DEVELOPMENT OF CORROSION RESISTANT GALVANISING ALLOYS

By

BO ZHANG

A thesis submitted to
The University of Birmingham
for the degree of
DOCTOR OF PHILOSOPHY

Metallurgy and Materials
School of Engineering
The University of Birmingham
July 2005

ABSTRACT

In this work an investigation into the effect of alloying additions (Mn, Cu, Sb and Zr) on microstructure and corrosion of Zn alloys and hot dip galvanised coatings was undertaken.

The first part of this thesis focuses on the effect of alloying additions on the corrosion of Zn alloys. The result shows that Mn is the most beneficial addition, which can significantly improve the resistance of Zn. The effect of Cu depends on its concentration. A high level of Cu addition has a deleterious effect on the corrosion resistance as the Cu-rich particles are catalytic cathodic sites for oxygen reduction. Additions of Zr and Sb were found to have minor effect on the corrosion behaviour of Zn alloys.

The effect of these additions on the microstructure of hot dip galvanised coatings was investigated in the second part. Both Zr and Mn can inhibit the layer growth of active steels with high Si content. Thus, Mn and Zr might be an alternative addition to Ni which can control the excessive reaction of the active steels. Addition of 0.8 wt % Cu significantly increases the coating thickness of the galvanised steel containing 0.02 wt % Si. The growth kinetics of the alloy layers follows a linear law.

The final part of this thesis focuses on the effect of these additions on the atmospheric corrosion resistance and electrochemistry of hot dip galvanised coatings. Among the alloying additions investigated in this study, Mn is the most beneficial addition to the Zn bath and can significantly improve the resistance of the hot dip galvanised coating to atmospheric corrosion. The effect of other additions on corrosion resistance is minor. The beneficial effect of Mn addition is mainly due to the formation of a Mn-rich oxide layer on the top surface during the galvanising process, which can greatly inhibit the cathodic reactivity of the hot dip galvanised coating. Coupled with the relatively low cost and ease of alloying of this element, these various factors suggest that Mn might have broader applications in general galvanising.

ACKNOWLEDGEMENTS

I would like to express my great thanks to my supervisor Dr Alison J. Davenport for her continuous help, support, and encouragement in this project.

I would also like to thank Joseph Ash Galvanising and UUK for the financial support for the project. A special thank to Adam Kent and Terry Felton in Joseph Ash Galvanising for providing materials, equipments, and discussion.

I would like to thank Dr Allan Walton in the Applied Alloy Chemistry Group for his help with preparing the master alloys. I would like to thank Chris Hardy for her help with XPS and Paul Stanley for his help with FEG ESEM. The help from Derek in the workshop was also very much appreciated.

I would also like to say thanks to Dr Stuart Lyon at UMIST, the University of Manchester and Dr Neil Short at Aston University for providing useful papers and suggestions.

I would like to thank all the people of the electrochemical group for their experimental help. The atmosphere in the group has always been friendly, and I have received help whenever I have asked for it.

Finally I would like to thank my wife, Lina Zhou, for her understanding and moral support and encouragement over the last four years.

TABLE OF CONTENTS

CHAPTER 1 INTRODUCTION

Hot dip galvanised coatings are widely used in industry for corrosion protection of steels. The steel is protected by the Zn coating through a barrier effect and a galvanic effect, in which Zn acts as the sacrificial anode while steel acts as the cathode. In most atmospheric environments, Zn corrodes much less than steel, by a factor of 10 to 100 times [1, 2] due to the formation of a protective layer consisting of a mixture of Zn oxide, Zn hydroxide and various basic Zn salts depending on the nature of the environment. Thus the protection of steel by a Zn coating is mainly through the barrier effect. However, at the places where the Zn coating is damaged and the steel underneath is exposed, such as at cuts or at scratches, the galvanic action between steel and Zn can protect the exposed steel from corrosion.

Although Zn has high corrosion resistance in most non-aggressive atmospheric environments, corrosion problems of Zn coatings have been often found in aggressive atmospheric environments where salt and sulphur dioxide are present. To overcome this problem, new types of Zn coatings with higher corrosion resistance are needed. In the literature some alloying additions (Al [3], Cu [4, 5], Mg [6, 7], Ni [8], Co [9, 10], Mn [11-14] , V [15], Cd [16] and Sb [17, 18] etc) have been reported to increase the corrosion resistance of Zn coatings. However, most of the Zn coatings were made by electrodeposition (e.g. Ni, Co and Mn), little work has been done towards the improvement of corrosion resistance of hot dip galvanised coating. One of the fundamental problems is that it is difficult to produce hot dip galvanised coating with alloying elements that possess high melting points compared to pure Zn. Another problem is that most of alloying elements have very low solubility in Zn (e.g. Cr) at the normal galvanising temperature (450°C) which gives rise to problems in making the alloying bath. Furthermore, the mechanisms of the effect of these additions are still not clear, since the information on their effect on the corrosion resistance and structure of the coating is rather controversial [2].

Nevertheless, it has been suggested that it is possible to develop better corrosion resistant galvanised steel by alloying [19]. In recent years, with the increasing requirements of industry for a longer service life for hot dip galvanised surfaces to offset the rapid rises in cost of maintenance in service, a need for the development of new types of hot dip galvanised coatings has been identified.

In this work, an investigation into the effect of alloying additions (Mn, Cu, Sb and Zr) on microstructure and corrosion of Zn alloys and hot dip galvanised coatings will be investigated with the aim of developing more corrosion-resistant alloys for hot dip galvanising.

CHAPTER 2 LITERATURE REVIEW

Zn coatings are widely used in industry for corrosion protection of steel structures because of their high corrosion resistance in atmospheric environments and sacrificial protection to steel [2, 20]. Nearly half of the Zn produced is used for this purpose [2]. Typical processing methods used in producing Zn coatings include hot dip galvanising, thermal spraying and electrodeposition [21]. Many electroplated Zn coatings alloying with Ni, Co, Mn and Fe have been demonstrated to have higher corrosion resistance than pure Zn coating [8-14]. However, due to the natural thermal process required for the hot dip galvanising, alloying additions to the Zn bath are limited. For example, a Zn-12 % Ni coating, which shows better corrosion resistance, can be successfully made by electroplating [22, 23]. But the same amount of Ni can not be added to the molten Zn bath to make hot dip galvanised coating due to the limitation of solubility of Ni in Zn at the galvanising temperature (450°C) [24]. Thus, this review will focus on hot dip galvanised coatings. The effect of the selected alloying elements on the microstructure and corrosion of both Zn alloys and hot dip galvanised coatings will be explored in the following four sections.

2.1 Microstructure of Zn and Zn alloys for hot dip galvanising

2.1.1 Impurities and alloying additions in commercially-pure Zn

Commercially-pure Zn is commonly used for hot dip galvanising. It is often produced by thermal and electrolytic processes, which give purities greater than 98 % and 99.95 % respectively [20]. The natural impurities, contaminants, and alloying additions present in commercial Zn are Pb, Fe, Cu, Al, Ti, Cd and Sn. Most of them have extremely limited solid solubility [24]. The effects on microstructure produced by these elements are reviewed below.

2.1.1.1 Pb

Pb is the main individual impurity in Zn produced by thermal processes. At room temperature, the solubility of Pb in solid Zn is extremely limited [20, 24]. Even in high-purity metal containing less than 0.001 wt % Pb, it can be detected as beads at the grain boundaries [20]. Pb appears in cast Zn and Zn alloys at the dendrite boundaries in the form of small, spherical droplets or surface films. In rolled Zn, the particles of Pb are elongated in the rolling direction and are not located preferentially at the recrystallized grain boundaries.

In galvanising, Pb is often deliberately added to industrial Zn baths. At the normal galvanising temperature, 450°C, the solubility of Pb in Zn is about 1.2 wt %. Any excess Pb sinks to the bottom of the bath [25]. Thus, Pb is often used as a molten layer underneath the molten Zn which makes it easier to remove the dross formed during hot dip galvanising [20, 25, 26]. It is claimed that Pb protects the bottom of the crucible, especially in case of overheating when there is a change from a parabolic to a linear type of attack [26]. It can also affect the crystalline structure of the hot dip galvanised coating (Section 2.2.4.3.3).

2.1.1.2 Fe

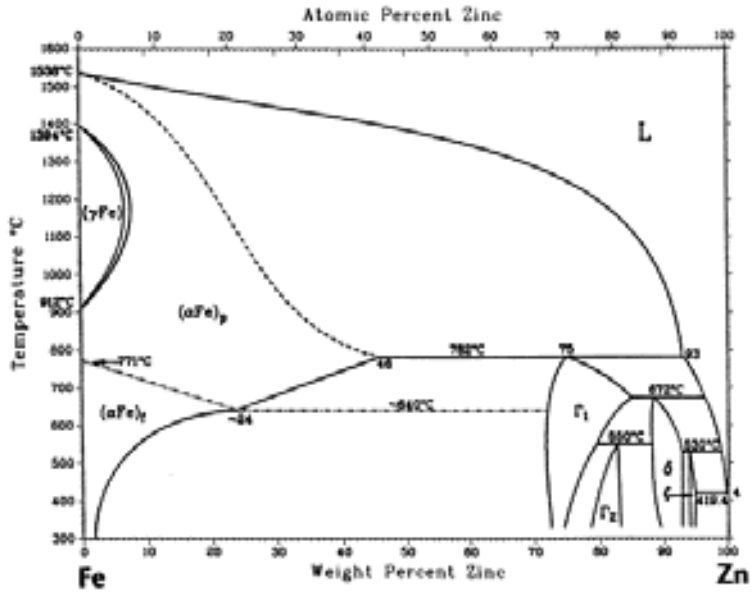

Fig 2.1 Zn-Fe equilibrium phase diagram [27]

The Fe-Zn alloys are of considerable importance in hot dip galvanising (see Section 2.2.2). The phase diagram of the Zn-Fe system is shown in Fig 2.1 [27]. Fe has very little solid solubility in Zn. It was reported that when the amount of Fe in Zn exceeds approximately 0.001 wt %, it appears in the microstructure as an intermetallic particle containing approximately 6 wt % Fe, possibly $FeZn_7$ [2, 20]. The particle size is controlled by the amount of iron present and the thermal history of the substrate. Fine particles formed during casting can coalesce to a coarser form by prolonged heating at 370^{o}C. The Fe-Zn intermetallic particles precipitate at dendrite boundaries [20]. In hot dip galvanising, a range of Fe-Zn intermetallic compounds form. The total thickness and the relative amount of each depend both on the steel composition and on the galvanising conditions (see Section 2.1.2).

2.1.1.3 Al

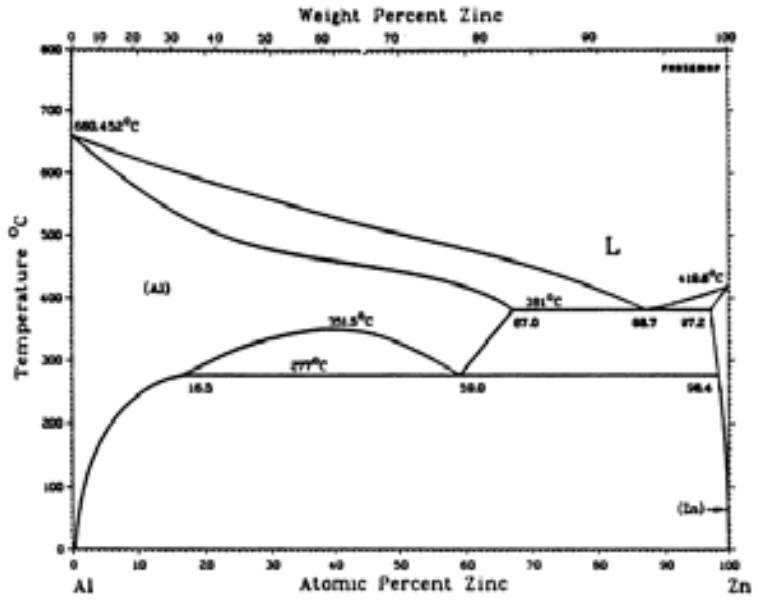

Fig 2.2 Zn-Al equilibrium phase diagram [28]

Al is an important alloying element in Zn. Many commercially important alloys were developed based on this system, such as the standard die-casting alloys and the galvanising alloys Galfan (5 wt % Al) and Galvalume (55 wt % Al). The Zn-Al phase diagram is shown in Fig 2.2. This system has a eutectic composition at about 5 wt % Al and a eutectoid at 22 wt % Al. Although the solid solubility of Al in Zn at the eutectic temperature is approximately 1 wt %, the solubility drops rapidly with temperature and casting alloys containing as little as 0.10 wt % Al display the eutectic structure in inter-dendritic areas.

Galfan is a Zn-5 wt % Al alloy coating, which is near the eutectic point in the Al-Zn equilibrium phase diagram, Fig 2.2. The Galfan composition corresponds to the Zn-Al eutectic (5 wt % Al) with additions of up to 0.5 wt % mischmetal. Mischmetal is a pyrophoric alloy of rare earth elements in various naturally occurring proportions. A typical composition includes approximately 50% Ce and 45% La. The addition of mischmetal is made to improve the wettability and fluidity of the molten bath without affecting the corrosion resistance of the coating [29]. It is also found to suppress bare spot

formation [30]. One of the objects in producing a Galfan coating was to develop a Zn-rich coating without intermetallics at the coating/steel interface for improved formability [21]. The microstructure of Galfan is characterized by a two-phase structure; a Zn-rich eta (η) proeutectoid phase surrounded by a eutectic type phase consisting of β Al and η Zn lamellae as shown in Fig 2.3 [31]. However, the microstructure can be varied depending upon cooling rate [32].

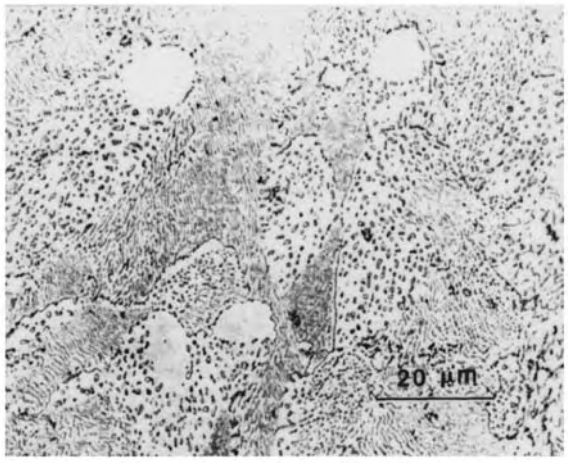

Fig 2.3 Planar view of the lamellar microstructure of a Galfan coating.

Another important Zn-Al galvanising alloy (Galvalume) was first developed by Bethlehem Steel Corporation [20]. This coating alloy, consisting of nominally 55 wt % Al, 43.4 wt % Zn and 1.6 wt % Si, has a higher corrosion resistance than conventional hot dip galvanised coatings and Galfan [33]. Si is added to the bath to prevent a very strong exothermic reaction between the Al–Zn bath and the steel sheet [20]. Without Si, rapid attack of the iron panel by the high Al containing Zn baths was controlled by the rate of Al diffusion in the liquid bath in contact with the iron panel [34]. Si suppresses the exothermic reaction by forming a solid interfacial layer that acts as a diffusion barrier or inhibition layer for the reactive species, which is probably Al [35]. Therefore, in order for a reaction between the bath and the iron substrate to occur, the Al has to diffuse through the solid phase in the interfacial layer, which is considerably slower than liquid state diffusion.

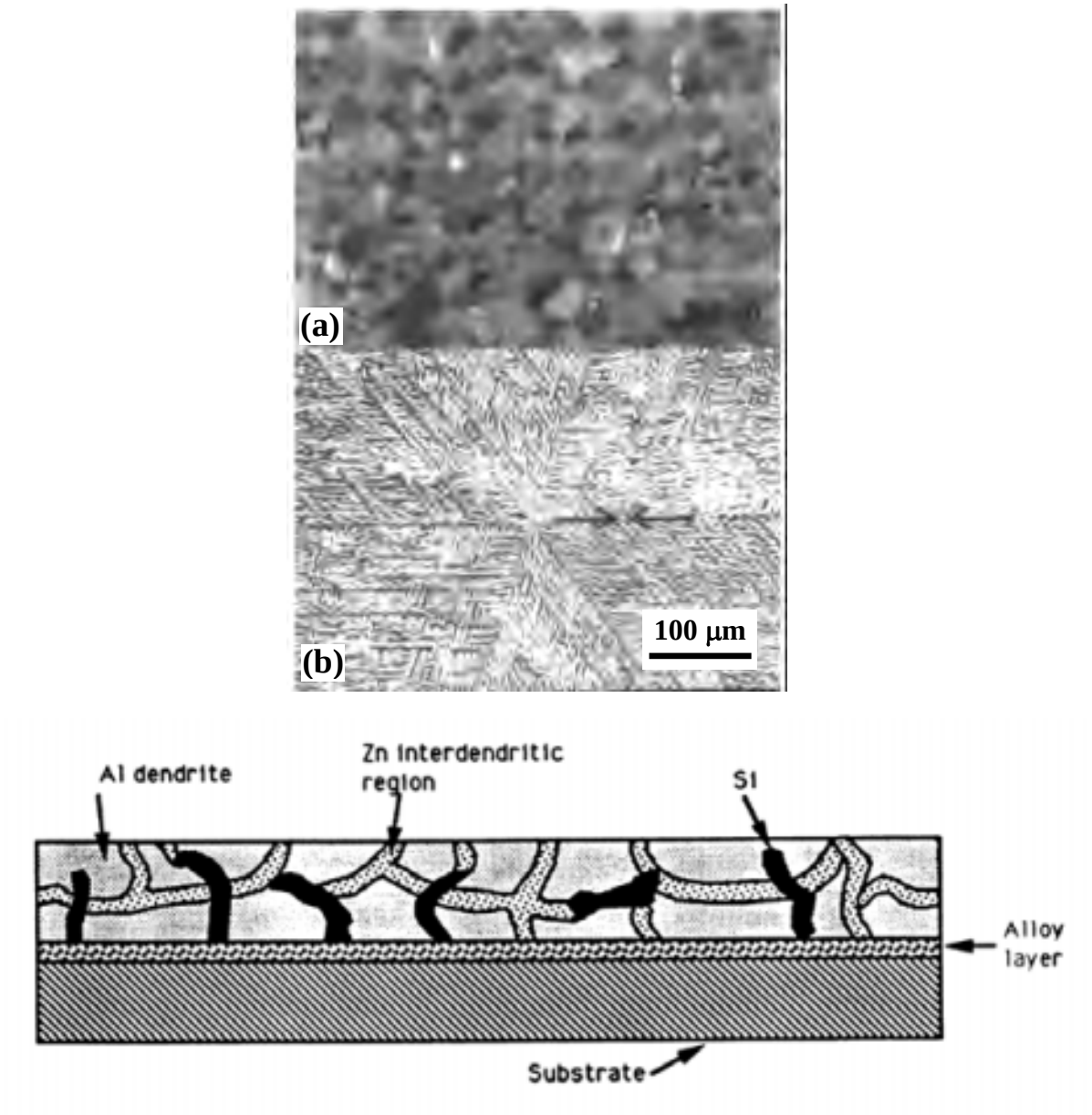

(c)

Fig 2.4 Microstructure of Galvalume coating: (a) spangle finish; (b) dendrite arm spacing; (c) cross-sectional view [31].

The surface of the Galvalume coating contains characteristic spangles, Fig 2.4 (a), that consist of Al dendrites with a clearly measurable dendrite arm spacing (DAS), Fig 2.4 (b). In cross-section, three features of the overlay are defined, Fig 2.4 (c): the

coating contains β Al dendrites, Zn-rich interdendritic regions and a fine dispersion of Si particles [20, 31].

2.1.1.4 Cu

Cu, when present in Zn, in amounts up to approximately 1 wt %, is in solid solution, and results in a cored structure. During hot rolling at approximately 205°C, the Cu is retained in supersaturated solid solution. Upon cooling, some of the Zn-Cu ε phase precipitates at the final recrystallized grain boundaries. During long exposures near room temperature, ε phase will continue to precipitate at grain boundaries and finally in the interior of the grains, ultimately forming a ternary eutectic structure. When cold rolled, the ε phase precipitates rapidly and abundantly in the cold-worked structure.

2.1.1.5 Ti

The solid solubility of Ti in Zn is very limited. It is reported to be smaller than 0.02 wt % Ti at 400°C [24]. At approximately 0.12 wt % Ti, a lamellar eutectic of Zn and $TiZn_{15}$ forms. The eutectic forms at dendrite boundaries in a casting. The $TiZn_{15}$ compound decreases the cast grain size of Zn and restricts grain growth in hot-rolled Zn. In rolled strip, particles of the compound are elongated in the rolling direction. Zn grain growth is limited to the spacing between the stringers of compound.

2.1.1.6 Cd and Sn

The Cd present in most commercial Zn products is in solid solution and produces no change in microstructure [20]. The solubility of Sn in solid Zn is extremely restricted, and the Zn-Sn eutectic appears in alloys containing as little as 0.001 wt % Sn [24].

2.1.1.7 Sb

In galvanising, Sb may be an interesting alloying addition to the Zn bath as it lowers the surface tension, which can make a uniform galvanised coating [36, 37]. The Zn-Sb phase diagram is shown in Fig 2.5. In the Zn-rich corner, this system has a eutectic composition at about 2.2 wt % Sb (412°C). However, no solubility of Sb in solid Zn was observed [24]. There are several intermetallic phases of Sb and Zn in a binary phase diagram of the Sb-Zn system [24]. According to Chang [38], the Sb-rich intermetallic particles formed in the η layer of a galvanised coating after the addition of Sb revealed Sb_2Zn_3 electron diffraction patterns.

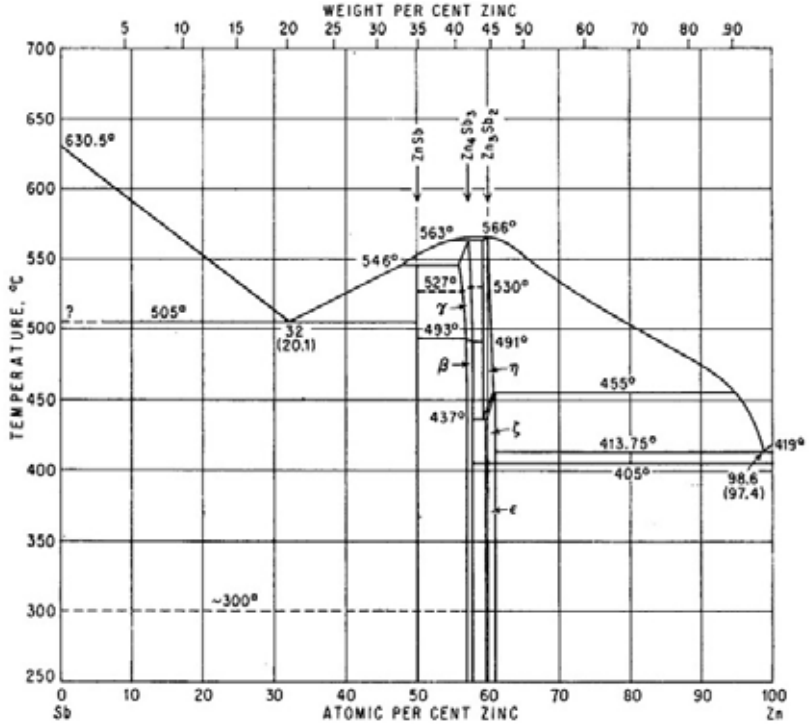

Fig 2.5 Zn-Sb equilibrium phase diagram [24]

2.1.1.8 Mn

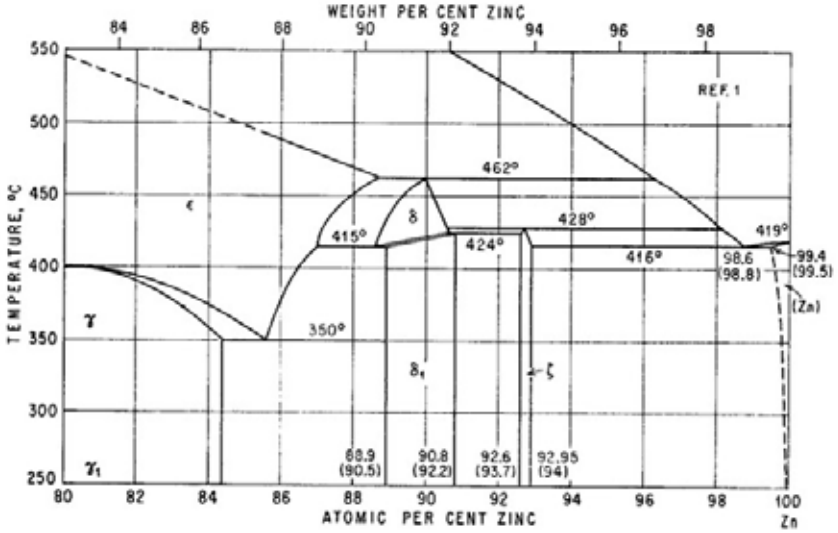

Fig 2.6 Zn-Mn equilibrium phase diagram (Zn-rich corner) [24]

The Zn-Mn phase diagram is shown in Fig 2.6. In the Zn-rich corner, this system has a eutectic composition at about 1.2 wt % Mn (419°C). Mn has relatively high solubility (about 0.5 wt %) in Zn at the eutectic temperature. But at 200°C the solubility of Mn in Zn drops to 0.02 wt % [24].

2.1.1.9 Zr

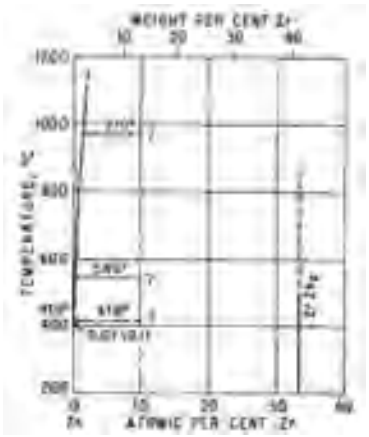

Fig 2.7 Zn-Zr equilibrium phase diagram (Zn-rich corner) [24]

The Zn-Zr phase diagram is shown in Fig 2.7. A eutectic at about 0.1 wt % Zr, 416°C was found [24]. Composition and crystal structure of the intermediate phases were not determined. The solubility of Zr in solid Zn is about 0.02 wt % at 400°C [24].

2.1.1.10 Bi

Some new galvanising alloys with Bi additions were developed recently [39, 40] as Bi improves bath fluidity [39, 41] and is not harmful for human health and the environment. However, the solubility of Bi in Zn is very small; a slowly cooled alloy with 0.1 wt % Bi was heterogeneous [24]. In resistivity measurements on Zn-Bi alloys quenched from 255°C, no solubility of Bi in solid Zn was observed [24].

2.1.2 Summary

Most of the impurities and alloying elements have very low solid solubility in Zn at room temperature. Thus, intermetallic particles are often found in commercially-pure Zn containing these elements even if the content is small. The effect of these elements on microstructure and corrosion resistance of hot dip galvanised coatings will be explored in the following sections.

2.2 Microstructure of hot dip galvanised coatings

2.2.1 Introduction

Hot dip galvanising is a process by which an adherent coating of Zn and Zn-Fe is produced on the surface of Fe or steel products by immersing them in a bath of molten Zn [20, 21]. A hot dipped coating will consist of three Zn-Fe alloy layers with decreasing Fe content on moving away from the steel surface. These layers are sometimes covered by a layer of solidified Zn, which is usually referred to as the pure Zn (eta phase) [21]. In this section, the Fe-Zn phase formation and growth will be discussed, followed by the effect of alloying additions on microstructure and growth of galvanised layers.

2.2.2 Fe-Zn phase formation

The most widely accepted Fe–Zn equilibrium phase diagram is that of Kubachewski shown in Fig 2.1 [27]. The Zn-rich corner of the Fe–Zn binary phase diagram is shown in Fig 2.8 . The primary phases formed during long immersion time galvanising are zeta (ζ), delta (δ), gamma1 (Γ1) and gamma (Γ). Although not represented in the equilibrium diagram, the η phase is a solid solution of Fe in Zn with a maximum Fe solubility of 0.003 wt % at 150°C. The characteristics of these Zn-Fe intermetallic phases are given in Table 2.1.

Table 2.1 Characteristics of Zn-Fe intermetallic phases [20, 21, 25]

Phase	Formula	Fe content (wt %)	Crystal structure	Density (g/cm^3)
η	Zn	Max 0.003	hcp	7.14
ζ	$FeZn_{13}$	5.7-6.3	monoclinic	7.18
δ	$FeZn_{10}$	7.0-11.5	hcp	7.24
Γ1	Fe_5Zn_{21}	17.0-19.5	fcc	-
Γ	Fe_3Zn_{10}	23.5-28.0	bcc	7.36

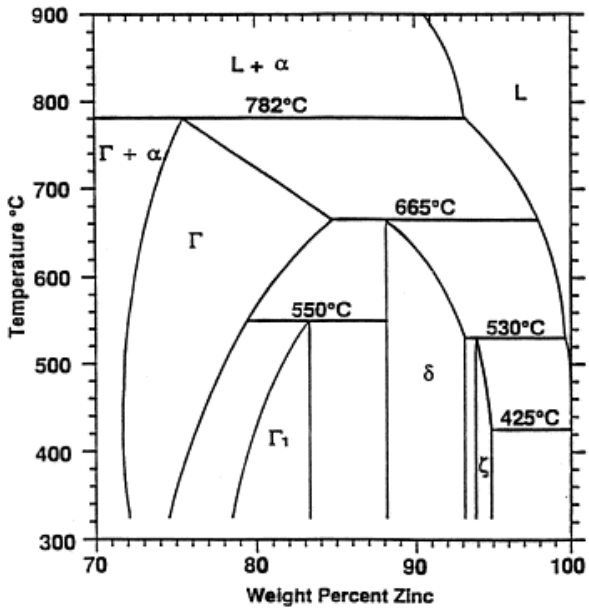

Fig 2.8 Zn rich end of the Fe–Zn equilibrium phase diagram [27].

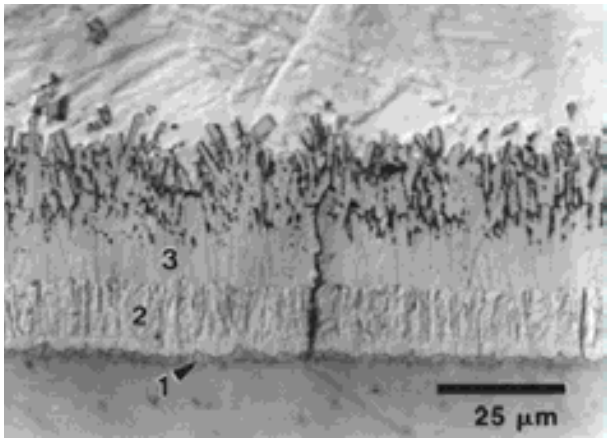

Fig 2.9 Microstructure of Zn coating formed after 300 s immersion in the Zn bath without Al addition at 450°C: (1) gamma phase, (2) delta phase, and (3) zeta phase [42].

A typical morphology found for a pure Zn hot dipped coating is shown in Fig 2.9 [42]. The Fe content of each of these phases has been confirmed by EPMA measurements. The gamma (Γ+Γ1) phases appear as a very thin layer with a planar interface between the steel substrate and the delta layer. The delta phase has a columnar morphology as a result of a preferred growth perpendicular to the interface in a direction along the (0001) basal plan of the hexagonal structure [30]. The zeta phase has two layers depending upon the supersaturation of Fe in the melt. Adjacent to the delta layer, the zeta phase grows in a columnar morphology that is supersaturated in Fe.

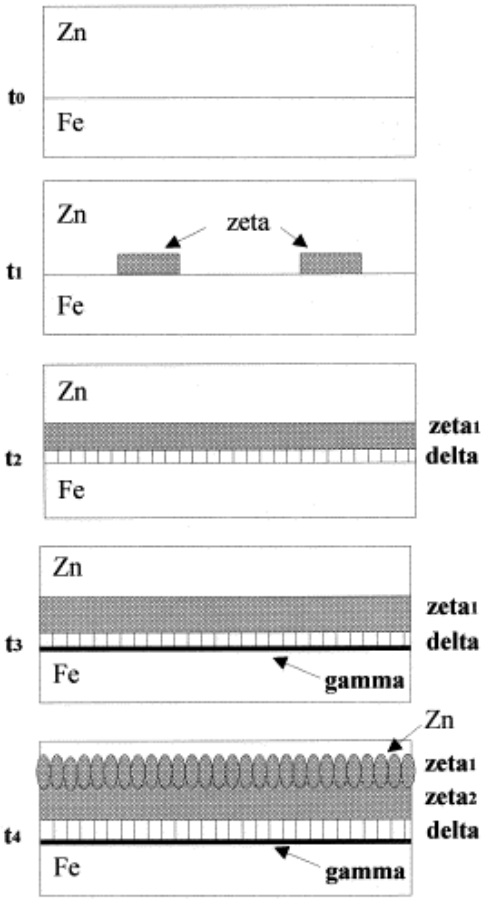

Fig 2.10 A schematic representation of Fe–Zn phase layer formation in the Zn bath without Al additions (t0 corresponds to zero time, and development occurs according to time such that t1<t2<t3<t4) [42].

When Fe is immersed in molten Zn at typical galvanising temperatures (450 - 490°C), the sequential nucleation of the Fe–Zn phases occurs at the interface beginning with (1) the zeta layer, followed by (2) the delta layer, and after an incubation time, (3) the gamma layer as shown schematically in Fig 2.10, where the reaction sequence is represented chronologically. There is no apparent delay in the formation of delta or zeta phases, as both are found to form a continuous layer after a 5 s immersion time. On the other hand, the gamma (Γ) phase is found to form after incubation time of 30 s (t_3) [42].

2.2.3 Fe-Zn phase reaction kinetics

Each layer in the Zn coating exhibits different growth kinetics [21, 25, 42-44]. At short immersion times up to 300 s at 450°C, Fig 2.11, the zeta phase layer grows rapidly at

first but then much more slowly, while the growth of the delta phase layer is at first slower than that of the zeta phase layer, but then becomes faster. The growth rate of the (Γ+Γ1) phase layer is very slow, and therefore this phase may not be observed with microscopy at short reaction times. Similar effects were reported at 457°C for times up to 6 h [25]. All of these transformations are governed by the diffusion of Zn into the Fe substrate [45, 46]. However, Fe probably also diffuses outward through the alloy phases into the Zn melt, but at a much slower rate [46].

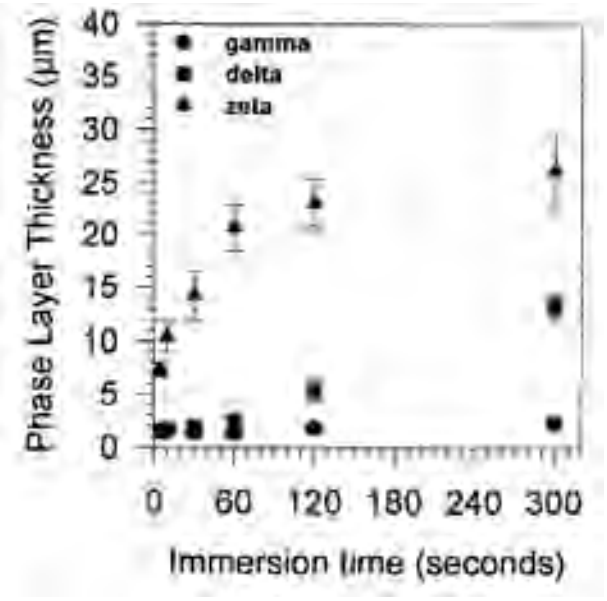

Fig 2.11 Individual Fe–Zn gamma (Γ) phase, delta (δ) phase, and zeta (ζ) phase layer growth for a ULC (ultra low carbon) steel substrate hot dipped at 450°C in a Zn bath without Al additions [42].

To evaluate the kinetics of Fe–Zn alloy layer growth, a power-law growth equation is generally used to interpret the growth rate data [44], as follows:

Equation 2.1 $Y = kt^n$

where Y is the layer thickness, k and n are growth rate constants, t is the reaction time.

The growth-rate constant n is an indication of the type of kinetics controlling the growth of the layer. An n value of 0.5 is indicative of parabolic diffusion-controlled growth, while an n value of 1.0 is representative of linear kinetics in which growth is interface

controlled [21, 25, 42, 44]. Mackowiak and Short [25] summarised the values n for a number of polished results as shown in Table 2.2. Although many of the studies were made on steel substrates with significant additions of carbon and other alloying elements, it was concluded from these results that in the lower parabolic range, values of n tend to be around 0.5 for delta layer growth and total layer growth. Values for the zeta layer and gamma layer growth were lower, around 0.35 and 0.25, respectively. In a more recent experiment [42] with short time immersions of up to 300 s at a temperature of 450°C, the results are remarkably close to the previous work. It was found that the zeta layer dominates the coating morphology [42], whereas for long times Allen [43] found that the delta layer dominates the coating structure.

Table 2.2 Values of n for growth of alloy layers in the lower parabolic range [25]

Source	gamma	delta	zeta	Total layer
Allen	0.25	0.65	0.35	0.55
Rowland	0.13	0.53	0.31	–
Blickwede	0.10	0.60	0.16	–
Horstmann and Peters	0.50	0.50	–	–
Sjoukes	0.23	0.58	0.26	–
Onishi et al.	0.23	0.49	0.36	0.43

2.2.4 Metallurgical properties of hot dip galvanised coating

The factors which determine the overall thickness and metallurgical properties of a hot dip galvanised coating are: the composition and metallurgy of the steel, bath temperature, immersion time, alloying additions to the Zn, withdrawal rate of article from the molten Zn, and surface condition and thickness of the steel [21]. In the following sections, the effect of the composition of the steel, bath temperature and alloying additions to Zn will be discussed.

2.2.4.1 Effect of bath temperature

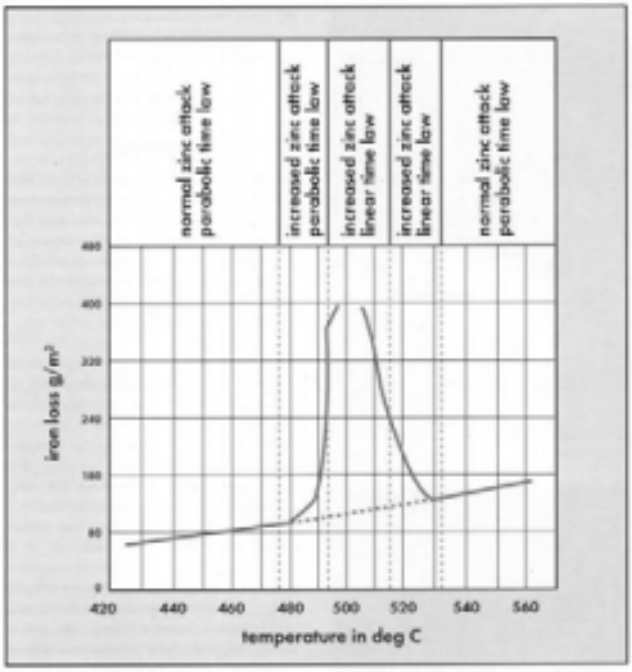

Fig 2.12 The influence of temperature on diffusion of Fe in molten Zn [47].

The reaction between Fe and molten Zn is influenced by bath temperature. With increasing temperature up to about 485°C, diffusion accelerates slowly, causing a slow but consistent increase in coating thickness, following a parabolic time law. Above 485°C and up to about 530°C, coating growth is almost linear with time (regardless of steel composition) after which the reaction reverts to a parabolic time law [21, 25]. Thus, hot dip galvanising at temperatures in excess of 470^{o}C is not recommended. Normal galvanising is carried out at temperatures below about 460°C.

2.2.4.2 Effect of the composition of the steel

2.2.4.2.1 C

The galvanising layers on steel (or cast iron) are similar to those obtained on pure Fe. However, the rate of attack depends on the amount of C present, and even more importantly on the form in which it is present. If the C is present as graphite (in cast iron)

or tempered martensite, the rate of alloy growth is little changed, but when the C is found in the steel as lamellar pearlite or spheroidized cementite, the rate of attack is increased by 5.5 times and 4 times, respectively [20, 21]. Two main reasons have been suggested for these changes in behaviour according to microstructure. Bablik *et al.* [48] suggested that the lamellar and globular structures increase the surface area on which the reaction could occur. Price and Charles [49] proposed that the actual alloy growth is modified by the presence of coarse Fe_3ZnC particles, which have been seen in the gamma and delta intermetallic layers.

2.2.4.2.2 Si (Sandelin effect)

Si was found to significantly promote the growth of the Zn-Fe alloy layer. The unusual activity of Si-containing steels was first studied by Sandelin in 1940 [50-52]. He showed that the presence of about 1 wt % Si in the steel led to a linear growth law for coatings obtained by galvanising in pure Zn baths, and he later [53] showed that smaller concentrations (about 0.1 wt %) also led to a linear growth. This phenomenon has been called the Sandelin effect ever since, and has been intensively investigated [54-57]. It became particularly troublesome to the galvanising industry with the advent of continuous casting in steelmaking practice, which involves killing with Si (The addition of Si is to remove oxygen from solution by the formation of silicon oxides so that no gas bubbles form and the steel is quiescent as it solidifies). This unpredictable reactivity may give rise to dull grey, brittle coatings of excessive thickness, and corrosion products which appear as unsightly black or brown deposits. Further problems may be caused by the inhomogeneous distribution of Si on the surface of the steel resulting in uneven coating formation [25].

Apart from its kinetic aspects, the Sandelin effect is characterized by modifications of the structure of the coatings, from the usual Fe-Zn stratified layers, to a mass of zeta crystallites surrounded by eta Zn [44]. The results of the detailed study by Kozdras [58] show that regardless of the Si content of the steel, the usual stratified structure of the coating is observed during the short immersion time (about 2 or 3 minutes), Fig 2.13. During this period, the growth kinetics are parabolic, as in the case of pure Fe. At

the end of this incubation period, the behaviour of the steels (morphology and growth kinetics) changes according to their Si content.

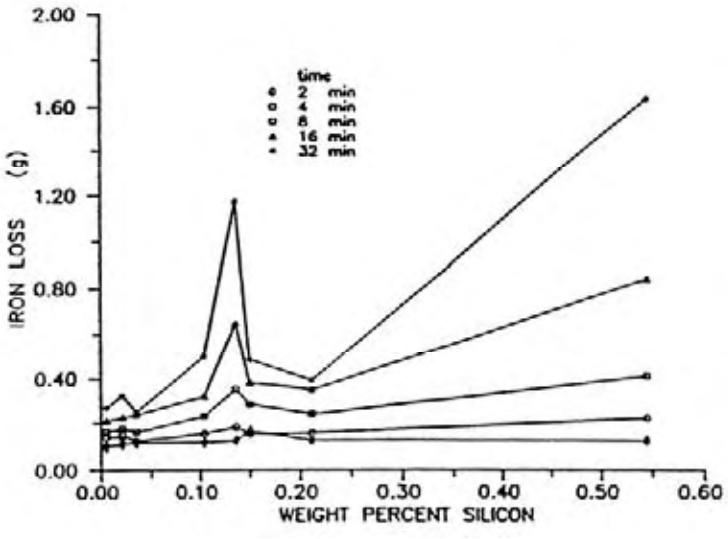

Fig 2.13 Comparison of Fe losses for different immersion times and different Si contents in the steel [58].

In order to overcome the detrimental effects of Si on the growth of the Zn–Fe intermetallic compounds, several studies were carried out. These research efforts have so far resulted in three solutions which have found their way to in-plant trials and even into industrial practice.

The problem is generally satisfactorily resolved by Al additions [25] which can suppress the formation of Fe-Zn alloy layer, especially for short immersion times (Section 2.2.4.3.1) .However, its industrial application has been limited because of the rather complicated surface preparation required prior to immersion in the galvanising bath. Another solution is based on a high temperature galvanising process [59], which leads to the elimination of the zeta phase at temperature above 530°C. However, increased pot and hardware corrosion and excessive dross formation strongly limit the success of this process. The most recent solution is the use of a Zn–Ni alloy [60-64]. The effect of Ni addition on the growth of galvanised layers is discussed in detail in Section 2.2.4.3.5.

2.2.4.2.3 P

P in steel also has deleterious effects on galvanising. The important role played by P has been recognised either in combination with Si or alone. It has been said that the influence of P as an accelerator is of equal importance to Si in the Fe/Zn reaction. Gladman *et al.* [65] note an increase in alloy growth rate with increasing P levels. Metallographically, P appears to suppress delta layer formation and encourage zeta phase growth while the gamma intermetallic becomes discontinuous. When considering Sandelin curves for coating mass, the behaviour of P is linked to that of Si and the following formula is to be used.

Equation 2.2 $\text{Si \%} + 2.5 \times \text{P \%} = \text{Si (equivalence) \%}$

2.2.4.2.4 Mn

Mn in steel has no significant effect on the layer growth and coating microstructures. Sebisty [66] reported that contents of up 1-2 wt % Mn in steel had very little effect on the growth of coating and its microstructures [67]. However, Dubois [67] suggested that changes in microstructures and phase distributions are possible when high Mn steel sheets are processed.

2.2.4.3 Effect of alloying additions to the Zn bath

2.2.4.3.1 Al

Al is probably the most important alloying element added to the hot dip galvanising bath, with different levels required in order to produce different properties in the bath [31]. Al levels of 0.005 wt % are added to brighten the initial coating surface. The effect is related to the formation of a continuous Al_2O_3 layer on the coating surface that inhibits atmospheric oxidation of the molten Zn bath by acting as a protective barrier layer [20, 21].

Al in the range of 0.1 - 0.3 wt % is added to the Zn bath to suppress the growth of brittle Fe-Zn intermetallic phases at the steel coating interface by forming the $Fe_2Al_5(Zn)$ inhibition layer. In this case, coatings with good ductility can be produced as only the eta layer and $Fe_2Al_5(Zn)$ layer are present in the coating.

The use of a high level of Al, e.g. 5 wt % (Galfan) and 55 wt % (Galvalume), was described in Section 2.1.1.3.

2.2.4.3.2 Fe

The galvanising bath after several runs will finally be saturated with about 0.03 wt % Fe at the normal galvanising temperature 450^{o}C. Thus, any quantity in excess of this amount will produce dross, which eventually settles at the bottom of the kettle during galvanising. Haughton in 1952 reported [68] that a bath unsaturated with Fe gave a coating with a thinner, smoother zeta layer than the saturated bath, although the variation was slight. The smooth effect of the bath unsaturated with Fe is probably due to the dissolution of zeta phase at the zeta/eta interface.

2.2.4.3.3 Pb and Bi

Pb is added to the galvanising bath to make the molten Zn more fluid, thus the conventional PWG (Prime Western Grade) Zn bath, which contains approximately 1% Pb,

has been extensively used [20, 39]. It was shown that Pb additions decrease the surface tension of the liquid phase [37, 69], increase the fluidity of the alloyed bath and improve liquid drainage [70]. Thus a high Pb content can result in an overall commercial saving. Krepski [70] observed that an increase in the Pb level from 0.03 wt % to 1.2 wt % resulted in a net decrease of up to 60 wt % in the amount of Zn dragged out from a galvanising bath. Pb also promotes “spangle” formation [20, 21, 71, 72]. Strutzenberger and Faderl [69] explained that Pb segregates ahead of growing dendrites, lowering the surface tension and allowing the growth velocity of the Zn dendrite to increase, resulting in larger grains or spangles. Similar interpretations were proposed by Fasoyino and Weinberg [37].

Sebisty and Edwards [73] reported that Pb has no effect on Fe-Zn alloy layer growth when galvanising low-C steels, but Krepski [70] notes a reduction in alloy growth. A recent study by Reumont and Perrot [74] indicated that Pb addition to the Zn does not disturb the existence, morphology, composition and kinetics of growth of the Fe-Zn intermetallic compounds.

Although Pb makes the molten Zn more fluid, it is considered detrimental for human health and the environment. In some countries as in the US, galvanising with Pb-containing alloys will no longer be permitted [40, 75]. A bath containing Bi has been proposed as an alternative to the traditional bath with Pb [41].

Bi was also found to promote spangle formation [17], has no significant effect on microstructure of hot dip galvanised coatings [17, 39] and improves the Zn drainage [39, 41]. As Bi improves bath fluidity and is not harmful for human health and the environment, some new galvanising alloys with Bi additions were developed recently [39, 40]. Fratesi [39] reported that a new Zn-0.04%Ni-0.1%Bi alloy can be successfully used to control the reactivity of the steels with high Si content (Si > 0.05 wt %). Another new galvanising alloy Galveco (Zn-0.05%Ni-1.8%Sn-0.5%Bi) was reported to be a solution for galvanising reactive steels. The excellent fluidity and low surface tension of Galveco reduces significantly the finishing work of the galvanised parts and improves the surface quality which is always shiny and spangled [40].

2.2.4.3.4 Cu

The effect of Cu has always been contentious [5, 36, 76, 77]. The addition of Cu up to 0.72 wt % has been found generally to increase alloy layer growth [78]. Sebisty and Palmer [36] reported that Cu promotes more rapid Zn attack on the steel surface and is also detrimental to coating surface appearance. However, Radeker *et al.* [5] claimed that an increase in the Cu content to 0.82 wt % causes a proportional decrease in the coating weight and thickness. Recently, Katisforis *et al.* [77] studied the influence of Cu (up to 3 wt %) on the structure and thickness of hot dip galvanised coatings. Their results indicated that the addition of Cu up to 0.6 wt % only slightly increases coating thickness without any change of the structure of the coating while the addition of Cu from 0.8 wt % to 3.0 wt % to the bath causes a substantial change to the structure of the coating. The presence of Cu in the galvanising baths favours the formation of the delta phase and hinders the zeta phase growth. At high Cu levels, the zeta phase was found to disappear completely while the delta crystals were dispersed in the eta phase [77]. Nell [76] proposed a mechanism to explain the effect of Cu addition: 1) Cu only takes part in the formation of the coating after it diffused through the zeta layer into the delta layer and further into the coating; 2) Cu has a loosening effect on the zeta layer, which produces instability and increases layer growth; 3) Finally a new modified zeta layer forms on top of the delta layer which stabilizes the reaction. Thus if the immersion time is less than the incubation time, the effect of Cu addition on layer growth can be ignored.

Not many studies were carried out on the growth kinetics of the alloy layer with Cu additions. In one study, Katisforis *et al*. [77] found that the growth of total thickness of the coating follows closely the linear time law for the addition of 1.6 wt % Cu.

2.2.4.3.5 Ni, Ti and V

Ni is added to an increasing number of galvanising baths to control the excessive reaction of some steels (particularly Si 0.04-0.12 wt %) with molten Zn [20]. The effect of Ni additions to overcome the detrimental effect of Si in steels has not been clearly identified [63]. Sebisty [79] suggested that with Ni additions, there appeared to be a

secondary reaction involving dissolution of the zeta phase to form intermetallic compounds at the Zn-zeta interface, thereby limiting growth of the zeta phase.

Sebisty and Palmer [79] reported that 0.01 wt % Ti can slightly decrease growth of Fe-Zn phases, especially zeta phase on non-reactive steel. Addition of more than 0.05 wt % Ti can significantly decrease the reactivity of Si steels, thus Ti could be the replacement for Ni in the Zn bath to overcome the detrimental effects of Si [80]. It was suggested by Reumont *et al.* [80] that Ti has almost the same properties as Ni, which is confirmed by the great similarities between the Fe-Zn-Ni and Fe-Zn-Ti ternary systems. A high content of Ti suppressed Fe-Zn alloy growth, but with 0.1 wt % Ti, a very non-uniform Zn layer with distinctive dispersion of intermetallic compounds formed. The intermetallic compounds were probably Fe_2TiZn_{22}, $TiZn_{15}$ or zeta as suggested by Reumont [80].

The combination of Ti and V has been successful, as reported by Adams *et al.* [81] in a recent work. Their results indicated that addition of 0.04 wt % V + 0.05 wt % Ti was successful in controlling reactivity effects for up to 1 wt % effective Si in the steel. This can be compared to the upper limit of 0.2 wt % effective Si which the well-known Ni-Zn process will control.

2.2.4.3.6 Sn, Sb and Cd

Sn and Sb have little effect on Fe-Zn alloy formation, but at high concentrations, Sn and Sb promoted spangle formation [17, 36-38]. The spangle is the result of the dendritic solidification of Zn. Sb lowers the bath viscosity and the surface tension of the molten Zn in the sheet, so that a uniform coating is effectively achieved [36, 37]. Katiforis *et al*. [77] found that up to 3 wt % Sn had no effect on thickness and structure of the galvanised coatings on normal steels. However Gilles *et al*. [82] found that the addition of Sn in concentrations of at least 2.5 wt % is very effective in neutralising the high reactivity of Si and P containing steels. A mechanism was proposed to explain the effect of Sn on the coating thickness. During galvanising, Sn is repelled while the Zn-Fe intermetallic phases are formed. Due to its low surface tension, it forms a thin film around the intermetallic phase, which is probably hinders the diffusion of Fe or Zn [82].

It was reported [36] that 0.05 wt % Cd tended to increase coating weight at longer immersion times. A more detailed study on the effect of Cd addition was carried out by Katiforis *et al.* [77] who found that more than 1.0 wt % Cd promotes zeta phase formation and hinders the growth of the delta phase, while lower content of Cd than 0.6 wt % has no effect on the structure of the coating with only slightly increasing the thickness of the alloy layer.

2.2.4.3.7 Mn

The addition of Mn to Zn baths has not been studied extensively. Palmer *et al.* [83] was probably the first to add Mn to the Zn bath. They found that Mn is incorporated into the Zn/zeta alloy layers with a high concentration throughout the zeta layer. Reumont *et al*. [80] found that addition of more than 0.5 wt % Mn can significantly decrease the reactivity of Si steels, thus Mn could also be a replacement for Ni in the Zn bath to overcome the detrimental effects of Si. A mechanism has also been proposed by Reumont that Mn can attract Si originating in the substrate to form Mn-Si compounds which are thermodynamically more stable than the FeSi compound. The FeSi compound formed during the first period of immersion is believed to be responsible for the excessive thickness of the coating [56].

2.2.4.3.8 Zr

The study on addition of Zr to Zn bath is very limited. Sebisty [79] reported that additions of 0.1 and 0.3 wt % Zr decreased the coating thickness. He suggested that the limiting growth of the zeta phase is probably due to the formation of the intermetallic particles rich in Fe and Zr which involves the dissolution of the zeta phase.

2.2.5 Summary

Among these alloying additions, Ni, Ti, V, Mn, Zr and Al in small amounts can inhibit the Fe-Zn phase growth. Pb and Bi increase the fluidity of molten Zn, thus they

have some beneficial effects on the galvanising process. Cu and Cd were found to increase the layer growth especially at high levels and long immersion times.

2.3 Corrosion of Zn and Zn Alloys

2.3.1 Electrochemical thermodynamics of Zn

Zn is an electrochemically active metal with a standard potential of -0.763 V (vs SHE). The potential-pH equilibrium Pourbaix diagram of the Zn-water system at 25°C is shown in Fig 2.14 [84]. According to the Pourbaix diagram, Zn is thermodynamically unstable in water and aqueous solutions, and tends to dissolve with the evolution of hydrogen over the whole pH range. In solution of pH range 8.5 - 12, Zn can be covered with a hydroxide film, which has the effect of inhibiting Zn dissolution.

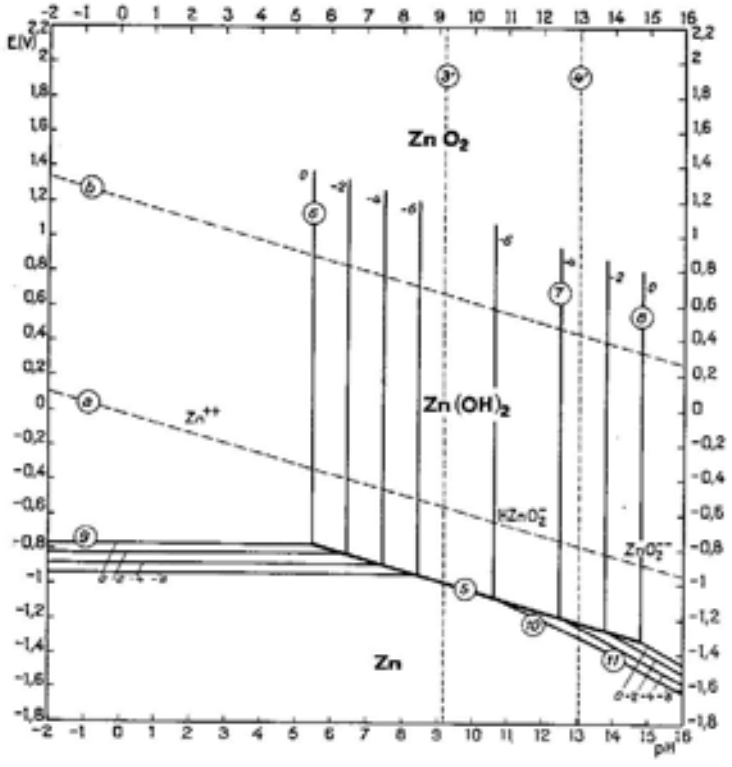

Fig 2.14 Potential-pH equilibrium diagram for the Zn-water system at 25°C [84].

2.3.2 Kinetics of corrosion

The kinetics of electrochemical reactions involving Zn, such as anodic dissolution, cathodic reactions, and surface film formation, have been the subject of many electrochemical studies.

2.3.2.1 Anodic dissolution

The mechanism of dissolution is different for acidic and alkaline solution and for complexing and noncomplexing solutions. In acidic or near neutral solutions, it is generally accepted that the dissolution occurs through a two-step charge transfer reaction: [85, 86]:

Equation 2.3 $Zn \rightarrow Zn^{+} + e^{-}$

Equation 2.4 $Zn^{+} \rightarrow Zn^{2+} + e^{-}$ (r.d.s.)

with the reaction in Equation 2.4 as the rate-determining step (r.d.s.). This dissolution mechanism gives a Tafel slope of $2.3 \times 2RT/3F$ (40 mV). The dissolution of Zn in acidic NaCl solution, although following Equation 2.3 and Equation 2.4, is diffusion-limited, probably because of the diffusion of chloro-Zn species (e.g., $ZnCl_4^{2-}$) away from the electrode surface [85].

In alkaline solutions, Bockris *et al*. [87] proposed a multistep reaction mechanism (Equation 2.5 to Equation 2.8) for the dissolution of Zn, with the rate-determining step being the reaction in Equation 2.7. Under steady-state conditions, the rate-determining step becomes the diffusion of zincate away Zn from the surface rather than the charge-transfer ? reaction (Equation 2.7) [88].

Equation 2.5 $Zn + OH^{-} \rightarrow Zn(OH) + e^{-}$

Equation 2.6 $Zn(OH) + OH^{-} \rightleftharpoons Zn(OH)_2^{-}$

Equation 2.7 $Zn(OH)_2^{-} + OH^{-} \rightarrow Zn(OH)_3^{-} + e^{-}$ (r.d.s.)

Equation 2.8 $Zn(OH)_3^{-} + OH^{-} \rightleftharpoons Zn(OH)_4^{2-}$

In neutral solutions, Cachet *et al.* [89] proposed a model for the dissolution of Zn in naturally-aerated sodium sulphate solution as shown in Fig 2.15. It appears that the dissolution process is particularly complex because it involves three parallel paths and three adsorbed intermediate species. The surface coverage by Zn_{ad}^{+} is always very small, whereas the two other adsorbed species, Zn_{ad}^{2+} and $ZnOH_{ad}$, are in competition for the surface occupancy. This competition is markedly affected by the electrode preparation and by the experimental procedure. It was claimed that the model opens a new outlook to account for the influence of various factors such as protective layers or composition and structure of the Zn electrode on the dissolution process.

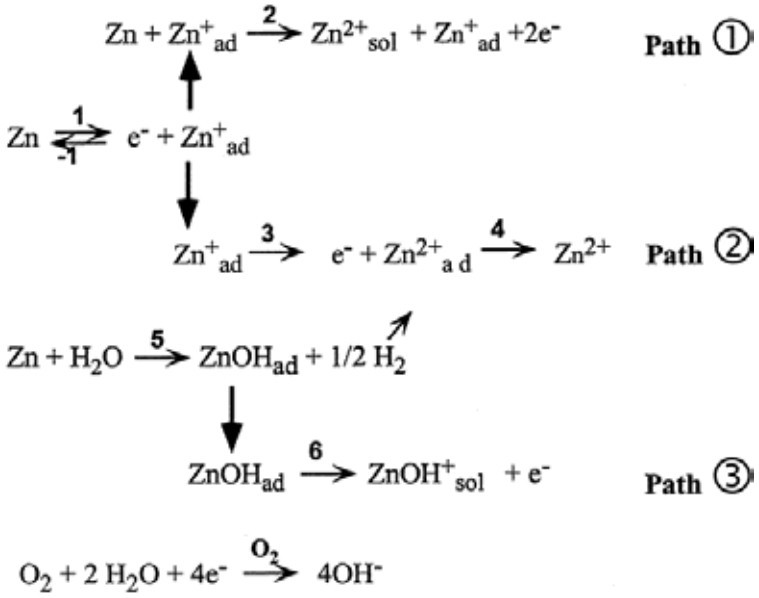

Fig 2.15 Reaction model accounting for Zn dissolution in naturally-aerated sulphate [89].

2.3.2.2 Hydrogen evolution

The hydrogen evolution reaction in acidic solution can be expressed by the following equation:

Equation 2.9 $2H^{+} + 2e^{-} \rightarrow H_2$

Whereas Equation 2.10 describes the reaction in neutral and alkaline solutions:

Equation 2.10 $2H_2O + 2e^{-} \rightarrow H_2 + 2OH^{-}$

The cathodic reaction current density (i) is dependent on the hydrogen overpotential (η), the exchange current density (i_o) and Tafel slope (b) through the Tafel equation:

Equation 2.11 $\eta = b \log i/i_o$, where $b = RT/\alpha F$

In most cases, the Tafel slope for hydrogen evolution on the Zn electrode is about 120 mV/decade. The exchange current density for hydrogen reduction on Zn is very low compared with that on other metals (e.g., Fe, Cu and Co). Thus, in neutral aerated solutions, hydrogen reduction is not the major cathodic process owing to its high overpotential on pure Zn, and the corrosion rate of Zn is normally controlled by the reduction of oxygen [2].

Impurities present in the Zn electrode may change the kinetics of hydrogen reduction [90-92]. In acid solutions, the presence of a trace amount of Pb in Zn results in a significant decrease in the rate of hydrogen evolution [92]. Lee [90] reported that Hg in Zn decreases the exchange current density for hydrogen reduction in alkaline solutions and reduces the Tafel slope. Mn and Cd were found to increase exchange current density significantly. Alloying with noble metals generally facilitates hydrogen evolution [2, 90].

2.3.2.3 Oxygen reduction

Oxygen reduction is, apart from hydrogen evolution, the most important cathodic reaction in metal corrosion processes. The electrode reaction for oxygen reduction in acid solution is [84]

Equation 2.12 $O_2 + 4H^+ + 4e^- \rightarrow 2H_2O$

And in neutral or alkaline solutions is

Equation 2.13 $O_2 + 2H_2O + 4e^- \rightarrow 4OH^-$

2.3.3 Pitting corrosion

Pitting corrosion is a form of localised attack that results in holes in a corroding metal. Pitting is a common form of corrosion of Zn in distilled water at room temperature,

as was reported as early as 1919 by Bengough and Hudson [93]. According to their observations, if Zn panels are placed vertically in distilled water, corrosion pits form, often arranged in straight rows of unconnected pits. According to Evans and Davies [94], the pits are the result of the gravitational sinking of solid corrosion products, which lodge at points where they shield the underlying Zn from oxygen, facilitating the anodic attack at those points. Pitting does not occur without oxygen. The local depletion of oxygen was found to be necessary for pitting corrosion.

The occurrence of pitting corrosion on Zn depends on the pH and solution composition. Lorking and Mayne [95] reported that solutions prepared from distilled water with addition of NaOH, at pH values from 5.8 to 11, could cause pitting on Zn. It was reported that the pitting rate increases with NaCl concentration [96] and the pit density generally increases with increasing halide ion concentration [93, 97, 98]. As reported recently by Assaf [99], the aggressivity of halide ions towards the stability of the passive film decreases in the order: $Cl^- > Br^- > I^-$ and the susceptibility of Zn to pitting corrosion is enhanced with increasing halide ion concentration and temperature, but decreases with the potential sweep rate. Pitting corrosion was also found in an SO_4^{2-} containing solution [100]. The numbers of pits and pit size greatly depend on the initial surface condition. In general, pitting corrosion of Zn is not likely to occur in acidic solutions and is most often found in slightly basic solutions.

Pitting corrosion of Zn was also found in atmospheric corrosion tests. In an ASTM atmospheric exposure programme, pits were observed on high-grade Zn and on a Zn - 1.0 wt % Cu alloy after two years of exposure in four different environments [101]. The corrosion of Zn in the presence of NaCl results in heavy pitting of the metal, which was found by Johansson in a laboratory study of the atmospheric corrosion of NaCl-treated Zn in air containing different concentrations of carbon dioxide [102, 103].

2.3.3.1 Mechanisms of pitting corrosion

The detailed processes of pitting corrosion are complicated. Whether pitting corrosion occurs depends on many factors. The physical imperfections on a metal surface (e.g. intermetallic particles) and chemical factors (e.g. O_2 and Cl^-) in the solution are the most important factors [2].

The theory of local acidification seems to be widely accepted for the pitting corrosion of Zn. To initiate and maintain an active pit, local acidification is considered to be necessary [94, 98, 104]. This local acidification is a result of metal dissolution:

Equation 2.14 $Zn \rightarrow Zn^{2+} + 2e^-$

Equation 2.15 $Zn^{2+} + H_2O \rightleftharpoons ZnOH^+ + H^+$

Equation 2.16 $ZnOH^+ + H_2O \rightleftharpoons Zn(OH)_2 + H^+$

According to this model, if the dissolution in a pit is not fast enough to maintain sufficient acidity to prevent repassivation, a new passive film will form and pitting corrosion can stop. The pitting potential is considered to be the minimum potential at which such acidification can be maintained [97].

2.3.4 Corrosion rate of Zn and Zn alloys in aqueous solutions

2.3.4.1 Effect of pH on the corrosion rate of pure Zn

The corrosion rate of Zn in distilled water as function of pH is shown in Fig 2.16. It indicates that the corrosion rate of Zn in water of pH 6-12 is relatively low. At pH values lower than 6 or higher than 12, the corrosion rate increases substantially. The low corrosion rate at pH values between 6 and 12 is primarily due to the formation of passive corrosion products on the surface of the Zn [105].

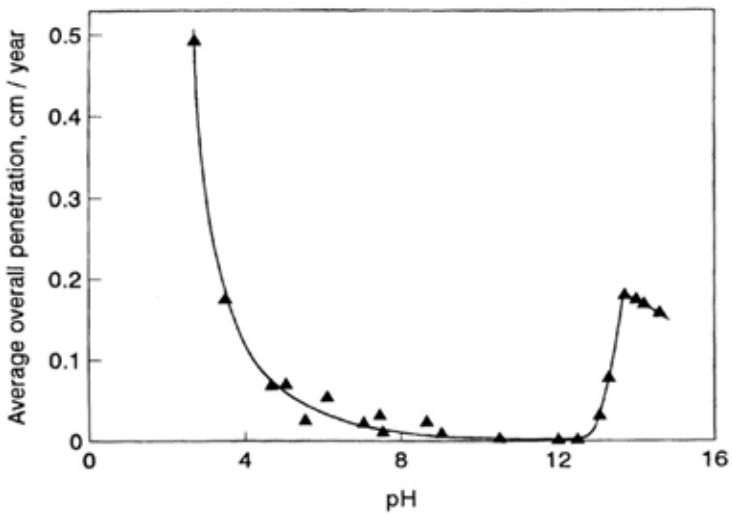

Fig 2.16 Corrosion rate of Zn in distilled water as a function of pH (addition of NaOH or HCl for pH adjustment) [105].

2.3.4.2 Corrosion rate of Zn alloys

The corrosion potential of a Zn alloy depends on both the equilibrium potential of Zn and that of the alloying element. Since Zn has a low position in the electrochemical series, alloying with most elements will result in a more positive corrosion potential. In general, addition of small amounts (a few percent) of other elements does not significantly alter the corrosion potential from that of pure Zn. The potential only becomes significantly different from that of pure Zn when a critical level of the alloying element is present. Compared with the corrosion potential, the corrosion currents of Zn alloys vary with the alloying element in a more complicated manner, as it is affected not only by the nature and quantity of the alloying element but also by the formation of intermetallic phases and the microstructure of the alloy.

Zn has been alloyed with many elements, such as Al, Mn, Fe, Ni, Ti and Cu. Fig 2.17 (from the work of Selvam and Guruviah [106]) shows the corrosion potentials and corrosion rates of Zn-Mn alloys in 3 % NaCl solution. The corrosion potentials of the alloys with Mn contents below 50 % are close to that of pure Zn, while the corrosion current is the lowest for alloys with Mn contents between 10 and 30 %.

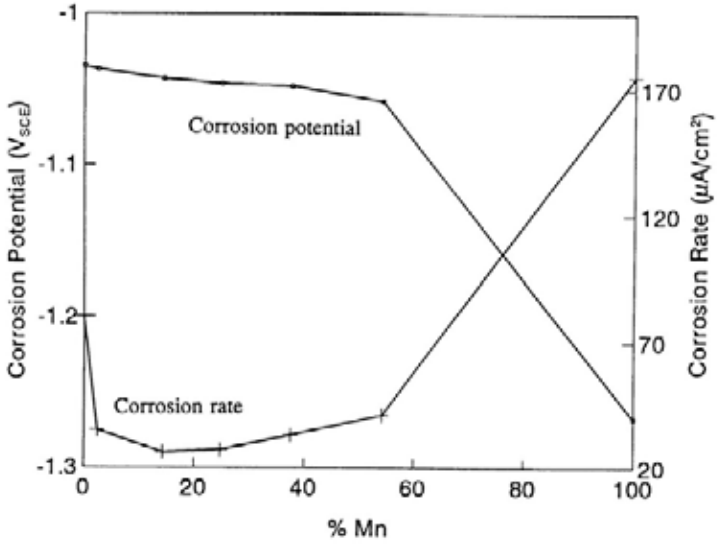

Fig 2.17 Corrosion potential and current of Zn-Mn alloys in 3 wt % NaCl as a function of Mn content [106].

For Zn-Cu alloys, Fig 2.18 shows that the corrosion potential is close to that of pure Zn when the Cu concentration is below 30% and is close to that of pure Cu when it is above 40% [107].

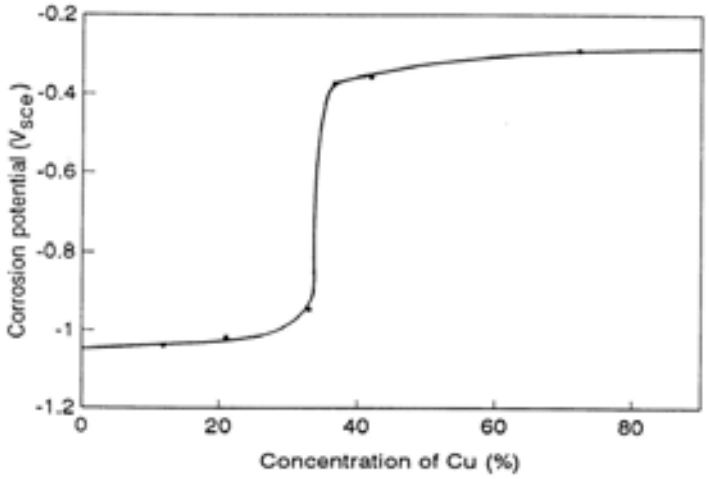

Fig 2.18 Potential of Zn-Cu alloys in air-saturated 3.5 wt % sodium chloride solution at 25°C as a function of Cu content [107].

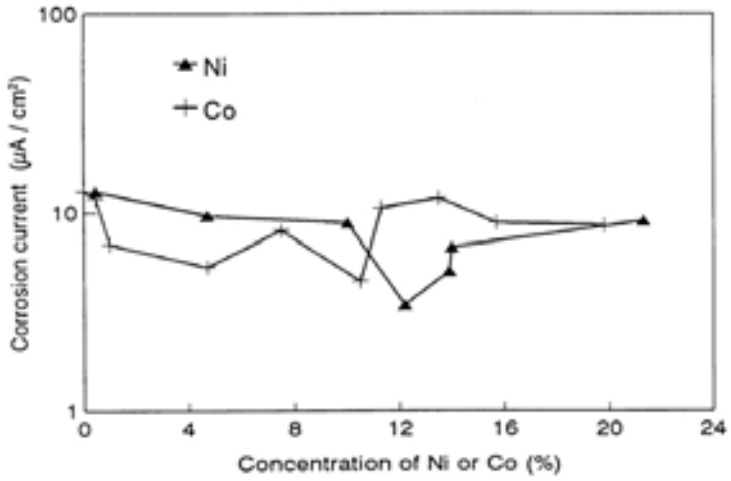

Fig 2.19 Effect of Ni and Co concentration on the average corrosion rate, between 20 and 40 days, of Zn alloy coatings in 5 wt % NaCl solution [108].

The corrosion current as a function of Co and Ni concentration is shown in Fig 2.19. According to Short *et al*. [108], the ennoblement of the potential with increasing Ni or Co content is associated with an increase in the anodic Tafel slope. They also found that for the electroplated Zn-Ni and Zn-Co alloy coatings more positive corrosion potentials are associated with lower corrosion currents. Similarly, Hosny *et al.* [9] found that the addition of 8g/l Co to Zn plating bath resulted in 25% reduction of corrosion current compared with pure Zn electroplated layer.

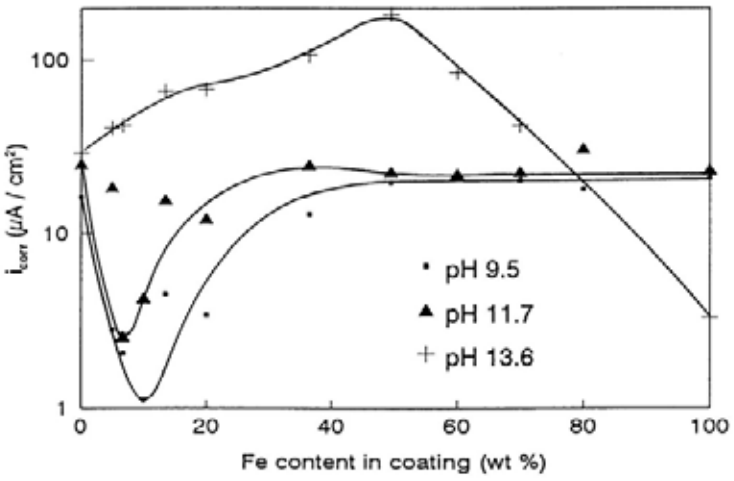

Fig 2.20 Relationship between corrosion density obtained from polarisation curves for Zn-Fe alloy coatings measured in alkaline 5 wt % NaCl solution and Fe content in the coating [109].

According to Sagiyama *et al.* [109], Zn-Fe alloys containing 4-27% Fe exhibit much lower corrosion currents than that of pure Zn and alloys containing more than 30 % Fe when tested in neutral 5% NaCl solution. The dependence of the corrosion current on Fe content is a function of the pH of the testing solution. At pH 9.5 and 11.7, the dependence of corrosion current on Fe content is similar to that observed in the neutral solutions as shown in Fig 2.20 [109]. The same figure shows that at pH 13.6, the corrosion current increases with Fe content up to about 50% Fe and then decreases with further increase in the Fe content. In another study, Chang and Wei [365] found that electrodeposited Zn-Fe alloys with 20-40% Fe have the lowest corrosion current in deaerated 0.1 M NaCl solution.

The corrosion of most Zn alloys is associated with a dezincification process, in which the Zn is preferentially dissolved. As a result of dezincification, the surface concentrations of the alloying elements increase. Thus, the corrosion potential and current tend to vary much more with time than in the case of pure Zn.

2.4 Corrosion of hot dip galvanised coatings

2.4.1 Protection of steel by Zn

Coating steel with Zn is one of the most common ways to prevent the steel from corroding in natural environments. The steel is protected by the Zn coating through a barrier effect and a galvanic effect, in which Zn acts as the sacrificial anode while steel acts as the cathode. The sacrificial properties of Zn can be seen in the galvanic series where the potential of Zn is less noble than steel in most environments at ambient temperatures.

In most atmospheric environments, Zn corrodes much less than steel, by a factor of 10 to 100 times [1, 2] due to the formation of a protective layer consisting of a mixture of Zn oxide, Zn hydroxide and various basic Zn salts depending on the nature of the environment. Thus the protection of steel by a Zn coating is mainly through the barrier effect. However, at the places where the Zn coating is damaged and the steel underneath is exposed, such as at cuts or at scratches, the galvanic action between steel and Zn can protect the exposed steel from corrosion.

2.4.2 Atmospheric corrosion

Atmospheric corrosion is the most prevalent type of corrosion of Zn, owing to extensive outdoor applications of galvanised steels. The corrosion behaviour of Zn depends greatly on environmental factors.

2.4.2.1 Film formation

Zn corrodes very slowly in clean dry air at room temperature with the formation of an oxide film. On a cleaved plane of a single crystal, an amorphous film is slowly produced; after a few weeks, it reaches a thickness of approximately 100 Å [110]. The oxide film prevents further oxidation of the metal. When in contact with condensed clean moisture in

the form of rain, mist, or dew, Zn corrodes with formation of Zn hydroxide according to the following reactions :

Anodic:

Equation 2.17 $Zn + 2H_2O \rightarrow Zn(OH)_2 + 2H^+ + 2e^-$

Cathodic:

Equation 2.18 $2H^+ + 2e^- \rightarrow H_2$ and/or

Equation 2.19 $O_2 + 2H_2O + 4e^- \rightarrow 4OH^-$

Over a certain period of time, ranging from a few days to a few weeks, this hydroxide layer then dehydrates to form oxide, or reacts with the carbon dioxide dissolved in the water to form the relatively less soluble Zn carbonate.

Equation 2.20 $Zn(OH)_2 \rightleftharpoons ZnO + H_2O$

or

Equation 2.21 $5Zn(OH)_2 + 2CO_2 \rightleftharpoons 2ZnCO_3 \cdot 3Zn(OH)_2 + H_2O$

or

Equation 2.22 $5ZnO + 2CO_2 + 3H_2O \rightleftharpoons 2ZnCO_3 \cdot 3Zn(OH)_2$

The formation of a carbonate film slows down the corrosion rate significantly. However, in aggressive environments, the corrosion rate increases significantly if Cl^- and SO_2 are present.

2.4.2.2 Effects of NaCl, CO_2 and SO_2

Although carbon dioxide is beneficial in forming the protective Zn carbonate film, the solubility of CO_2 in moisture may lower the pH to a range in which the carbonate is not stable and can be dissolved [111]. Falk [112] found that in the absence of NaCl, CO_2 enhances the corrosion rate slightly. This was considered to be due to the acidification of the surface electrolyte, giving rise to higher surface conductivity and an enhanced

dissolution of the surface film. In contrast, it was reported that in the presence of NaCl, the corrosion rate decreases considerably when CO_2 is added. To explain the slowing down of corrosion by CO_2, it was proposed [103] that CO_2 enhances the formation of simonkolleite, $Zn_5(OH)_8Cl_2 \cdot H_2O$. This results in a decreased conductivity as chloride is removed from the surface electrolyte. The results indicate that the corrosion products and the corrosion process as a whole are fundamentally influenced by CO_2 [102].

The presence of sodium chloride and sulphur dioxide in the atmosphere can cause a significant increase in the corrosion rate of Zn [2, 102]. It has been reported that the corrosion of Zn in the presence of NaCl results in heavy pitting of the metal in a laboratory study of atmospheric corrosion [102, 103].

The theory of the role of sulphur dioxide in the corrosion process of metals is commonly accepted as the one which involves the acidification of a film of moisture through hydration and oxidation of sulphur dioxide to sulphuric acid and the reduction of hydrogen ions in the moisture to promote the corrosion of Zn [111]:

2.4.2.3 Corrosion products

Corrosion products greatly affect the corrosion behaviour of the metal by producing a barrier between the metal and the environment. In various types of atmospheric environments, a sequence of formation of various Zn compounds in the corrosion products were found [113-115].

In a rural environment [113], Zn hydroxycarbonate, $Zn_5(CO_3)_2(OH)_6$, forms initially and transforms to $Zn_4SO_4(OH)_6 \cdot 4H_2O$ under sheltered conditions. In marine environments [114], the initial step consists of the formation of basic Zn carbonate, $Zn_5(CO_3)_2(OH)_6$, which is subsequently transformed into Zn hydroxychloride, $Zn_5(OH)_8Cl_2 \cdot H_2O$. Later, sodium zinc chorohydroxysulfate, $NaZn_4Cl(OH)_6SO_4 \cdot 6H_2O$, is formed. In urban and industrial environments [115], the initial step is the formation of $Zn_5(CO_3)_2(OH)_6$, followed by the formation of hydroxysulfate, $Zn_4SO_4(OH)_6 \cdot nH_2O$, and eventually by the formation of Zn chlorohydroxysulfate, $Zn_4Cl_2(OH)_4SO_4 \cdot 5H_2O$.

Generally, a corrosion product layer that is insulating, compact, adherent, and insoluble serves as a good barrier against a corroding environment. It has been found in several studies [116-118] that certain Zn compounds are more protective than others. Kawafuku *et al.* [118] considered that $ZnCl{\cdot}4Zn(OH)_2$ is a more compact corrosion product than ZnO because the c axis of the hexagonal close-packed structure of $ZnCl{\cdot}4Zn(OH)_2$ is parallel to the direction of the film growth. Others have suggested that the inhibitive effect of the corrosion products composed mainly of $ZnCl{\cdot}4Zn(OH)_2$ is probably due to a decrease of the oxygen reduction rate on $ZnCl{\cdot}4Zn(OH)_2$ [117]. However, it was suggested [119, 120] that simonkolleite $Zn_5(OH)_8Cl_2{\cdot}H_2O$ does not seem to be very protective for the Zn surface while $Zn_4SO_4(OH)_6{\cdot}nH_2O$ offer high protection. $NaZn_4Cl(OH)_6SO_4{\cdot}6H_2O$ was also found to have better protective properties against corrosion than $Zn_4Cl_2(OH)_4SO_4{\cdot}5H_2O$ [120].

There is very little systematic information about the corrosion products formed on Zn alloys. Satoh *et al.* [117] reported that the corrosion product formed on Zn-Ni alloys is more concentrated with $ZnCl{\cdot}4Zn(OH)_2$ than that formed on galvanised steel. In a study by Short *et al.* [108], the corrosion product of a Zn-Ni coating formed during an immersion test in 5 wt % NaCl was identified to be mainly $ZnCl{\cdot}4Zn(OH)_2$, and the coating after removal of the corrosion products was found to be rich in Ni.

2.4.3 Effects of alloying additions

Although Zn coatings have high corrosion resistance in non-aggressive atmospheric environments, corrosion problems for galvanised steel have been found in aggressive atmospheric environments where sodium chloride and sulphur dioxide are found [111]. With the increasing requirements of industry for a longer service life for hot dip galvanised surfaces, new types of Zn coatings need to be developed. It is suggested that it is possible to develop a better corrosion resistant galvanised steel by alloying [19].

Electrodeposition and hot dip galvanising are the two fundamental processes to produce Zn coatings. The addition of alloying elements to Zn coatings has been mainly

achieved by electrodeposition [8, 12, 121-123], where well established methods are commonly carried out. For hot dip galvanised coatings, the addition of alloying elements (e.g. Ni, V and Al) to the galvanising bath is mainly used to control the coating microstructure on reactive steels as reviewed in Section 2.2.4.3. Little work has been done towards the improvement of the corrosion resistance. The main reason for this lack of interest is probably related to the fundamental problems involved in producing Zn coatings with alloying elements that possess high melting points compared with Zn. Another reason is that most elements have very low solid solubility in both solid Zn and molten Zn, which gives rise to problems in making the alloying bath. Since the Zn alloyed coatings have to be made at higher temperatures, consumption of Zn by excessive dross formation and oxidation of molten Zn is rapid, which causes increased cost.

In the following sections, the effect of alloying additions on the corrosion behaviour of hot-dip galvanised coatings will be reviewed. It should be noted that the effect of alloying elements on the atmospheric corrosion performance of Zn coatings is complex. The data concerning the effects of these alloys are often contradictory.

2.4.3.1 Al

Al is probably the most successful alloying element used to improve the corrosion resistance of hot dip galvanised coatings. When present in small quantities, Al reduces the atmospheric corrosion resistance with a maximum effect at a concentration of 0.32 wt % [5] as shown in Fig 2.21. With the addition of more than 1 wt % Al as shown in Fig 2.22, the atmospheric corrosion resistance of Zn coatings increases with Al content up to 4-7 wt %, beyond which the corrosion resistance decreases with Al content to about 21 wt %; between 21 wt % and 70 wt % Al, corrosion resistance increases almost linearly with Al content [124].

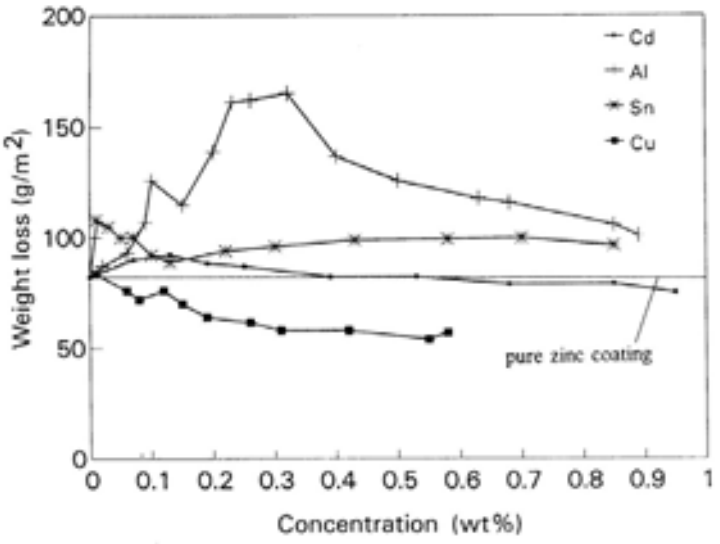

Fig 2.21 Coating loss in 2.25 years for galvanised steel produced in baths containing different amounts of various alloying elements [5].

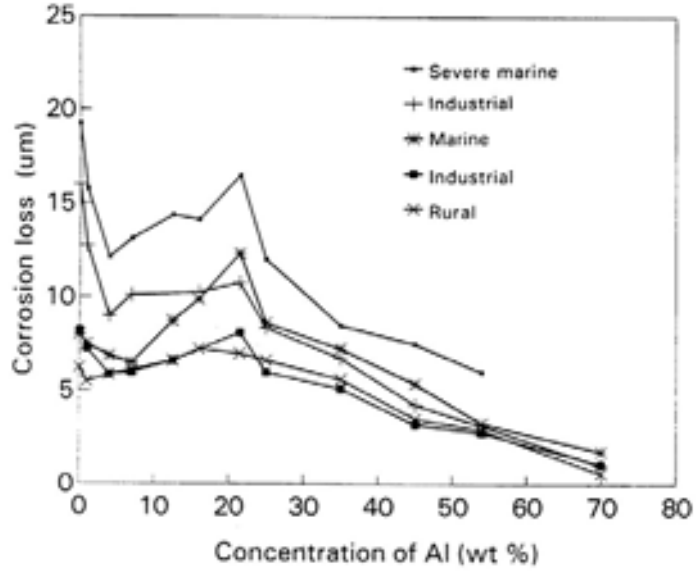

Fig 2.22 Effect of Al content on corrosion of Zn-Al alloy coatings after 5-year exposure in various atmospheric environments [124].

Two major commercial Zn-Al alloy coatings, Galfan (5 wt % Al) and Galvalume (55 wt Al %), have been developed for the production of more corrosion-resistant steel sheets. In non-marine (industrial) environments, the Galfan corrosion mechanism occurs by a two-step process: in the first step, a temporary protective Al oxide passive layer forms on the surface, followed by a step of dissolution of Zn in which a Zn sulphate layer forms on

top of the oxide layer [125]. The last step is much slower than the first step because of the necessity for diffusion through the oxide layer, which explains why Galfan coatings corrode slower than pure Zn galvanised coatings. It has also been shown that the Zn-rich eta phase in both the proeutectic and eutectic lamella microstructure corrodes preferentially [3]. After 10-year outdoor exposure tests, Zn-5 wt % Al alloy coated sheet steel had at least twice the corrosion resistance of galvanised steel sheet as shown in Fig 2.23.

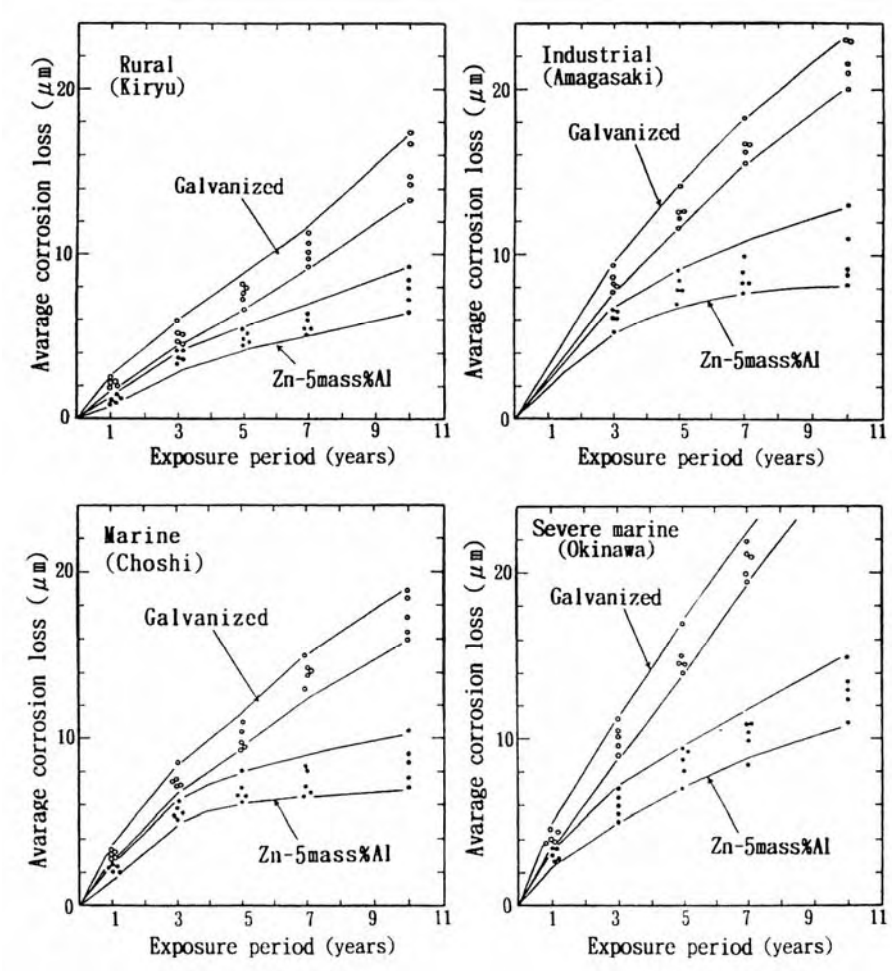

Fig 2.23 Corrosion loss of coating layer after atmospheric exposure test [3].

The improved protection afforded by Galvalume is due to its microstructure and corrosion mechanism. The microstructure of Galvalume is composed of large Al-rich dendrites with a Zn-rich phase filling the interdendritic spaces [126]. Initially, the Zn-rich interdendritic phase corrodes preferentially until the buildup of corrosion products prevents

further activity in this area. Such areas are small, so the initial corrosion rate is slower than conventional galvanised materials and Galfan. As the Zn-rich phase becomes depleted, corrosion protection is provided by the major Al-rich phase by means of oxide/hydroxide formation commonly associated with Al coatings.

2.4.3.2 Cu

The effect of Cu additions on the corrosion of Zn is contradictory. Some authors reported that Cu additions can increase the atmospheric corrosion resistance of hot dip galvanised coatings [4, 5], while others claimed that it decreases the corrosion resistance [101]. It was reported that addition of up to 0.82 wt % Cu increased the corrosion resistance by as much as 20 % in a two-year industrial exposure test [5]. Gilbert also found that a 2 wt % Cu alloy increased corrosion resistance by up to 20 % [4]. However, Dunbar and Showak [101] reported that adding 1 wt % Cu to rolled Zn sheet decreased the corrosion resistance in a severe marine environment. In salt spray tests, Gilbert [4] found that 2 wt % Cu decreased the corrosion resistance. This enhancement of the corrosion rate was attributed to the galvanic cell effect between Zn matrix and Cu-rich intermetallic phase which is always found to be an effective cathode site. Thus distinct pits were more likely to be developed during corrosion of Cu-containing Zn alloys [101].

2.4.3.3 Mg

Mg additions at 0.03 wt % have been claimed to give increased corrosion resistance [6, 7], but Townsend [127] found that 0.04 wt % Mg had no significant effect on the life of hot dip galvanised coatings in various atmospheric environments. The commercial use of Mg additions is only made in conjunction with other elements, notably Al.

2.4.3.4 Mn

Mn was found to increase corrosion resistance of Zn [11-13]. However, the mechanism is not completely understood. The effect of additions of Mn on the corrosion resistance of Zn has not been studied extensively. Boshkov *et al.* [12] reported that an 11 wt % Zn-Mn alloy produced by electrodeposition shows increased corrosion resistance and protective ability. The high corrosion resistance is due to the rapid formation of $Zn_5(OH)_8Cl_2 \cdot H_2O$ (ZHC) on the Zn-Mn alloy. Boshkov proposed that dissolution of Mn causes a slight increase of the pH of the medium up to a value which favours the formation of ZHC. ZHC appears also on pure Zn. But ZHC appears more slowly on the pure Zn coating compared to Zn–Mn alloys. By using ion beam assisted deposition (IBAD), Munz [13] made several Zn/Mn multilayer coatings and found that Zn-Mn coatings show high corrosion resistance under salt spray tests. Munz suggested that the improvement noted with alloy coatings is attributed to the passive nature of Mn alloying additions. In the case of Zn–Mn, γ-Mn_2O_3 is reported to be beneficial as it suppresses oxygen reduction at the cathode, slowing the corrosion process [13]. The use of Mn additions to hot dip galvanising was reported recently, but only up to 1 wt % Mn were successfully added to molten Zn [11]. The results obtained from potentiodynamic polarisation curves showed that 0.5 wt % Mn can slightly increase the corrosion resistance. The corrosion resistance of Zn-Mn coatings is attributed to a mixture of Mn oxides formed on the surface when the galvanised steel was withdrawn from the galvanising bath [14].

2.4.3.5 Pb

Anderson [128] reported that Pb was not harmful to alloy layer formation and no significant differences in corrosion rates were found among different grades of Zn with Pb concentrations of 0.0055, 0.049 and 0.82 wt % after 20 years of atmospheric exposure. However, Sere [129] reported that an increase in the Pb content produced a crystallographic preferential orientation with the pyramidal family of planes parallel to the coating surface,

which deteriorates not only the surface appearance but also the corrosion resistance of the galvanised steel sheets.

2.4.3.6 Ni

The addition of a small amount of Ni (about 0.05 wt %) to the galvanising bath is mainly used to control the coating microstructure on reactive steels. Little work has been done concerning its effect on the corrosion resistance of hot dip galvanised coatings. High levels of Ni addition to Zn have been successfully achieved by electrodeposition [8, 121, 122] and pulse-plating [130]. It was reported that 12 wt % Ni in Zn increases the corrosion resistance of Zn coating in a humid tropical climate and accelerated chloride and sulphur dioxide cabinet tests [8]. In another study, Alfantazi *et al.* [130] claimed that the corrosion resistance of pulse-plated Zn-Ni (up to 62 wt %) alloy coatings was superior to that of the pure Zn by potentiodynamic polarisation and the neutral salt-spray tests. However, in alkaline solutions, Short *et al.* [121] found that Zn-Ni electrogalvanised coatings had poor corrosion resistance which was attributed to microcracking of the coatings in this solution.

2.4.3.7 Sb

In the literature, the beneficial effect of Sb addition on the improvement of corrosion resistance of hot dip galvanised coating was reported [17, 18]. Rädeker [17] reported that Sb reduced weight loss over 3 years in an industrial atmosphere by 20 %.

2.4.3.8 Co

Co addition was also mainly used in electrodeposition. It was reported that Co up to 1.0 wt % can increase corrosion resistance of electrogalvanised coating [10].

2.4.3.9 Other additions

A 15-year urban atmospheric exposure showed that addition of 0.08 wt % V slightly increases the corrosion resistance of galvanised coatings [15]. Cd was also found to slightly increase the corrosion resistance [16]. Sn has no significant effect. However, Sn induces intergranular corrosion in Zn-Al alloys. The concentration of Sn must be maintained below 0.002 wt %.

2.5 Summary

Although the data concerning the effects of alloying elements are often contradictory, additions of Al, Cu, Mg, Ni, Co, Mn, V, Cd and Sb etc have been found to increase corrosion resistance of Zn coatings. Unfortunately, most of them were successfully added to Zn either by electrodeposition (e.g. Ni and Co) or a more complicated method. The main reason for this is probably related to the fundamental problems involved in producing Zn coatings with alloying elements that possess high melting points compared to Zn. Another reason is that most elements have very low solid solubility in both solid Zn and molten Zn, which gives rise to problems in making the alloying bath.

Nevertheless, Al, Mn, Cu and Sb have been shown to have some beneficial effect on the corrosion resistance of hot dip galvanised coatings. Due to the complicated surface treatment of steels before galvanising when the Al content is higher than 0.01 wt %, Al additions higher than 0.01 wt % are not considered in this study. Thus Mn, Cu and Sb are chosen in this work. Furthermore, Zr is possibly a beneficial element which can inhibit the alloy layer growth. Meanwhile, the combinations of these alloying elements were also considered.

In the present work, the effects of Mn, Cu, Sb and Zr on microstructure and corrosion resistance of hot dip galvanised coating will be investigated. The mechanisms whereby these alloying elements improve the corrosion resistance of hot dip galvanised alloy coatings will be discussed with an aim to developing more corrosion-resistant alloys for hot dip galvanising.

CHAPTER 3 EXPERIMENTAL METHOD

3.1 Materials

3.1.1 General

Hot dip galvanising is a process by which an adherent coating is produced on the surface of steel products by immersing them in a bath of molten Zn. Due to the nature of the process of hot dip galvanising, the amounts of alloying additions added to the bath are limited according to equilibrium phase diagrams. The alloying additions used in this study were carefully selected based on the literature and equilibrium phase diagrams. Both Zn alloys and hot dip galvanised coatings were investigated after successfully melting the selected alloying additions.

3.1.2 Zn bath compositions

All Zn alloy baths were produced based on commercially pure Zn (Z-CP). Its chemical composition is shown in Table 3.1. Small additions of Cu, Sb, Zr and Mn were selected as alloying elements. The amounts of additions were carefully chosen with their details shown in Table 3.2. The bath chemical compositions were measured by inductively coupled plasma (ICP). All these additions were successfully melted in the galvanising bath. In order to reduce the rate of oxidation of molten Zn, lower Al additions (about 0.005 % Al) were added to the galvanising bath. Some baths without 0.005 % Al were also produced as comparisons. Another commercial Zn alloy (Z-Pb) with Pb as the impurity was also used in this study as a comparison, its composition shown in Table 3.1.

Table 3.1 Chemical composition of commercially pure Zn (Z-CP) and (Z-Pb) (wt %)

	Pb	Cu	Fe	Sn	Ni	Cd
Z-CP	0.03	-	<0.01	<0.01	-	-
Z-Pb	0.96	0.04	0.02	0.17	0.05	0.01

Table 3.2 Chemical composition of Zn baths with alloying additions (wt %)

Addition in bath (aim to make)	Composition				
	Cu	Zr	Sb	Mn	Al
0.2%Cu	0.16	-	-	-	-
0.2%Cu	0.21	-	-	-	0.005
0.8%Cu	0.84	-	-	-	-
0.8%Cu	0.77	-	-	-	0.005
0.2%Zr[a]	-	0.2	-	-	-
0.3%Sb	-	-	0.34	-	0.005
1.0%Sb[a]	-	-	1.0	-	-
0.4%Mn	-	-	-	0.41	0.005
0.8%Mn	-	-	-	0.68	0.005
0.2%Cu-0.8%Mn	0.26	-	-	0.70	0.005
0.8%Cu-0.8%Mn	0.81	-	-	0.66	0.005

[a] nominal value

3.1.3 Zn and Zn alloys

All Zn and Zn alloys were made directly from the molten Zn baths (see Section 3.1.1) at 450^{o}C. Water-quenched (wq) and air-cooled (air) Zn alloy slugs were made after removal from the molten bath. The defined names and chemical compositions of these Zn alloys measured by inductively coupled plasma (ICP) are shown in Table 3.3.

Table 3.3 Zn alloys and their chemical compositions (wt %) by inductively coupled plasma (ICP)

Definition of Zn alloys	Cu	Mn	Zr	Sb	Pb	Al	Cooling method
Z-0.2Cu-wq	0.16	-	-	-	-	-	water quench
Z-0.2Cu-Al-air	0.21	-	-	-	-	0.005	air cool
Z-0.2Cu-Al-wq	0.21	-	-	-	-	0.005	water quench
Z-0.8Cu-wq	0.84	-	-	-	-	-	water quench
Z-0.8Cu-Al-air	0.77	-	-	-	-	0.005	air cool
Z-0.8Cu-Al-wq	0.77	-	-	-	-	0.005	water quench
Z-0.4Mn-wq	0.41	-	-	-	-	-	air cool
Z-0.4Mn-Al-air	0.41	-	-	-	-	0.005	air cool
Z-0.4Mn-Al-wq	0.41	-	-	-	-	0.005	water quench
Z-0.8Mn-Al-air		0.68	-	-	-	0.005	air cool
Z-0.8Mn-Al-wq		0.68	-	-	-	0.005	water quench
Z-0.8Mn-0.2Cu-Al-wq	0.26	0.70	-	-	-	0.005	water quench
Z-0.8Mn-0.2Cu-Al-air	0.26	0.70	-	-	-	0.005	air cool
Z-0.8Mn-0.8Cu-Al-wq	0.81	0.66	-	-	-	0.005	water quench
Z-0.8Mn-0.8Cu-Al-air	0.81	0.66	-	-	-	0.005	air cool
Z-Sb-wq[a]	-	-	-	1.0	-	-	water quench
Z-CP-wq	-	-	-	-	0.03	-	water quench
Z-CP-Al-wq	-	-	-	-	0.03	0.005	water quench
Z-CP-Al-air	-	-	-	-	0.03	0.005	air cool
Z-Pb-wq	-	-	-	-	0.96	0.005	water quench
Z-Pb-Al-wq	-	-	-	-	0.96	0.005	water quench
Z-Pb-Al-air	-	-	-	-	0.96	0.005	air cool

[a] nominal value

3.1.4 Hot dip galvanised coatings

3.1.4.1 Steel types

It has been reported that more than 0.07 wt % Si in steel significantly increased the thickness of hot dip galvanised coatings [50-52, 54-58]. To study the effect of alloying elements on the thickness of hot dip galvanised coatings, two types of steels with 0.02 wt % and 0.2 wt % Si content were used. The steel with 0.02 wt % Si is characterised

as “hypo-Sandelin” steel and the steel with 0.2 wt % Si is characterised as “hyper-Sandelin” steel. The chemical compositions are given in Table 3.4. Because the roughness of the as received “hyper-Sandelin” steel is high, to reduce its effect on the coating thickness, the steel surfaces were polished to 800 grit with SiC paper before galvanising.

Both hot dip galvanised coatings made on two steel substrates were used for corrosion measurements.

Table 3.4 Chemical composition of steel substrates

	C	Si	S	P	Mn	Ni	Cr	Mo
Hyper-Sandelin	0.15	0.19	0.013	0.009	0.62	0.03	0.01	<0.01
Hypo-Sandelin	0.18	0.02	0.011	0.009	0.65	0.02	0.01	<0.01

3.1.4.2 Pre-treatment procedures

Table 3.5 Procedure for preparation of galvanised samples

1. Pickling	Immersion in a standard solution of by volume 50% tap water and 50% commercial hydrochloric acid (36%) with an addition of 30 g/l iron sulphate
2. Rinsing	in cold tap water for 1 minute
3. Fluxing	Flux for 5 minutes in solution saturated with Zn ammonium chloride double salt ($ZnCl_2$•$2NH_4Cl$)
4. Drying	Dry using warm blown air
5. Galvanising	The small scale tests were done in a 1 kg Zn bath: sample size 3 × 6 cm. The large scale tests were done in a 5 kg Zn bath: sample size 7.5 × 10 cm.

Before galvanising, the steel substrates were thoroughly cleaned. The pre-treatment procedure is described in Table 3.5.

3.1.4.3 Galvanising

Galvanising was carried out in Zn baths of 1 kg and 5 kg in an electrically heated crucible furnace. Most of the galvanised samples were made at 450°C for 90 s. To study the

kinetics of galvanised alloy layer growth, the steel samples were dipped for 5, 10, 30, 90, 300 and 900 s. The samples were withdrawn manually at a speed of about 3 cm/s.

The defined names and chemical compositions of the hot dip galvanised coatings measured by inductively coupled plasma (ICP) are shown in Table 3.6.

Table 3.6 Definition of hot dip galvanised coatings and the relative bath composition (wt %) determined by inductively coupled plasma (ICP)

Definition of coatings	Cu	Mn	Zr	Sb	Pb	Al	Cooling method
G-0.2Cu-wq	0.16	-	-	-	-	-	water quench
G-0.2Cu-Al-air	0.21	-	-	-	-	0.005	air cool
G-0.2Cu-Al-wq	0.21	-	-	-	-	0.005	water quench
G-0.8Cu-wq	0.84	-	-	-	-	-	water quench
G-0.8Cu-Al-air	0.77	-	-	-	-	0.005	air cool
G-0.8Cu-Al-wq	0.77	-	-	-	-	0.005	water quench
G-0.4Mn-wq	0.41	-	-	-	-	-	Water quench
G-0.4Mn-Al-air	0.41	-	-	-	-	0.005	air cool
G-0.4Mn-Al-wq	0.41	-	-	-	-	0.005	water quench
G-0.8Mn-Al-air		0.68	-	-	-	0.005	air cool
G-0.8Mn-Al-wq		0.68	-	-	-	0.005	water quench
G-0.8Mn-0.2Cu-Al-wq	0.26	0.70	-	-	-	0.005	water quench
G-0.8Mn-0.2Cu-Al-air	0.26	0.70	-	-	-	0.005	air cool
G-0.8Mn-0.8Cu-Al-wq	0.81	0.66	-	-	-	0.005	water quench
G-0.8Mn-0.8Cu-Al-air	0.81	0.66	-	-	-	0.005	air cool
G-1.0Sb-wq[a]	-	-	-	1.0	-	-	water quench
G-0.3Sb-Al-wq	-	-	-	0.34	-	0.005	water quench
G-0.3Sb-Al-air	-	-	-	0.34	-	0.005	air cool
G-CP-wq	-	-	-	-	0.03	-	water quench
G-CP-Al-wq	-	-	-	-	0.03	0.005	water quench
G-CP-Al-air	-	-	-	-	0.03	0.005	air cool
G-Pb-wq	-	-	-	-	0.96	0.005	water quench
G-Pb-Al-wq	-	-	-	-	0.96	0.005	water quench
G-Pb-Al-air	-	-	-	-	0.96	0.005	air cool

[a] nominal value

3.2 Sample preparation

3.2.1 Zn alloys

All Zn alloys were mounted in contact with a conductive wire in epoxy resin with an exposed area of about 1 cm^2. For corrosion tests, the samples were ground to 1200 or 4000 grit with SiC paper, cleaned with deionised water and ethanol, and dried with warm air. The samples were then used immediately for corrosion measurements, especially for polarisation tests. In some cases, the samples were also polished to 1 μm before corrosion tests. For microstructural examination, all samples were polished down to 1 μm with diamond paste. Then the samples were etched either in 2% Nital (20 ml 70% HNO_3 + 980 ml ethanol) or in a second etchant (40 g CrO_3 + 1.5 g Na_2SO_4 + 200 ml H_2O for 5 s followed immediately by a rinse in 3 g Na_2SO_4 + 200 ml H_2O), especially for Cu-containing alloys.

3.2.2 Hot dip galvanised coatings

Hot dip galvanised coatings were used as received without any surface treatment. Before corrosion measurements, the samples were cleaned with deionised water and ethanol. If a beaker cell (Section 3.3.1.1) was used, a lacquer was applied to each sample to give an exposed area of about 1 cm^2. For the microelectrochemical cell (Section 3.3.1.2), no lacquer was applied to samples.

To investigate the microstructure of coatings, the samples were cut carefully and mounted in conductive bakelite. The cross section of these samples were ground with SiC paper and polished to 1 μm diamond paste with a Struers polisher. The samples were then etched in 2% Nital, thoroughly rinsed with deionised water, dried with warm air and stored in a desiccator.

3.3 Electrochemical tests

The electrochemical cell used was usually a three-electrode cell, containing the working electrode, the reference electrode and the counter electrode. There were three types of reference electrodes used in different types of experimental setups. The saturated calomel electrode (SCE) was used in cells containing chloride ions. The second type of electrode, a saturated mercury/mercurous sulphate electrode (MSE) was used in chloride-free electrolytes. For comparison purposes, the potential scale was referred to against the SCE (by adding a value of 0.4 V). The third electrode type was a small Ag/AgCl electrode (3M NaCl, -35 mV with respect to SCE at 25°C), and was used in the microelectrochemical cell (3.3.1.2). The quoted potential-scale was either SCE or Ag/AgCl. The counter electrode was a pure platinum mesh or a coil of pure platinum wire. The electrode was cleaned prior to the experiment by being dipped in concentrated HNO_3 and flamed.

Electrochemical experiments were performed on Solartron corrosion measurement systems (model no.1285 and 1280) or ACM potentiostats. All experiments were conducted at room temperature (20 ± 2°C).

Most of the electrochemical experiments were repeated at least three times unless good reproducibilities were achieved.

3.3.1 Electrochemical Cells

3.3.1.1 Beaker Cell

The working electrode, the reference electrode and the counter electrode were arranged in corrosive electrolytes with a beaker as the container. Most potentiodynamic polarisations and linear polarisations were performed in the so called beaker cells on both Zn alloys and hot dip galvanised coatings. In most cases, the volume of the corrosive electrolytes was about 250 ml.

3.3.1.2 Microelectrochemical Cell

The microelectrochemical cell makes contact between the sample and the electrolyte at the tip of a pipette mounted on a cell containing the platinum counter electrode and a small Ag/AgCl reference electrode as shown in Fig 3.1. The plastic pipette has a tip diameter about 1 mm. The position of the electrolyte can be controlled with a syringe. The sample's x, y and z location relative to the droplet can be adjusted using the stage of the microscope. The cell was attached to the lens holder of an optical microscope; electrochemical measurements can be easily repeated on a fresh area by moving the sample on the microscope stage.

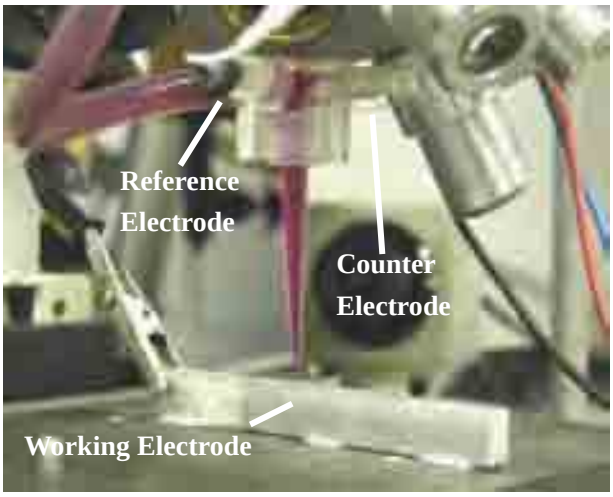

Fig 3.1 Microelectrochemical cell

The use of the microelectrochemical cell allows multiple measurements on one sample and the sample does not need to be lacquered. The microelectrochemical cell was used only on hot dip galvanised coatings.

3.3.2 Electrolytes

All electrolytes were prepared with analytical grade chemicals and deionised water purified with a water purification system (Millipore). Several electrolytes were used in this study, with compositions as shown in Table 3.7.

Electrolytes A, B and C are aggressive corrosion testing media. They were mainly used for potentiodynamic polarisation measurements. Electrolyte D and E were used to simulate a marine atmosphere environment. Cyclic tests and linear polarisation were carried out in these electrolytes for both Zn alloys and hot dip galvanised coatings. Similar 'accelerated' electrolytes were reported to successfully simulate marine atmosphere environments for Zn [120].

Table 3.7 Chemical composition of corrosion electrolytes

	NaCl	Na_2SO_4	$NaHCO_3$	pH	Used as
A	0.01 M	-	-	6.0	Standard testing solution
B	0.1 M	-	-	6.0	Standard testing solution
C	-	0.1 M	-	5.8	Standard testing solution
D	0.1 M	0.1 M	0.01 M	8.4	Accelerated solution
E	0.01 M	0.01 M	0.001 M	8.4	Accelerated solution

3.3.3 Potentiodynamic polarisation

After polishing, samples were quickly transferred to the test solution and a polarisation scan was carried out immediately either in the anodic or cathodic direction at a rate of 1 mV s^{-1} from OCP. All tests were repeated to check reproducibility. Cyclic polarisation measurements were performed by sweeping the voltage from open circuit in an anodic direction with a sweep rate of 1 mV s^{-1} and reversing the sweep at an anodic current density of 500 μA cm^{-2}.

3.3.4 Linear polarisation resistance

The linear polarisation resistance (LPR) technique has been widely used in industrial monitoring because of its ability to respond instantaneously to a corrosion situation or change in corrosion rate. It is based on the linear relationship that exists between applied potential and anodic and cathodic current densities, provided the applied potentials are small. Furthermore, it has the advantage that the small changes in potential required in the determination do not disturb the system significantly. The technique was

originally developed based on Stern–Geary theory where the corrosion current density, i_{corr}, is given by

Equation 3.1 $$i_{corr} = \frac{\beta_a \beta_c}{2.3(\beta_a + \beta_c)} \frac{1}{R_p} = \frac{B}{R_p}$$

Where β_a, β_c are Tafel constants, B is the Stern–Geary constant, and R_p is the polarisation resistance. The constant B can be determined from the anodic and cathodic polarisation curves.

In this study, the instantaneous R_p was measured by using a continuous LPR technique which can be carried out using Corrware electrochemical measurement software. At each setting, the polarisation resistance was measured by scanning at a rate of 1 mV s^{-1} over ± 5 mV against the open-circuit potential (OCP). During the intervals in between measurements, the OCP was measured against time (approximately 1h) until the next LPR scan was carried out.

3.3.5 Cyclic test

The cyclic test is an accelerated corrosion testing method that has been developed recently to simulate atmospheric corrosion of Zn and hot dip galvanised coatings. In this study, the cyclic wet-dry conditions were achieved by exposing the samples to an alternate condition of 1 h immersion in the accelerated solution and 23 h (or 3 h)-drying in air. During the 1 h immersion in solution, the LPR was recorded every 30 minutes. After being taken out, the samples were hung in air without any attempt to dry the solution that remained on the surfaces. Only the accelerated solutions D and E were used for cyclic tests.

3.4 Atmospheric corrosion tests

Atmospheric corrosion tests were carried out in Lyme Regis (light marine atmosphere) and Birmingham (industrial atmosphere) in the UK.

3.4.1 Marine atmosphere (light)

Before atmospheric corrosion tests, the samples were cleaned with deionised water and ethanol. Lacquers were applied to each sample with only one side exposed. The exposed area was about 8 cm^2 for small samples and 40 cm^2 for large samples. The specimens were exposed at 30^o to the horizontal on a wooden frame facing the sea in Lyme Regis (light marine atmosphere) as shown in Fig 3.2. All samples were exposed for 4 months from Feb 2004 to June 2004. The surface morphologies of the coatings were taken before and after atmospheric corrosion testing.

Fig 3.2 (a) Marine atmospheric (light) corrosion test site at Lyme Regis, and (b) Hot dip galvanised coatings on a wooden frame exposed facing the sea in a garden.

3.4.2 Industrial atmosphere

The specimens were exposed at 30^o to the horizontal on a wooden frame on the roof in Birmingham (industrial atmosphere) as shown in Fig 3.3. All samples were exposed for 4 months from March 2004 to July 2004. The surface morphologies of the coatings were evaluated before and after atmospheric corrosion test.

Fig 3.3 (a) Industrial atmospheric corrosion test site at Birmingham, and (b) Hot dip galvanised coatings on a wooden frame exposed on the roof.

3.4.3 Weight loss measurements

Before atmospheric corrosion tests, the samples were cleaned with deionized water and ethanol. The coatings were weighed before lacquers were applied to each sample with only one side exposed. After atmosphere test, the lacquers were removed first. Weight loss of coatings without lacquers was determined gravimetrically with the accuracy of $\pm$ 0.02 mg/cm^2 after the removal of corrosion products in saturated ammonium acetate solution for up to 10 minutes.

3.5 Characterisation of the surfaces

3.5.1 Optical Microscopy

An optical microscope connected to a computer with KS 300 3.0 software (Imaging Associates) was used to examine the sample before and after corrosion tests. In-situ observations while monitoring the electrochemical behaviour during potentio-dynamic polarisation were also performed.

3.5.2 Scanning electron microscope (SEM)

The microstructure and surface morphology of etched, polished and corroded surfaces were characterised using scanning electron microscopy (JEOL 6300, Philip XL 30 or FEG ESEM). Elemental composition was analysed using energy dispersive X-ray analysis (EDX) attached to the scanning electron microscope. EDX mapping and line scans were used to determine microstructure, pit initiation sites and distribution of particles in both Zn alloys and hot dip galvanised coatings.

3.5.3 Digital Imaging

Imaging of samples of larger dimensions was performed with a Nikon digital camera and a microscope using a CCTV camera and magnification lens (0.25 ×, 0.5 × and 2 ×) connected to computer with AxioVision 3.0 software (Imaging Associates) to take digital images.

3.5.4 XPS and AES

Both X-ray photoelectron spectroscopy (XPS) and Auger electron spectroscopy (AES) were performed by a VG Escalab II surface analysis facility. MgK_{α} excitation was used for XPS analysis with 0.5 and 0.1 eV step size for survey and high resolution spectra, respectively. AES was obtained with a 5 keV electron beam with 0.2 μA current incident at 60^{o}C normal to the surface in the N(E) mode. Cleaning of the surface for the measurements and depth profile was achieved with Ar^{+} sputtering with a beam energy of 4 keV.

CHAPTER 4 MICROSTRUCTURE AND CORROSION OF ZINC ALLOYS

In this chapter, the microstructure and corrosion of Zn alloys with additions of Cu, Sb, Zr and Mn are investigated. The effect of these additions on pitting corrosion, anodic activity and cathodic reduction reactions of Zn alloys were mainly investigated with the aim of identifying the beneficial alloying elements for improving the corrosion resistance of Zn.

Most Zn alloys used in this study were made by water quenching from molten Zn baths. However, for comparison with the hot dip galvanising process, Zn alloys containing 0.005 wt % Al were also made from molten Zn baths by air cooling, especially for the Zn alloys containing Mn additions. Low levels of Al (0.005 wt %) are used in galvanising baths to reduce the rapid rate of oxidation of molten Zn.

4.1 Microstructure of Zn alloys

4.1.1 Commercially-pure Zn

Two commercially pure zincs, namely Z-CP (99.95 wt %) and Z-Pb (98.75 wt %), were used in this study. Their chemical compositions were given in Table 3.1 (see Section 3.1.2). Fig 4.1 shows the typical microstructure of commercially-pure Zn (Z-CP). No coarse intermetallic particles were found on the etched surface. However, very small Pb globules (< 1 μm) were occasionally found in some samples as shown by the arrow A in Fig 4.1 (b). Water-quenched and air-cooled alloys show a similar microstructure except that the air-cooled alloy has a larger grain size (~15 μm) than that of water-quenched alloys (~5 μm).

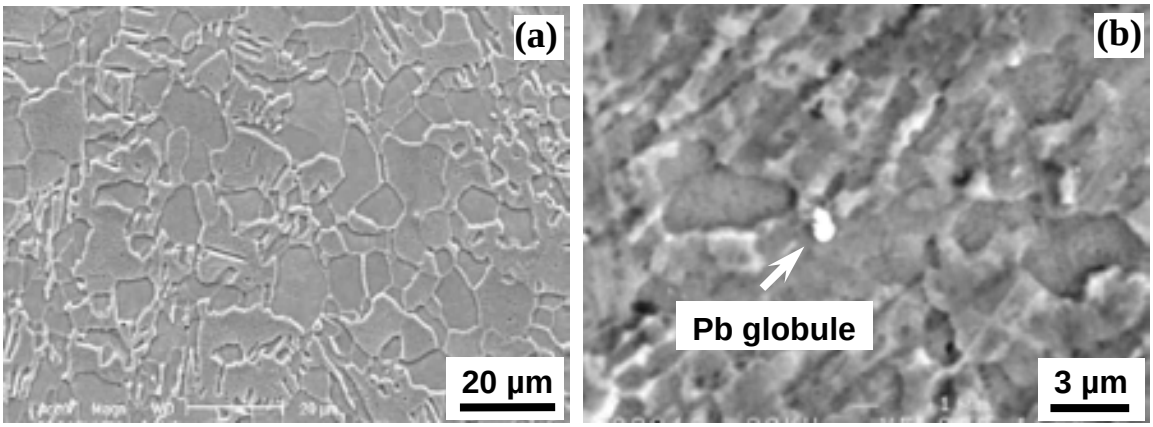

Fig 4.1 SEM images of etched commercially-pure Zn (a) Z-CP-air, and (b) Z-CP-wq.

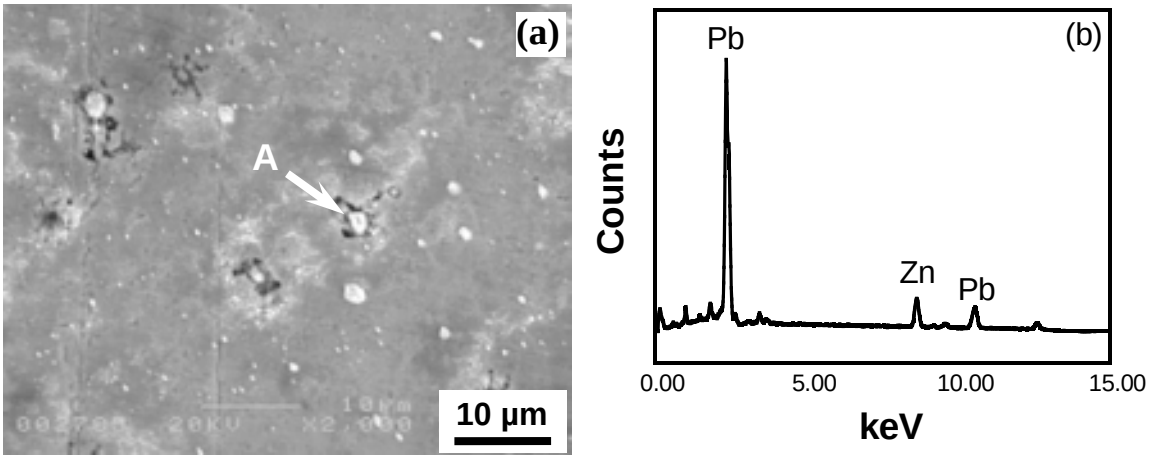

Fig 4.2 (a) SEM image of etched Z-Pb-wq, and (b) EDX spectrum of Pb globule as shown by arrow A in (a).

Fig 4.2 (a) shows the microstructure of the commercially-pure Zn (Z-Pb) which contains about 1 wt % Pb. There are significant numbers of particles present. EDX analysis indicated that the particles are Pb globules (Fig 4.2 (b)). No detectable Pb was found in the matrix by SEM/EDX. This result is consistent with the literature [20] that Pb globules are frequently found in Pb-containing commercially-pure Zn alloys.

4.1.2 Sb additions

The typical microstructure of Zn alloys with 1 wt % Sb is shown in Fig 4.3. Similar to Z-Pb, there were significant intermetallic particles present. EDX analysis (Fig 4.3 (b)) of larger particles indicated that they were Sb-rich intermetallic particles

which were mainly precipitated on grain boundaries. There are several intermetallic phases of Sb and Zn in a binary phase diagram of the Sb-Zn system [24]. The Sb-rich particles found in this study are probably Sb_2Zn_3 according to Chang [38], who found that Sb-rich intermetallic particles formed in the eta layer of a hot dip galvanised coating with Sb additions revealed Sb_2Zn_3 electron diffraction patterns. No detectable Sb was found in the matrix by SEM/EDX, this is not surprising because the solubility of Sb in Zn is extremely low at room temperature [24].

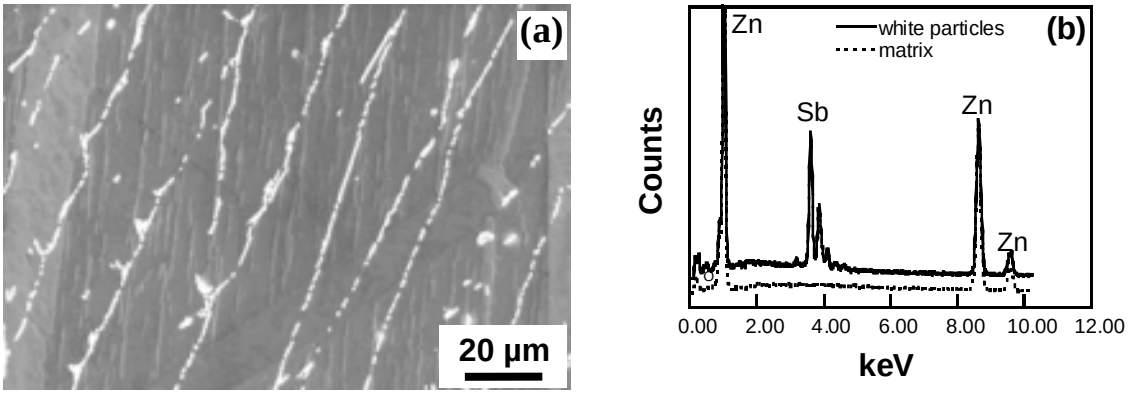

Fig 4.3 (a) SEM image of Z-Sb-wq, and (b) EDX spectrum of Sb-rich phases visible as white particles in (a).

4.1.3 Cu additions

Two levels of Cu additions, 0.2 wt % Cu and 0.8 wt % Cu, were used in this study. Cu has a relatively higher solid solubility in Zn than that of other alloying additions over a range of temperatures. For example, the solubility of Cu in Zn is 0.3 wt % at 100^{o}C and 2.5 wt % at 400^{o}C, respectively [24]. Thus it is possible to dissolve 0.8 wt % Cu in a molten Zn bath. Fig 4.4 shows the typical microstructure of air-cooled Zn alloys with 0.8 wt % Cu (Z-0.8Cu-air) after etching. Cu-rich intermetallic particles (probably Zn-Cu ε phase) were found in this alloy, as shown in EDX spectrum (Fig 4.4 (b)). EDX quantitative analysis on polished samples without etching revealed that there is about 0.3 ± 0.05 wt % Cu (average of ten measurements) dissolved in the matrix. The EDX result is consistent with the solubility of Cu in Zn at room temperature.

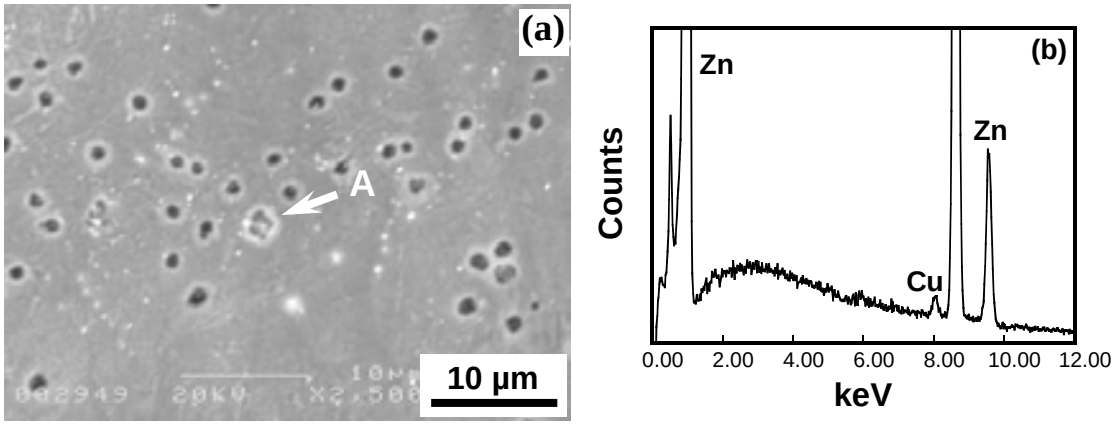

Fig 4.4 (a) SEM image of etched Z-0.8Cu-air, and (b) EDX spectrum of a Cu-rich particle as shown with arrow A in (a).

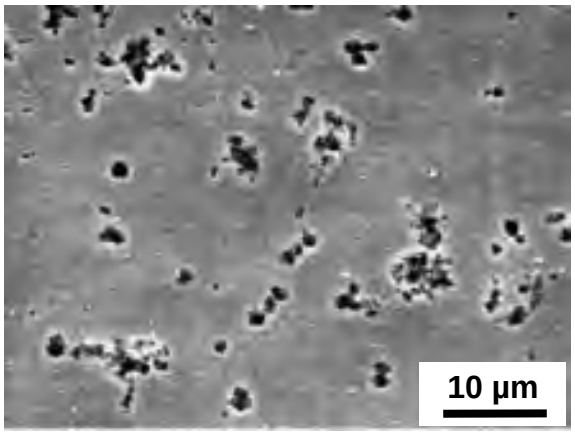

Fig 4.5 SEM image of etched Z-0.8Cu-wq.

The microstructure of a water-quenched Zn alloy with 0.8 wt % Cu (Z-0.8Cu-wq) is shown in Fig 4.5. No detectable Cu-rich intermetallic particles were found in this alloy although there were many pits on the surface after etching in 2 % Nital. EDX quantitative analysis on polished samples without etching revealed that there is about 0.8 wt % Cu (average of ten measurements) in the matrix. It is possible that Cu-rich intermetallic particles of size finer than the resolution limit of the SEM could be present in the alloy. The pits appearing on the etched surface are probably due to these tiny particles. However, no further analysis was carried out to confirm this.

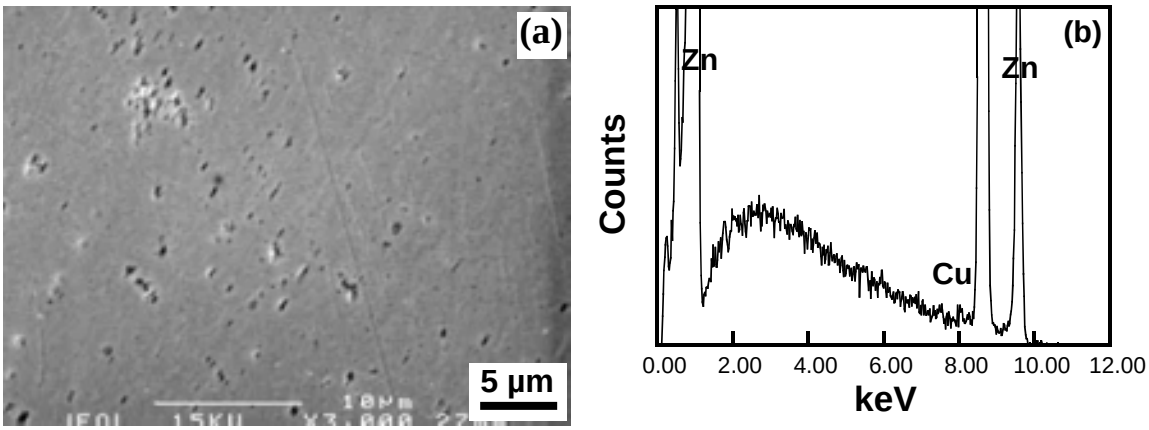

Fig 4.6 (a) SEM image of Z-0.2Cu-wq, and (b) EDX spectrum of the matrix.

For the water-quenched Zn alloy with addition of 0.2 wt % Cu, no intermetallic particles were detected in this alloy, as shown in Fig 4.6 (a). However, it is possible that Cu-rich intermetallic particles of size finer than the resolution limit of the SEM could be present in the alloy. About 0.2 wt % Cu was found to be dissolved in the matrix as shown by EDX analysis of the matrix in Fig 4.6 (b). Further analysis of air-cooled Zn alloys with 0.2 wt % Cu was also carried out. The result revealed that it shows a similar microstructure to that of the water quenched sample.

4.1.4 Zr additions

Fig 4.7 shows the microstructure of the water-quenched Zn alloy with addition of 0.2 wt % Zr (Z-0.2Zr-wq). Zr-rich intermetallic particles were found on the etched surface as shown in Fig 4.7 (a) and (b). No detectable Zr was found dissolved in the matrix. Due to the considerable difference in the melting points of both Zr and Zn, it was found that it is difficult to melt Zr in Zn bath. As no further chemical composition analysis was carried out on this alloy, it was not clear if the required amount of Zr had been completely dissolved in molten Zn bath.

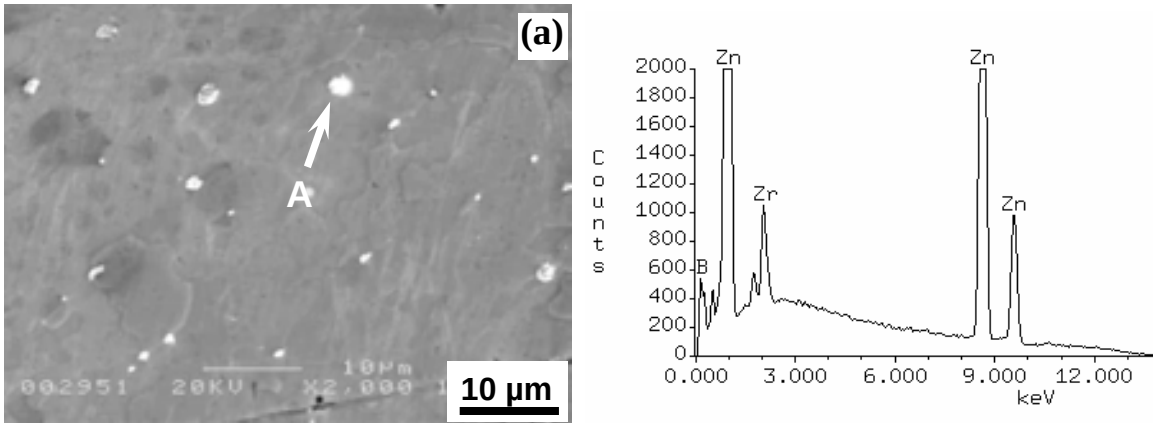

Fig 4.7 (a) SEM image of Z-0.2Zr-wq, and (b) EDX spectrum of one Zr-rich particle as shown with arrow A in (a).

4.1.5 Mn additions

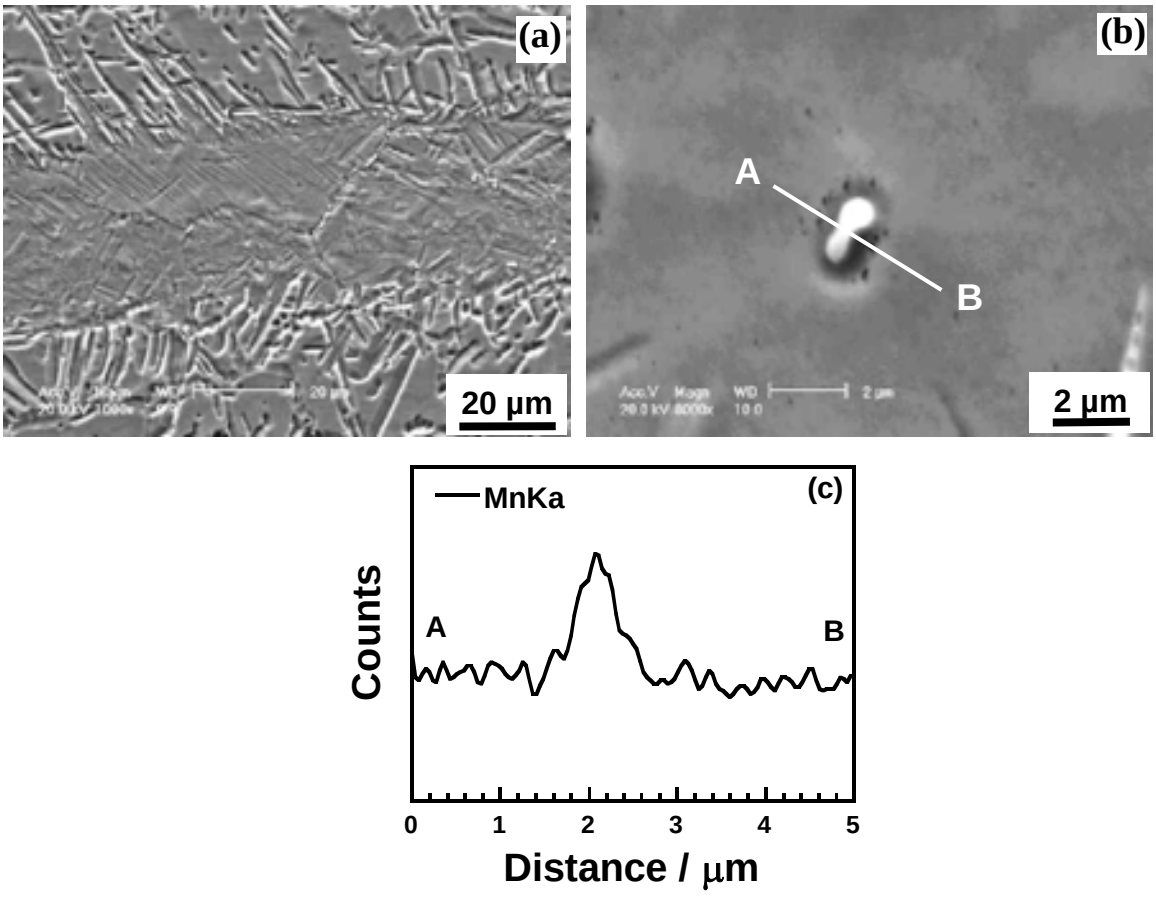

Fig 4.8 (a) Low magnification, (b) high magnification SEM images of etched Z-0.4Mn-Al-air, and (c) EDX line scan across Mn-rich particles as shown with a white line in (b).

Fig 4.8 shows the microstructure of air-cooled Zn alloys with 0.4 wt % Mn (Z-0.4Mn-Al-air). Intermetallic particles were found on the surface as shown in Fig 4.8 (a) and (b). The EDX line scan (Fig 4.8 (b)) across a typical particle indicated that it is Mn-rich; the intermetallic particles were mainly formed on grain boundaries as shown in Fig 4.8 (a).

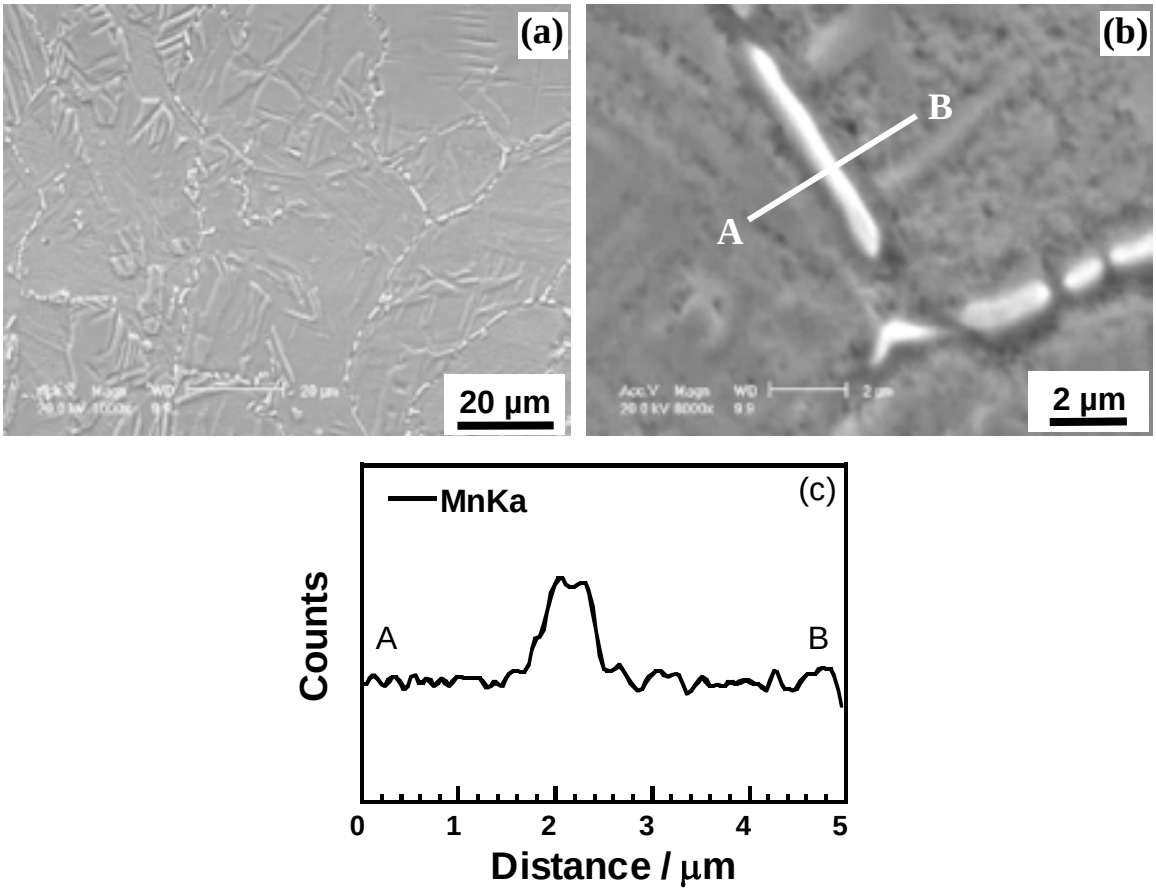

Fig 4.9 (a) low magnification, (b) high magnification SEM images of Z-0.8Mn-Al-air, and (c) EDX line scan across Mn-rich particles as shown with a white line in (b).

Fig 4.9 shows the microstructure of air-cooled Zn alloys with 0.8 wt % Mn (Z-0.8Mn-Al-air). Intermetallic particles were found on the surface as shown in Fig 4.9 (a), (b) and (c). EDX line scans (e.g. Fig 4.9 (c)) across the particles indicated that they were Mn-rich intermetallic particles which were mainly formed on grain boundaries. Compared with the sample containing 0.4 wt % Mn, the Mn-rich particles in Z-0.8Mn-Al-air are larger than that in Z-0.4Mn-Al-air and there are more Mn-rich particles in Z-0.8Mn-Al-air

than those in Z-0.4Mn-Al-air which can be seen from a comparison of Fig 4.8 (b) and Fig 4.9 (b).

Significant numbers of Mn-rich intermetallic particles were also found in the water-quenched Zn alloys with addition of 0.8 wt % Mn as shown in Fig 4.10 (b). Only a few particles were found when 0.4 wt % Mn was added to the Zn, as shown in Fig 4.10 (a). EDX quantitative analysis on polished samples was carried out to identify the Mn content dissolved in the matrix in the different alloys. The results are given in Table 4.1. A slightly higher Mn content in the matrix was found for water-quenched Zn alloys, especially for Zn alloys with 0.8 wt % Mn.

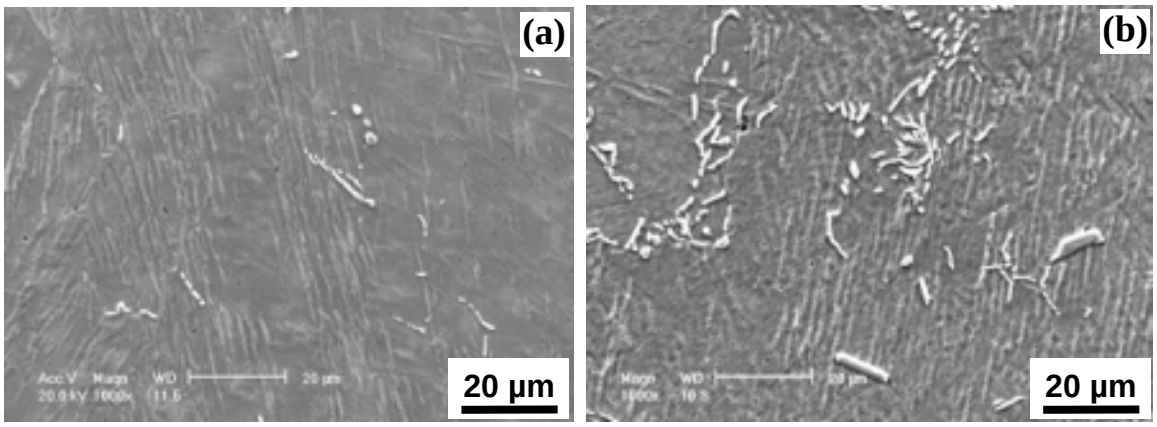

Fig 4.10 SEM images of water-quenched Zn alloys (etched) (a) Z-0.4Mn-Al-wq, and (b) Z-0.8Mn-Al-wq

Table 4.1 EDX analysis of Mn content in the matrix of Zn alloys with Mn additions

Zn alloy	Mn content (wt %)
Z-0.4Mn-Al-wq	0.36 ± 0.06
Z-0.4Mn-Al-air	0.34 ± 0.04
Z-0.8Mn-Al-wq	0.63 ± 0.05
Z-0.8Mn-Al-air	0.5 ± 0.04

4.1.6 Combined additions of Mn and Cu

The combination of Mn and Cu additions was also investigated with the aim of developing more corrosion resistant Zn alloys for hot dip galvanising. The combinations of 0.8 wt % Mn with 0.2 wt % Cu and 0.8 wt % Cu were used in this study. Fig 4.11 shows the typical microstructure of the water-quenched Zn alloys (Z-0.8Mn-0.2Cu-Al-wq and Z-0.8Mn-0.8Cu-Al-wq) with the Mn and Cu alloying elements. Significant numbers of intermetallic particles were found in both Zn alloys. EDX line scan (Fig 4.12) across a typical particle indicated that it was Mn-rich and not Cu-rich. This result indicated that Mn-rich particles are the main coarse intermetallic particles found in Z-0.8Mn-0.8Cu-Al-wq. In the matrix, both Mn and Cu were found. The content of Mn and Cu in the matrix is listed in Table 4.2. The result is comparable with the Zn alloys of only one type of additions (Mn or Cu) which is described in Section 4.1.3 and 4.1.5. It is possible that Cu-rich intermetallic particles of a size finer than the resolution limit of the SEM could be present in the Mn-Cu containing alloys. Cu was mainly dissolved in the matrix with the possibility of some small Cu-rich particles precipitated at grain boundaries for the water-quenched Zn alloy (Z-0.8Cu-wq) (Section 4.1.5).

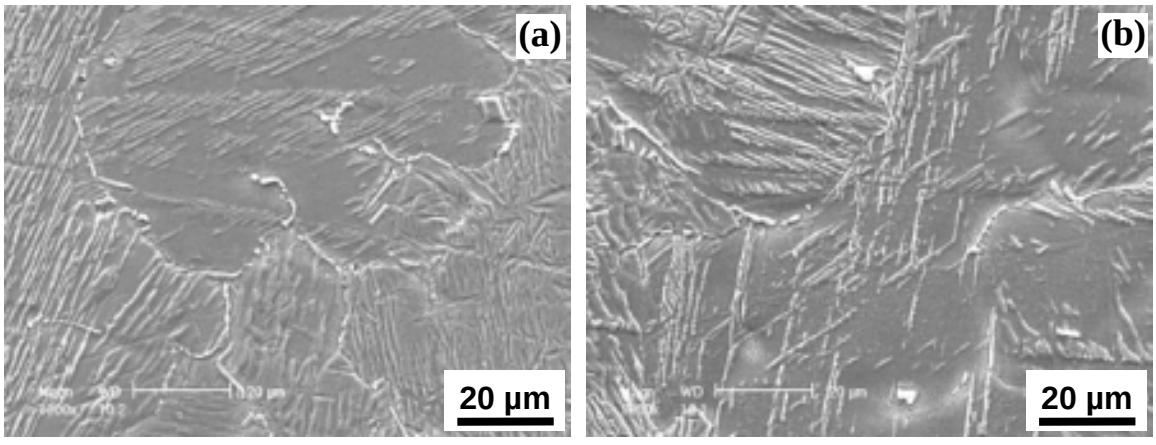

Fig 4.11 SEM images of water-quenched Zn alloys (etched) (a) Z-0.8Mn-0.2Cu-Al-wq, and (b) Z-0.8Mn-0.8Cu-Al-wq

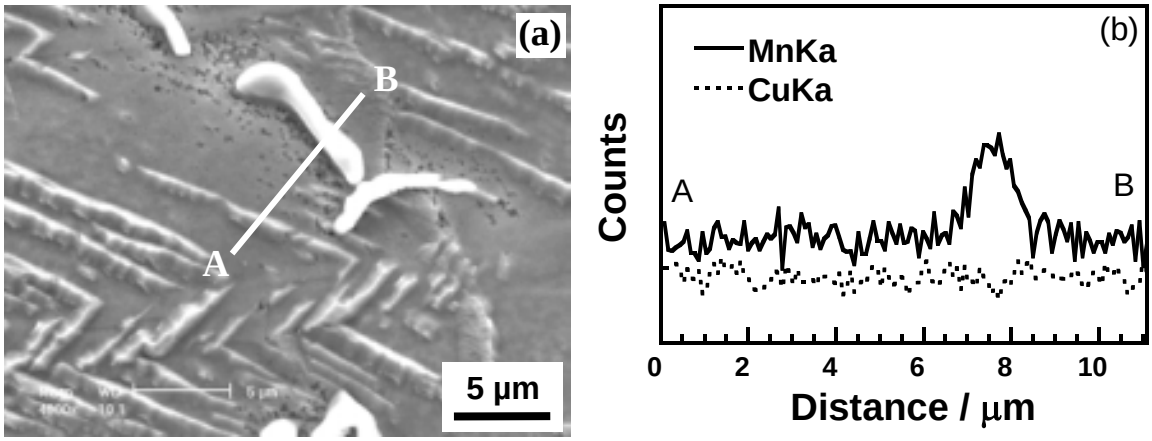

Fig 4.12 (a) SEM images of etched Z-0.8Mn-0.8Cu-Al-wq, and (b) EDX line scan from A to B across a Mn-rich particle as shown with a white line in (a).

Table 4.2 EDX analysises of Mn and Cu content in the matrix of Zn alloys with Mn and Cu additions

Zn alloy	Mn content (wt %)	Cu content (wt %)
Z-0.8Mn-Al-wq	0.63 ± 0.05	
Z-0.8Mn-0.2Cu-Al-wq	0.60 ± 0.05	0.2 ± 0.02
Z-0.8Mn-0.8Cu-Al-wq	0.60 ± 0.05	0.8 ± 0.05

4.2 Corrosion of Zn alloys

4.2.1 Electrochemical polarisation

4.2.1.1 In 0.1 M NaCl solution

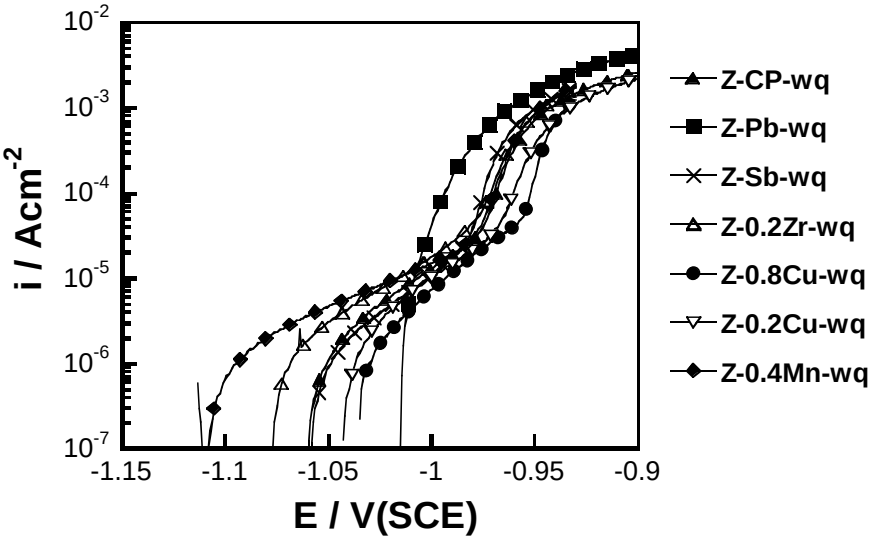

Fig 4.13 Potentiodynamic anodic polarisation curves for water-quenched Zn alloys in naturally-aerated 0.1 M NaCl at pH 6 with a scan rate of 1 mV/s; tests were started immediately after samples were polished and rapidly transferred into solution.

Fig 4.13 shows the anodic polarisation curves for water-quenched Zn alloys with alloying additions of Cu, Sb, Zr and Mn in naturally-aerated 0.1 M NaCl solution at pH 6. Tests were started immediately after samples were polished and rapidly transferred into solution. Details of the content of alloying elements can be found in Table 3.3. It was found that there is a passive plateau for most of these alloys except Z-Pb-wq. A sharp increase in current density occurred for each alloy after the breakdown potential which is associated with pitting. All Zn alloys suffered pitting as a result of the anodic polarisation. Pitting corrosion of these alloys was confirmed by SEM images of corrosion morphologies after potentiodynamic polarisation to the potential of -0.93 V(SCE) as shown in Fig 4.14 and Fig 4.15. The data for the pitting potentials at -1.0 V(SCE) are listed in Table 4.3. Among these alloys, Z-0.8Cu-wq shows the highest pitting potential and the lowest passive current

density. This result indicates that the addition of 0.8 wt % Cu can slightly decrease the dissolution of Zn and inhibit pitting compared with commercially-pure Zn without any alloying additions (Z-CP-wq). The pitting potential of Z-0.2Cu-wq was slightly higher than that of Z-CP-wq. There is no distinct passive plateau for the other commercially-pure Zn alloy with 1 wt % Pb additions (Z-Pb-wq). This indicates that Pb promotes anodic activity of Zn. Additions of Sb and Zr had no significant effect on pitting potential of Zn. Addition of Mn (0.4 wt % Mn) was also found to have no significant effect on pitting potential, but significantly decreased the open circuit potential (OCP) compared with Z-CP-wq.

Table 4.3 Comparison of corrosion behaviour of water-quenched Zn alloys after anodic polarisation tests in 0.1 M NaCl solution

Zn alloys	Pitting potential [a] (V *vs* SCE), ± 0.005	Pit density[b] (mm^{-2}), ± 5
Z-0.8Cu-wq	-0.95	50
Z-0.2Cu-wq	-0.96	70
Z-0.2Zr-wq	-0.98	130
Z-CP-wq	-0.97	160
Z-Sb-wq	-0.98	80
Z-Pb-wq	-1.0	260
Z-0.4Mn-wq	-0.97	100

[a] The pitting potential is defined as the potential where the current density reaches 50 $\mu A/cm^2$.

[b] Pits were counted manually based on 4 SEM images as shown in Fig 4.14.

In addition, pit sizes and densities are significantly different especially for Z-Pb-wq and Z-Cu-wq compared with Z-CP-wq as shown in Fig 4.14. The pit density of Z-Pb-wq was found to be higher than that of Z-CP-wq, whereas Z-0.8Cu-wq and Z-0.2Cu-wq showed fewer but larger pits. Pit densities of Z-0.2Zr-wq are similar to that of Z-CP-wq. Addition of 0.4 wt % Mn was found to decrease the pit size and density as shown in Fig 4.15 (surfaces were polished to 1 μm) after potentiodynamic anodic polarisation up to the potential of -0.93 V (*vs* SCE). SEM/EDX analysis of a large number of pits revealed that no detectable intermetallic particles were responsible for pit initiation for both Zn alloys. Therefore coarse Mn-rich particles found in Mn-containing Zn alloys (see Section 4.1.5) may not be pit initiation sites.

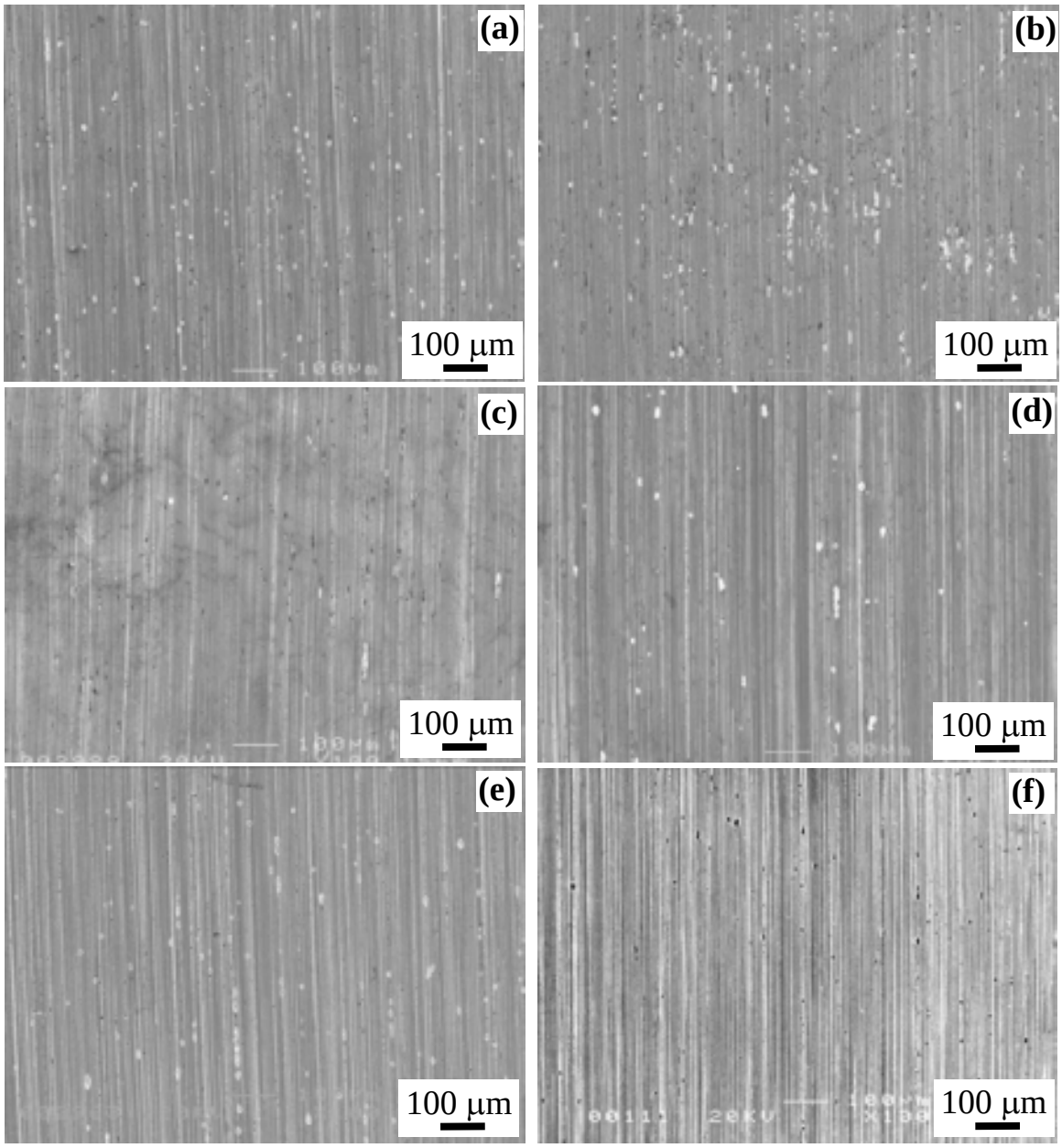

Fig 4.14 Corrosion morphologies of (a) Z-CP-wq, (b) Z-Pb-wq, (c) Z-0.2Cu-wq, (d) Z-0.8Cu-wq, (e) Z-0.2Zr-wq, and (f) Z-Sb-wq after potentiodynamic polarisation to the potential of -0.93 V (*vs* SCE) in naturally-aerated 0.1 M NaCl at pH 6.

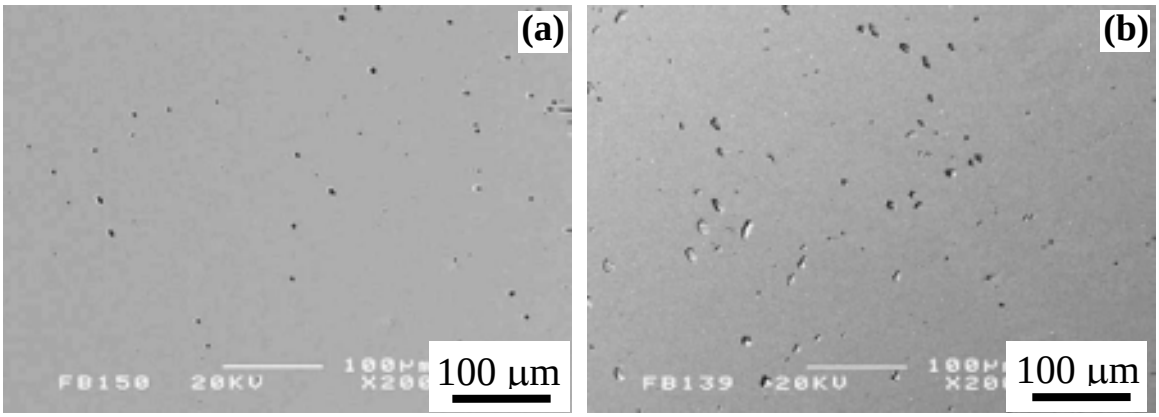

Fig 4.15 Corrosion morphologies of (a) Z-0.4Mn-wq and (b) Z-CP-wq after potentiodynamic polarisation to the potential of -0.93 V (*vs* SCE) in naturally-aerated 0.1 M NaCl at pH 6.

Pit initiation sites were also identified for other Zn alloys after potentiodynamic polarisation to the potential of -0.93 V (vs SCE) in naturally-aerated 0.1 M NaCl at pH 6. The results are shown in Fig 4.16. Pb globules, Zr-rich particles and Cu-rich particles were responsible for pit initiation, while Sb-rich particles were not pit initiation sites as shown in Fig 4.16 (d), where it can be seen that a pit did not initiate from Sb-rich particles (the surface of Z-Sb-wq was etched after anodic polarisation to show the Sb-rich particles). Similar to Z-0.4Mn-wq, no detectable particle was responsible for pit initiation sites for Z-CP-wq and Z-0.2Cu-wq.

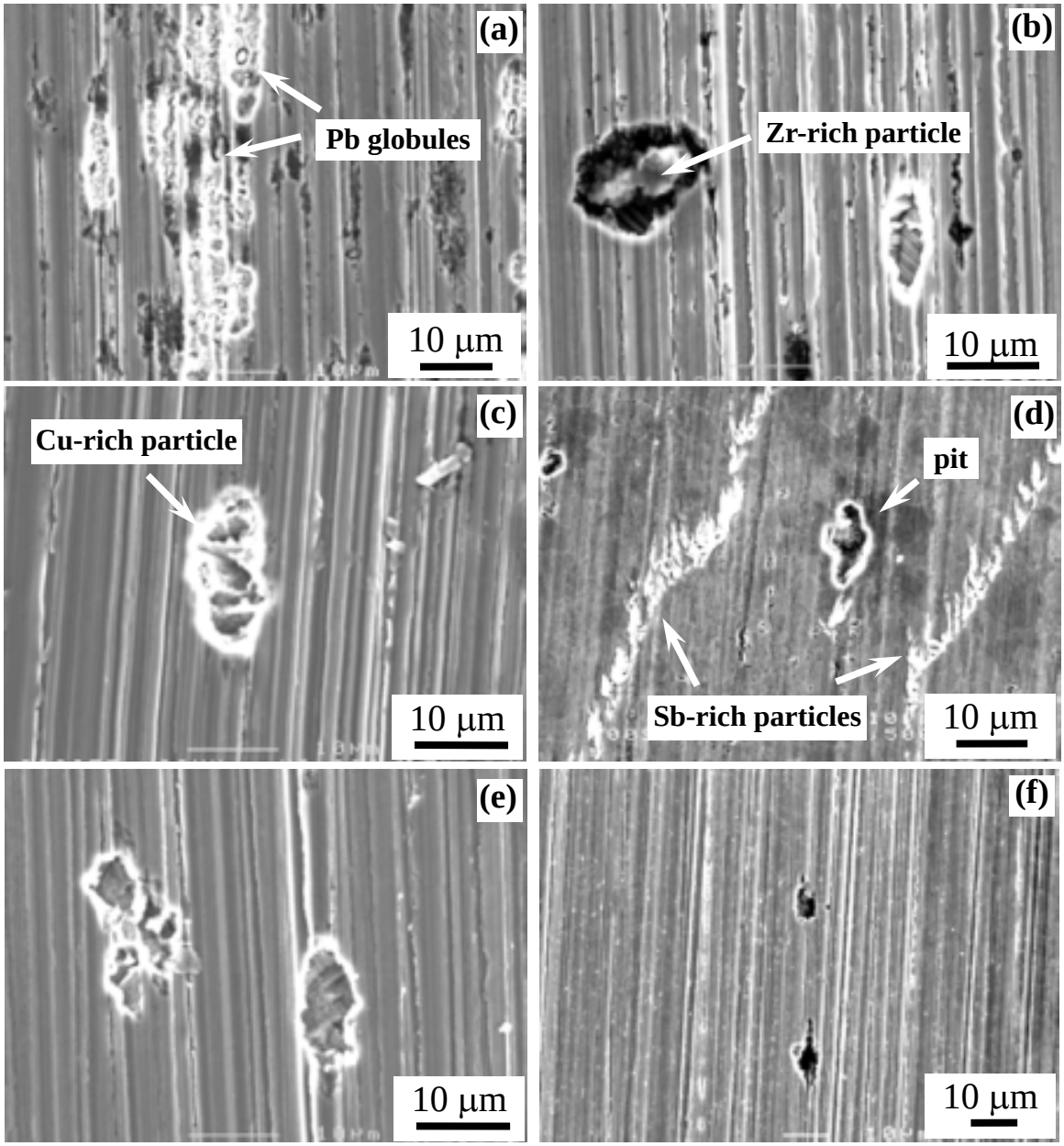

Fig 4.16 SEM images of (a) Z-Pb-wq, (b) Z-0.2Zr-wq, (c) Z-0.8Cu-wq, (d) Z-Sb-wq, (e) Z-CP-wq, and (f) Z-0.2Cu-wq after potentiodynamic polarisation to the potential of -0.93 V (*vs* SCE) in naturally-aerated 0.1 M NaCl at pH 6.

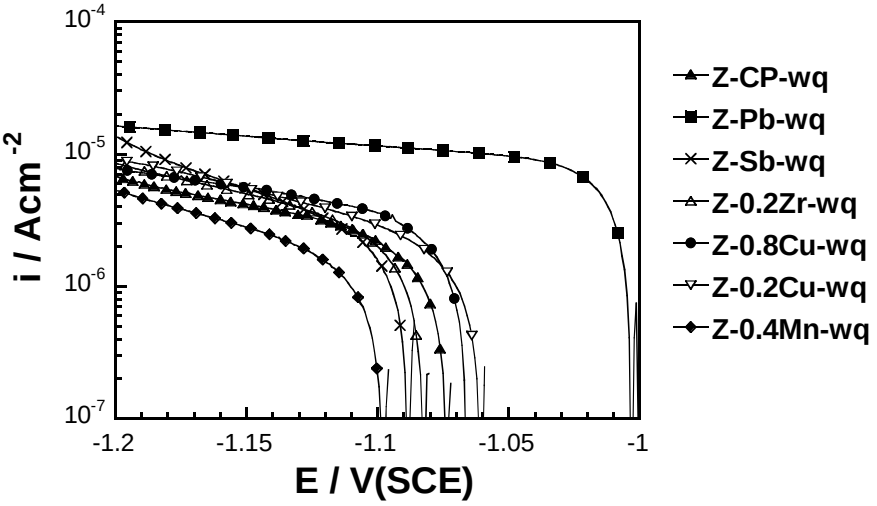

Fig 4.17 Potentiodynamic cathodic polarisation curves for water-quenched Zn alloys in naturally-aerated 0.1 M NaCl at pH 6 with a scan rate of 1 mV/s; tests were started immediately after samples were polished and then rapidly transferred into solution.

Fig 4.17 shows the cathodic polarisation curves for water-quenched Zn alloys with Cu, Sb, Zr and Mn additions in naturally-aerated 0.1 M NaCl at pH 6. It can be seen from these curves that the cathodic reaction of each alloy is controlled by diffusion of oxygen. Comparison of the cathodic current density of each alloy at potential -1.2 V (*vs* SCE) is listed in Table 4.4. It is obvious that the commercial Zn alloy Z-Pb-wq has significantly higher cathodic reaction current than Z-CP-wq, indicating that Pb globules are catalytic sites for oxygen reduction reaction on Zn. Z-0.2Cu-wq and Z-0.8Cu-wq have a slightly higher cathodic current density than Z-CP-wq, especially at potentials close to OCP. This result indicates that Cu-rich intermetallic particles are probably the catalytic sites for cathodic reduction, i.e., oxygen reduction on Zn. Z-Sb-wq shows a similar cathodic current density to Z-CP-wq at potential close to OCP (Fig 4.17). It was shown in the previous results that there are significant numbers of Sb-rich particles in Z-Sb-wq. This result indicated that the Sb-rich intermetallic particles are not catalytic sites for oxygen reduction. Addition of 0.4 wt % Mn was found to significantly decrease the cathodic current density as shown in Fig 4.17. As Mn has less effect on the anodic reaction of Zn, it is not surprising that the OCP of Z-0.4Mn-wq is lower than that of Z-CP-wq as shown in Fig 4.13 and Fig 4.17.

Table 4.4 Comparison of cathodic current density of water-quenched Zn alloys after the cathodic polarisation tests in 0.1 M NaCl at pH 6

Zn alloys	Cathodic current density ($\mu A/cm^2$) at -1.2 V (*vs* SCE), ± 1.0
Z-0.8Cu-wq	8.0
Z-0.2Cu-wq	9.0
Z-0.2Zr-wq	9.0
Z-CP-wq	7.0
Z-Sb-wq	13.0
Z-Pb-wq	17.0
Z-0.4Mn-wq	5.0

4.2.1.2 In 0.1 M Na_2SO_4 solution

To further confirm the effect of alloying additions on the anodic and cathodic activity of Zn, polarisation measurements were also carried out in 0.1 M Na_2SO_4 at pH 6. The second type of reference electrode, a saturated mercury/mercurous sulphate electrode (MSE) was used in this solution. For comparison purposes, the potential scale was referred to against SCE (by adding a value of 0.4 V). The anodic polarisation curves for water-quenched Zn alloys with alloying additions of Cu, Sb, Zr and Mn in naturally-aerated 0.1 M Na_2SO_4 solution are given in Fig 4.18. They are similar to those in 0.1 M NaCl solution. Most of the Zn alloys exhibit passive behaviour except Z-Pb-wq and Z-0.8Cu-wq. Z-Pb-wq exhibits higher anodic activity than that of Z-CP-wq. This indicates that Pb globules promote anodic dissolution of Zn. Z-0.8Cu-wq shows the highest pitting potential but it is very close to its open circuit potential (OCP). In this solution, it was found that the OCP of Z-0.8Cu-wq shifts in the anodic direction very quickly after transferring the fresh polished sample into solution. The shift of the OCP in the anodic direction is probably due to the enhanced cathodic reaction on Cu-rich particles after the rapid dissolution of Zn oxide formed in air. The anodic polarisation curves of the other alloys are quite similar, which indicates that the additions of Cu (0.2 wt %), Sb (1.0 wt %), Zr (0.2 wt %) and Mn (0.4 wt %) had no significant effect on anodic dissolution of Zn in this solution.

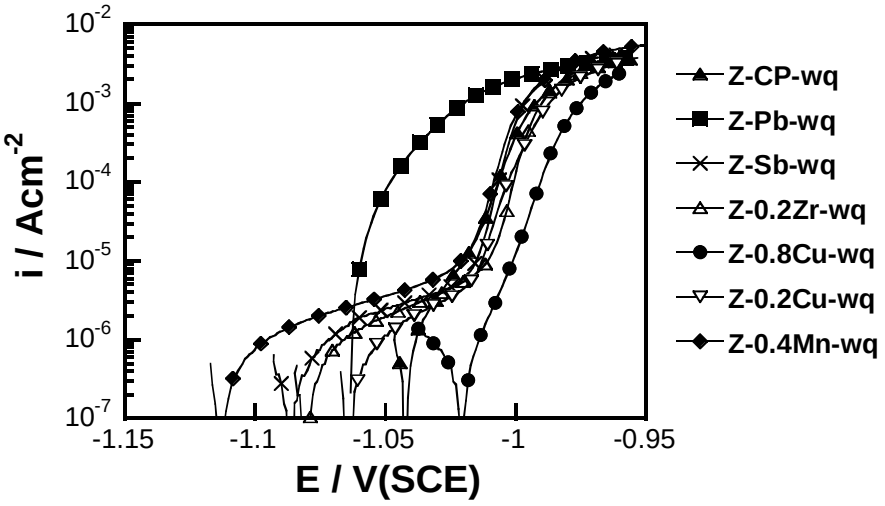

Fig 4.18 Potentiodynamic anodic polarisation curves for water-quenched Zn alloys in naturally-aerated 0.1 M Na_2SO_4 at pH 6 with a scan rate of 1 mV/s; tests were started immediately after samples were polished and then rapidly transferred into solution.

The corrosion morphologies after anodic polarisation tests were shown in Fig 4.19. Obvious pits were only found for Z-Pb-wq, Z-0.2Cu-wq and Z-0.8Cu-wq after potentiodynamic polarisation to the potential of -0.95 V (vs. SCE). However, unlike that in 0.1 M NaCl solution no obvious pits were found for other alloys in this solution. In literature pitting corrosion of Zn was found in Na_2SO_4 solutions [100]. It was reported that in the pH range 6.0 - 7.5, active dissolution and pitting corrosion are at their lowest. Above and below this pH range, both general and pitting corrosion are enhanced. This may probably explain why there are no obvious pits on the corroded surface of the Zn alloys without significant cathodic sites (e.g., Z-CP-wq). It is assumed that the rapid increase of the anodic current is associated with the active dissolution of Zn due to the presence of SO_4^{2-} ions. SO_4^{2-} ions could promote the anodic dissolution of Zn due to the formation of ion pairs between Zn^{2+} ions and SO_4^{2-} ions [85]. This ion pair formation is assumed to decrease the activation energy for dissolution and hence increase the dissolution current. The accelerating influence of SO_4^{2-} ions could also be related to theirs adsorption on the metal surface and subsequent participation in the active dissolution process [100]. In SO_4^{2-} neutral media, two opposing effects control the rate of dissolution at this pH; oxide formation tending to inhibit the process and ion pair formation tending to accelerate it [85].

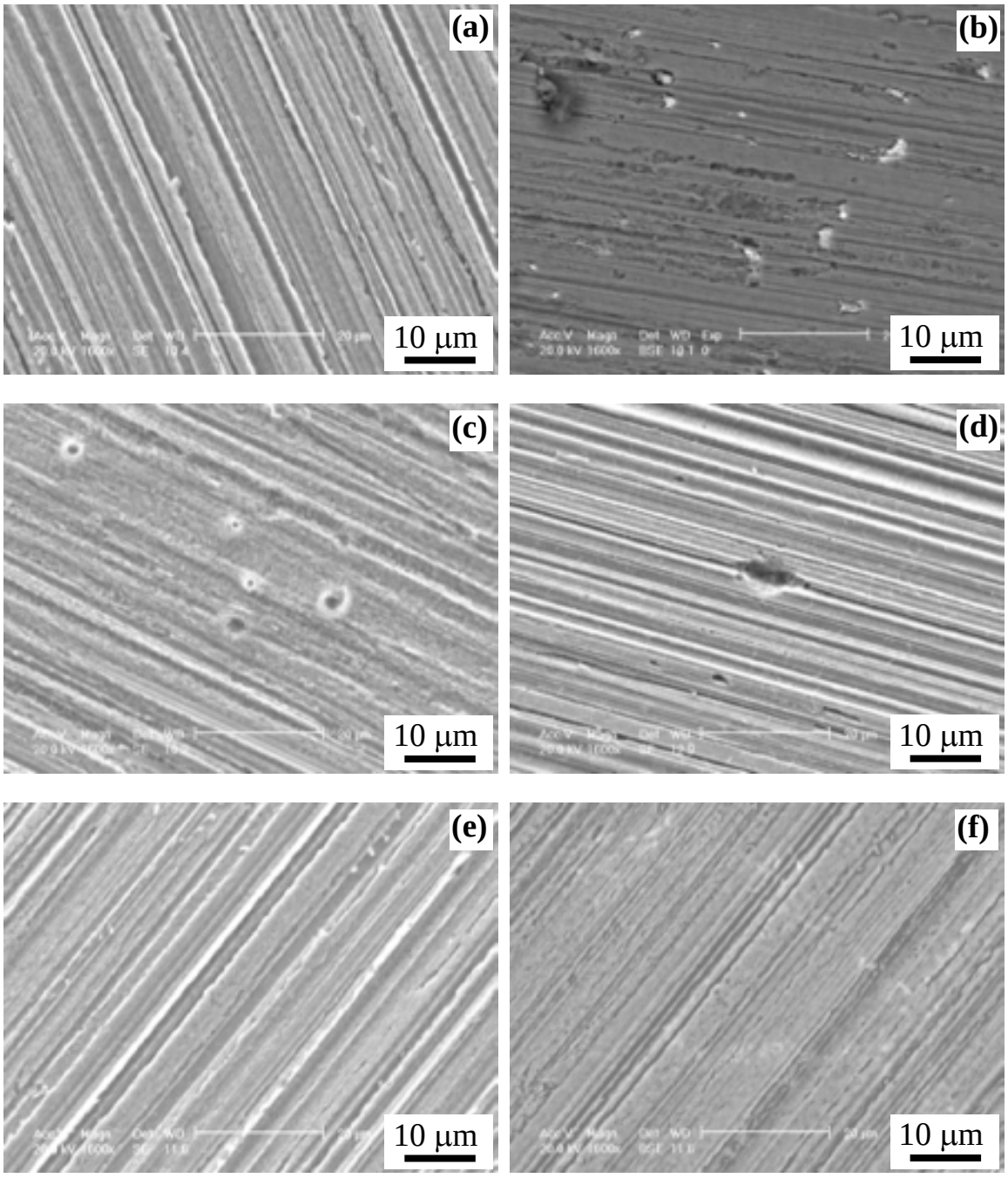

Fig 4.19 Corrosion morphology of (a) Z-CP-wq, (b) Z-Pb-wq, (c) Z-0.2Cu-wq, (d) Z-0.8Cu-wq, (e) Z-0.2Zr-wq, and (f) Z-Sb-wq after potentiodynamic polarisation to the potential of -0.95 V (*vs* SCE) in naturally-aerated 0.1 M Na_2SO_4 at pH 6.

Fig 4.20 shows the cathodic polarisation curves for water-quenched Zn alloys in naturally-aerated 0.1 M Na_2SO_4. Similar to the behaviour in 0.1 M NaCl, Z-Pb-wq shows the highest cathodic reaction activity among these alloys. It is notable that Z-0.4Mn-wq,

Z-0.2Zr-wq and Z-Sb-wq show lower cathodic current density than Z-CP-wq. For Cu additions, Z-0.2Cu-wq has no significant effect while Z-0.8Cu-wq exhibits a higher cathodic reduction reaction than that of Z-CP-wq. This result indicates that Pb globules and Cu-rich particles are catalytic sites for cathodic reduction reactions whereas Zr-rich particles and Sb-rich particles are not. The cathodic current density of each alloy at -1.2 V (*vs* SCE) is listed in Table 4.5. Compared with the behaviour in 0.1 M NaCl, it seems that the cathodic current densities of most Zn alloys are higher in 0.1 M Na_2SO_4. For example, the cathodic current density of Z-CP-wq is 12 $\mu A/cm^2$ in 0.1 M Na_2SO_4 compared with 7 $\mu A/cm^2$ in 0.1 M NaCl.

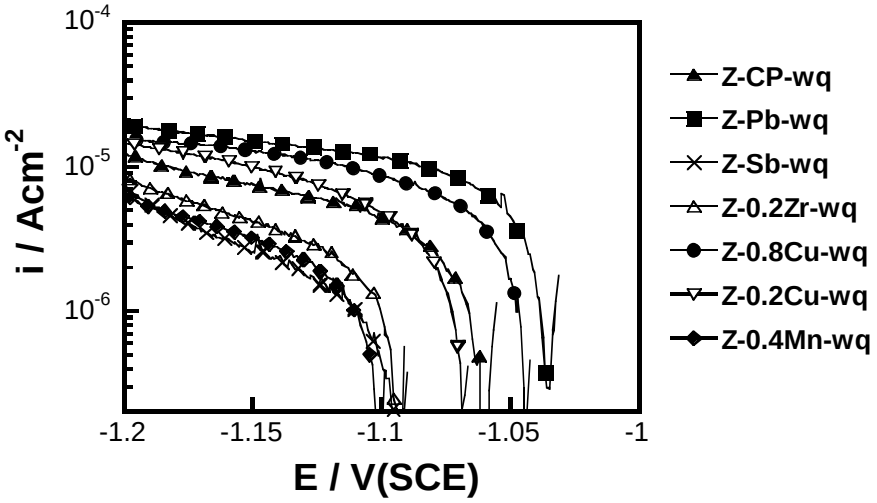

Fig 4.20 Potentiodynamic cathodic polarisation curves for water-quenched Zn alloys in naturally-aerated 0.1 M Na_2SO_4 at pH 6 with a scan rate of 1 mV/s; tests were started immediately after samples were polished and then rapidly transferred into solution.

Table 4.5 Comparison of cathodic current density of water-quenched Zn alloys after the cathodic polarisation tests in 0.1 M Na_2SO_4 at pH 6

Zn alloys	Cathodic current density ($\mu A/cm^2$) at -1.2 V (*vs* SCE), ± 2.0
Z-0.8Cu-wq	16.0
Z-0.2Cu-wq	14.0
Z-0.2Zr-wq	9.0
Z-CP-wq	12.0
Z-Sb-wq	8.0
Z-Pb-wq	20.0
Z-0.4Mn-wq	5.0

4.2.1.3 In accelerated solution

An accelerated solution to simulate the marine environment developed in the literature [120] was used in this study. It contains NaCl, Na_2SO_4, and $NaHCO_3$ (the composition is given in Section 3.3.2). The composition of the solution must be as close as possible to that of natural waters with which Zn can be in contact when it is exposed to the atmosphere. Sulphate and chloride ions are included because they are known to enhance the corrosion of Zn [131, 132]. $NaHCO_3$ additions were made in order to simulate the beneficial effect of CO_2 in providing a passivating species, HCO_3^-, on the Zn surface. The selection of a slightly alkaline pH (8.4) might be surprising for thick electrolyte layers on Zn surfaces considering the pH values of, for example, acid rain and fog. Nevertheless, Keddam *et al.* have noted that reducing the electrolyte thickness of a neutral chloride solution from bulk solution to 50 μm, as often occurs during atmospheric corrosion on a Zn electrode, leads to an increase of the interfacial solution pH [119].

The accelerated solution is mainly used for immersion tests where linear polarisation resistance (LPR) measurements can be carried out at OCP (see Section 4.2.3). To better understand the corrosion failure in this solution, potentiodynamic polarisation measurements in this solution were also carried out.

The anodic polarisation curves for water-quenched Zn alloys with alloying additions of Cu, Sb, Zr and Mn in the accelerated solution are shown in Fig 4.21. The effects of alloying additions on anodic behaviour of Zn are similar to that in 0.1 M Na_2SO_4. In this solution, Cu (0.8 wt %) increases the pitting potential, although it is very close to its open circuit potential (OCP). Pb was found to be the only element to promote anodic activity. The additions of Cu (0.2 wt %), Sb (1.0 wt %), Zr (0.2 wt %) and Mn (0.4 wt %) have no significant effect on anodic activity of Zn. Compared with anodic polarisation curves in 0.1 M NaCl (Fig 4.13) and 0.1 M Na_2SO_4 solution (Fig 4.18), the pitting potential of most Zn alloys in the accelerated solution are higher than those in 0.1 M Na_2SO_4 solution but lower those that in 0.1 M NaCl solution. The data for pitting potentials in these solutions are listed in Table 4.6.

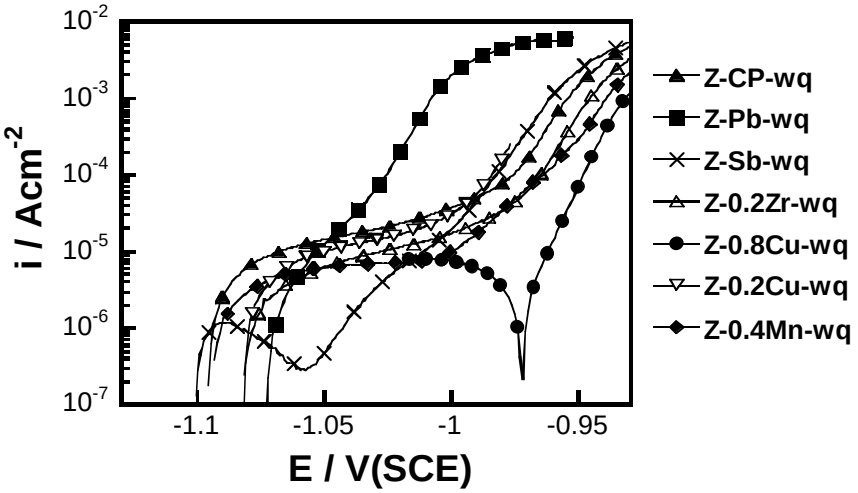

Fig 4.21 Potentiodynamic anodic polarisation curves for water-quenched Zn alloys in the accelerated solution (0.1 M NaCl + 0.1 M Na_2SO_4 + 0.01 M $NaHCO_3$) at pH 8.4 with a scan rate of 1 mV/s; tests were started immediately after samples were polished and then rapidly transferred into solution.

Table 4.6 Pitting potentials of water-quenched Zn alloys in different solutions (± 0.005 V (*vs* SCE), more than three measurements)

Zn alloys	0.1 M NaCl	0.1 M Na_2SO_4	accelerated solution
Z-CP-wq	-0.97	-1.02	-0.99
Z-Pb-wq	-1.00	-1.05	-1.03
Z-0.2Cu-wq	-0.96	-1.01	-0.99
Z-0.8Cu-wq	-0.95	-0.99	-0.95
Z-0.2Zr-wq	-0.98	-1.00	-0.97
Z-Sb-wq	-0.98	-1.01	-0.99
Z-0.4Mn-wq	-0.97	-1.01	-0.97

Note：The pitting potential is defined as the potential where the current density reaches 50 μA/cm^2.

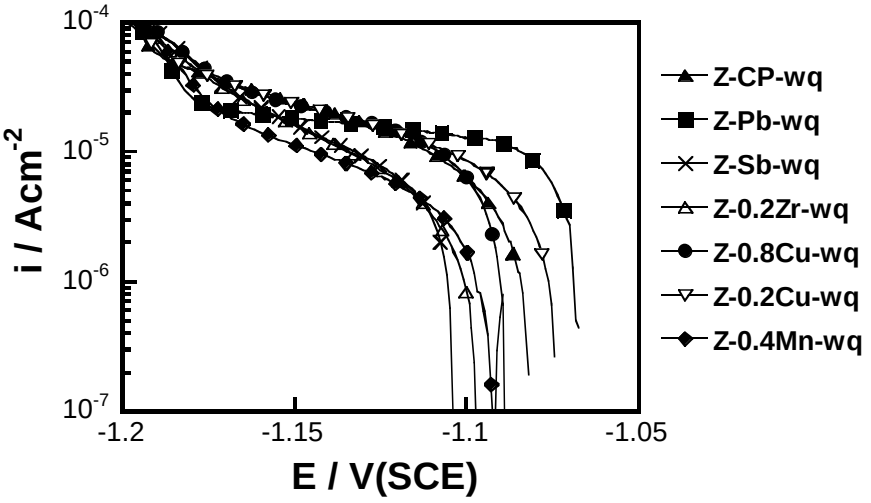

Fig 4.22 Potentiodynamic cathodic polarisation curves for water-quenched Zn alloys in the accelerated solution (0.1 M NaCl + 0.1 M Na_2SO_4 + 0.01 M $NaHCO_3$) at pH 8.4 with a scan rate of 1 mV/s; tests were started immediately after samples were polished and then rapidly transferred into solution.

The typical cathodic polarisation curve for water-quenched Zn alloys in the accelerated solution is show in Fig 4.22. Z-Pb-wq shows the highest cathodic reaction activity among these alloys. Z-0.2Zr-wq, Z-Sb-wq and Z-0.4Mn-wq exhibit lower cathodic current density compared with Z-CP-wq. For Cu additions, Z-0.2Cu-wq has no significant effect while Z-0.8Cu-wq exhibits higher cathodic current density than that of Z-CP-wq. This result further confirms that Pb globules and Cu-rich particles are catalytic sites for cathodic reduction reactions.

4.2.2 In-situ observation of corrosion

In order to investigate the pitting corrosion of Zn alloys, in-situ observation of corrosion morphology during anodic polarisation and immersion tests were also carried out. This study is mainly focused on the effect of Cu as an alloying element due to its significant effect on pitting corrosion of Zn. The surface morphologies were recorded using a video camera attached to an optical microscope. Still images were taken from the video recording. Fig 4.23 shows the result of an in-situ investigation for Z-0.8Cu-wq during anodic polarisation in naturally-aerated 0.1 M NaCl at pH 6. The pitting corrosion was clearly seen in this investigation as shown in Fig 4.23 (b). The corrosion morphology was found to change with potential. At a potential of -0.97 V (*vs* SCE) a pit was found to initiate on the surface. On further increasing the potential, the pit became larger and more pits initiated at other sites. It was also found that during the pitting corrosion, no hydrogen evolution occurred on the surface.

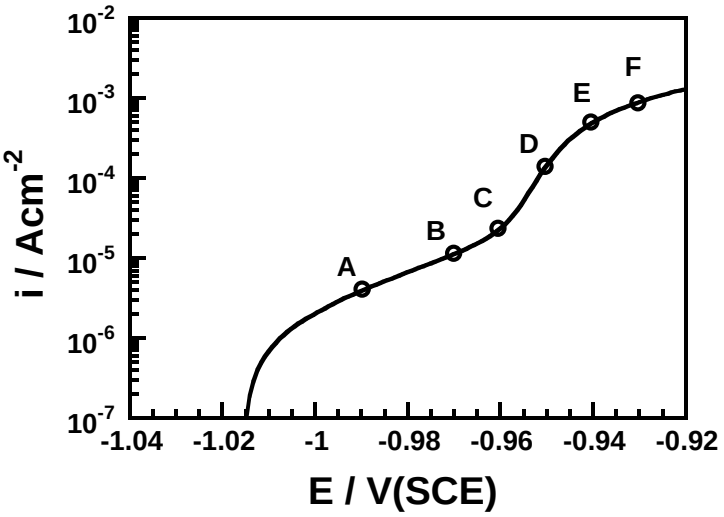

(a)

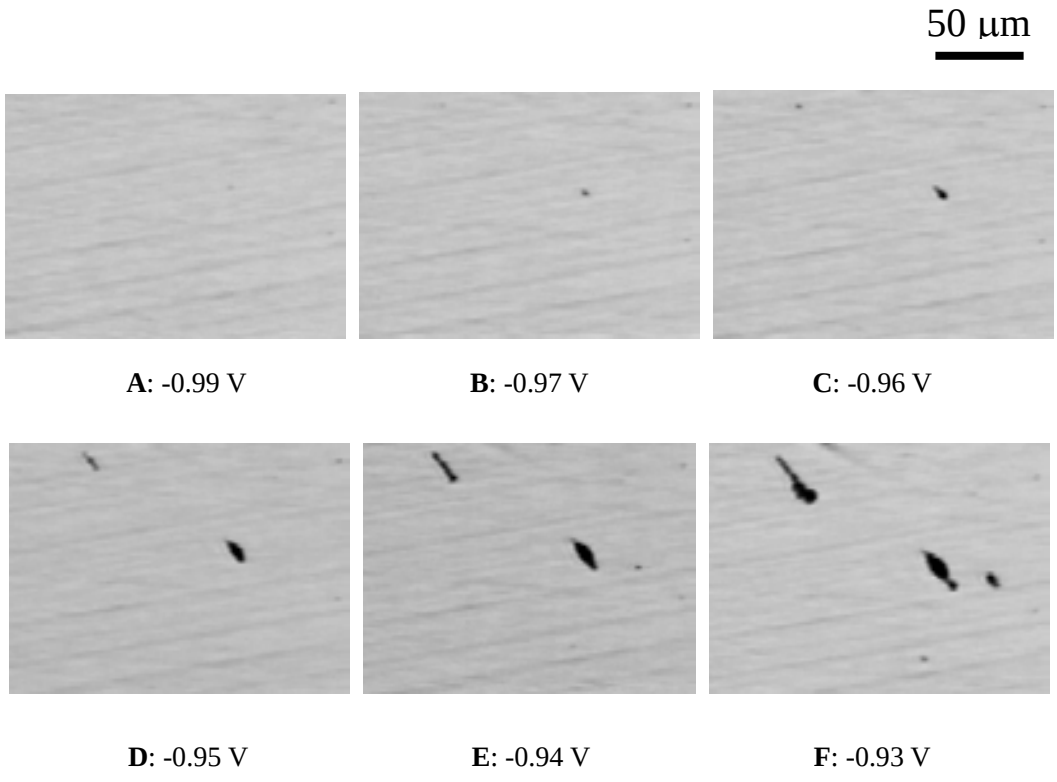

(b)

Fig 4.23 In-situ investigation of pit initiation for Z-0.8Cu-wq during anodic polarisation in naturally-aerated 0.1 M NaCl at pH 6 with a scan rate of 1 mV/s: (a) anodic polarisation curve and (b) In-situ images taken from video camera at different potentials (V (*vs* SCE)) indicated by the frames marked A to F in (a).

In-situ immersion tests of Z-CP-wq, Z-0.2Cu-wq and Z-0.8Cu-wq in naturally-aerated 0.1 M NaCl at pH 6 was also conducted. The corrosion morphologies were monitored and recorded during the immersion test. The typical corrosion morphology after a 1 h immersion test is shown in Fig 4.24. The result indicates that pitting corrosion is the main corrosion form for all these Zn alloys. It shows that pits formed on Z-0.2Cu-wq are smaller while number of pits is larger than that on Z-CP-wq. No hydrogen evolution was observed during in-situ optical microscopy investigation from the pits as well as on the surface. This is not surprised as the overpotential of hydrogen evolution on Zn is high. At pH 6, the cathodic reaction of hydrogen evolution can be neglected.

SEM/EDX analysis showed that corrosion pits initiated from Cu-rich intermetallic phases for Z-0.8Cu-wq as shown in Fig 4.25(b). No particles were detected at pit initiation sites for Z-CP-wq and Z-0.2Cu-wq, although significant pitting corrosion occurred on the surface. Impurities and intermetallic particles that are finer than the resolution limit of the SEM, could be pit initiation sites for Z-CP-wq. For example, Fe impurities present in Zn, which act as cathodic sites for hydrogen evolution, can significantly increase the corrosion rate of Zn in acidic environment.

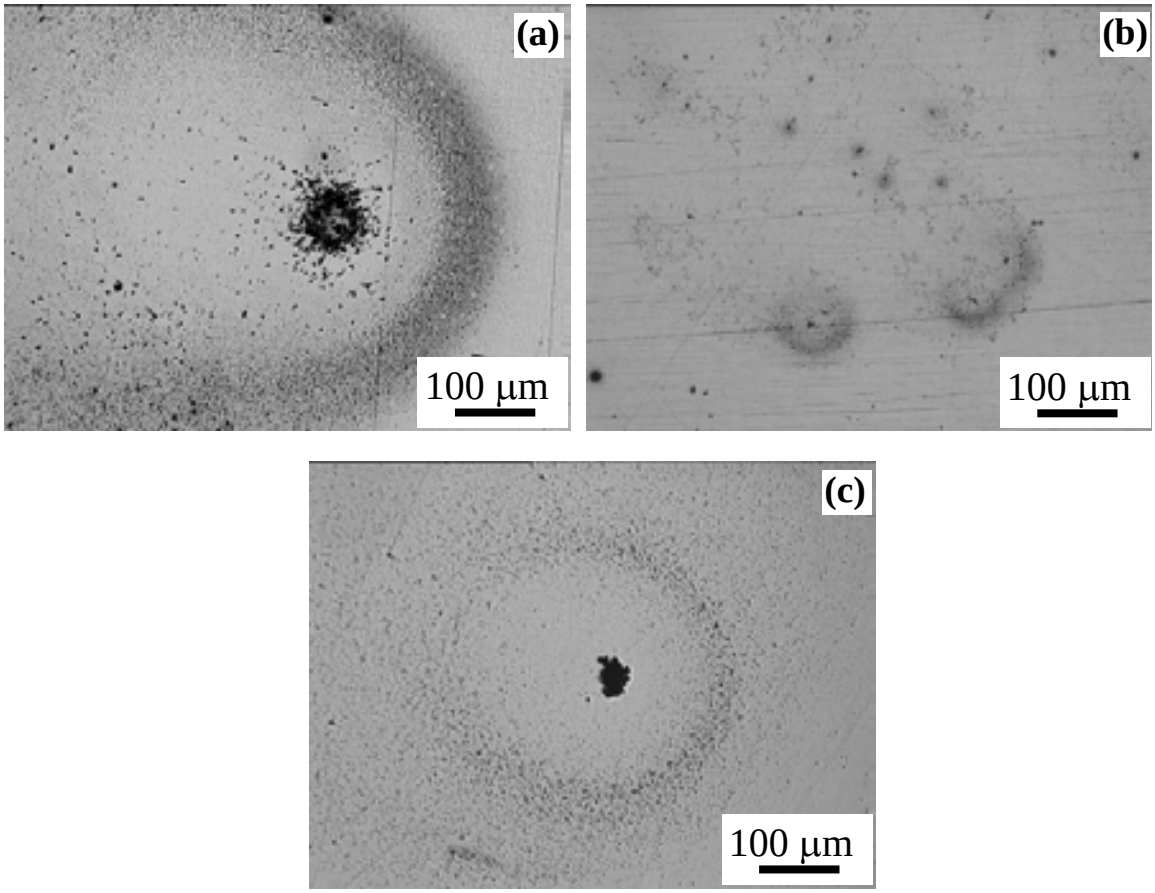

Fig 4.24 In-situ optical micrographs of (a) Z-CP-wq, (b) Z-0.2Cu-wq, and (c) Z-0.8Cu-wq after 1h immersion in naturally-aerated 0.1M NaCl at pH 6.

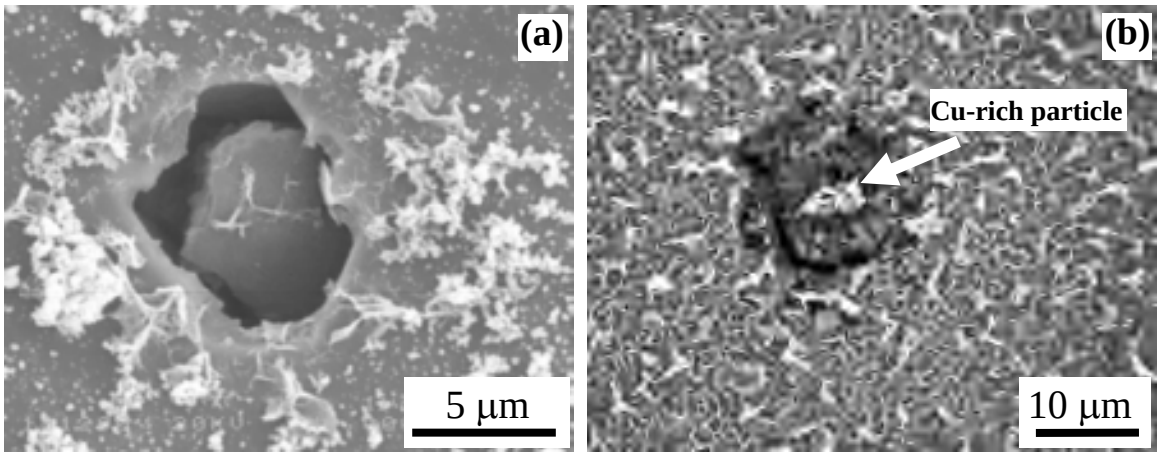

Fig 4.25 SEM images of (a) Z-CP-wq and (b) Z-0.8Cu-wq after 1h immersion in naturally-aerated 0.1 M NaCl at pH 6; Cu-rich particles were responsible for pit initiation as shown in (b).

4.2.3 Linear polarisation resistance (LPR)

The potentiodynamic polarisation experiments described above were relatively short in duration. Meanwhile all electrochemical polarisation measurements were controlled by a potentiostat, which can supply as much current as is needed to support anodic dissolution of the Zn alloys. In reality, for example, in atmospheric corrosion, corrosion occurs under free corrosion conditions, where local cathodes on the surface supply cathodic current to support anodic reactions at the local anodes. To investigate this type of exposure, long term immersion tests were carried out in an accelerated testing solution (described in Section 3.3.2) with an aim of simulating the marine atmosphere corrosion and evaluate the effect of alloying elements on corrosion resistance of Zn.

All Zn alloys were immersed in the air-exposed "accelerated" solution. Linear polarisation resistance (LPR) measurements were carried out at OCP during immersion tests. The LPR technique has been widely used in industrial monitoring because of its ability to react instantaneously to a corrosion situation or change in corrosion rate. The technique was originally developed based on the Stern–Geary theory as described in Section 3.3.4 (Chapter 3). According to this theory, a high LPR corresponds to a low corrosion rate. In this study, the instantaneous R_p was monitored by using a continuous LPR technique which can be achieved by Corrware software for electrochemical measurements.

Fig 4.26 shows the LPR of water-quenched Zn alloys with and without alloying elements as a function of immersion time in the accelerated solution. Except for Z-0.8Cu-wq and Z-Pb-wq, the LPR of all other Zn alloys increases with immersion time after an initial period of 2 h during 20 h immersion tests. Comparison of the LPR after 20 h is given in Fig 4.27. The results show that the addition of Mn significantly increases LPR (inversely related to the corrosion rate) compared with the commercially-pure Zn (Z-CP-wq). The effect of the addition of Cu depends on the concentration, 0.2 wt % Cu shows a beneficial effect while 0.8 wt % Cu shows a deleterious effect on corrosion

resistance. Both 0.2 wt % Zr and 1.0 wt % Sb were found to have no effect on LPR in the accelerated solution. The worse case was found for Z-Pb-wq, which has the lowest LPR among all the Zn alloys. The result is consistent with previous electrochemical polarisation measurements which indicated that Pb promotes pitting corrosion and enhances cathodic reduction reaction.

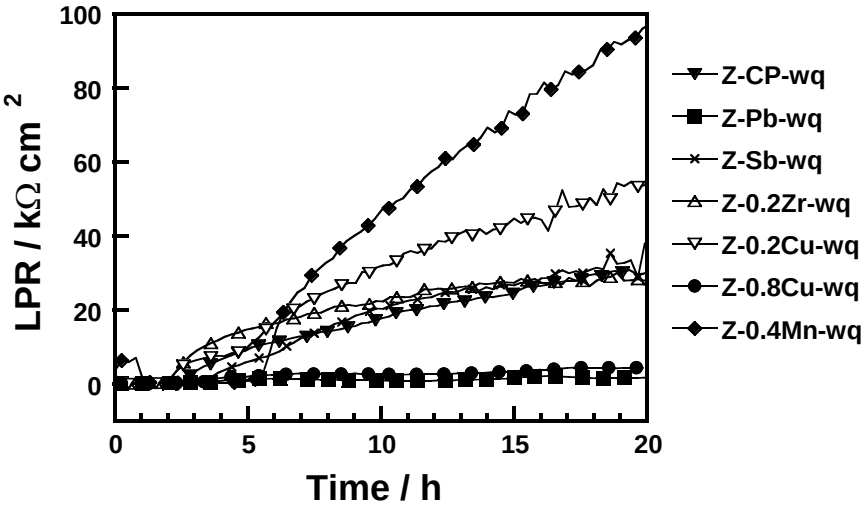

Fig 4.26 Linear polarisation resistance (LPR) of water-quenched Zn alloys as a function of immersion time in the accelerated solution (0.1 M NaCl + 0.1 M Na_2SO_4 + 0.01 M $NaHCO_3$).

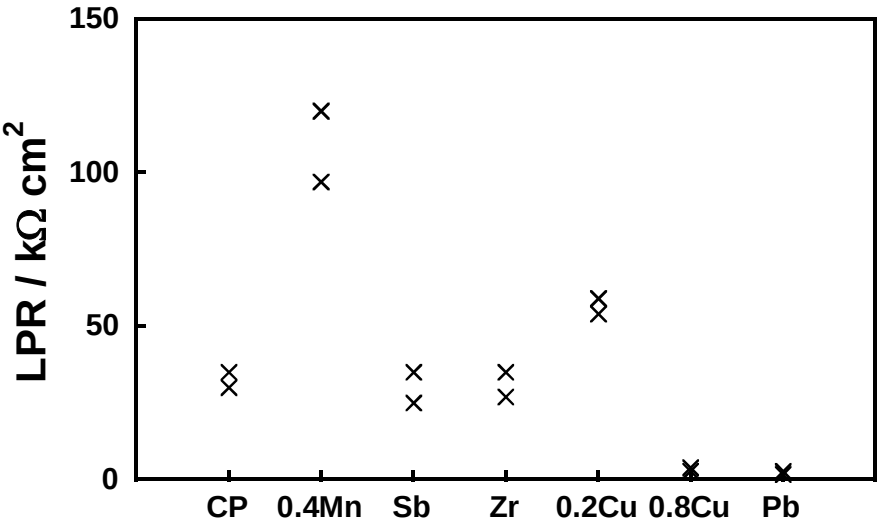

Fig 4.27 Comparison of linear polarisation resistance (LPR) of water-quenched Zn alloys after 20 h immersion test in the accelerated solution (0.1 M NaCl + 0.1 M Na_2SO_4 + 0.01 M $NaHCO_3$).

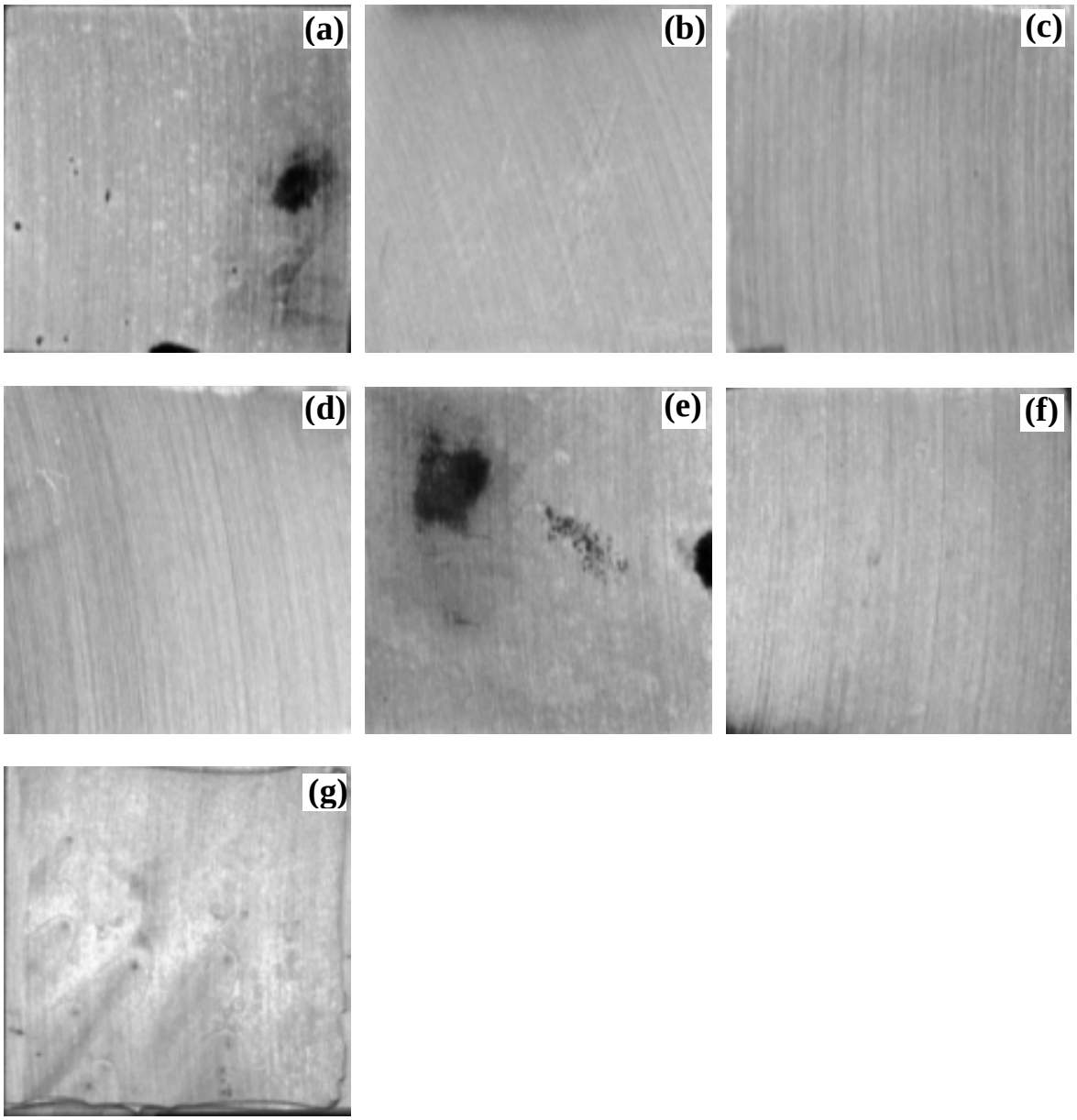

Fig 4.28 Optical images of (a) Z-0.8Cu-wq, (b) Z-Sb-wq, (c) Z-CP-wq, (d) Z-0.2Zr-wq, (e) Z-Pb-wq, (f) Z-0.2Cu-wq, and (g) Z-0.4Mn-wq after LPR tests in the accelerated solution (0.1 M NaCl + 0.1 M Na_2SO_4 + 0.01 M $NaHCO_3$) for 20 h.

Fig 4.28 shows corrosion morphologies of Zn alloys after 20 h immersion tests in the accelerated solution. Localised corrosion occurred on the surface of both Z-0.8Cu-wq and Z-Pb-wq, while other Zn alloys show uniform corrosion on the surface. As shown in previous experiments, Cu-rich intermetallic particles and Pb globules are pit initiation sites and promote cathodic reduction reactions. The very low LPR for both Z-0.8Cu-wq and

Z-Pb-wq is due to pitting corrosion initiated from Cu-rich particles and Pb globules respectively.

4.2.4 Combined additions of Mn and Cu

The previous experiments showed that the addition of Mn inhibits the cathodic reduction reaction and increases LPR in the accelerated solution, while other additions have no effect or a deleterious effect on the corrosion resistance of Zn. Thus Mn was chosen as the main addition to the Zn bath. In this section, the effect of Mn, Cu and their combination on the corrosion of Zn alloys were investigated. Their effect on corrosion of hot dip galvanised coatings will be explored in the following chapters. Cu was chosen as it has a beneficial effect on corrosion at a low level. In addition, about 0.005 wt % Al was added to molten Zn to assist with the hot dip galvanising process. The Zn alloys were subsequently made by air cooling. The detailed chemical compositions of these Zn alloys can be found in Table 3.3.

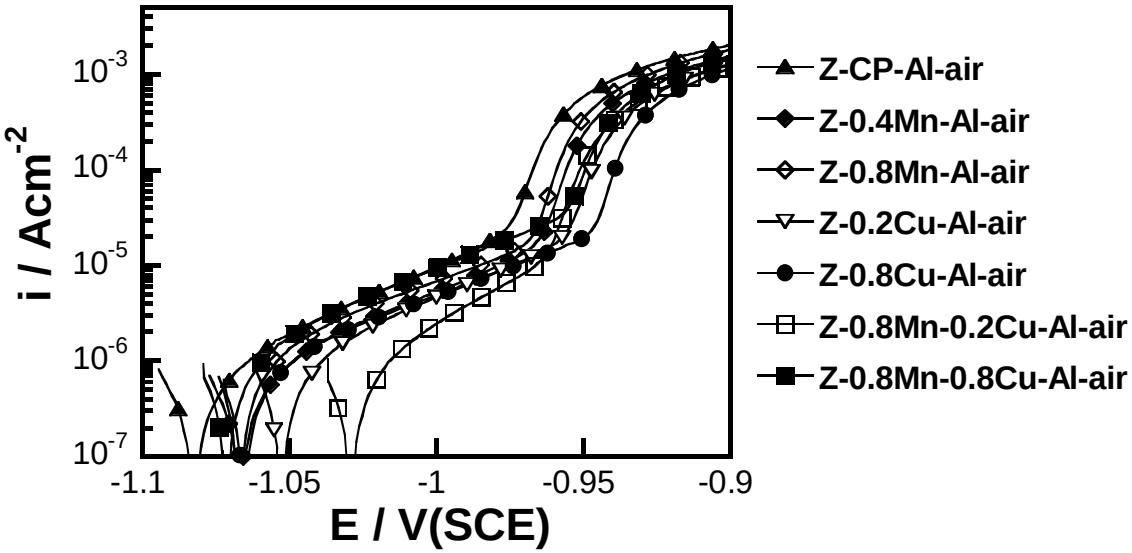

Fig 4.29 Potentiodynamic anodic polarisation curves for air-cooled Zn alloys with Mn, Cu and Al additions in naturally-aerated 0.1 M NaCl at pH 6 with a scan rate of 1 mV/s (tests were started immediately after samples were polished and then rapidly transferred into solution). Before corrosion tests, samples were polished to 4000 grit with SiC paper.

Fig 4.29 shows potentiodynamic anodic polarisation curves for air-cooled Zn alloys with Mn, Cu and Mn-Cu additions in naturally-aerated 0.1 M NaCl at pH 6. A

passive plateau was found for all of the Zn alloys. All Zn alloys with these alloying elements show lower passive currents and higher pitting potential than those without alloying element (Z-CP-Al-air). A Zn alloy with Mn-Cu additions (Z-0.8Mn-0.2Cu-Al-air) showed the lowest passive current density. The data for the pitting potentials and passive currents (at -1.0 V vs SCE) are listed in Table 4.7. The results indicated that Z-0.8Cu-Al-air has the highest pitting potential while Z-CP-Al-air has the lowest value.

The corrosion morphologies of these Zn alloys after anodic polarisation tests are shown in Fig 4.30. Pitting corrosion occurred for all these Zn alloys. It is interesting that pit sizes and densities of these Zn alloys are different (especially for the Cu-containing alloys) from those of Z-CP-Al-air. The pit density of Z-0.8Cu-Al-air was found to be lowest, whereas Z-CP-Al-air showed the highest pits density. Alloys with combined additions of Mn and Cu show fewer but larger pits as shown in Fig 4.30 (f) and (g).

Table 4.7 Comparison of corrosion behaviour of air cooled Zn alloys after anodic polarisation tests in 0.1 M NaCl solution

Zn alloys	Pitting potential [a] (V *vs* SCE), ± 0.005	Passive current density[b] ($\mu A/cm^2$), ± 1.0
Z-CP-Al-air	-0.97	9.5
Z-0.2Cu-Al-air	-0.95	5.0
Z-0.8Cu-Al-air	-0.94	5.0
Z-0.4Mn-Al-air	-0.96	5.0
Z-0.8Mn-Al-air	-0.96	7.0
Z-0.8Mn-0.2Cu-Al-air	-0.955	2.5
Z-0.8Mn-0.8Cu-Al-air	-0.955	9.5

[a] The pitting potential is defined as the potential where the current density reaches 50 $\mu A/cm^2$.

[b] Passive current density is the value at potential of -1.0 V (*vs* SCE) (average of three measurements).

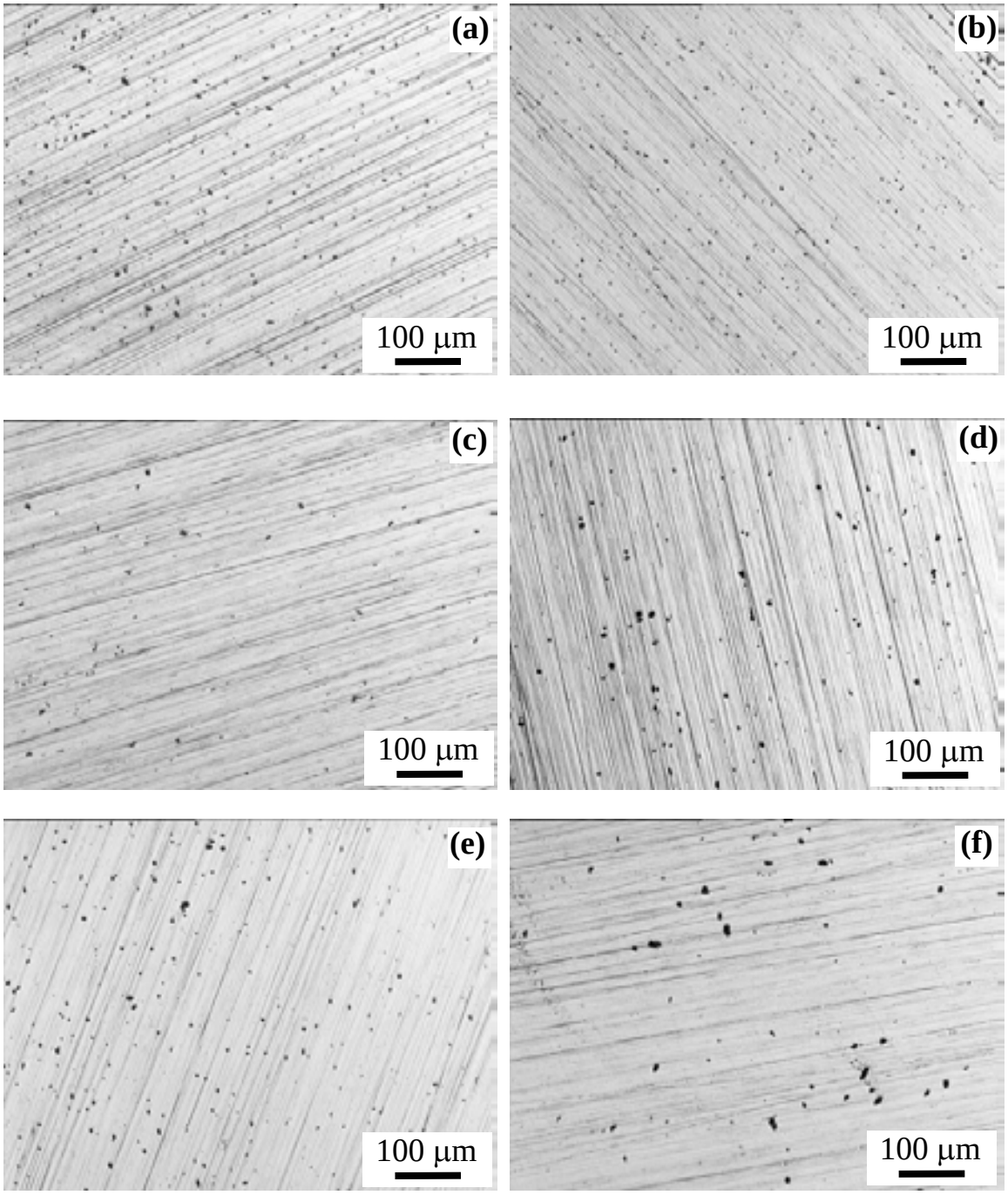

(to be continued)

Fig 4.30 Corrosion morphologies of (a) Z-CP-Al-air, (b) Z-0.2Cu-Al-air, (c) Z-0.8Cu-Al-air, (d) Z-0.4Mn-Al-air, (e) Z-0.8Mn-Al-air, (f) Z-0.8Mn-0.2Cu-Al-air and (g) Z-0.8Mn-0.8Cu-Al-air after potentiodynamic polarisation to the potential of -0.9 V (*vs* SCE) in naturally-aerated 0.1 M NaCl at pH 6.

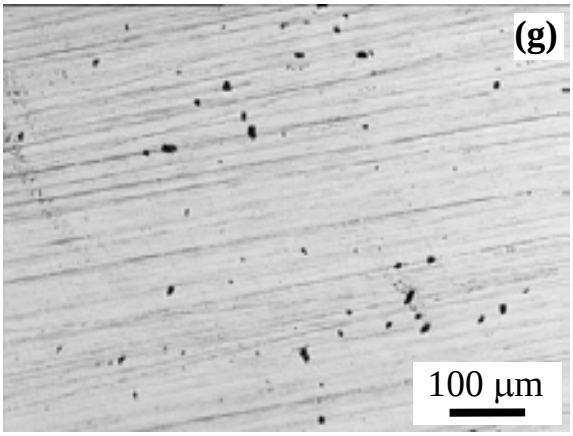

(continued)

Fig 4.30 Corrosion morphologies of (a) Z-CP-Al-air, (b) Z-0.2Cu-Al-air, (c) Z-0.8Cu-Al-air, (d) Z-0.4Mn-Al-air, (e) Z-0.8Mn-Al-air, (f) Z-0.8Mn-0.2Cu-Al-air and (g) Z-0.8Mn-0.8Cu-Al-air after potentiodynamic polarisation to the potential of -0.9 V (*vs* SCE) in naturally-aerated 0.1 M NaCl at pH 6.

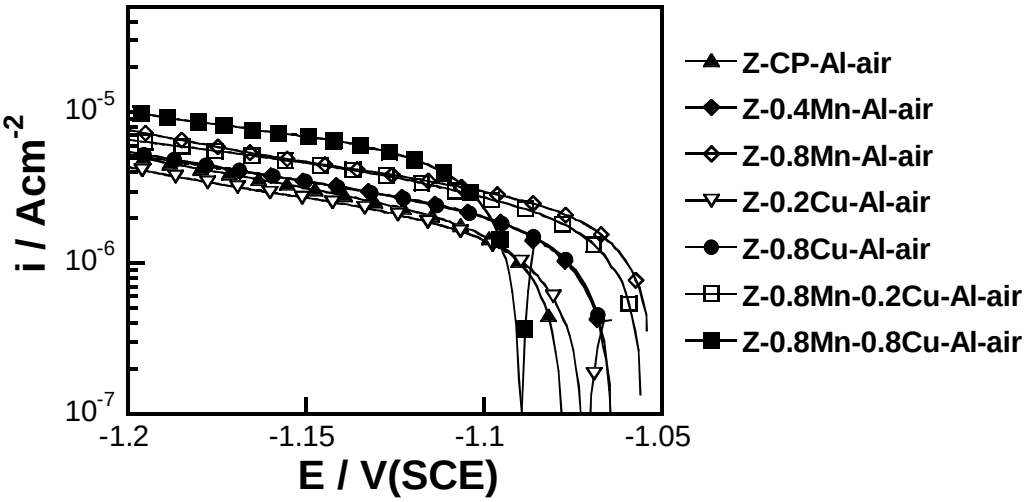

Fig 4.31 Potentiodynamic cathodic polarisation curves for air-cooled Zn alloys with Mn, Cu and Al additions in naturally-aerated 0.1 M NaCl at pH 6 with a scan rate of 1 mV/s (tests were started immediately after samples were polished and then rapidly transferred into solution). Before corrosion tests, samples were polished to 4000 grit with SiC paper.

Cathodic polarisation curves of these alloys in 0.1 M NaCl solution are shown in Fig 4.31. The cathodic current densities at -1.2 V (vs SCE) is summarised in Table 4.8. For comparison, the data of water-quenched Zn (Z-CP-wq) is also listed in Table 4.8. It was found that the cathodic current density of Z-CP-Al-air is lower than that of Z-CP-wq. The reason for this is not clear. A low content of Mn has no effect on cathodic reaction, but a

high content of Mn was found to enhance the cathodic reduction reaction. As shown in the previous section, Mn-rich intermetallic particles were found on Mn-containing Zn alloys especially those with a high level of Mn. It is suggested that the Mn-rich intermetallic particles promote the cathodic reduction reaction on Zn in naturally-aerated 0.1 M NaCl solution. Previous results indicate that a low level of Cu shows no effect, while a high level of Cu promotes the cathodic reduction reaction. The combination of Mn and Cu shows no significant effect on the cathodic reaction when a low level of Cu is added but significantly increases cathodic reaction when a high level of Cu is used. This result suggested that high levels of Cu should be avoided in galvanising if a high corrosion resistance for Zn is required.

Table 4.8 Comparison of cathodic current density of air cooled Zn alloys with Mn and Cu alloying elements in 0.1 M NaCl solution (average of three measurements)

Zn alloys	Cathodic current density at -1.2 V (vs SCE), ($\mu A/cm^2$, ± 1.0)
Z-CP-Al-air	5.0
Z-0.2Cu-Al-air	4.5
Z-0.8Cu-Al-air	5.5
Z-0.4Mn-Al-air	5.5
Z-0.8Mn-Al-air	8.0
Z-0.8Mn-0.2Cu-Al-air	7.0
Z-0.8Mn-0.8Cu-Al-air	10
Z-CP-wq	7.0
Z-0.4Mn-wq	5.0

4.2.4.1 Linear polarisation resistance (LPR)

To investigate the long term corrosion behaviour of the Zn alloys with Mn, Cu and Al additions, LPR measurements of these Zn alloys were also carried out in an accelerated testing solution (described in Section 3.3.2) with an aim of simulating the marine atmosphere corrosion and evaluate the effect of these alloying elements on the corrosion resistance of Zn.

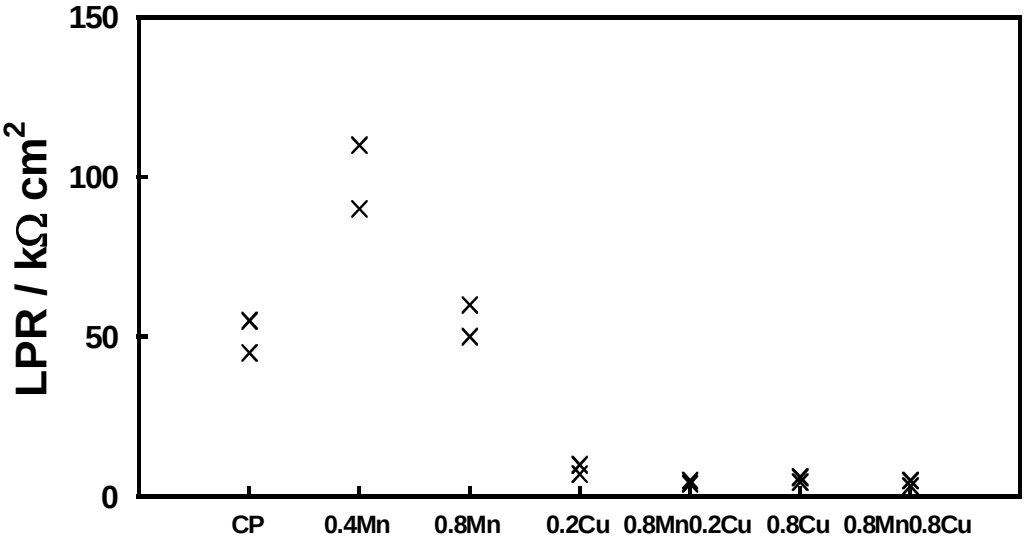

Fig 4.32 Comparison of linear polarisation resistance (LPR) of air cooled Zn alloys with Mn and Cu additions after 20 h immersion test in the accelerated solution (0.1 M NaCl + 0.1 M Na_2SO_4 + 0.01 M $NaHCO_3$).

All of the Zn alloys were immersed in this air-exposed accelerated solution. Linear polarisation resistance (LPR) measurements were carried out at OCP during immersion tests. A comparison of the LPR results after 20 h is given in Fig 4.32. The results show that addition of 0.4 wt % Mn significantly increases LPR (inversely related to the corrosion rate) compared with the commercially-pure Zn (Z-CP-Al-air). This result is in good agreement with the previous results of the water-quenched samples (see Section 4.2.3). Addition of 0.8 wt % Mn had no significant effect on LPR after 20 h exposure in the accelerated solution, although it was found to promote the cathodic reaction on Zn. All other additions significantly decrease LPR.

Fig 4.33 shows the corrosion morphology of air cooled Zn alloys after a 20 h immersion test in the accelerated solution. Localised corrosion occurred on the surface of all Zn alloys except the commercially-pure Zn Z-CP-Al-air. It is suggested that Cu-rich particles are responsible for the pitting corrosion of Cu-containing alloys. The reason for the low LPR of Z-0.2Cu-Al-air compared with the high LPR of Z-0.2Cu-wq is not clear. In this study, the Cu content (0.21 wt %) in Z-0.2Cu-Al-air is higher than that in Z-0.2Cu-wq (0.16 wt %). Thus more tiny Cu-rich particles are likely to form on the surface of

Z-0.2Cu-Al-wq. Although addition of 0.4 wt % Mn increases LPR, localised corrosion was also found on the surface. The high LPR is probably because the corrosion product formed around the pits of Z-0.4Mn-Al-air is protective and subsequently inhibits the dissolution. The corrosion product can be clearly seen on the surface of Z-0.4Mn-Al-air and Z-0.8Mn-Al-air. However, no further study was carried out to confirm this hypothesis. Both Zn alloys with the combination of Mn and Cu (Z-0.8Mn-0.2Cu-Al-air and Z-0.8Mn-0.8Cu-Al-air) showed significantly lower LPR than the commercially-pure Zn (Z-CP-Al-air). This result indicates that Mn additions combined with Cu (0.2 wt % and 0.8 wt %) have deleterious effects on the corrosion resistance of Zn. The Cu-rich particles were not detected in the Mn-Cu containing alloys by SEM (Section 4.1.6). However, Cu-rich intermetallic particles, of a size finer than the resolution limit of the SEM, could be also present in these Cu-containing alloys. As shown in the previous sections, Cu-rich particles are the effective cathodic sites which can significantly decrease the corrosion resistance of Zn.

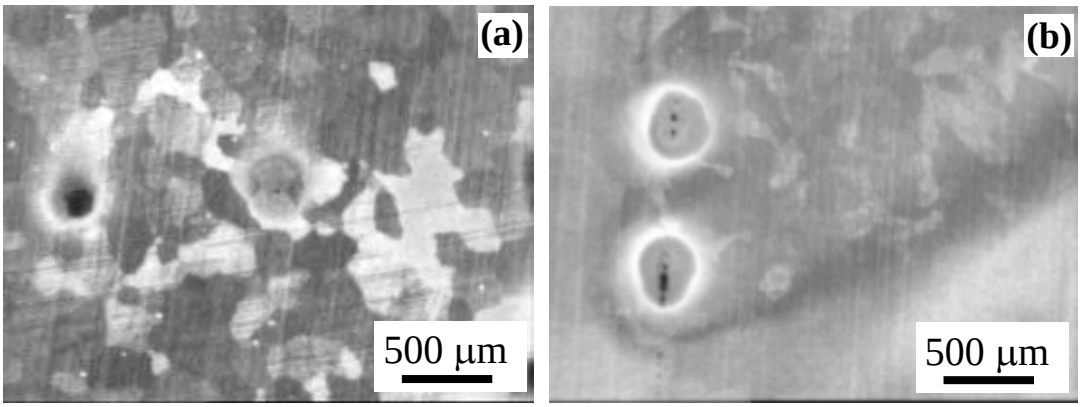

(to be continued)

Fig 4.33 Optical images of (a) Z-0.2Cu-Al-air, (b) Z-0.8Cu-Al-air, (c) Z-0.4Mn-Al-air, (d) Z-0.8Mn-Al-air, (e) Z-0.8Mn-0.2Cu-Al-air, (f) Z-0.8Mn-0.8Cu-Al-air, and (g) Z-CP-Al-air after LPR tests in the accelerated solution (0.1 M NaCl + 0.1 M Na_2SO_4 + 0.01 M $NaHCO_3$) for 20 h.

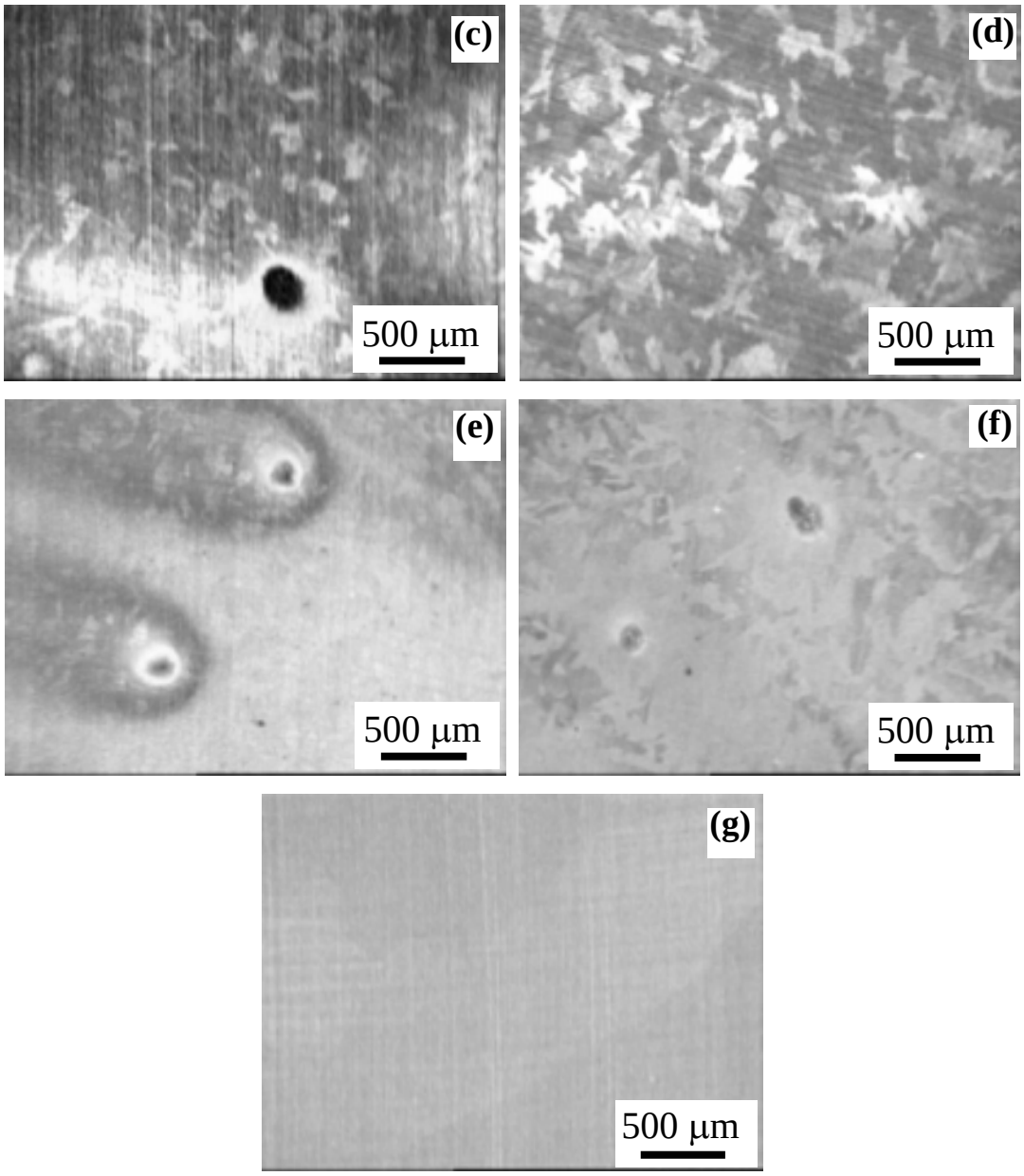

(continued)

Fig 4.33 Optical images of (a) Z-0.2Cu-Al-air, (b) Z-0.8Cu-Al-air, (c) Z-0.4Mn-Al-air, (d) Z-0.8Mn-Al-air, (e) Z-0.8Mn-0.2Cu-Al-air, (f) Z-0.8Mn-0.8Cu-Al-air, and (g) Z-CP-Al-air after LPR tests in the accelerated solution (0.1 M NaCl + 0.1 M Na_2SO_4 + 0.01 M $NaHCO_3$) for 20 h.

4.3 Discussion

4.3.1 Effect of Cu

The present work has shown that the effect of Cu on the corrosion of Zn depends on its content. For the Zn alloys with 0.8 wt % Cu (Z-0.8Cu-wq), pitting corrosion occurred on the surface after immersion and anodic polarisation tests. The Cu-rich particles present in Z-0.8Cu-wq were found to be the catalytic sites for the oxygen reduction reaction as shown in Section 4.2.1. This result indicates that a high content of Cu has a deleterious effect on corrosion resistance of Zn. This was further confirmed by the LPR measurements in the accelerated solution. The low corrosion resistance in the accelerated solution is due to the deleterious effect of the Cu-rich intermetallic particles on enhancing the cathodic reactivity of Zn. The enhanced cathodic reaction at the Cu-rich particles will significantly increase dissolution of Zn around the particles. Thus pits are likely to initiate at the Cu-rich particles as shown in Fig 4.16 and Fig 4.25. Dunbar and Showak [101] reported that adding 1.0 wt % Cu to rolled Zn sheet decreased the corrosion resistance in a severe marine environment. This enhancement of the corrosion rate was attributed to the galvanic cell effect between the Zn matrix and the Cu-rich intermetallic phase which is always found to be an effective cathode site [101]. Nevertheless, the present work also shows that additions of 0.8 wt % Cu slightly increases pitting potential when measurements start immediately upon immersion of the fresh polished samples in the solution. These contradictory effects for Cu content may be explained as follows.

The slightly higher pitting potential after the addition of 0.8 wt % Cu is probably due to the beneficial effect of the dissolved Cu in solid solution. Cu is a more noble element than Zn. It is supposed that Cu atoms will accumulate at the Zn surface as a result of the selective dissolution of Zn, e.g. inside of pits. Therefore the dissolution of Zn will be inhibited due to the blocking effect of the accumulated noble Cu atoms. According to the theory of local acidification for pitting of Zn [94, 98, 104], if the dissolution of Zn is inhibited and not fast enough to maintain sufficient acidity to prevent repassivation, a new

passive film will form and the growth of the pit can stop. This hypothesis provides an explanation of the beneficial effect of dissolved Cu in solid solution. In the literature [133], the pitting potential of the alloy was found to increase with increasing Cu content in solution treated Al-Cu alloys. The alloying elements were found to modify the pitting potential by changing the anodic behaviour of the alloy in the pit-like solution. The maintenance of a localized acidification on the metal-solution interface is the main cause for pitting in Al-Cu alloys [134]. Although this investigation is only made on Al-based alloys, the theory of localized acidification is suitable for both Al and Zn alloy systems [135].

It seems that there is a competition between Cu in the intermetallic particles and the dissolved Cu in the matrix. Under the conditions of open circuit in aerated solutions, the rate of cathodic reduction of oxygen controls the corrosion process. Cu-rich particles are cathodic sites that facilitate oxygen reduction, which drives the corrosion process. Thus, localised corrosion is likely to develop at these areas and the corrosion resistance is then significantly reduced. It is therefore expected that more Cu in solid solution and less in intermetallic particles would make a Zn-Cu alloy with higher corrosion resistance.

Based on the above discussion, additions of 0.2 wt % Cu may have a beneficial effect on the corrosion resistance of Zn as there are no detectable Cu-rich intermetallic particles in this alloy (Fig 4.6). The results show that addition of 0.2 wt % Cu has no detectable effect on both the anodic and cathodic reactivity. As Cu-rich particles in Zn alloys have deleterious effects on corrosion resistance, the corrosion resistance of Zn alloys with Cu additions is mainly depend on whether the Cu is completely dissolved in the Zn matrix. With the addition of 0.2 wt % Cu, both higher (Fig 4.26) and lower LPR (Fig 4.32) values were found in the accelerated solution. This is probably because the Zn alloy used for the LPR tests (Fig 4.32) has a slightly higher Cu content (0.21 wt % Cu) than that (0.16 wt % Cu) used for the LPR tests (Fig 4.26). Thus more Cu-particles are likely to be developed in the alloy with more Cu content.

4.3.2 Effect of Mn

Mn has been shown to be the most promising alloying element for increasing the corrosion resistance of Zn alloys. The results of electrochemical polarisation confirmed its beneficial effect.

Without small Al additions (0.005 wt %), addition of 0.4 wt % Mn can decrease the cathodic reactivity of Zn, but has no significant effect on the anodic activity. When small Al additions were also made to the Zn bath, addition of 0.4 wt % Mn had no detected effect on both anodic and cathodic reactivity; while addition of 0.8 wt % Mn slightly increases the cathodic reactivity. This result indicates that Mn-rich particles are effective cathodic sites. However, Mn-rich intermetallic particles were not found to be pit initiation sites (see Section 4.2.1.1).

The inhibition of the cathodic reduction reaction is probably due to the formation of passive film or Mn_2O_3 on the surface, which is reported to suppress oxygen reduction at the cathode, slowing the corrosion process [13]. Mn-rich intermetallic particles were found in the Mn-containing alloys especially with a high level of Mn (0.8 wt %). Electrochemical cathodic polarisation shows that Mn-rich particles slightly enhance the cathodic reactivity of Zn. Thus, from a corrosion point of view, Mn-rich intermetallic particles in Zn may not have a deleterious effect on corrosion resistance.

The present work has also shown that Mn additions can increase the LPR after 20 h in the accelerated solution (Fig 4.26 and Fig 4.32). Corrosion products were formed on the surface of Mn-containing alloys after 20 h LPR tests as shown in Fig 4.33. The higher LPR indicates that the corrosion products formed on the Mn-containing alloys are more protective against corrosion. In the literature, Boshkov *et al.* [12] reported that a Zn-11 wt % Mn alloy has higher corrosion resistance than pure Zn. He suggested that the high corrosion resistance is due to the rapid formation of corrosion product $Zn_5(OH)_8Cl_2{\cdot}H_2O$ (ZHC) on the Zn-Mn alloy. Mn is electrochemically a more negative element than Zn: it dissolves first as Mn^{2+}, causing evolution of hydrogen and consequently

a slight increase in pH, which favours the formation of ZHC. It is general believed that ZHC is more compact than ZnO [118] and it can decrease the oxygen reduction rate [117]. Thus it is supposed that the high corrosion resistance achieved by the addition of Mn to Zn is due to the formation of a more compact corrosion product which can decrease the cathodic reactivity of Zn. From the long term corrosion point of view, the ability to form a more protective corrosion product is very important.

4.3.3 The combined effect of Mn-Cu additions

The combination of Mn and Cu shows no significant effect on the rate of the cathodic reaction when a low level of Cu is added but significantly increases the rate of the cathodic reaction when high level of Cu is used. This result indicates that the Cu addition dominates the corrosion behaviour of Zn when the combined additions of Mn and Cu are used. The results of LPR measurements in the accelerated solution show that the combination of Mn and Cu decreases the LPR compared with commercially-pure Zn (Z-CP-wq). The low corrosion resistance in the accelerated solution is probably due to the deleterious effect of the Cu-rich intermetallic particles which increase the cathodic reactivity of Zn.

4.3.4 Effect of Pb

Pb has been shown to have deleterious effect on corrosion resistance of Zn alloys. This is because Pb globules promote both anodic and cathodic reactivity of Zn. Pb has very low solubility in Zn and thus significant amount of Pb globules can be found in Zn. Pb was reported to promote anodic activity of Zn in the literature [38, 129, 136, 137]. It was suggested that the interstitial localisation of Pb can cause tension in the crystalline lattice, creating greater heterogeneity in the surface, and therefore increasing the surface activity [137]. Pyun [136] found that the alloying element Pb promotes anodic dissolution of the hot-galvanised Zn layer over all potential ranges in alkaline solution. The present work has also demonstrated that Pb enhances the cathodic reactivity of Zn. Thus Zn alloy

containing Pb shows the lowest corrosion resistance.

4.3.5 Effect of Sb

The present work has shown that addition of Sb had no significant effect on both anodic and cathodic reactivity of Zn. This is consistent with the observation that Sb-rich particles are not pit initiation sites as shown in Fig 4.16. Meanwhile, LPR measurements show no obvious difference after the addition of Sb to Zn. In literature, there is no published work concerning the effect of Sb on the corrosion of Zn alloys. However, Sb was found to have a slightly beneficial effect on corrosion resistance of hot dip galvanised coatings [17, 18]. It has been reported by Rädeker [17] that Sb reduced weight loss over 3 years in an industrial atmosphere by 20 %.

4.3.6 Effect of Zr

The Effect of Zr additions on the corrosion of Zn has not been reported in the literature. Its effect on corrosion behaviour of Zn is complex. It was found in the present study that Zr can slightly decrease the cathodic reactivity of Zn (Fig 4.17, Fig 4.20 and Fig 4.22). However, LPR of Z-0.2Zr-wq after 20h in the accelerated solution does not show a higher value than that of Z-CP-wq. The mechanism for the effect of Zr on cathodic reactivity of Zn is not clear. It was also found that Zr-rich particles acted as pit initiation sites as shown in Fig 4.16. Surprisingly, in the accelerated solution, no obvious pitting was observed on Z-0.2Zr-wq. Thus, further work is required to propose an explanation for this result.

As Zr has no beneficial effect on the improvement of the corrosion resistance of Zn, atmospheric corrosion tests of the Zr-containing coatings were not investigated in this study.

4.4 Summary

Pitting is the main form of corrosion of Zn, and the corrosion rate is mainly controlled by the cathodic reduction of oxygen in naturally-aerated solutions. Among the alloys developed in this study, Mn shows the greatest promise for improving the corrosion resistance of Zn. The beneficial effect of Mn addition is probably due to the formation of Mn oxide that can great inhibit the cathodic reactivity of Zn. Although Mn-rich particles slightly promote the cathodic reaction, the corrosion products formed around this particle can effectively protect Zn from further dissolution.

Pb globules and Cu-rich intermetallic particles are catalytic sites for the oxygen reduction reaction and are also the initiation sites for pitting. Thus addition of Pb and a high content of Cu have a deleterious effect on the corrosion resistance of Zn. However, Cu if in solid solution was found to increase the corrosion resistance of Zn.

Sb-rich particles are not catalytic sites for the oxygen reduction reaction or pit initiation sites, thus no significant effect can be observed after the addition of Sb to Zn. No significant effect of Zr additions on the corrosion behaviour of Zn was observed, although Zr-rich particles were found to be pit initiation sites.

The effect of the addition of Mn and Cu in combination mainly depended on the Cu content. Mn combined with a high Cu content can significantly decrease the corrosion resistance of Zn.

CHAPTER 5 MICROSTRUCTURE OF HOT DIP GALVANISED COATINGS

In this chapter, the effects of alloying additions (Cu, Sb, Zr and Mn) on the microstructure and alloy layer thickness of hot dip galvanised coatings were investigated. As shown in the previous results (see Chapter 4), Mn has the greatest beneficial effect on improving the corrosion resistance of Zn. Thus, the work in this chapter will focus on the effect of Mn additions. The effect of the alloying elements on corrosion behaviour of hot dip galvanised coatings will be explored in Chapter 6.

5.1 Effect of alloying elements on the microstructure of galvanised layers

5.1.1 Commercially-pure Zn

Fig 5.1 (a) and (b) show the typical microstructure of a water-quenched hot dip galvanised coating on 0.2 wt % Si steel at 450^{o}C after 90 s immersion in a commercially-pure Zn bath with and without addition of 0.005 wt % Al, respectively. It is evident that both coatings show similar microstructure and coating thickness, which indicates that the small Al addition has no effect on both the microstructure and alloy layer growth of hot dip galvanised coatings.

It is shown in Fig 5.1 that different layers of alloy phases (eta, zeta and delta) can be clearly seen on the etched surface. The gamma phase should be present between the steel substrate and the delta phase layer. However, it is difficult to see due to the low thickness (less than 1 μm). Identification of each of these phases (except gamma) was supported by quantitative SEM/EDX measurements of the Fe content. The delta phase has a columnar morphology, probably due to preferred growth perpendicular to the interface in a direction along the (0001) basal plane of the hexagonal structure [21]. The zeta phase also

has a columnar morphology adjacent to the delta phase layer.

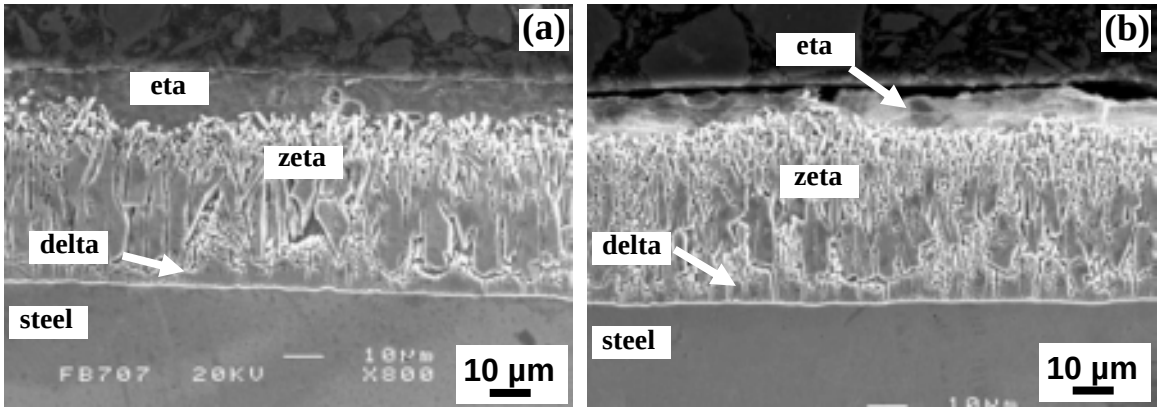

Fig 5.1 SEM image of an etched hot dip galvanised coating on 0.2 wt % Si steel after immersion at 450^{o}C for 90 s: (a) G-CP-Al-wq, and (b) G-CP-wq.

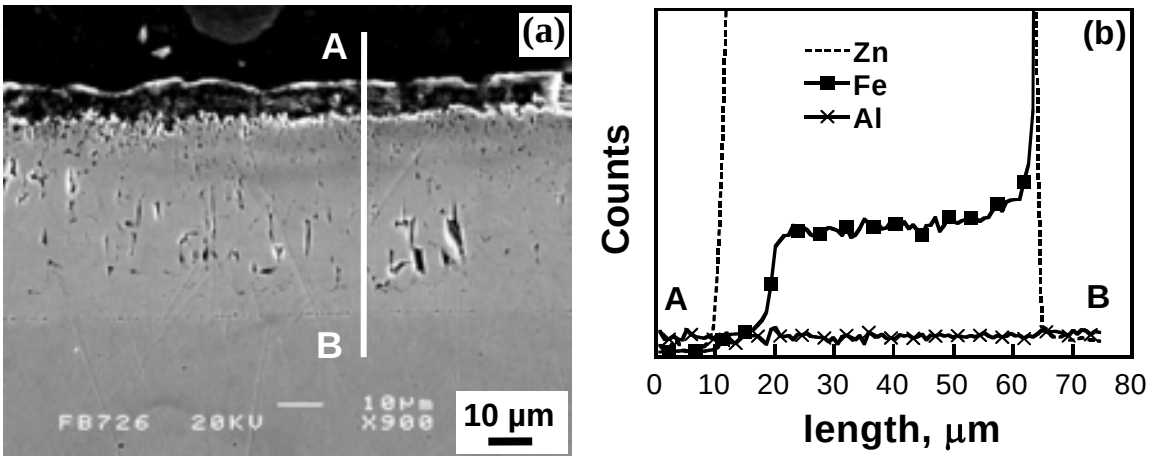

Fig 5.2 (a) SEM image of the as polished hot dip galvanised coating G-CP-Al-wq on 0.2 wt % Si steel at 450^{o}C for 90 s, and (b) EDX line scan across coating layer from A to B in (a).

EDX line scans were carried out across coating layers on unetched samples to determine the distribution of alloying elements. The EDX line scans of G-CP-Al-wq are shown in Fig 5.2. The Fe content was found to increase rapidly when the line scan reached the zeta layer and then increase gradually towards the steel substrate. A sharp increase of Fe content occurred again at the steel substrate. This result is consistent with previous findings of the Fe distribution in the coating [21].

It has been reported that there are Al oxides on the top surface of hot dip galvanised coatings with small Al additions [20, 21]. However SEM line scans reveal that

there is no detectable Al in the coating, as shown in Fig 5.2. This is not surprising since the oxide is very thin, beyond the resolution limit of the SEM.

5.1.2 Commercial Zn containing Pb

The microstructure of a hot dip galvanised coating on 0.2 wt % Si steel at 450^{o}C after a 90 s immersion in a commercial Zn bath containing about 1.0 wt % Pb (G-Pb-wq) is shown in Fig 5.3. A similar coating structure of alloy layers was found to that for the coating G-CP-wq. Pb globules were mainly found in the eta phase layer by SEM backscattered electron imaging as shown in Fig 5.3 (b). This result is in agreement with previous results that Pb globules are present in Pb-containing commercial Zn alloys (Section 4.1.1).

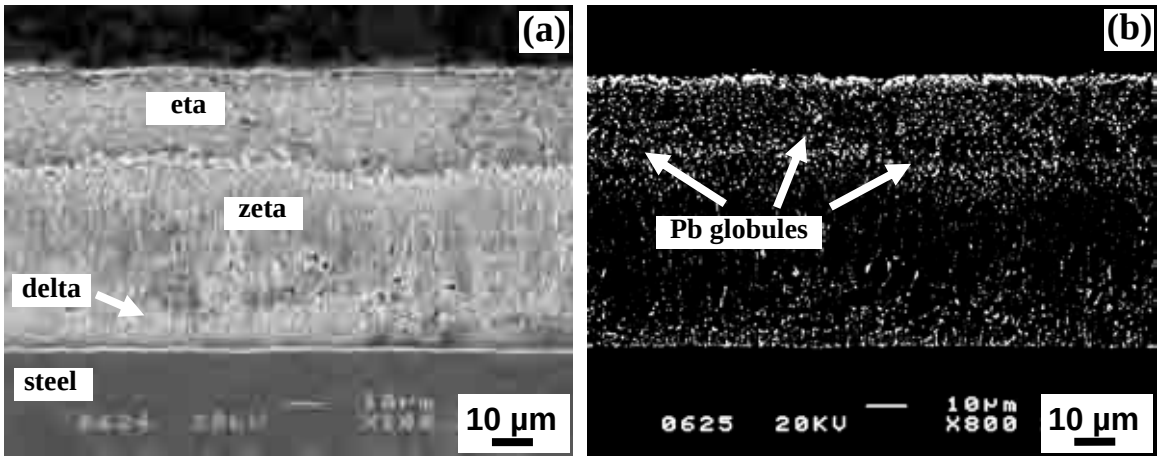

Fig 5.3 SEM images of an etched hot dip galvanised coating of G-Pb-wq on 0.2 wt % Si steel at 450^{o}C for 90 s: (a) secondary electron (SE) image, and (b) backscattered electron (BE) image showing Pb globules mainly precipitated in the eta layer.

5.1.3 Addition of Sb

The microstructure of a hot dip galvanised coating with the addition of 1.0 wt % Sb (G-Sb-wq) is shown in Fig 5.4. Both delta and zeta phase layers show typical columnar morphology. The SEM/EDX analysis reveals that there is no detectable Sb in the alloy phase matrix. However significant numbers of Sb-rich particles are found in the eta

phase layer as shown in Fig 5.4 (b). This is reasonable as the solubility of Sb in solid Zn is extremely low at room temperature [24]. EDX analysis of the particles shows that apart from the Sb peak, a small Fe peak was also found in the EDX spectrum of the Sb-rich particles as shown in Fig 5.4 (c).

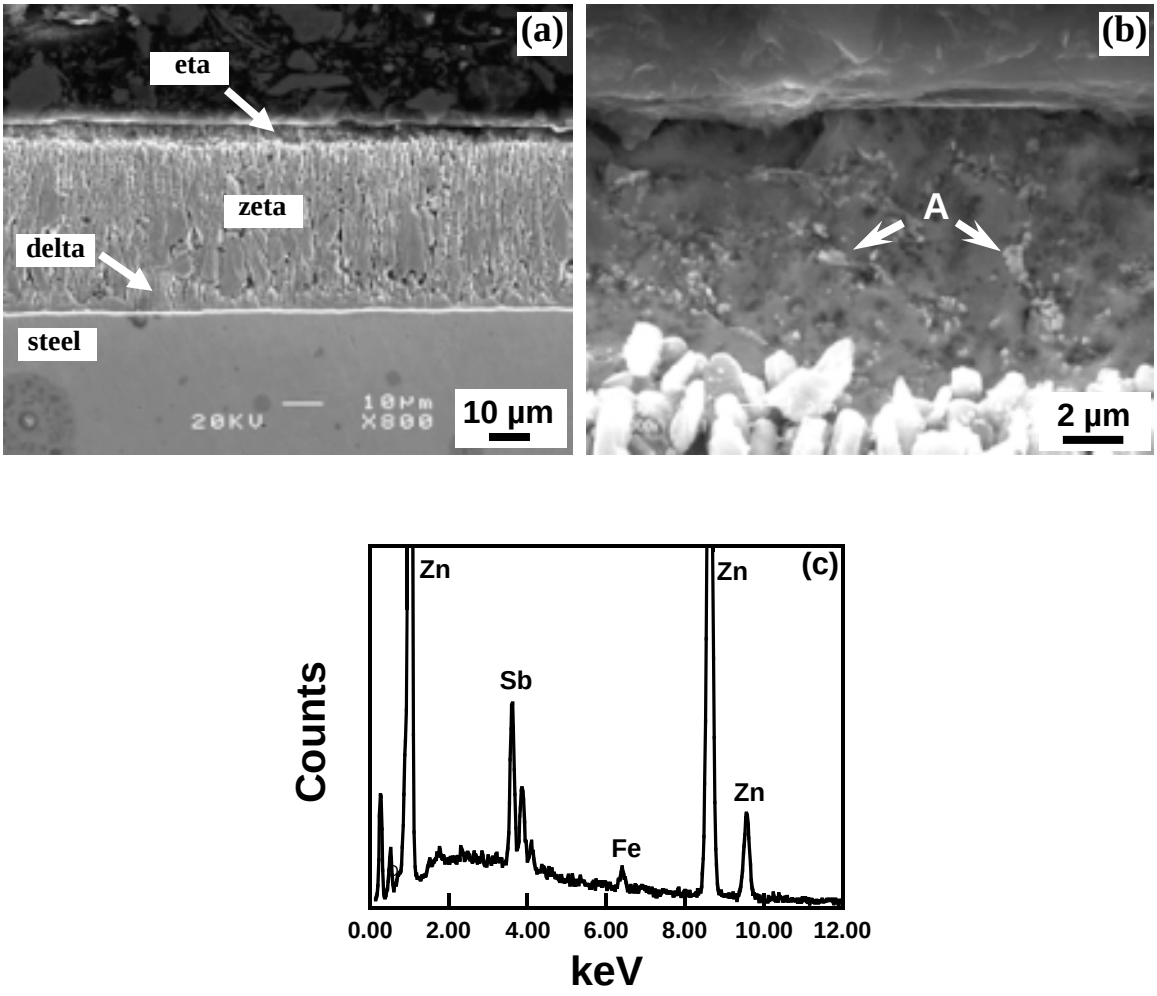

Fig 5.4 SEM images of the etched hot dip galvanised coating G-Sb-wq on 0.2 wt % Si steel at 450^{o}C for 90 s: (a) the coating, and (b) eta phase layer; (c) EDX spectrum of Sb-rich particles as shown with arrow A in (b).

5.1.4 Addition of Zr

The typical microstructure of the hot dip galvanised coating on 0.2 wt % Si steel at 450^{o}C for 90 s immersion with the addition of 0.2 wt % Zr (G-0.2Zr-wq) is shown in Fig 5.5. Both delta and zeta phase layers show typical columnar morphology. A smooth zeta-eta interface boundary was observed for this coating as shown in Fig 5.5. No Zr was detected in the alloy phase matrix. However, Zr-rich intermetallic particles (about 2 μm in size) were found in the eta phase layer as shown in Fig 5.5. The EDX line scans and spectra reveal that these intermetallic particles are rich in both Fe and Zr.

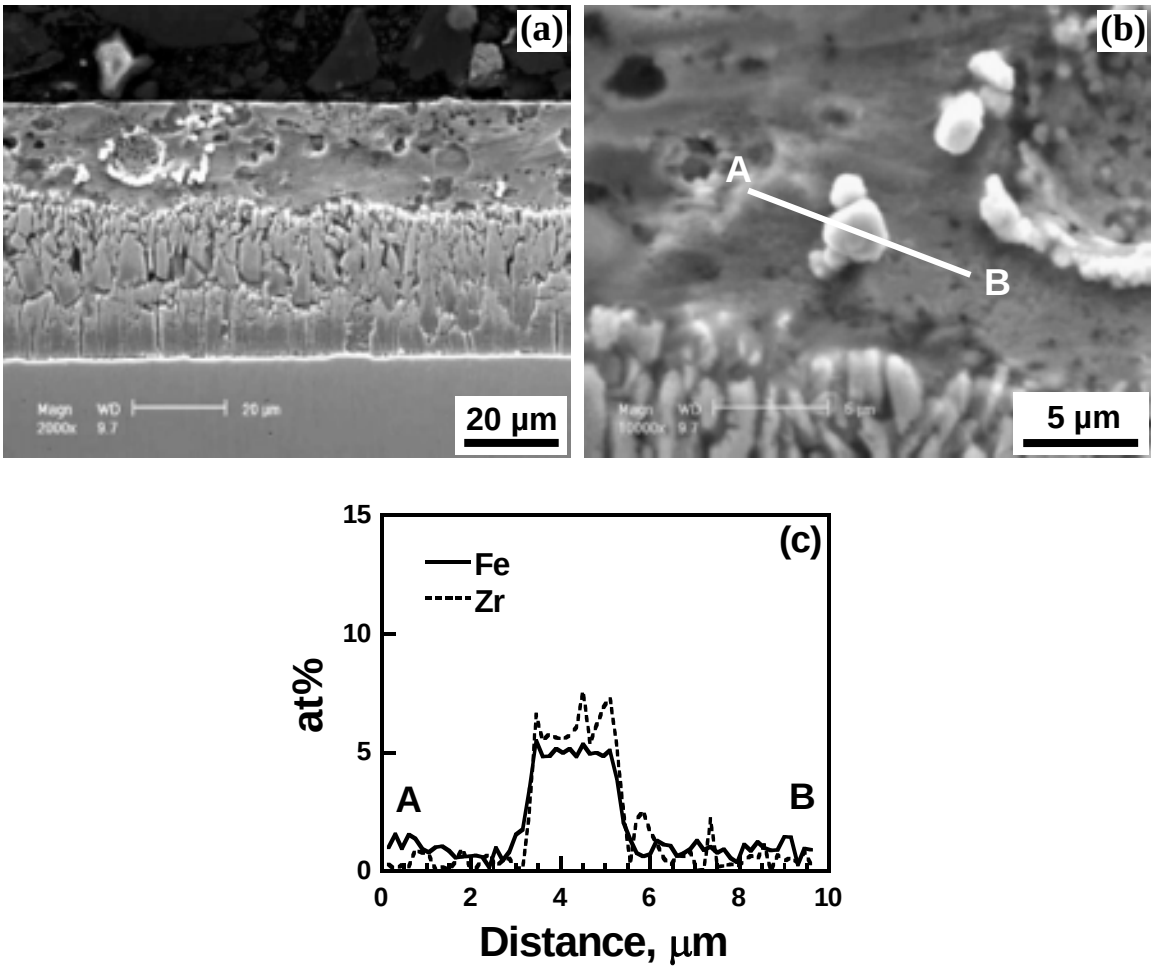

Fig 5.5 SEM images of etched hot dip galvanised coating G-0.2Zr-wq on 0.2 wt % Si steel at 450^{o}C for 90 s: (a) the coating, and (b) eta layer; (c) EDX line scan across Zr-rich particles as shown by the white line from A to B in (b).

5.1.5 Addition of Cu

The typical microstructures of the coating on 0.2 wt % Si steel at 450^{o}C for 90 s after immersion in the galvanising bath containing up to 0.8 wt % Cu are shown in Fig 5.6. The coating morphology was found to depend on the concentration of Cu additions. The addition of 0.2 wt % Cu has no effect on the coating morphology compared with G-CP-wq as shown in Fig 5.1 (b) and Fig 5.6 (a). However, the addition of 0.8 wt % Cu to the bath has an effect on the coating morphology (Fig 5.6 (b)). EDX line scans of the cross section of G-0.2Cu-wq and G-0.8Cu-wq indicates that Cu is incorporated into the Fe-Zn alloy layer of both hot dip galvanised coatings as shown in Fig 5.6 (c) and (d). No detectable Cu-rich particles were found in the eta layer of both coatings.

EDX microanalysis of the alloy phases on G-0.2Cu-wq reveals that there is about 0.8 wt % Cu and 0.6 wt % Cu incorporated into the zeta phase and delta phase, respectively. Table 5.1 summaries the compositions of the phases in the hot dip galvanised coating G-0.8Cu-wq indicated with the arrows C, D, E and F in Fig 5.6 (b). The result indicates that the alloy layers are ternary Zn-Fe-Cu compounds. The compositions of the phases at positions D and E are quite similar, containing about 3 wt % Cu, 6 wt % Fe and 91 wt % Zn. The Fe content of this phase is somewhat similar to the Fe content of the zeta phase in the binary Fe-Zn system. Similar results were also found by Katisforis *et al* [77], who studied the influence of Cu (up to 3 wt %) on the structure and thickness of hot dip galvanised coatings. They found that about 3 wt % Cu was incorporated into the alloy layers to form a ternary Zn-Fe-Cu phase. They claimed that the ternary phase containing 3 wt % Cu and 6 wt % Fe was not zeta phase but delta phase based on X-ray diffraction investigations [77]. This implies that 0.8 wt % Cu promotes the formation of delta phase and inhibits the growth of zeta. The delta layer becomes thicker at the expense of the zeta phase, which practically disappears. Above it, and up to the surface of the coating there is a mixture of fragmented crystals and some crystals interspersed in a matrix of Zn.

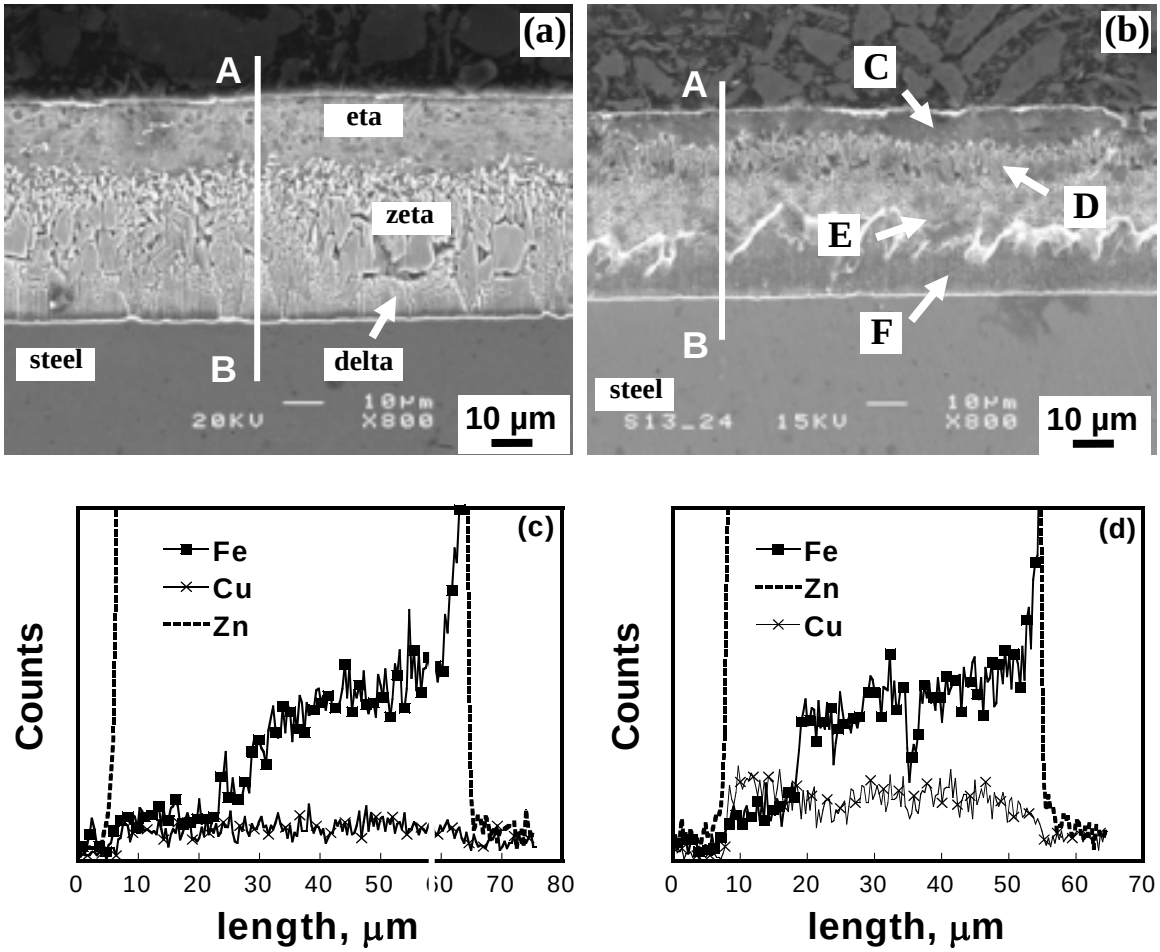

Fig 5.6 SEM images of the etched hot dip galvanised coating on 0.2 wt % Si steel at 450^{o}C for 90 s: (a) G-0.2Cu-wq, and (b) G-0.8Cu-wq; (c) EDX line scan across coating layer (G-0.2Cu-wq) from A to B in (a), and (d) EDX line scan across coating layer (G-0.8Cu-wq) from A to B in (b). Points C, D, E and F show the location of EDX measurements shown in Table 5.1.

Table 5.1 EDX microanalysis of the phases of hot dip galvanised coating G-0.8Cu-wq on 0.2 wt % Si steel at 450^{o}C for 90 s immersion

position	Fe, wt %	Cu, wt %
C (eta)	-	0.8 ± 0.1
D (delta)	5.5 ± 0.2	3.3 ± 0.1
E (delta)	6.1 ± 0.2	3.1 ± 0.1
F (delta)	9.7 ± 0.3	1.7 ± 0.1

5.1.6 Addition of Mn

5.1.6.1 The microstructure of galvanised layers

Fig 5.7 shows the typical microstructure of the water-quenched hot dip galvanised coating on 0.2 wt % Si steel in a Zn bath containing 0.4 wt % Mn. Different layers of alloy phases (eta, zeta and delta) can be clearly seen on the etched surface. Both delta and zeta phases have compact columnar morphologies. No obvious Mn-rich particles are found in the eta layer as shown in Fig 5.7 (b).

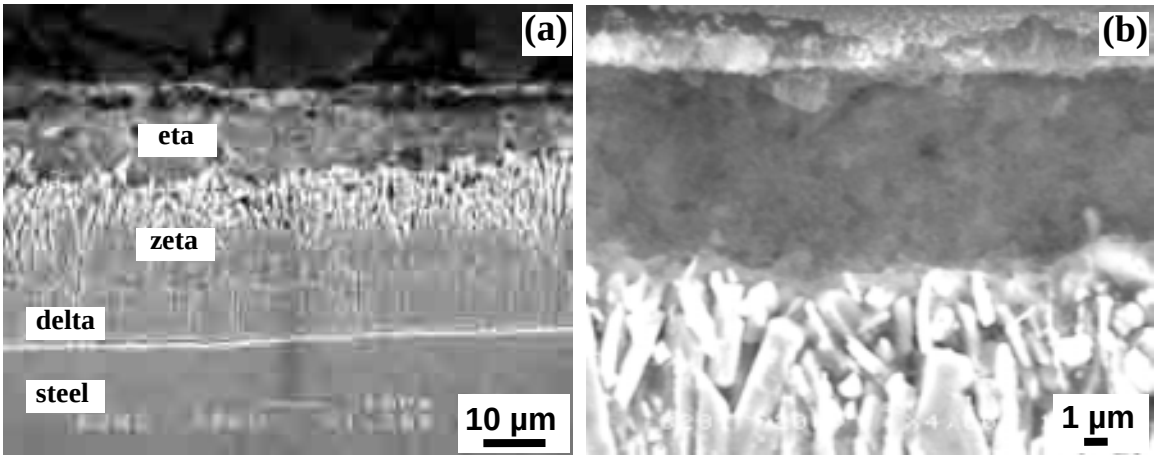

Fig 5.7 SEM image of an etched hot dip galvanised coating (G-0.4Mn-wq) on 0.2 wt % Si steel at 450^{o}C for 90 s: (a) the coating, and (b) the eta layer.

The variations in Mn and Fe concentrations across the Mn-containing coating (0.4 wt % Mn) are shown in Fig 5.8. The level of Mn in the eta layer was relatively constant, but increased rapidly to a maximum at about 0.9 wt % at the outer edge of the zeta phase. Across the zeta phase, a declining composition gradient was indicated. This was followed by a sudden drop at the zeta/delta interface and a further continuous decrease through the delta phase until a minimum was reached near the gamma boundary. Beyond this minimum in the delta layer, there was a rise in Mn in the interface of alloy layer/steel. This is not surprising as there is about 0.65 wt % Mn in the steel substrate. It would appear, therefore, that the zeta phase has a high affinity for Mn. The minimum Mn content located

in the delta phase indicated that the Mn in the coating was derived primarily from the galvanising bath (0.4 wt % Mn) and not the steel substrate. Furthermore, it is obvious that there is maximum peak of Mn content across the top surface of the hot dip galvanised coating. This indicates that Mn segregates on the top surface. A close view of the cross section of the Mn-rich layer is shown in Fig 5.9 (a). EDX line scan analysis (Fig 5.9 (b)) confirms the above observations that there is a Mn-rich layer on the top surface. The thickness of this layer is estimated to be 0.75 μm.

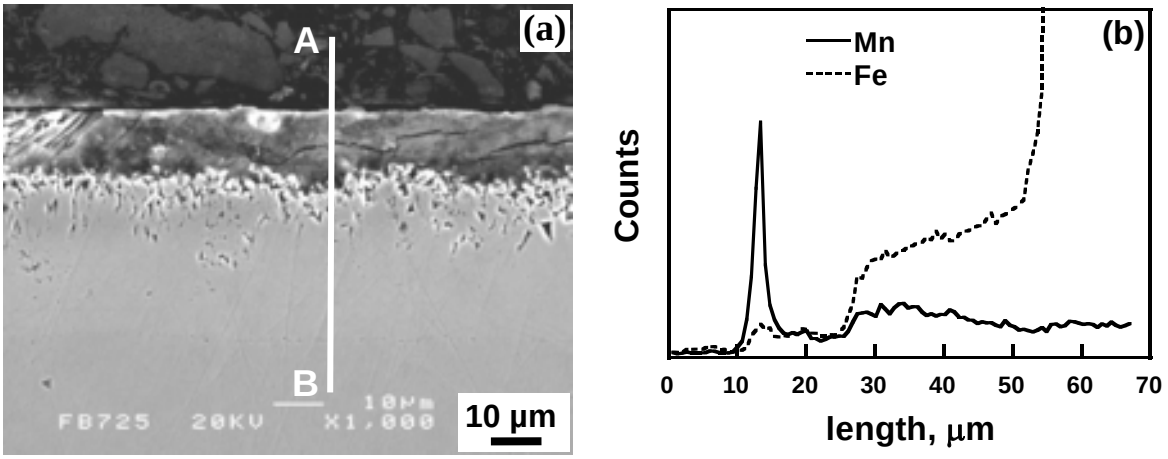

Fig 5.8 (a) SEM image of as polished hot dip galvanised coating on 0.2 wt % Si steel at 450°C for 90 s (water-quenched G-0.4Mn-wq), and (b) EDX line scan across whole coating as shown by the white line from A to B in (a).

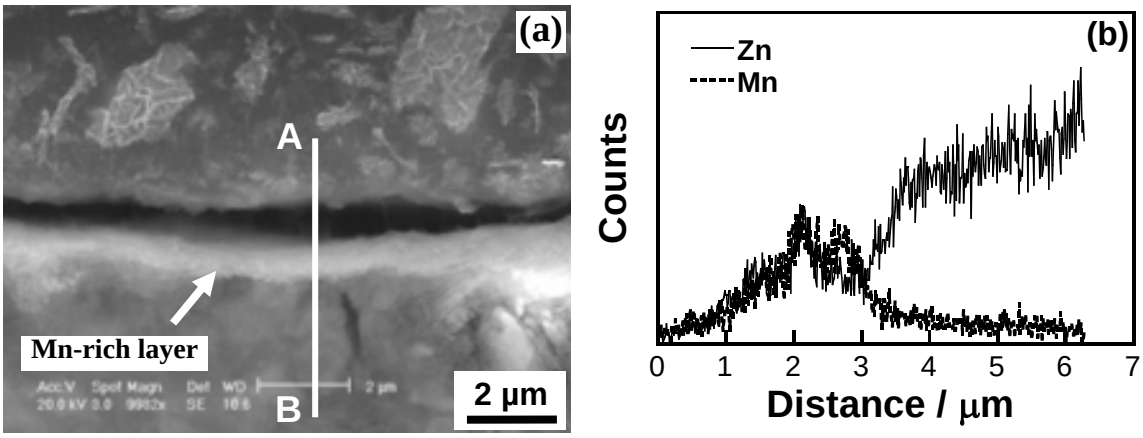

Fig 5.9 (a) SEM image of the cross section of the top surface of the hot dip galvanised coating on 0.2 wt % Si steel at 450°C for 90 s (as polished G-0.4Mn-wq), and (b) EDX line scan across top surface from A to B in (a).

To suppress the oxidation of the molten Zn, a small addition of 0.005 wt % Al was added to the galvanising bath. The microstructure and EDX line scan analysis of the Mn-containing coating after addition of 0.005 wt % Al (G-0.4Mn-Al-wq) is shown in Fig 5.10. It was found that the Mn peak across the top surface disappeared. These localized areas of Mn concentration of G-0.4Mn-wq are also verified by the EDX elemental maps as shown in Fig 5.15. Significant Mn concentration can be clearly seen at the cross section of the top surface and in the Zn-Fe alloy layers. But for the coating with addition of 0.005 wt % Al (G-0.4Mn-Al-wq), no Mn enrichment was observed at the top surface as shown in Fig 5.12. This result indicates that Al can inhibit the formation of the relatively thick Mn-rich layer on the top surface of the Mn-containing coatings during hot dip galvanising. Due to the resolution limit of SEM, further XPS and AES were carried out on the hot dip galvanised coating G-0.4Mn-Al-wq. The result will be shown in Section 5.1.6.3.

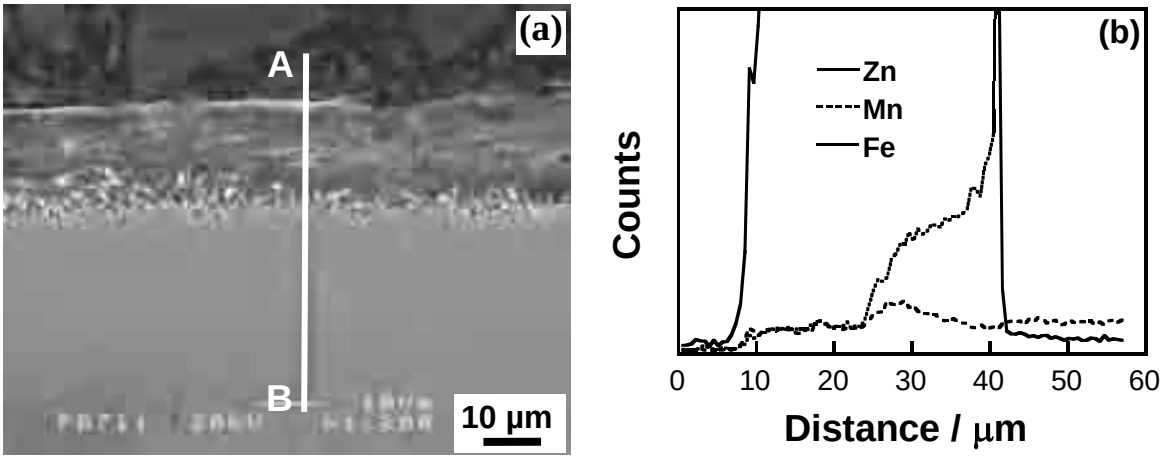

Fig 5.10 (a) SEM image of the as polished hot dip galvanised coating (G-0.4Mn-Al-wq) on 0.2 wt % Si steel, and (b) EDX line scan across whole coating from A to B in (a).

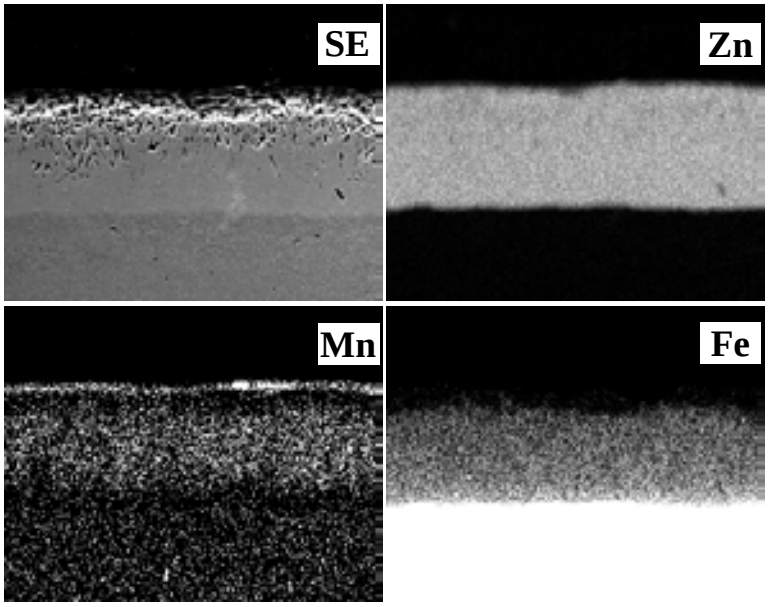

Fig 5.11 SEM image and EDX maps of cross section of hot dip galvanised coating on 0.2 wt % Si steel at 450^{o}C for 90 s (G-0.4Mn-wq)

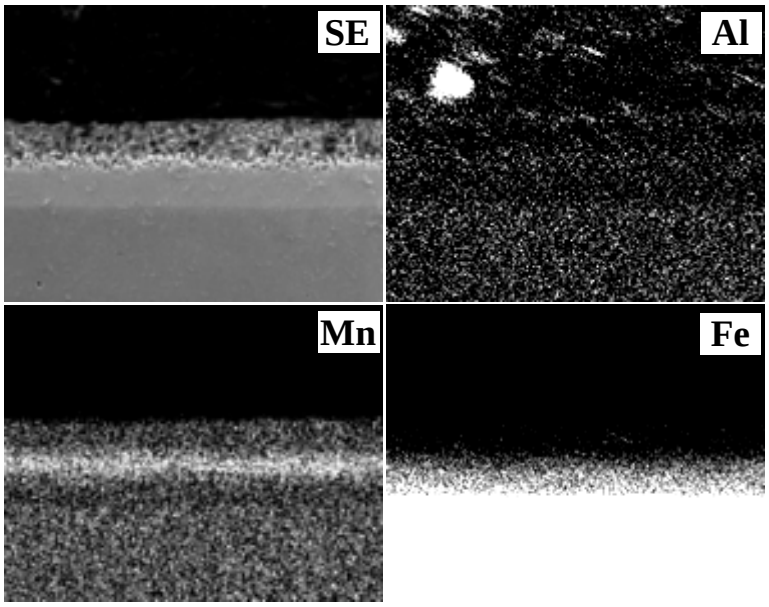

Fig 5.12 SEM image and EDX maps of cross section of hot dip galvanised coating on 0.2 wt % Si steel at 450^{o}C for 90 s (G-0.4Mn-Al-wq)

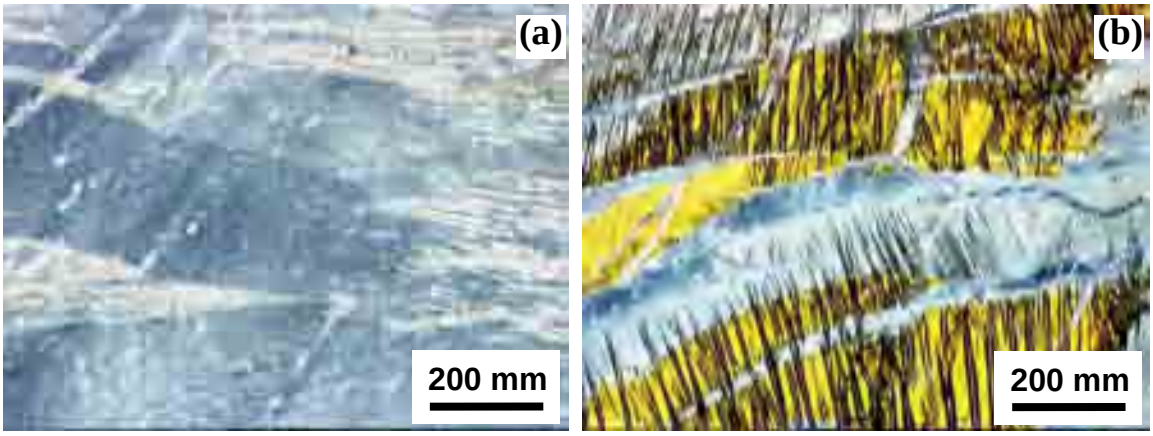

Fig 5.13 The colourful top surface of galvanised coatings G-0.4Mn-wq: (a) shiny surface, and (b) dull surface.

Fig 5.14 The shiny surface of galvanised coatings G-0.4Mn-Al-wq

The top surface of G-0.4Mn-wq has a blue and yellow colour as shown in Fig 5.13 (a) and (b). After the addition of Al to the Mn-containing bath, the thick colourful Mn-rich oxide disappeared, while a shiny surface with very light yellow color was produced as shown in Fig 5.14.

Fig 5.15 shows the typical microstructure of the air-cooled hot dip galvanised coating on 0.02 wt % Si steel at 450^{o}C for 90 s after immersion in the Zn bath with the addition of 0.4 and 0.8 wt % Mn. The coating microstructure is similar to that formed on steel substrates with 0.2 wt % Si. Different phase layers (eta, zeta and delta) can be clearly seen on the etched surface. Both coatings of different Mn content show compact columnar

morphologies. With the addition of 0.4 wt % Mn, no obvious Mn-rich particles are present in the eta layer as shown in Fig 5.15 (a). However, Mn-rich particles can be clearly seen in the eta layer for the coating with 0.8 wt % Mn as shown in Fig 5.15 (b) and Fig 5.16 (a). The EDX spectrum and line scan on the larger particles reveal that there is no Fe in the Mn-rich particles as shown in Fig 5.16 (b) and Fig 5.17 (b).

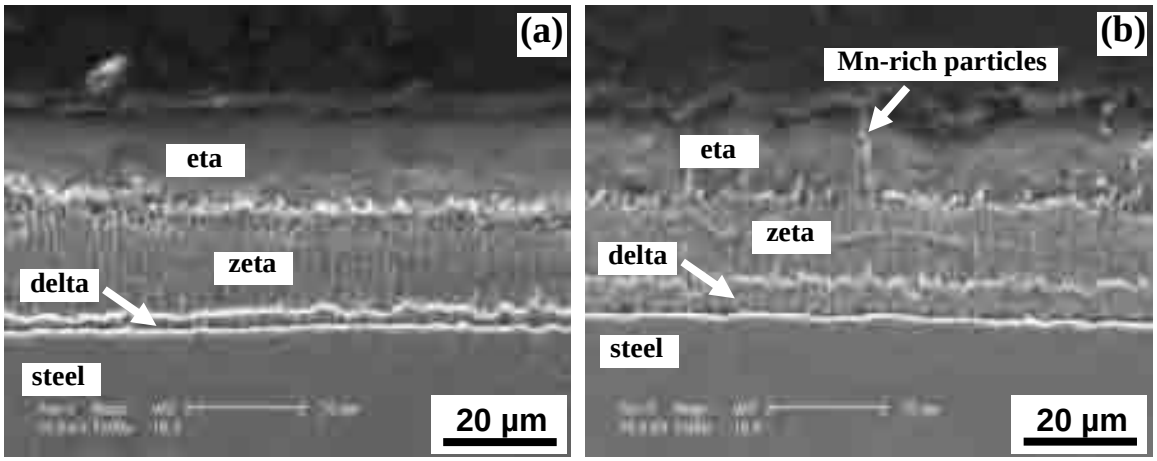

Fig 5.15 SEM images of the etched hot dip galvanised coating on 0.02 wt % Si steel: (a) air-cooled G-0.4Mn-Al-air, and (b) air-cooled G-0.8Mn-Al-air.

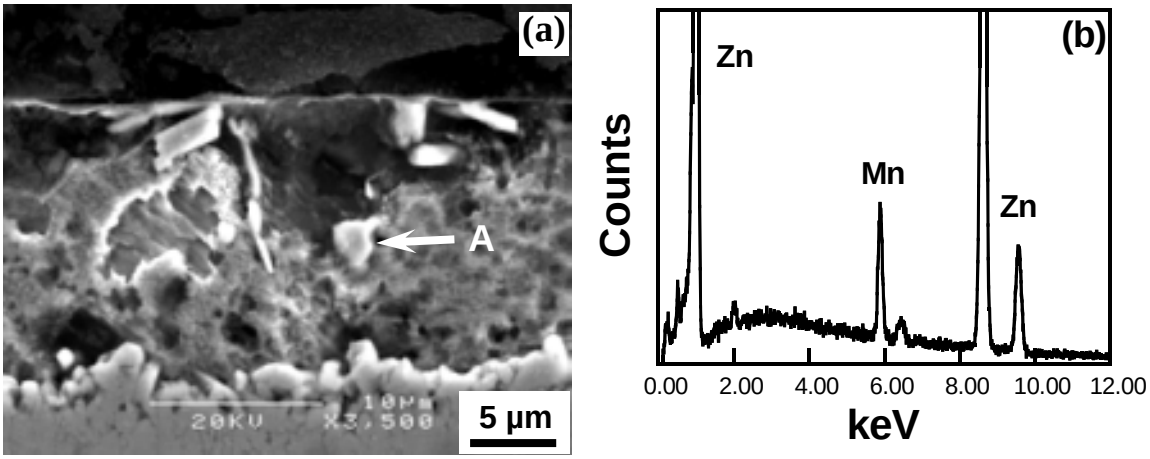

Fig 5.16 (a) SEM images of the eta layer of etched hot dip galvanised coating G-0.8Mn-Al-air, and (b) EDX spectrum of Mn-rich particles as shown with arrow A in (a).

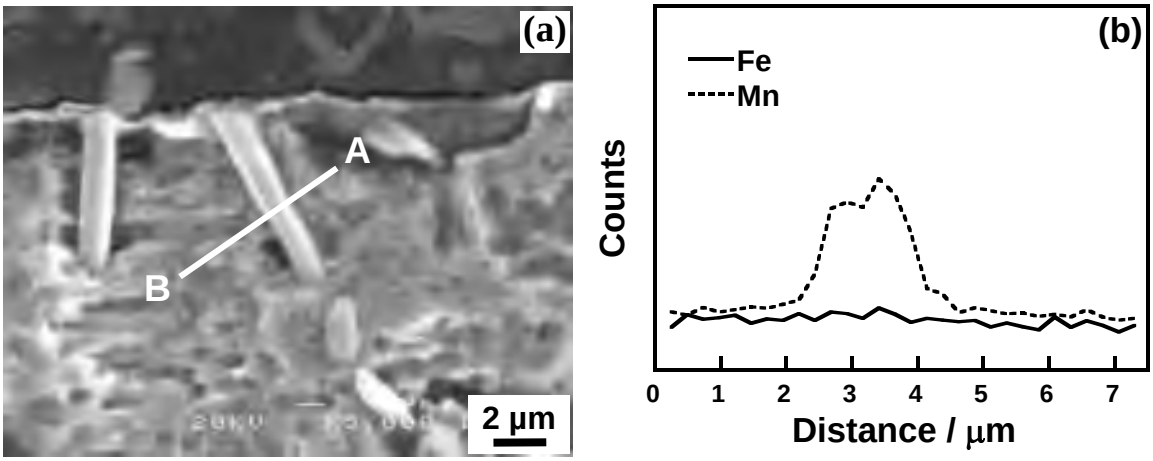

Fig 5.17 (a) SEM image of the as polished eta layer of the hot dip galvanised coating G-0.8Mn-Al-air, and (b) EDX line scan across a Mn-rich particle in eta layer as shown by the white line in (a).

The variations in Fe and Mn concentration across the Mn-containing coatings G-0.4Mn-Al-air and G-0.8Mn-Al-air are shown in Fig 5.18 and Fig 5.19, respectively. Similar to that of water quenched G-0.4Mn-Al-wq, a maximum Mn content was found at the outer edge of the zeta phase for both Mn-containing coatings. At the peak, the Mn and Fe contents are 2.2 ± 0.2 wt % and 2.3 ± 0.3 wt %, respectively. The observation of a low Fe content in the zeta phase implies that Mn may have substituted for Fe in the zeta phase layer.

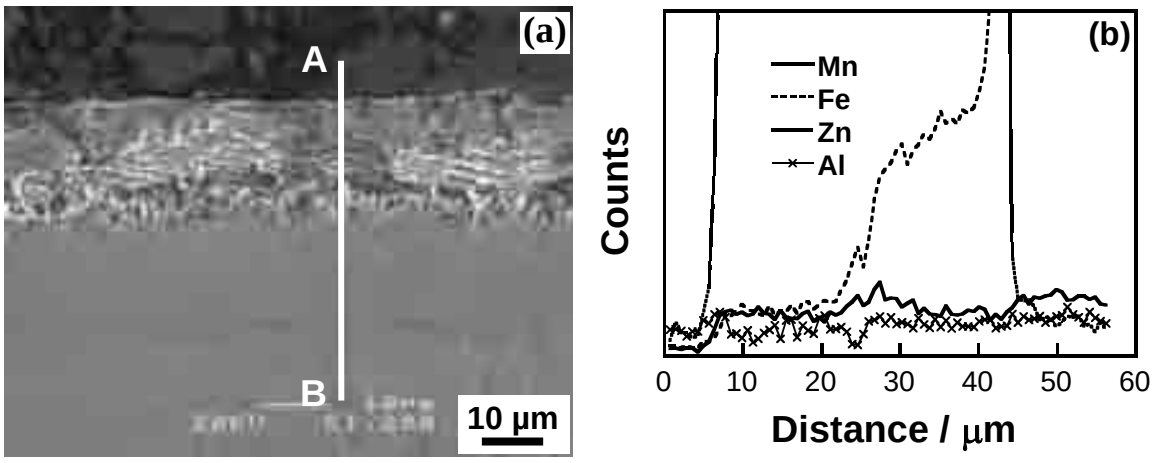

Fig 5.18 (a) SEM image of as polished hot dip galvanised coating G-0.4Mn-Al-air, and (b) EDX line scan across whole coating as shown by the white line from A to B in (a).

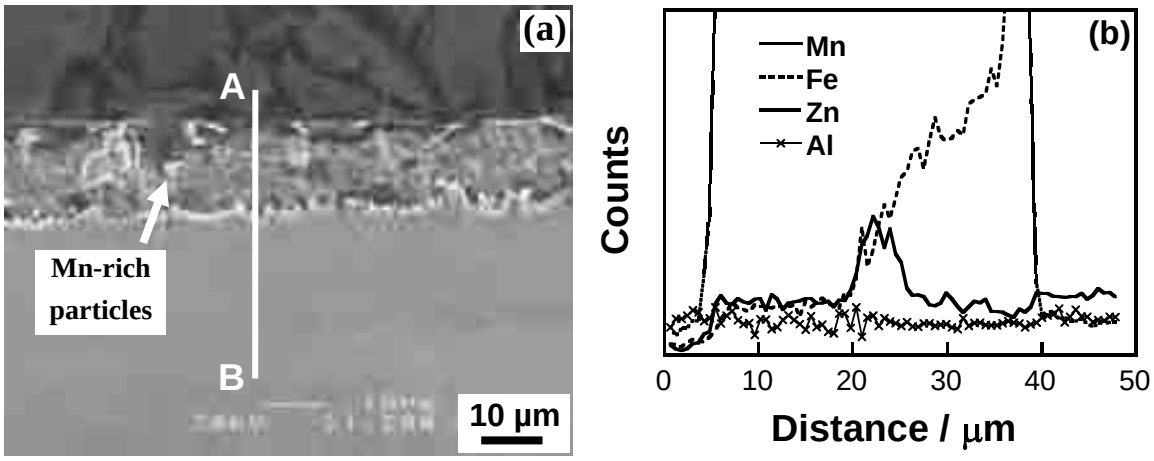

Fig 5.19 (a) SEM image of as polished hot dip galvanised coating G-0.8Mn-Al-air, and (b) EDX line scan across whole coating as shown by the white line from A to B in (a).

5.1.6.2 The microstructure of top surface of Mn-coatings

Fig 5.20 shows the surface morphology of the Mn-containing hot dip galvanised coating G-0.4Mn-Al-air. The results indicated that there are intermetallic particles on the surface. Most of them are adjacent to grain boundaries. EDX line scan reveals that these intermetallic particles are rich in Mn as shown in Fig 5.21. The surface morphologies of the Mn-containing hot dip galvanised coating G-0.8Mn-Al-air is shown in Fig 5.22. The distribution density of the Mn-rich intermetallic particles on the coating surface increased with the Mn amount in the bath.

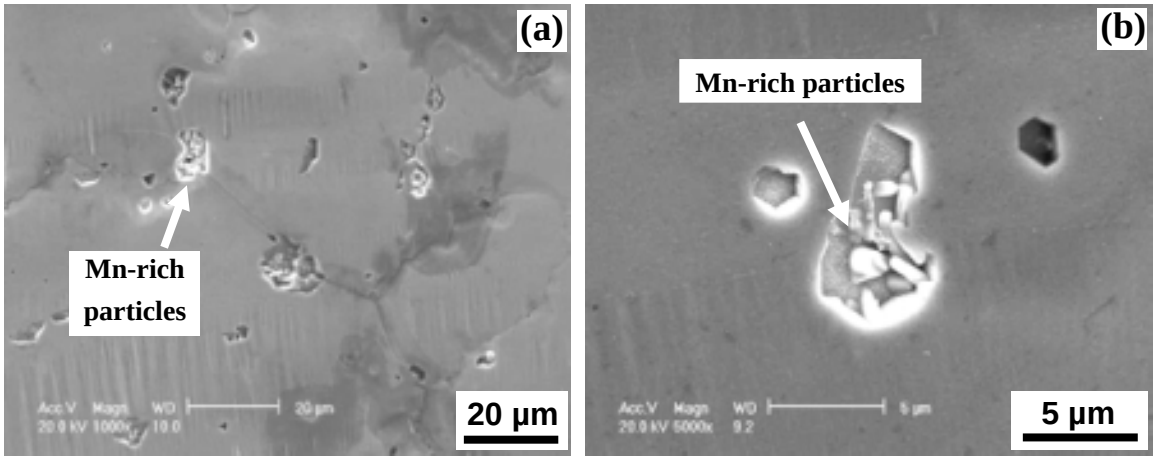

Fig 5.20 SEM images of top surface of as received hot dip galvanised coating G-0.4Mn-Al-air: (a) low magnification, and (b) high magnification.

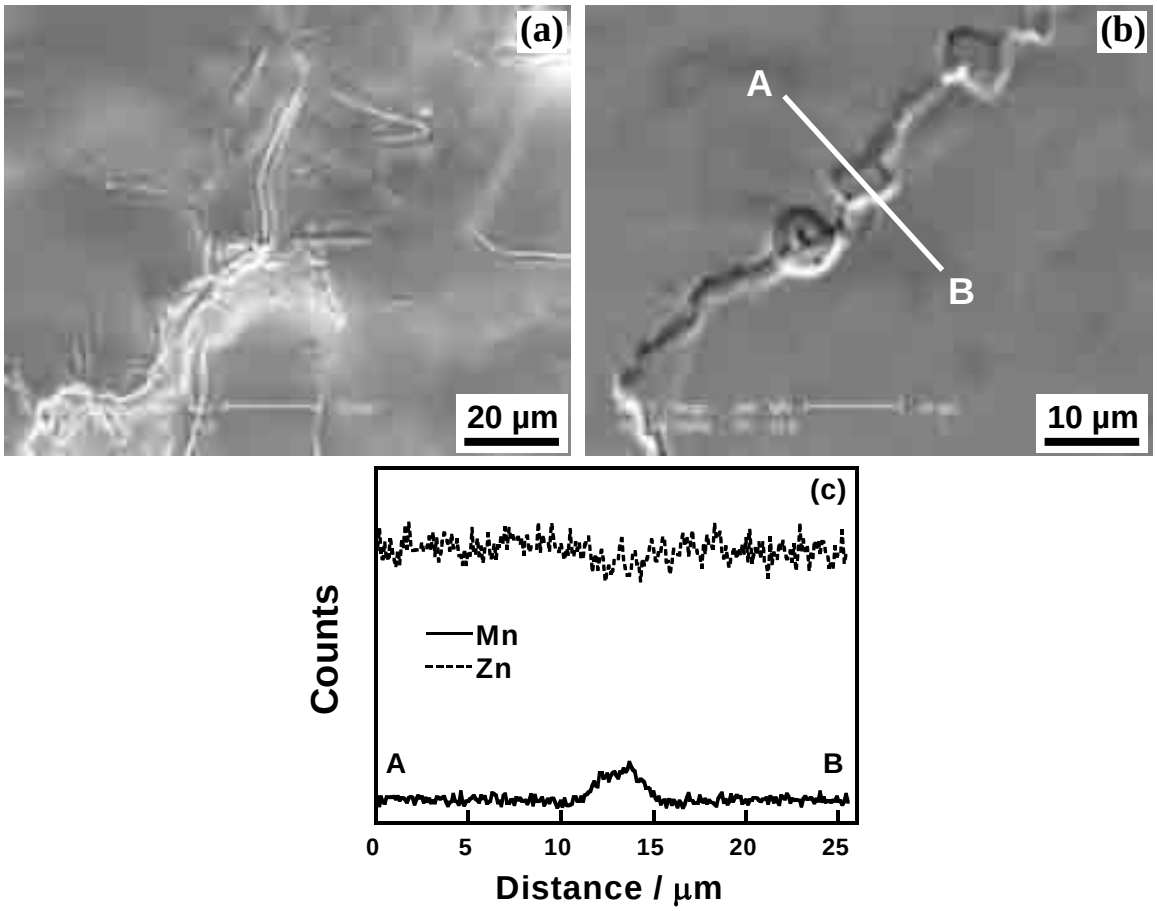

Fig 5.21 (a) and (b) SEM images of top surface of air-cooled hot dip galvanised coating G-0.4Mn-Al-air, and (c) EDX line scan Mn-rich particles as shown by the white line from A to B in (b).

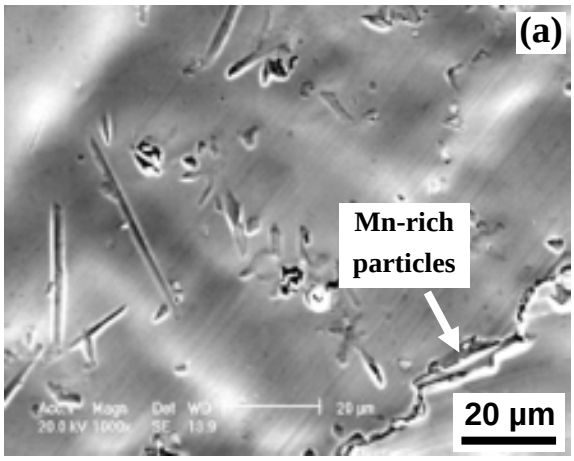

Fig 5.22 SEM image of top surface of air-cooled hot dip galvanised coating G-0.8Mn-Al-air.

5.1.6.3 Surface composition analysis

It was shown in the previous SEM/EDX results that there was a Mn-rich layer on the top surface of G-0.4Mn-wq. After the addition of 0.005 wt % Al, no Mn-rich layer was detectable by SEM/EDX. Analysis of the top surface was made with Auger Electron Spectroscopy (AES) and X-ray Photoelectron Spectroscopy (XPS). The Auger depth profile of the film is shown in Fig 5.23. The depth profile of the layer on the top surface shows a Mn-rich oxide film with a small contribution from Al and Zn oxide. The depth profile also shows that Al only consists in some depth of the whole oxide layer, while Mn goes through the whole layer. This result suggests that the whole layer is probably a mixture Mn and Al oxides above a layer of Mn oxide.

Fig 5.24 presents the XPS spectrum of the oxide film after sputtering for 2 minutes. The XPS spectrum shows peaks corresponding to Mn, Zn, Al, O, and C. The peaks not identified correspond to Auger and secondary peaks of these elements. Fig 5.25 shows the high-resolution spectra of Mn $2p_{3/2}$, Zn $2p_{3/2}$, and O 1s core-level excitations for the oxide layer on the Zn-Mn coating G-0.4Mn-Al-wq. In the Mn $2p_{3/2}$ region (Fig 5.25 (a)) the corresponding peak is 640.9 eV. This suggests that the oxide contains Mn oxide, MnO, Mn_3O_4 [138] or possibly Zn_2MnO_4 [14]. The Zn $2p_{3/2}$ peak at 1021.9 eV indicates the presence of Zn^{2+}. The Al 2p peak at 74.7 eV suggests that Al oxide is also present on the surface.

It is concluded that the oxide layer formed on G-0.4Mn-Al-wq mainly consists of Mn and Al oxides.

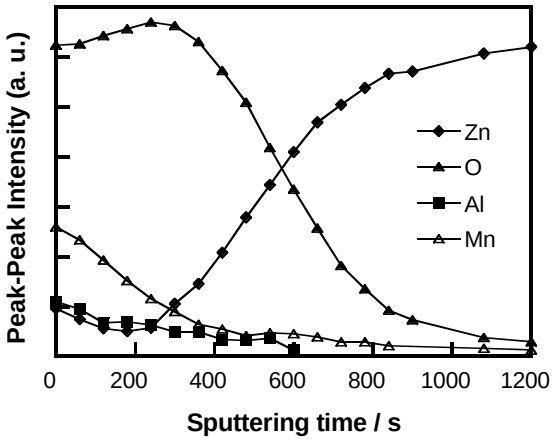

Fig 5.23 AES depth profile of alloying elements for hot dip galvanised coating G-0.4Mn-wq-Al.

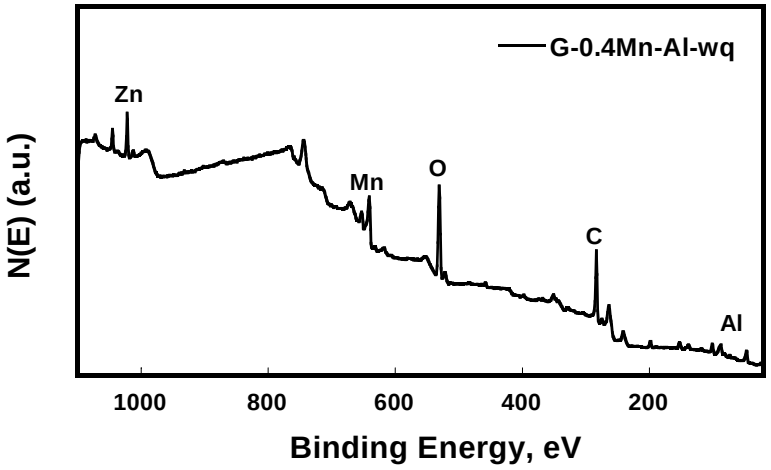

Fig 5.24 XPS survey spectra of hot dip galvanised coating G-0.4Mn-Al-wq.

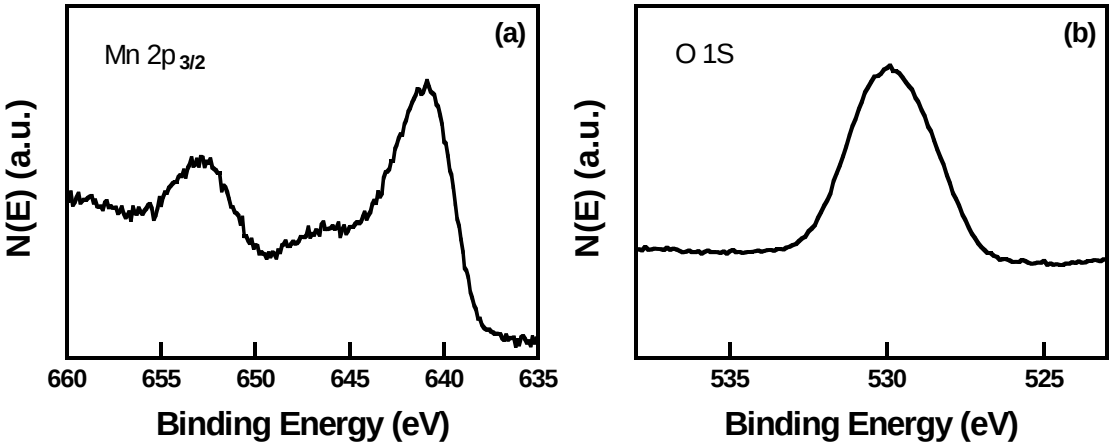

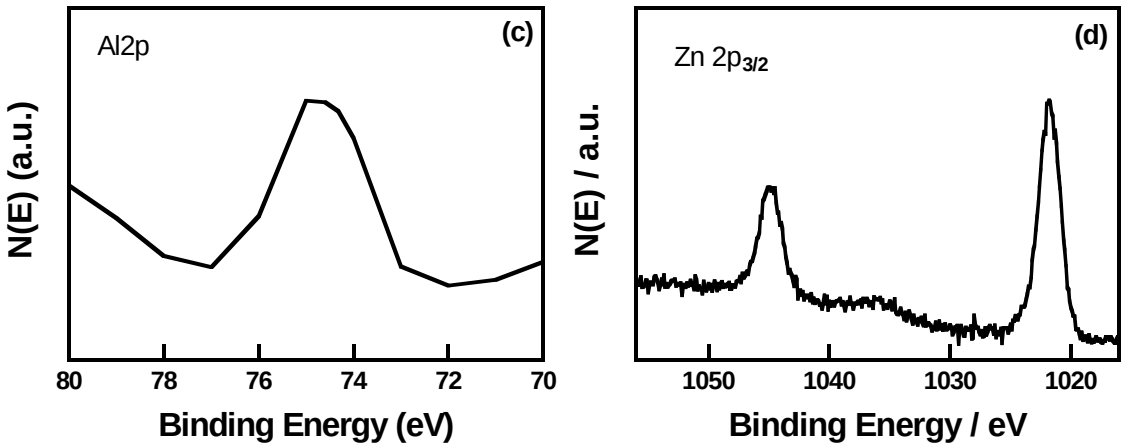

Fig 5.25 High-resolution XPS spectra of hot dip galvanised coating G-0.4Mn-Al-wq in the (a) Mn 2p, (b) O 1s, (c) Al 2p, and (d) Zn 2p energy windows.

5.2 Effects of alloying additions on coating thickness

The previous experiments showed that the addition of Mn increases the corrosion resistance of Zn. In this section, the effect of Mn, Cu and their combination on coating thickness and growth kinetics of hot dip galvanised coating were investigated. The steel containing 0.02 wt % Si was chosen as the coating substrate. Its chemical composition is given in Section 3.1.4.1.

5.2.1 The growth kinetics of the alloy layer

Measurements of the coating thickness for 10 – 900 s immersions were carried out with an aim of studying the reaction kinetics of alloy layer growth. The alloy layers were measured over four fields of SEM images (ten measurements / field) at a magnification of × 800 and average and standard deviation values were calculated from the compiled alloy layer thickness data.

The total Fe-Zn alloy layer thickness was measured for each reaction time studied, and the growth data for the alloyed hot dip galvanised coatings are shown in Fig 5.26 and Fig 5.27. The cross section morphologies of the galvanised hypo-Sandelin steels for 10 - 900 s immersion are shown in Fig 5.28 - Fig 5.33.

The result reveals that addition of 0.2 wt % Cu has no detectable effect on alloy layer thickness for 10 s - 900 s immersion, but addition of 0.8 wt % Cu shows a great effect on the growth kinetics of the alloy layer. Before 30 s as shown in Fig 5.30 (a) and (b), two alloy layers (zeta and delta) can be seen. However, after 90 s only one alloy layer dominated the growth. It is not clear if the alloy layer is zeta or delta phase. Quantitative EDX measurements show that the composition of this alloy is about 3.0 wt % Cu, 6.0 wt % Fe and 91.0 wt % Zn, which is consistent with the observation of Katiforis [77].

Additions of Mn up to 0.8 wt % have no significant effect on alloy layer growth for short immersion times and only slightly decrease the alloy layer thickness after 900 s immersion as shown in Fig 5.27. The cross section morphologies of the Mn-containing

coatings (Fig 5.31 and Fig 5.32) are similar to that of G-CP-Al-wq after immersion in the bath for up to 900 s.

The combined Mn (0.8 wt %) and Cu (0.2 wt % and 0.8 wt %) additions were found to significantly increase the alloy layer thickness. The cross section morphologies are similar to those of the coating G-0.8Cu-Al-wq, especially for the coating with a high level of Cu as shown in Fig 5.33 and Fig 5.34. Adjacent to the eta layer, it can be clearly seen that there are eta phases dispersed into this alloy layer as shown in Fig 5.33 (c) and Fig 5.34 (c).

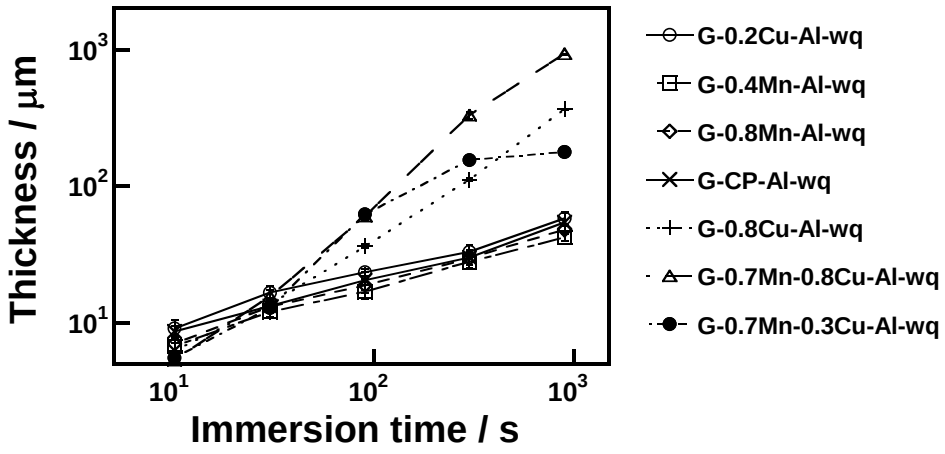

Fig 5.26 Total alloy layer growth for water-quenched hypo-Sandelin steels hot dip galvanised in Zn bath with different additions.

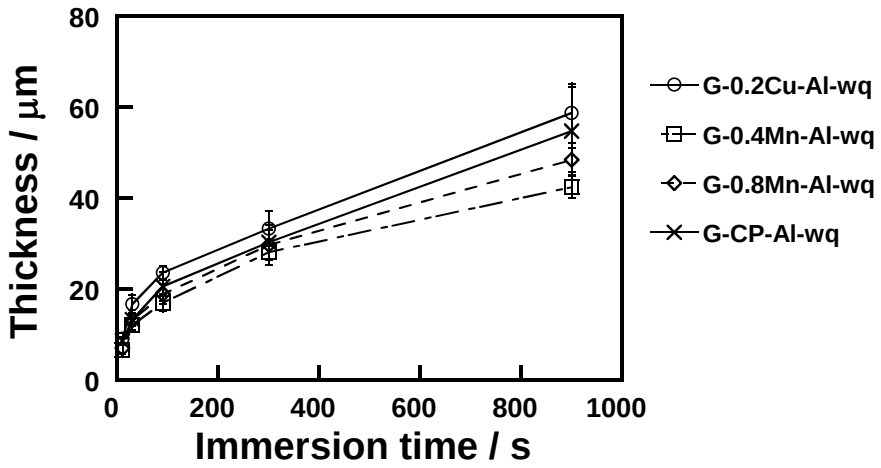

Fig 5.27 Total alloy layer growth for water-quenched hypo-Sandelin steels hot dip galvanised in Zn bath with different additions.

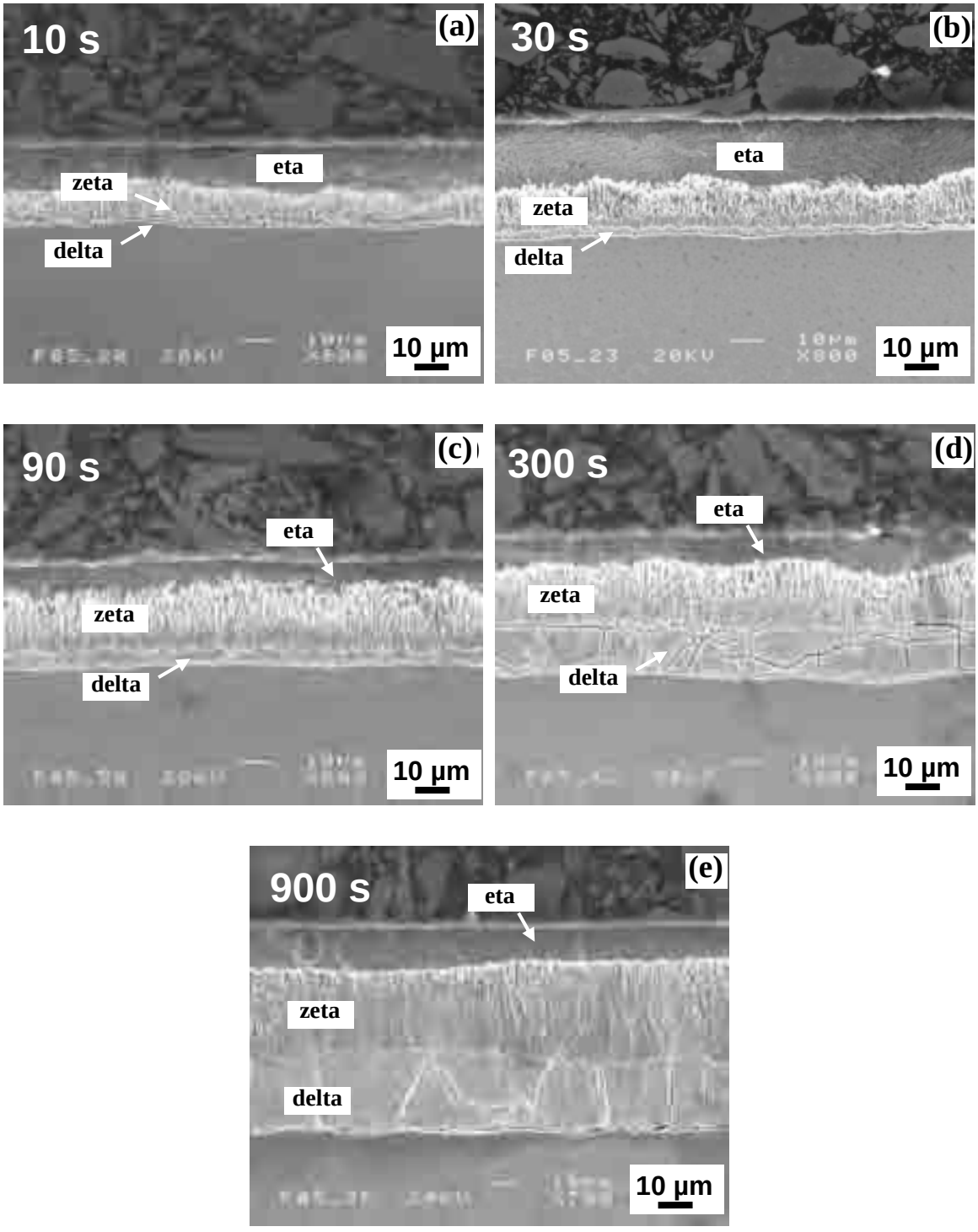

Fig 5.28 SEM images of etched hot dip galvanised coatings (G-CP-Al-wq) on Hypo-Sandelin steel (0.02 wt % Si) at 450^{o}C for different immersion times: (a) 10 s, (b) 30 s, (c) 90 s, (d) 300 s, and (e) 900 s

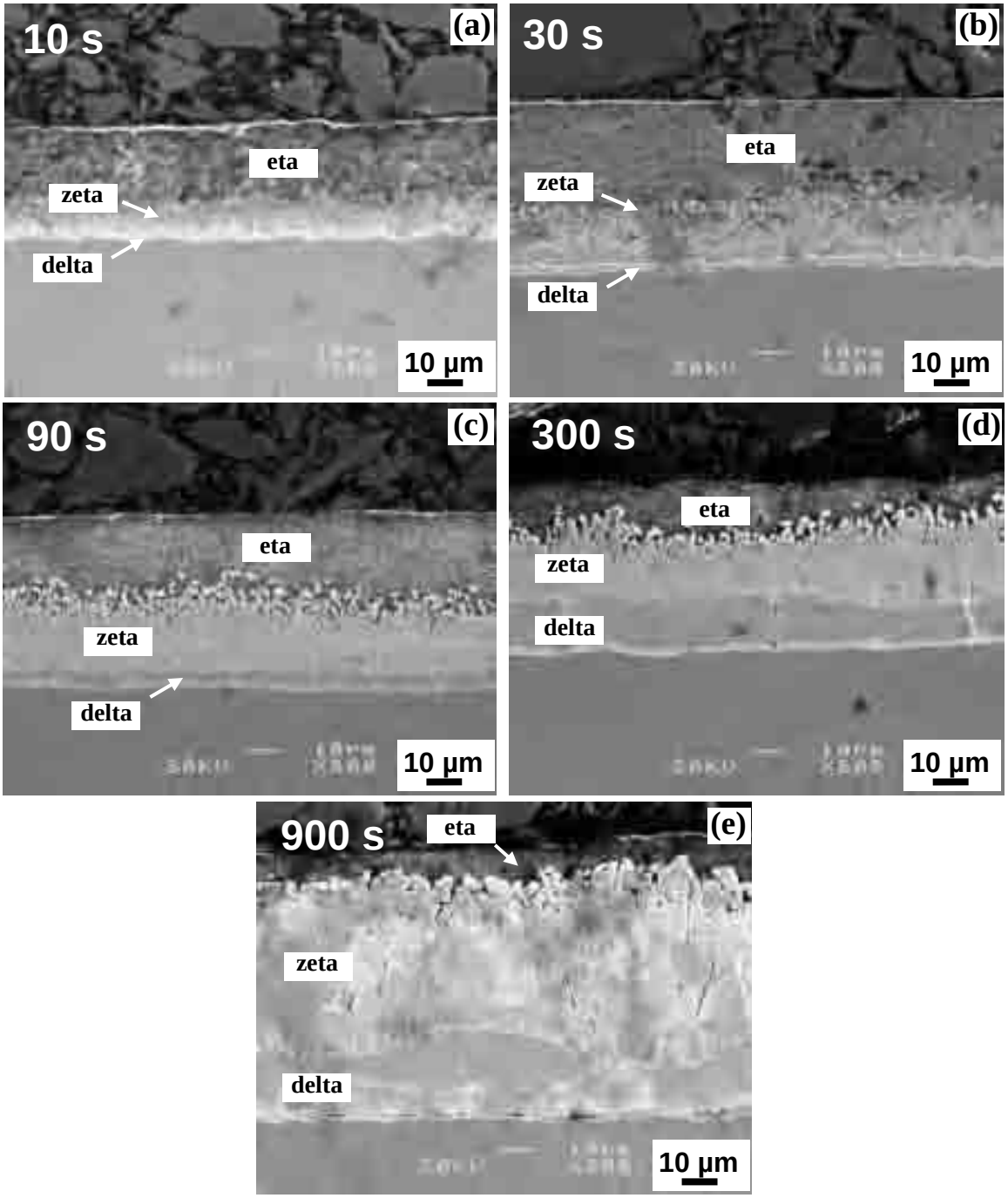

Fig 5.29 SEM images of etched hot dip galvanised coatings (G-0.2Cu-Al-wq) on Hypo-Sandelin steel (0.02 wt % Si) at 450^{o}C for different immersion times: (a) 10 s, (b) 30 s, (c) 90 s, (d) 300 s, and (e) 900 s

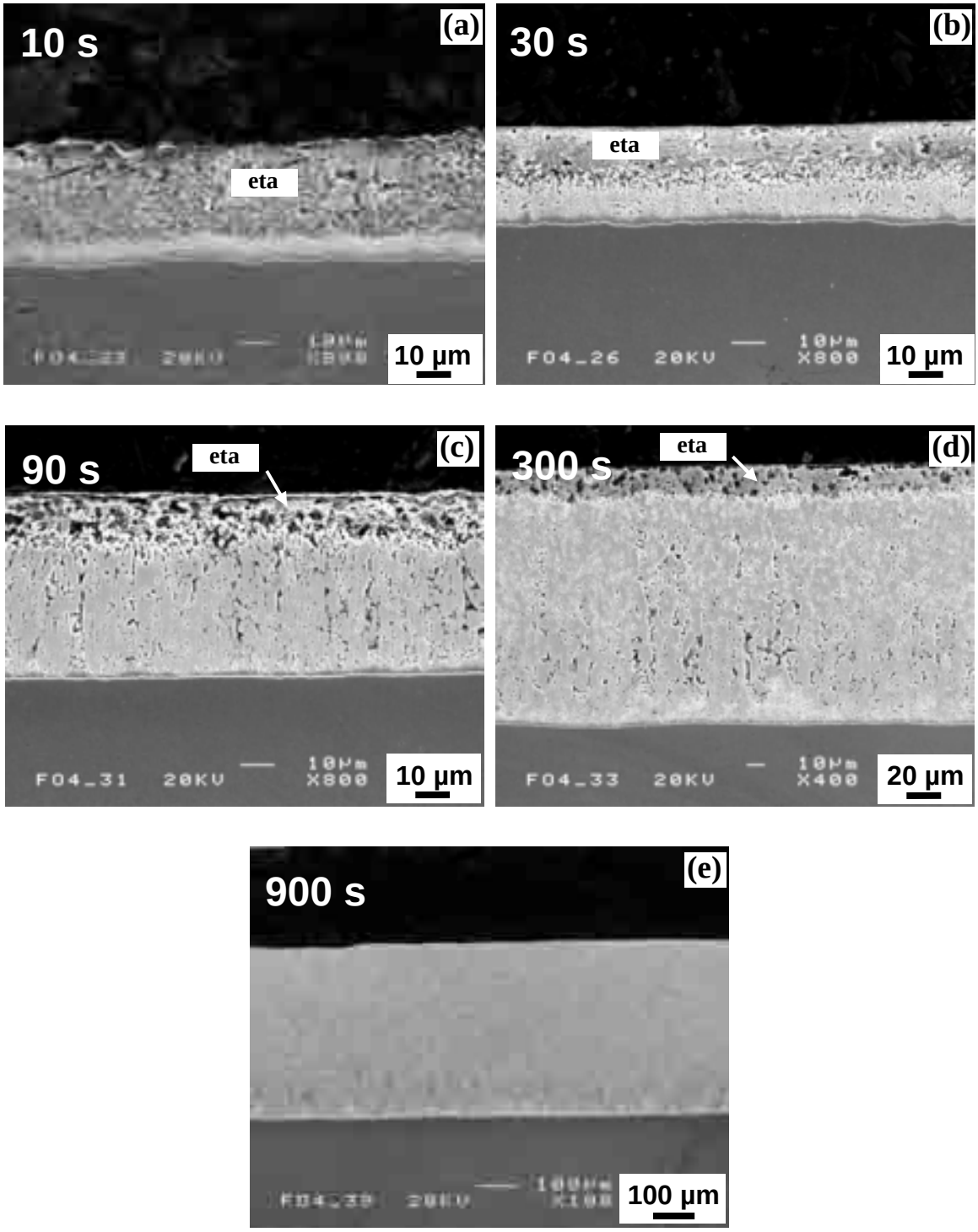

Fig 5.30 SEM images of etched hot dip galvanised coatings (G-0.8Cu-Al-wq) on Hypo-Sandelin steel (0.02 wt % Si) at 450^{o}C for different immersion times: (a) 10 s, (b) 30 s, (c) 90 s, (d) 300 s, and (e) 900 s.

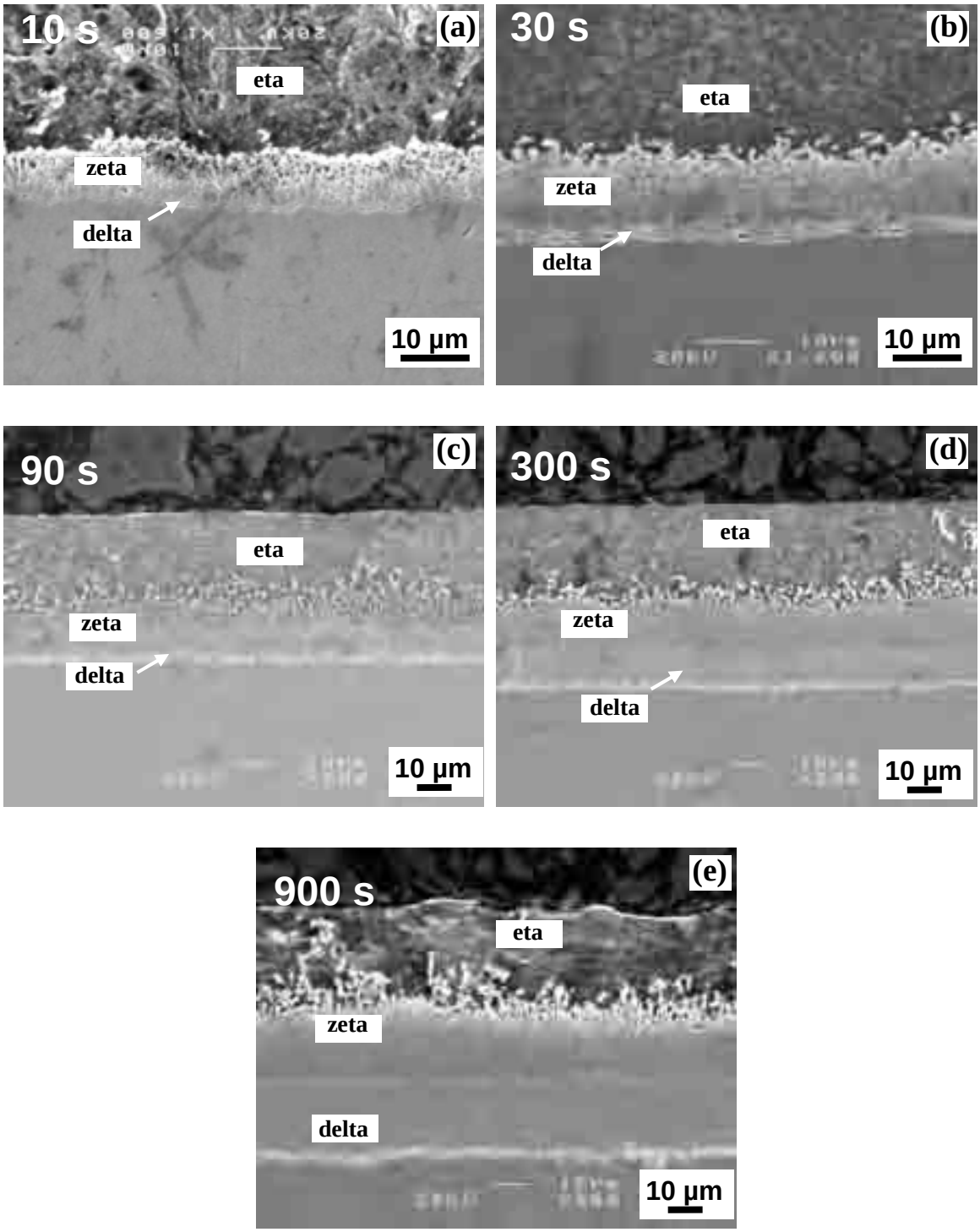

Fig 5.31 SEM images of etched hot dip galvanised coatings (G-0.4Mn-Al-wq) on Hypo-Sandelin steel (0.02 wt % Si) at 450^{o}C for different immersion times: (a) 10 s, (b) 30 s, (c) 90 s, (d) 300 s, and (e) 900 s.

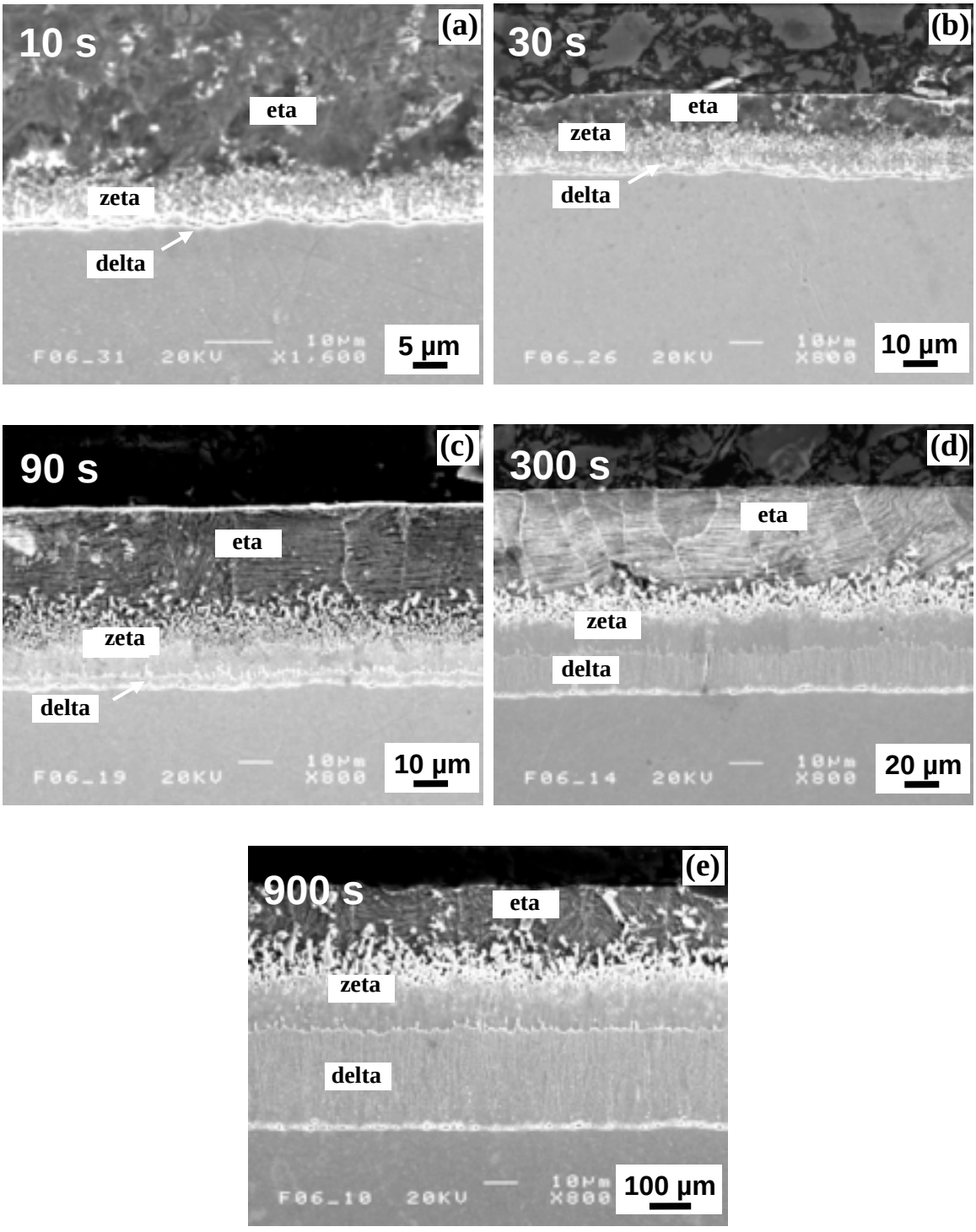

Fig 5.32 SEM images of etched hot dip galvanised coatings (G-0.8Mn-Al-wq) on Hypo-Sandelin steel (0.02 wt % Si) at 450^{o}C for different immersion times: (a) 10 s, (b) 30 s, (c) 90 s, (d) 300 s, and (e) 900 s.

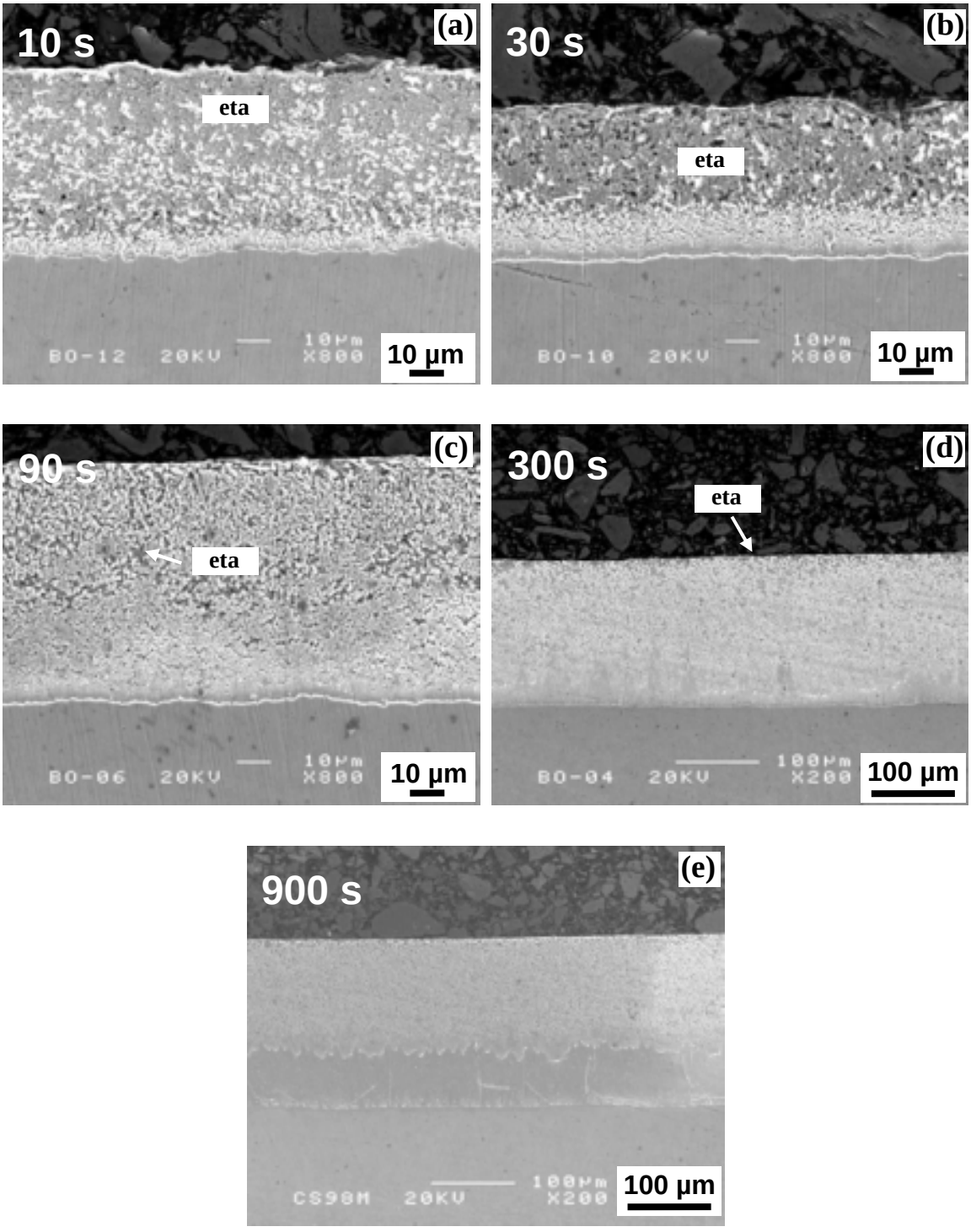

Fig 5.33 SEM images of etched hot dip galvanised coatings (G-0.8Mn-0.2Cu-Al-wq) on Hypo-Sandelin steel (0.02 wt % Si) at 450^{o}C for different immersion times: (a) 10 s, (b) 30 s, (c) 90 s, (d) 300 s, and (e) 900 s.

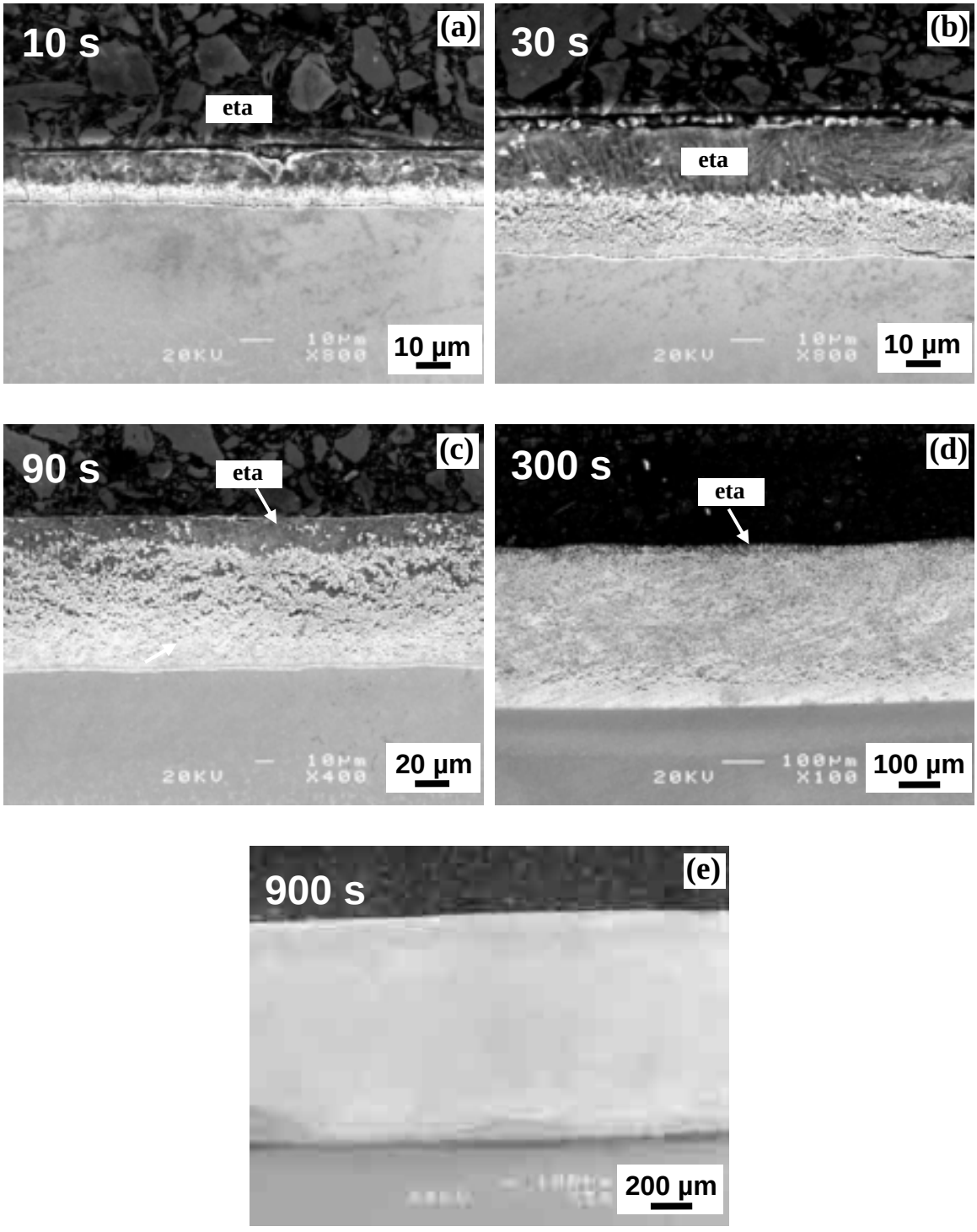

Fig 5.34 SEM images of etched hot dip galvanised coatings (G-0.8Mn-0.8Cu-Al-wq) on Hypo-Sandelin steel (0.02 wt % Si) at 450^{o}C for different immersion times: (a) 10 s, (b) 30 s, (c) 90 s, (d) 300 s, and (e) 900 s.

To evaluate the kinetics of Fe–Zn alloy layer growth, a power-law growth equation was used to interpret the growth rate data.

Equation 5.1 $Y = kt^n$

Y is growth layer thickness, k is growth rate constant, t is reaction time, and n is growth-rate time constant. The growth-rate time constant n is an indication of the type of kinetics controlling the growth of the layer. An n value of 0.5 is indicative of parabolic diffusion-controlled growth, while an n value of 1.0 is representative of linear kinetics in which growth is interface controlled [21, 25, 42, 44].

The total alloy layer was analysed to determine growth-rate time constant values. The n values were determined from a general curve fit (power) in the software program KaleidaGraph and are shown in Table 5.2. Mn and 0.2 wt % Cu additions had no effect on the growth kinetics of the alloy layer. The total alloy layer had the same growth rate time constant n value of 0.4 as that of G-CP-Al-wq without addition. The n values are in agreement with the n values (0.33-0.55) reported previously in the literature [25, 42]. An n value of 0.5 is indicative of parabolic diffusion-controlled growth. The relatively low n value of 0.4 is probably because the total alloy layer growth is controlled by diffusion along intermetallic phase layer grain boundaries instead of the bulk Fe and Zn interdiffusion [42].

Table 5.2 Total alloy layer growth-rate time constant, n, values for hypo-Sandelin steels hot dip galvanised in a Zn bath with and without additions.

Samples	n
G-0.2Cu-Al-wq	0.40 ± 0.03
G-0.8Cu-Al-wq	1.10 ± 0.03
G-0.4Mn-Al-wq	0.40 ± 0.01
G-0.8Mn-Al-wq	0.40 ± 0.02
G-0.8Mn-0.2Cu-Al-wq	-
G-0.8Mn-0.8Cu-Al-wq	1.00 ± 0.06
G-CP-Al-wq	0.40 ± 0.03

Addition of 0.8 wt % Cu significantly affects the growth kinetics of the alloy layer. The growth-rate time constant n value was found to be 1.1 as shown in Table 5.2. This indicates that the alloy layer growth is interface controlled [21, 25, 42, 44].

The combination of Mn and Cu additions (0.8Mn-0.8Cu) also has great effect on the growth kinetics of the alloy layer with the growth-rate time constant close to 1 indicating an interface controlled growth of the alloy layer. The growth of the alloy layer of G-0.8Mn-0.2Cu-Al-wq shows linear kinetics for short immersion times up to 300 s. However, after 900 s immersion, linear kinetics was not observed.

The cooling method has also an effect on the thickness of the alloy layer as shown in Fig 5.35. For 90 s immersion, additions of 0.4 wt % Mn, 0.8 wt % Mn and 0.2 wt % Cu have no effect on the thickness, independent of the cooling method. However, addition of 0.8 wt % Cu and combined additions of Mn and Cu significantly increase the alloy layer thickness, and air cooling has a further effect increasing the thickness. This indicates that the growth of the alloy layers can continue even at a lower temperature than the galvanising temperature when addition of 0.8 wt % Cu or combined additions of Mn and Cu are added to the Zn bath.

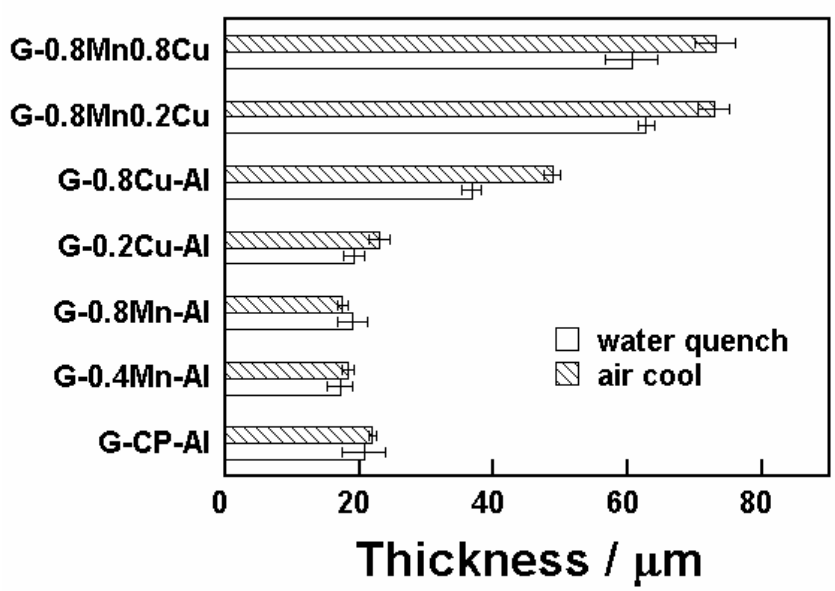

Fig 5.35 Effect of alloying additions on the thickness of the alloy layer of water-quenched and air-cooled hot dip galvanised coatings on steels with 0.02 wt %Si after 90 s in molten Zn at 450 ºC.

5.2.2 Hyper-Sandelin steel

As stated in the literature review, more than 0.07 wt % Si in steel can significantly increase the coating thickness [50-52, 54-58]. Alloying is found to be an effective way to overcome the detrimental effects of Si on the growth of the Zn–Fe intermetallic compounds [20]. In this section, the effect of Zr, Mn, Sb and Cu on the coating thickness of galvanised steel containing 0.2 wt % Si was investigated with an aim to identify the beneficial alloying elements to overcome the Sandelin effect (see Section 2.2.4.2.2).

Fig 5.36 shows the comparison of the alloy layer thickness of the water-quenched hot dip galvanised coating obtained when galvanising the industrial steel containing 0.2 wt % Si (hyper-Sandelin steel) at 450^{o}C for 90 s in different alloyed Zn baths. The typical morphologies of the cross section of the hot dip galvanised coatings with and without the alloying additions have been shown in Section 5.1.

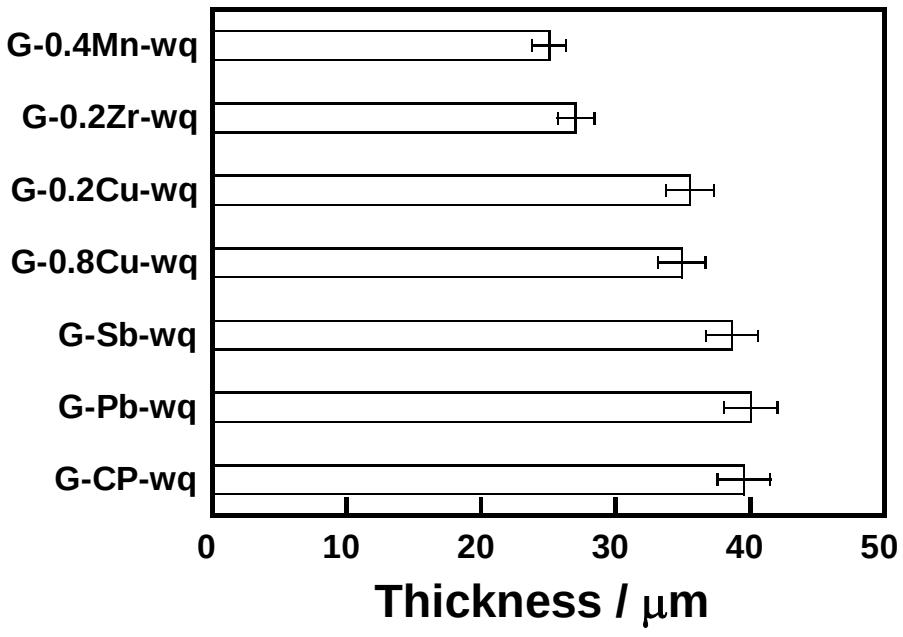

Fig 5.36 Effect of alloying additions on the thickness of the alloy layer of water-quenched hot dip galvanised coatings made on steel with 0.2 % Si after 90 s in molten Zn at 450 ºC.

It was found that addition of 0.2 wt % Zr decreased the Zn-Fe alloy layer thickness significantly compared with the conventional hot dip galvanised coating G-CP-wq. The addition of 0.2 wt % Zr inhibits the growth of the alloy layers, especially the zeta phase layer (see Fig 5.1 (a) and Fig 5.5 (a)). Similar results were reported by Sebisty [79], whose studies showed that additions of 0.1 and 0.3 wt % Zr decreased the coating thickness and a dispersion of very fine intermetallic particles was observed in the eta layer. The mechanism of the effect of Zr on coating thickness is not clear. As suggested by Sebisty [79], the smooth interface is probably produced by the dissolution of the zeta phase as a result of Fe depletion around the intermetallic particles rich in Fe and Zr. This result implies that Zr could be a possible replacement for Ni in the Zn bath to overcome the detrimental effects of Si.

In addition to Zr, the addition of 0.4 wt % Mn to the bath also decreased the Zn-Fe alloy layer thickness significantly. Reumont *et al.* [80] found that addition of more than 0.5 wt % Mn can significantly decrease the reactivity of Si steels. Thus Mn could also be a possible replacement for Ni in the Zn bath to overcome the detrimental effects of Si.

The additions of Cu up to 0.8 wt % slightly decrease the alloy layer thickness. Similar results were reported by Radeker *et al.* [5]. Their results indicated that an increase in the Cu content to 0.82 wt % causes a proportional decrease in the coating weight and thickness. However, the effect of Cu on increasing the coating thickness were also reported in this study (Section 5.2.1) and the literature [36, 77, 78]. The contradictory results on the effect of Cu are probably due to the different experimental conditions used in the literature. For example, the immersion time and the type of steels used in the literature were found to be different [5, 36, 77, 78]. More details on the effect of Cu will be discussed in the Section 5.3.1.2.

Sb and Pb have no significant effect on the alloy layer growth as shown in Fig 5.36. This result is consistent with the observations in the literature [36, 73, 74].

5.3 Discussion

5.3.1 Effect of Cu

5.3.1.1 Modification of the structure

The addition of Cu was found to cause a substantial change to the structure of the hot dip galvanised coating especially at high level of addition (0.8 wt %). The modified structure can be clearly seen in Fig 5.30, where the smooth interface between delta and zeta and the stratified structure of the coating disappeared with only one thick alloy layer observed. EDX analysis of this phase layer showed that it is a ternary Zn-Fe-Cu phase containing about 3 wt % Cu, 6 wt % Fe and 91 wt % Zn. Identification of this ternary phase was not carried out in this study. It is possibly the zeta phase as the Fe content of this phase is somewhat similar to the Fe content of the zeta phase in the binary Fe-Zn system. Similar results were also found by Katisforis *et al.* [77] who studied the influence of Cu (up to 3 wt %) on the structure and thickness of hot dip galvanised coatings. They found that about 3 wt % Cu was incorporated into the alloy layers to form a ternary Zn-Fe-Cu phase. However, they claimed that the ternary phase was not zeta phase but had the hexagonal structure of the delta phase based on the X-ray diffraction investigations [77]. They explained that the total content of this phase in Fe and Cu (9 wt %) is within the limit of the Fe content of the delta phase. The Fe atoms could be substituted in the hexagonal structure of the delta phase by the Cu atoms as the Cu and Fe atoms have very similar atomic diameters, varying only by 3 % (d_{Fe} = 0.2482 nm, d_{Cu} = 0.2556 nm) [77, 139]. Nevertheless, it was pointed out by Jordan [42] that X-ray diffraction analysis of the gamma, delta and zeta phase layers results in severe peak overlap, especially for the delta and zeta phases. Thus it is still not clear what the crystal structure of the ternary phase Fe-Zn-Cu is. Nell [76] also found that Cu was incorporated into the Fe-Zn alloy layer, but the maximum content of Cu in alloy layers was only 0.7 wt % for the coating galvanised in a bath containing 0.72 wt % Cu. As the immersion time for Nell's experiments was 8 h [76], her results may not

be compared with the results in this study (10 s - 900 s) and in the literature (180 s) [77]. Furthermore, the slightly lower content of Cu addition (0.72 wt %) that Nell used may also cause the lower content of Cu in the alloy layers.

In this study, it was also found that the effect of the addition of Cu on the coating structure depends on the Cu content. The addition of 0.2 wt % Cu to the bath has no effect on the coating structure as shown in Fig 5.6 (a) and Fig 5.29 compared with the commercially-pure Zn coating. EDX composition analysis of the alloy phases of G-0.2Cu-wq reveals that there is about 0.8 wt % Cu and 0.6 wt % Cu incorporated into zeta phase and delta phase respectively.

5.3.1.2 Effect on coating thickness

5.3.1.2.1 Hypo-Sandelin steel

The addition of Cu to the bath was found to have a great effect on the coating thickness of the galvanised hypo-Sandelin steels (0.02 wt % Si) as shown in Fig 5.35 and Fig 5.26. It is evident that addition of 0.8 wt % Cu can significantly increase the coating thickness especially at longer immersion times (more than 90 s). However, at short immersion times (10 s), the reverse effect was found, as shown in Fig 5.37. Similar results were found by Sebisty and Palmer [36] who reported that Cu tended to reduce Fe-Zn alloy formation and coating weight at immersion times of up to 60 s, but these effects were reversed at 120 s. Nell [76] also found that the additions of Cu up to 0.72 wt % generally increased alloy layer growth. Recently, Katisforis *et al.* [77] studied the influence of Cu (up to 3 wt %) on the structure and thickness of hot dip galvanised coatings. Their results indicated that the additions of Cu from 0.8 wt % to 3.0 wt % to the bath cause a substantial change to the structure of the coating and the presence of Cu in the galvanising baths favours the formation of the delta phase and hinders the zeta phase growth. However, Radeker *et al.* [5] reported that an increase in the Cu content to 0.82 wt % causes a proportional decrease in the coating weight and thickness. It seems that the results of the effect of Cu on coating thickness in the literature are contradictory. However, it is noted

that the immersion time used in the work of Radeker *et al.* [5] is only 15 s. For short immersion times, Cu was found to decrease the coating thickness in this study and in the literature [36].

Table 5.3 summarises the experimental conditions used in the literature and in this study. It can be concluded that addition of Cu at high levels (e.g., 0.8 wt %) can decrease the coating thickness at short immersion times, but increase the coating thickness at long immersion times.

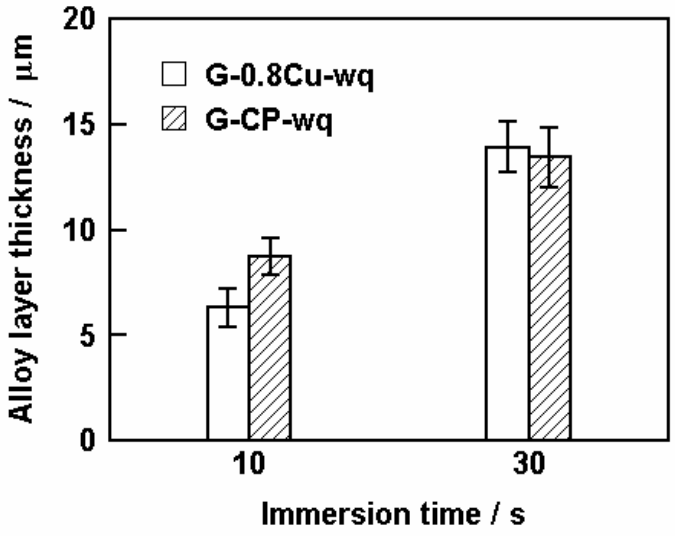

Fig 5.37 Effect of alloying additions on the thickness of alloy layers of air-cooled hot dip galvanised coatings made on steels with 0.02 wt % Si after 90 s in molten Zn at 450 ºC.

Table 5.3 Effect of Cu addition on coating thickness and the galvanising condition used in the literature and this study.

Source	Immersion time	Si and P in steel (wt %)	Cu addition (wt %)	Effect on thickness
Nell [76]	0.5 - 32 h	P 0.000, Si 0.000	0.09 - 0.72	increase
Sebisty and Palmer [36]	15 - 120 s	P 0.012, Si 0.002	0.05, 1.25	decrease before 60 s increase after 120 s
Katisforis *et al.* [77]	180 s	Si 0.01	0.3 - 3.0	increase
Radeker *et al.* [5]	15 s	P 0.054, Si 0.000	0 - 0.82	decrease
This study	90 s	P 0.009, **Si 0.19**	0.2, 0.8	decrease
	10 - 900 s	P 0.009, Si 0.02	0.2, 0.8	decrease before 30 s increase after 90 s

Nell [76] proposed a mechanism to explain the effect of Cu addition: 1) Cu only takes part in the formation of the coating after it diffused through the zeta layer into the delta layer and further into the coating; 2) Cu has a “loosening” effect on the zeta layer, which produces instability and increases layer growth; 3) Finally a new modified zeta layer forms on top of the delta layer which stabilizes the reaction. This mechanism implies that if the immersion time is not enough for Cu to diffuse through the zeta layer into the delta layer, the effect of Cu addition on layer growth can be ignored. This mechanism provides an explanation of the time dependent effect of Cu on coating thickness found in both the current and previous work [36].

Addition of 0.8 wt % Cu significantly affects the growth kinetics of the alloy layer. The growth-rate time constant n value was found to be 1.1 as shown in Fig 5.42. This indicates that the alloy layer growth is interface controlled. Not many studies were carried out on the growth kinetics of the alloy layer with Cu additions. In one study, Katisforis *et al.* [77] found that the growth of total thickness of the coating follows closely the linear time law for the addition of 1.6 wt % Cu.

5.3.1.2.2 Hyper-Sandelin steel

For the hyper-Sandelin steels (0.2 wt % Si), additions of Cu up to 0.8 wt % were found to slightly decrease the coating thickness of the hot dip galvanised coating after immersion time of 90 s as shown in Fig 5.36. In the literature, no report has been found related to the effect of Cu additions on the coating thickness of galvanised Sandelin steels. It is expected that Cu will increase the coating thickness at the long immersion times. However, as no further work has been carried out, the mechanism why Cu has such an effect on the coating thickness is still not clear. Further work under these conditions would be required to propose an explanation for these results.

5.3.2 Effect of Mn

In this study, Mn has been found to have a great effect on surface appearance,

structure and thickness of coating.

5.3.2.1 Modification of the top surface

In general, the results obtained in this study demonstrate that during the galvanising process in the Mn-containing Zn bath, an important segregation of alloying elements (Mn and Al) takes place towards the surface, causing the composition of the coatings' outer surface to be rather different from the chemical composition of the bath. XPS and SEM/EDX results showed that Mn-rich oxide layers were always found on the top surface of both Mn-containing coatings with and without Al addition. Without Al addition, the Mn-rich oxide layer is relatively thick (about 0.75 μm) with the surface has a blue and yellow colour as shown in Fig 5.13. It was observed that this Mn-rich oxide layer formed at the galvanising temperature (450°C) during the withdrawal of samples from the molten Zn bath. A similar result was also reported in the previous work [14] and it was suggested that the Mn-rich oxide layer is most likely Zn_2MnO_4. This result suggests that Mn oxide is thermodynamically more stable than the Zn oxide. The rapid formation of the Mn-rich oxide layer also occurred on the top surface of the molten Zn bath. This will lead to rapid consumption of Mn in the bath. To overcome this problem, addition of small amount of Al can be made. Al addition is widely used in industry to retard the surface oxidation of the molten Zn. The results indicate that Al additions (0.005 wt %) can also significantly inhibit the rapid oxidation of the molten Mn-containing Zn bath. After the addition of Al to the Mn-containing bath, the thick colourful Mn-rich oxide disappeared, while a shiny surface with a very light yellow colour was produced (Fig 5.14). It seems likely that the Al_2O_3 present on the outer surface of the coating obstructs both the Mn and Zn oxidation. XPS analyses confirmed the present of Al oxide (see Section 5.1.6.3).

5.3.2.2 Modification of the structure

Mn addition has a great effect on the coating structure. The solubility of Mn in Zn is 2.0 wt % at 450°C [24, 80]. This value drops to 0.02 % at 200°C [24]. Thus it is not

surprising that Mn-rich intermetallic particles form in the eta phase layer of the Mn-containing coatings, especially for the high content of Mn (0.8 wt %). In this study, however, a high Mn content in solid solution of the eta layer was found. It is possible that Mn-rich intermetallic particles of size finer than the resolution limit of the SEM are present in the eta layer.

Mn was incorporated into the Zn/Fe alloy layers in some depth. The Mn peak is normally at the outer edge of the zeta phase with about 0.9 wt % and 2.2 wt % for the coating with 0.4 wt % and 0.8 wt % Mn additions. For the coating with 0.8 wt % Mn, EDX composition analysis shows that the Fe content of the zeta phase of the Mn-containing coating is relatively lower than the typical value of the zeta phase (6.0 wt %). For example, the Fe content was found to be only 2.3 wt % at the Mn peak and about 4.0 wt % further inside the zeta phase. This result suggests that the Fe atoms are substituted in the zeta phase by the Mn atoms. Palmer *et al.* [83] also studied the effect of 0.5 wt % Mn on coating structure. They reported that Mn was incorporated into the zeta alloy layers with a maximum concentration of 0.9 wt % at the outer edge of the zeta phase. However, they found that the composition limit of Fe in the zeta phase was not affected by the presence of considerable amount of Mn in the zeta phase. This is probably due to the concentration effect of Mn as the addition of 0.4 wt % Mn was also found to have no significant effect on the Fe content of the zeta phase in this study.

Metallographically, the effect of Mn was to produce a uniform and compact zeta layer, and a uniform delta layer as shown in Figure 5.38 and Figure 5.39 although some separated zeta phases were also found in the eta layer.

5.3.2.3 Effect on coating thickness

The effect of Mn addition on the coating thickness was found to depend on the type of steel substrate. For the galvanised steels containing 0.02 wt % Si, the effect of Mn on the coating thickness can be neglected, while for the galvanised steels containing 0.2 wt % Si, Mn addition decreases the coating thickness by about 30 % compared with the

commercially-pure Zn coating. Reumont *et al.* [80] also found that addition of more than 0.5 wt % Mn can significantly decrease the reactivity of Si steels. Thus Mn could also be the replacement of Ni in the Zn bath to overcome the detrimental effects of Si. A mechanism has been proposed to explain the effect of Mn on the reactive steels [80]. According to Foct [56], when galvanising reactive Si steels in a pure Zn bath, the excessive thickness of the coating is due to the formation of a thin liquid layer enriched with Si in the vicinity of the steel substrate during the first period of immersion. The high Si content prevents the nucleation of zeta crystals on the substrate and thus it nucleates and grows far from the substrate in the liquid, where the Si content becomes negligible. When galvanising reactive steels in a Zn bath with added Mn, the Si originating from the substrate is attracted by Mn in order to form Mn-Si compounds that are thermodynamically more stable than the FeSi compound. Such an effect is not observed for the low Si steel. It implies that the effect of Mn in the zeta layer on diffusion of Zn inward and Fe outward, which control the alloy layer formation, can be neglected.

5.3.3 Effect of Zr

Zr has also a great effect on the thickness of the alloy layers, especially the zeta phase layer. It was found that the addition of 0.2 wt % Zr decreased the Zn-Fe alloy layer thickness significantly compared with the commercially-pure hot dip galvanised coating G-CP-wq. Similar results were reported by Sebisty [79] whose results showed that additions of 0.1 and 0.3 wt % Zr decreased the coating thickness and a dispersion of very fine intermetallic particles was observed in the eta layer. The fine intermetallic particles were also found in this study as shown in Figure 5.10. Sebisty [79] suggested that the limiting growth of the zeta phase is probably due to the formation of the intermetallic particles rich in Fe and Zr which involves the dissolution of the zeta phase. It is supposed that the Fe in solution in the bath is effectively depleted by formation of intermetallic particles rich in Fe and Zr, and the unstable condition arising from incomplete Fe saturation results in more aggressive attack of the zeta phase boundary crystals. As shown in Fig 5.38,

a Fe-rich intermetallic particle was found adjacent to the smooth zeta-eta interface boundary which could be produced by the dissolution of the zeta phase due to depletion of Fe in solution. This result may provide evidence for the above dissolution mechanism of Zr additions.

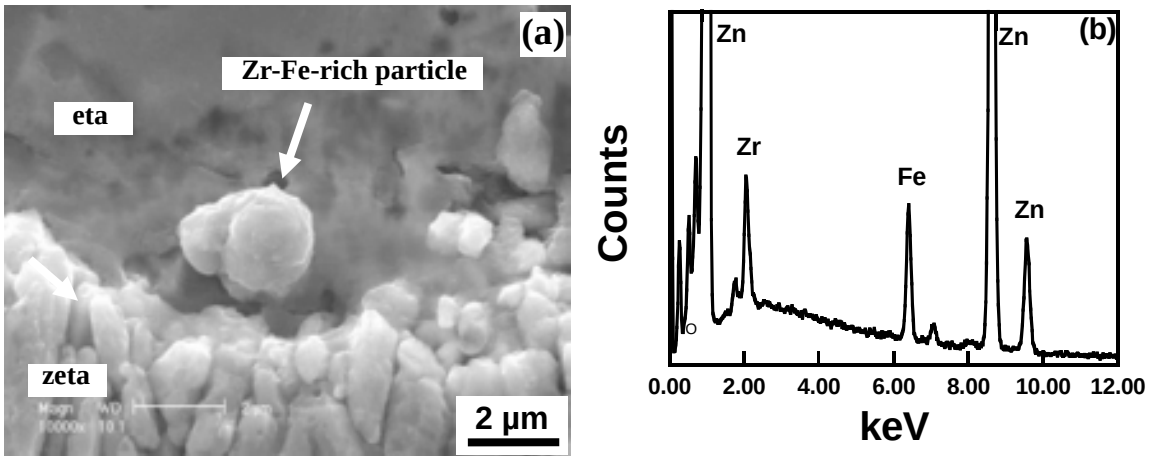

Fig 5.38 (a) SEM images of the interface between eta and zeta phase layers for hot dip galvanised coating G-0.2Zr-wq on 0.2 wt % Si steel at 450^{o}C for 90 s, and (b) EDX spectrum of a Zr-Fe-rich particle as shown in (a).

5.3.4 Effect of Pb and Sb

It has been shown that Pb has no effect on the thickness of the alloy layer. This further confirms the results observed in the previous work [73, 74], although Krepski [70] notes a reduction in alloy layer growth. Two reasons could explain the effect of Pb. EDX analysis shows that there is no detectable Pb in the alloy layer, thus its effect on diffusion of Zn and Fe, which control the alloy layer formation, can be neglected. Furthermore, there is no detectable Fe in the Pb globules found in the eta layer. It is therefore expected that Pb has no effect on the formation of zeta layer.

Fig 5.39 Macro optical image of the top surface appearance of G-Pb-Al-air showing larger grains (spangles) on the surface.

Although Pb has no effect on coating thickness, Pb has great effect on coating appearance. Significant larger grains (or spangles) were often found on the top surface of the air-cooled hot dip galvanised coating as shown in Fig 5.39. This result is consistent with those reported in the literature [20, 21, 71, 72]. The spangle is the result of the dendritic solidification of Zn. Strutzenberger *et al.* [69] explained that Pb segregates ahead of the growing dendrite, lowering surface tension and allowing the growth velocity of the Zn dendrite to increase, resulting in larger spangles. This mechanism was supported by Fasoyino *et al.* [37].

The effect of Sb is similar to Pb. Sb also has little effect on the rate of Fe-Zn alloy formation, but at high concentrations, Sb promotes spangle formation. Spangles were also reported in the literature [17, 36-38] for coatings with Sb additions. Sb lowers the bath viscosity and the surface tension of the molten Zn on the sheet, so that a uniform coating is effectively achieved [36, 37].

5.3.5 Combined additions of Mn and Cu

It has been found that Mn has no significant effect on the coating thickness of galvanised hypo-Sandelin steels, while Cu has a great effect depending on the concentration. It is therefore expected that the coating thickness could be determined

mainly by the Cu if both Mn and Cu are added to the galvanising bath. This is true for the combined addition of high level of Cu (0.8 wt % Cu). The combined additions of 0.8 wt % Mn and 0.8 wt % Cu significantly increase the thickness and growth kinetics of the alloy layer. The growth-rate time constant n value is close to 1.0 as shown in Table 5.2, which indicates the alloy layer growth is interface controlled. In general, the effect of the combined addition of 0.8 wt % Mn and 0.8 wt % Cu is similar to that of the addition of 0.8 wt % Cu only.

For a low level of Cu (0.2 wt %) additions combined with 0.8 wt % Mn, significant effects on increasing coating thickness were also found especially at short immersion times as shown in Fig 5.26 and Fig 5.33. The mechanism why the combined Mn with a low level of Cu has such an effect on coating thickness is not clear. Further work is required to propose an explanation for this result.

5.4 Summary

This chapter has concentrated on the investigation of the microstructure of galvanising coatings.

- **Low levels of Al:** No observed effect on the coating thickness and microstructure was found when low levels of Al are added to the Zn bath. Al addition (0.005 wt %) was only found to significantly change the appearance of the Mn-containing coating from the thick colourful Mn-rich oxide to a shiny surface with a very light yellow colour.
- **Cooling method: The** cooling method has no significant effect on the microstructure and coating thickness of the alloy layers (apart from the 0.8 wt % Cu and Mn-Cu additions). However, the cooling method has a great effect on the appearance of the coating with Pb and Sb additions. Air-cooled coatings show larger spangles while there are no observed spangles on the top surface of water-quenched coatings.
- **Cu:** Cu is incorporated into the Fe-Zn alloy layer of hot dip galvanised coating in some depth. The effect of Cu additions on coating thickness depends on its concentration and the type of steel substrate. For hypo-Sandelin steels (0.02 wt % Si), addition of 0.2 wt % Cu has no effect on either coating structure or alloy layer growth. However, the addition of 0.8 wt % Cu to the bath causes a substantial change to the structure of the coating and significantly increases the rate of alloy layer growth. The total alloy layer growth follows linear kinetics. For the hyper-Sandelin steels (0.2 wt % Si), additions of Cu up to 0.8 wt % were found to slightly decrease the coating thickness of the hot dip galvanised coating after an immersion time of 90 s.
- **Mn:** Mn-rich particles are found on the top surface and in the eta phase of the Mn-containing coatings (0.4 wt % and 0.8 wt % Mn). Mn-rich oxide layers are presented on the top surface of both Mn-containing coatings with and without Al addition. Mn is incorporated into the Zn/Fe alloy layers in some depth, with a high concentration throughout the zeta layer. Mn addition has no significant effect on the thickness and growth kinetics of the alloy layer for the galvanised steel containing

0.02 wt % Si. However, Mn addition decreases the coating thickness of galvanised steels containing 0.2 wt % Si to about 30 % compared with the commercially-pure Zn coating.

- **Zr:** Metallographically, the effect of Zr is to produce a smooth zeta-eta interface boundary. Zr-rich intermetallic particles are found in the eta phase layer. No Zr is detected in the alloy phase matrix. The addition of 0.2 wt % Zr inhibits the growth of the alloy layers, especially the zeta phase layer, of the galvanised steels containing 0.2 wt % Si.
- **Sb:** Addition of Sb produces spangles on the top surface. Significant amounts of Sb-rich particles are found in the eta layer. Sb has no effect on the microstructure and thickness of the alloy layer.
- **Pb:** Similar to Sb, Pb produces larger spangles on the top surface. Significant amounts of Pb globules are found in the eta layer. Pb has no effect on the thickness of the alloy layer.

CHAPTER 6 CORROSION OF HOT DIP GALVANISED COATINGS

6.1 Potentiodynamic polarisation

6.1.1 Water-quenched coatings

Fig 6.1 shows the anodic polarisation curves for water-quenched hot dip galvanised coatings with additions of Cu, Sb, Zr and Mn in the accelerated solution. In contrast with the anodic behaviour of polished Zn alloys in the accelerated solution (see Fig 4.21) there is no distinct passive range for the as-received hot dip galvanised coatings in the same solution. The average values of the electrochemical parameters obtained from the polarisation measurements are shown in Table 6.1. Compared with the polished Zn alloys, the anodic potentials at the same current density (50 $\mu A/cm^2$) of the galvanised coatings were found to be slightly higher, as shown in Table 6.1.

Among the hot dip galvanised coatings, G-0.4Mn-wq has a significantly lower corrosion current density. This result indicates that Mn addition to the Zn bath can reduce the anodic activity of the hot dip galvanised coating. Compared with the commercially-pure Zn coating, G-CP-wq, no significant difference in the anodic activity of the coating was found with the additions of Cu, Zr and Sb. As shown in Table 6.1 all coatings with these additions show similar corrosion current densities to the commercial Zn coating (G-CP-wq). This indicates that the additions of Zr, Cu and Sb have no significant effect on the anodic activity of the hot dip galvanised coating in the accelerated solution. It was also found that the commercial hot dip galvanised coating with 1 wt % Pb (G-Pb-wq) has the highest corrosion current density. This indicates that Pb promotes anodic activity of the hot dip galvanised coating, which is in agreement with the previous results, where Pb was also found to promote anodic activity of commercial Zn (Z-Pb-wq).

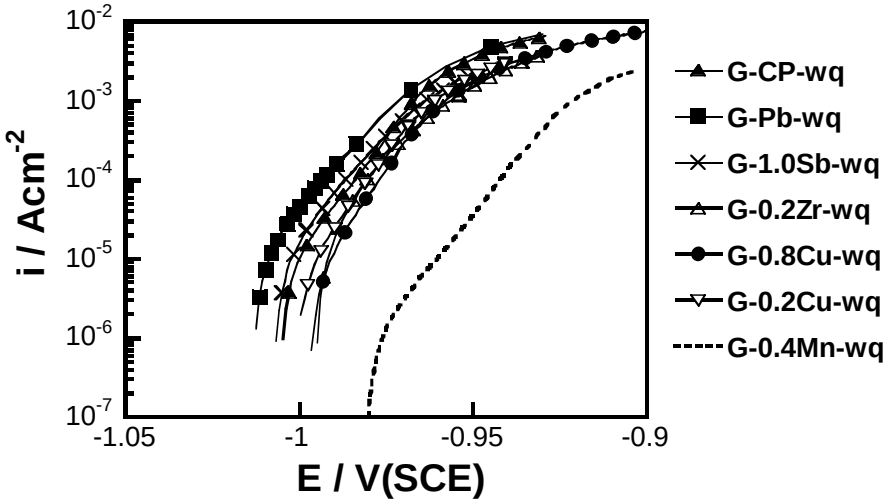

Fig 6.1 Potentiodynamic anodic polarisation curves for water-quenched hot dip galvanised coatings in the accelerated solution (0.1 M NaCl + 0.1 M Na_2SO_4 + 0.01 M $NaHCO_3$) with a scan rate of 1 mV/s, tests started immediately after samples were transferred into solution.

Table 6.1 Electrochemical parameters for the water-quenched hot dip galvanised coatings in the accelerated solution based on the anodic polarisation curves (Fig 6.1) (average of three measurements).

Hot dip galvanised coating	OCP (V *vs* SCE)	Anodic Tafel slope b_a (mV)	[a]Corrosion current density i_{corr} (μA/cm^2)	Potential of coating at 50 μA/cm^2	Potential of polished Zn alloys at 50 μA/cm^2
G-0.8Cu-wq	-1.00	16	6.0 ± 2.5	-0.99	-0.99
G-0.2Cu-wq	-1.00	18	8.0 ± 2.0	-1	-1.03
G-0.2Zr-wq	-0.99	18	12.0 ± 3.0	-0.99	-0.99
G-CP-wq	-1.01	19	8.0 ± 2.3	-0.98	-0.95
G-1.0Sb-wq	-1.01	20	10.0 ± 3.5	-0.99	-0.97
G-Pb-wq	-1.01	20	17.0 ± 3.0	-0.99	-0.99
G-0.4Mn-wq	-0.98	19	1.0 ± 0.5	-0.95	-0.97

[a] Corrosion current densities were determined from extrapolation of the anodic Tafel slope to the open circuit potential, average of three measurements.

The typical cathodic polarisation curves for water-quenched hot dip galvanised coatings with additions of Cu, Sb, Zr and Mn in the accelerated solution are shown in Fig 6.2. The result shows that Mn addition can significantly reduce cathodic current density of G-0.4Mn-wq compared with that of G-CP-wq. The additions of Zr, Cu and Sb have no

significant effect on the cathodic reactivity of the hot dip galvanised coating as shown in Fig 6.2.

Table 6.2 Comparison of the cathodic current density of water-quenched hot dip galvanised coatings after the cathodic polarisation tests in the accelerated solution with pH 8.4

Hot dip galvanised coating	Cathodic current density ($\mu A/cm^2$) at -1.1 V (*vs* SCE)
G-0.8Cu-wq	31.0
G-0.2Cu-wq	29.0
G-0.2Zr-wq	32.0
G-CP-wq	29.0
G-1.0Sb-wq	29.0
G-Pb-wq	36.0
G-0.4Mn-wq	7.0

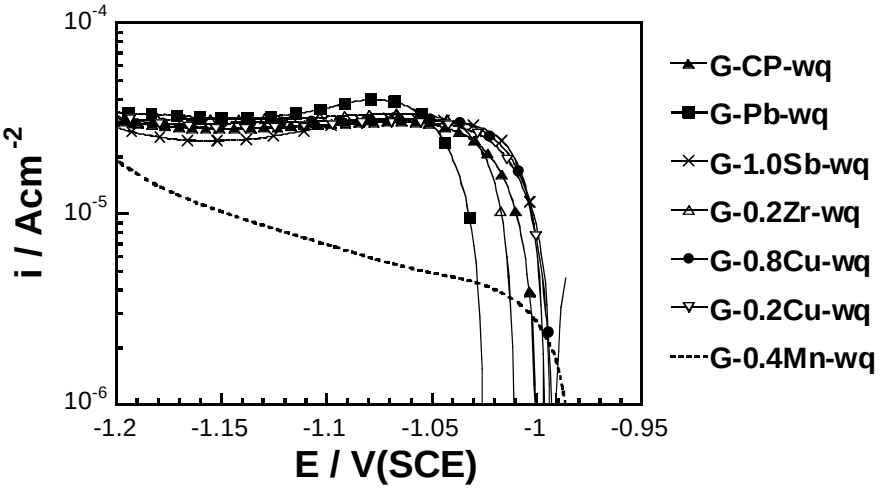

Fig 6.2 Potentiodynamic cathodic polarisation curves for water-quenched hot dip galvanised coatings in the accelerated solution (0.1 M NaCl + 0.1 M Na_2SO_4 + 0.01 M $NaHCO_3$) with pH 8.4 with a scan rate of 1 mV/s, tests started immediately after samples were transferred into solution.

Table 6.2 summarises the cathodic current density of each hot dip galvanised coating at potential of -1.1 V (*vs* SCE). Apart from the Mn-containing coating G-0.4Mn-wq, which shows a significantly lower cathodic current density than that of G-CP-wq, all other coatings with the additions (Cu, Zr and Sb) have similar cathodic current densities to that of G-CP-wq. It was also found that the effect of Pb on promoting the cathodic reaction on Zn is reduced when it is present in the hot dip galvanised coating.

Mn additions can reduce both the anodic and cathodic reactivity of hot dip galvanised coatings. It is therefore the most beneficial addition which could improve the corrosion resistance of hot dip galvanised coating in atmospheric environments. In practice, 0.005 wt % Al is often added deliberately to the molten Zn bath to significantly reduce the rapid oxidation of molten Zn during hot dip galvanising. In addition, most of the hot dip galvanised coatings are made by air cooling after withdrawal of the sample from the molten Zn bath. Thus, in the following section, the corrosion behaviour of air-cooled Mn-containing hot dip galvanised coatings with addition of 0.005 wt % Al will be mainly investigated.

6.1.2 Polarisation curves of Mn-containing coatings

6.1.2.1 Effect of Al addition to the bath

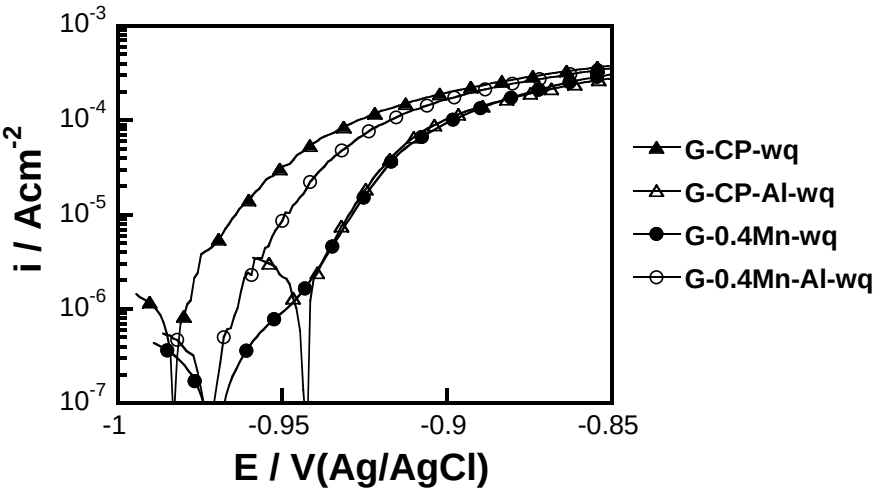

Fig 6.3 Effect of 0.005 wt % Al additions on potentiodynamic anodic polarisation curves for water-quenched hot dip galvanised coatings with and without 0.4 wt % Mn in naturally aerated 0.1 M NaCl with pH 6 with a scan rate of 1 mV/s, tests started immediately after samples were transferred into solution.

To evaluate the effect of small Al additions (0.005 wt %) on the corrosion behaviour of hot dip galvanised coating, preliminary experiments were carried out on water-quenched hot dip galvanised coatings G-CP-wq and G-0.4Mn-wq. Al addition was

found to affect the corrosion behaviour of hot dip galvanised coatings, especially on the cathodic reactivity. The typical results are shown in Fig 6.3 and Fig 6.4.

Fig 6.3 shows the typical anodic polarisation curves for water-quenched hot dip galvanised coatings with additions of Mn and Al in naturally aerated 0.1 M NaCl with pH 6. It was found that the addition of 0.005 wt % Al can significantly decrease the anodic activity of G-CP-wq, but for G-0.4Mn-wq, the addition of Al increases the anodic activity. The reason that Al has such an effect is not clear. For the cathodic polarisation curves as shown in Fig 6.4, the addition of 0.005 wt % Al can decrease the cathodic reactivity of G-CP-wq, but increase the cathodic reactivity of G-0.4Mn-wq.

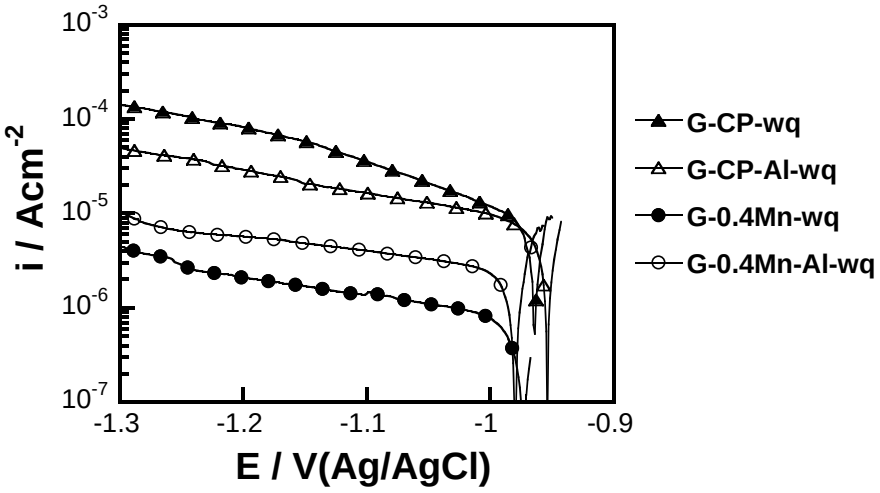

Fig 6.4 Effect of 0.005 wt % Al addition on potentiodynamic cathodic polarisation curves for water-quenched hot dip galvanised coatings with and without 0.4 wt % Mn in 0.1 M NaCl with pH 6 with a scan rate of 1 mV/s, tests started immediately after samples were transferred into solution.

Table 6.3 summarises the cathodic current densities of each hot dip galvanised coating at a potential of -1.1 V (vs SCE). The absolute values of cathodic current densities of the hot dip galvanised coatings were found to increase in the following order: G-0.4Mn-wq < G-0.4Mn-Al-wq < G-CP-Al-wq < G-CP-wq. Under free corrosion conditions in neutral solution, where local cathodes on the surface supply cathodic current to support anodic reactions at the local anodes, the corrosion rate of Zn is normally controlled by the reduction of oxygen [2]. As G-0.4Mn-Al-wq has a significantly lower

cathodic current density than that of G-CP-Al-wq, its corrosion rate in atmospheric environments should also be lower than that of the commercially-pure hot dip galvanised coating. The results of atmospheric corrosion will be explored in Section 6.5.

Table 6.3 Comparison of cathodic current density of water-quenched hot dip galvanised coatings after the cathodic polarisation tests in 0.1 M NaCl solution with pH 6 (average of three measurements)

Hot dip galvanised coating	Cathodic current density ($\mu A/cm^2$) at -1.1 V (*vs* SCE)
G-CP-wq	36.0 ± 5.0
G-CP-Al-wq	16.0 ± 2.0
G-0.4Mn-wq	2.0 ± 1.0
G-0.4Mn-Al-wq	6.0 ± 2.0

6.1.2.2 Comparison of air-cooled and water-quenched Mn coatings

In practice, most hot dip galvanised coatings were made by air cooling after withdrawal from the molten Zn bath. In this section, the corrosion behaviour of air-cooled and water-quenched Mn-containing coatings was examined. The commercially-pure Zn coating and the coatings with addition of Mn (0.4 and 0.8 wt %) were examined for this purpose with all coatings containing 0.005 wt % Al.

The cathodic polarisation curves for air-cooled and water-quenched hot dip galvanised coatings with additions of Mn and Al in naturally aerated 0.1 M NaCl with pH 6 is shown in Fig 6.5. The cathodic current densities of the hot dip galvanised coatings at a potential of -1.1 V (*vs* SCE) are summarised in Table 6.4. The results reveal that air cooling has only a slight effect on the corrosion behaviour. For the commercially-pure Zn coating, the air-cooled coating shows a slightly lower cathodic current density than the water-quenched coating, while for the Mn-containing hot dip galvanised coatings, air-cooled coatings show slightly higher cathodic current densities than the water-quenched coatings. It was also found that the cathodic current densities of the Mn-containing coatings

(with addition of 0.4 wt % and 0.8 wt % Mn) were almost same. Both of the air-cooled Mn-containing coatings (G-0.4Mn-Al-air and G-0.8Mn-Al-air) have approximately 50 % of the cathodic current density of the commercially pure Zn coating (G-CP-Al-air).

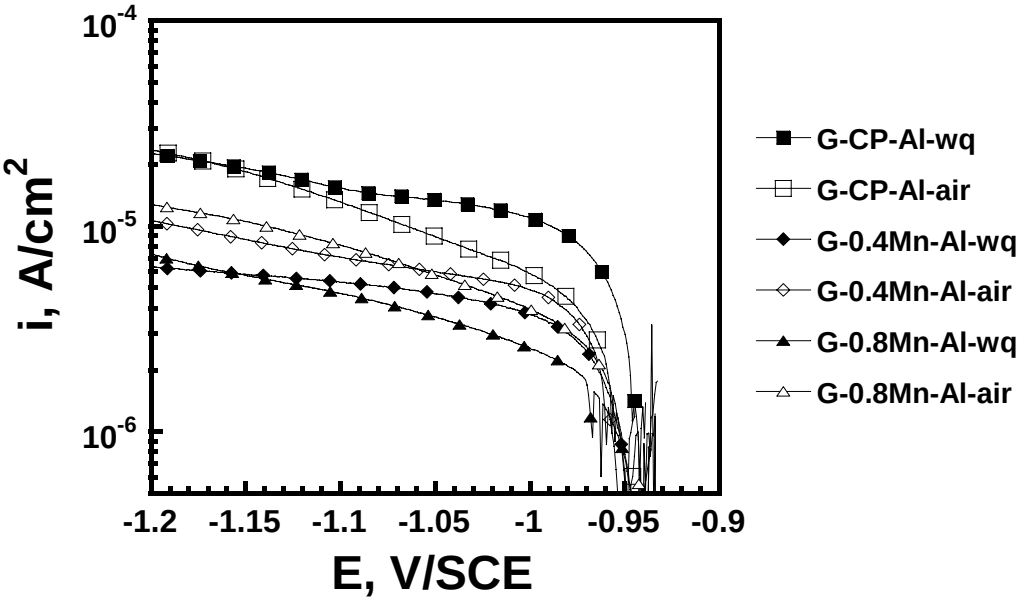

Fig 6.5 Potentiodynamic cathodic polarisation curves for water-quenched and air-cooled hot dip galvanised coatings with Mn and Al additions in 0.1 M NaCl with pH 6 with a scan rate of 1 mV/s, tests started immediately after samples were transferred into solution.

Table 6.4 Comparison of cathodic current density of air-cooled and water-quenched hot dip galvanised coatings after the cathodic polarisation tests in 0.1 M NaCl solution with pH 6 (average of three measurements)

Hot dip galvanised coating	Cathodic current density ($\mu A/cm^2$) at -1.1 V (*vs* SCE)
G-CP-Al-wq	16.0 ± 2.0
G-CP-Al-air	13.0 ± 3.0
G-0.4Mn-Al-wq	6.0 ± 2.0
G-0.4Mn-Al-air	8.0 ± 1.0
G-0.8Mn-Al-wq	6.0 ± 1.0
G-0.8Mn-Al-air	8.0 ± 2.0

Fig 6.6 shows the anodic polarisation curves for air-cooled and water-quenched hot dip galvanised coatings with additions of Mn and Al in naturally aerated 0.1 M NaCl with pH 6. It was found that both air-cooled and water-quenched coatings showed similar

anodic behaviour. This result indicates that cooling method has no significant effect on the anodic activity of hot dip galvanised coating.

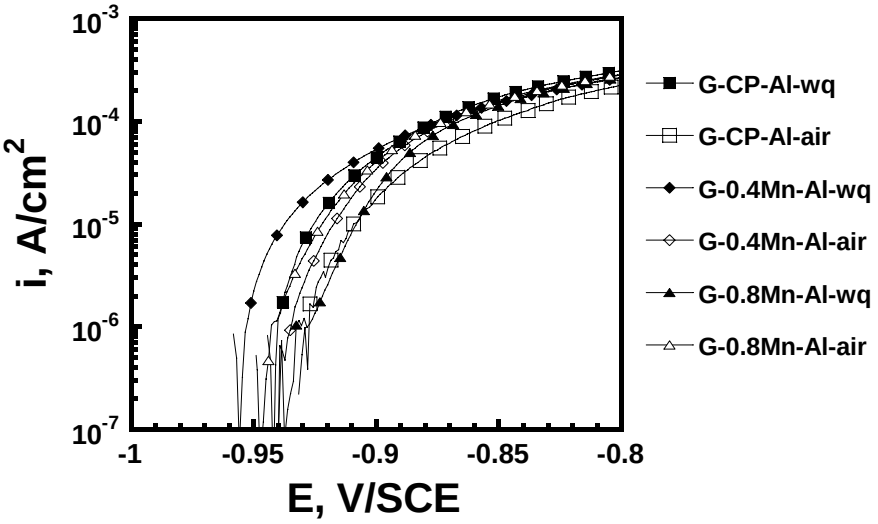

Fig 6.6 Potentiodynamic anodic polarisation curves for water-quenched and air-cooled hot dip galvanised coatings with Mn and Al additions in 0.1 M NaCl with pH 6 with a scan rate of 1 mV/s, tests started immediately after samples were transferred into solution.

6.1.3 Air-cooled coatings with a combination of Mn and Cu additions

The corrosion behaviour of the air-cooled hot dip galvanised coatings (containing 0.005 wt % Al) with additions of Cu, Sb, Mn and Mn-Cu were investigated in this section. Potentiodynamic polarisation measurements were carried out in 0.1 M NaCl solution by using the droplet cell. The advantage of using the microelectrochemical cell is to allow multiple measurements on one sample and the sample does not need to be lacquered. Detail description of the microelectrochemical cell is described in Section 3.3.1.2.

Fig 6.7 shows the anodic polarisation curves for the air-cooled hot dip galvanised coatings with additions of Cu, Sb, Mn and Mn-Cu combinations in naturally aerated 0.1 M NaCl with pH 6. In contrast with the anodic behaviour of polished Zn alloys in sodium chloride solution, there is no distinct passive range for the as-received air-cooled hot dip galvanised coatings in the same solution. The result indicates that the coatings

G-CP-Al-air, G-Pb-Al-air, G-0.2Cu-Al-air, G-0.8Cu-Al-air and G-0.8Mn-0.8Cu-Al-air exhibit similar anodic behaviour, while the coating G-0.4Mn-Al-air, G-0.8Mn-Al-air and G-0.8Mn-0.2Cu-Al-air show similar anodic behaviour. Apart from G-0.8Mn-0.8Cu-Al-air, all other Mn-containing coatings have lower OCP (open circuit potential) and slightly higher anodic current densities than G-CP-Al-air.

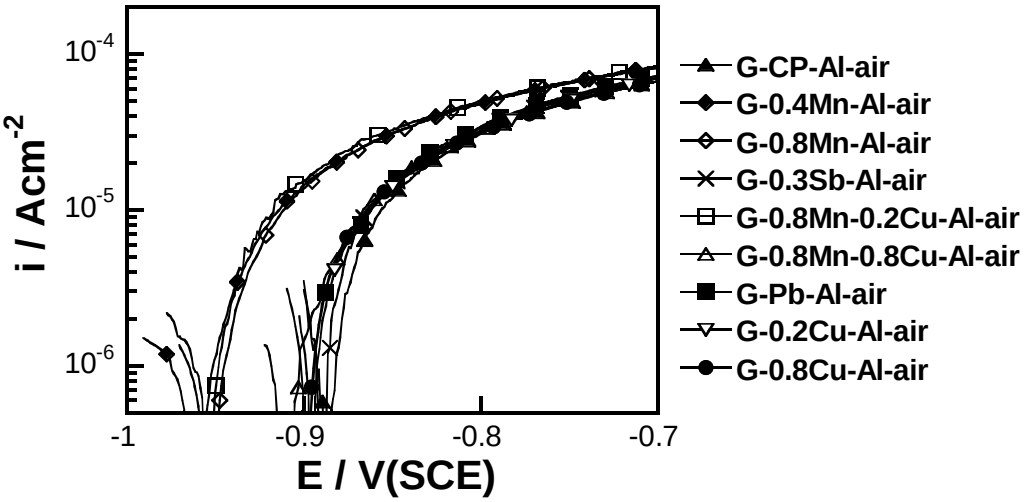

Fig 6.7 Potentiodynamic anodic polarisation curves for air-cooled hot dip galvanised coatings with Mn and Al additions in 0.1 M NaCl with pH 6 with a scan rate of 1 mV/s. Tests were carried out by using the droplet cell.

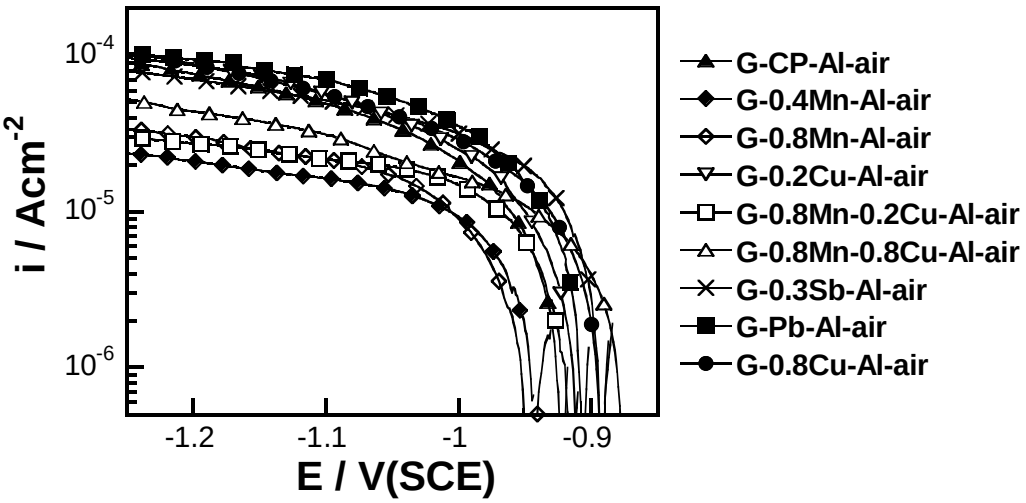

Fig 6.8 Potentiodynamic cathodic polarisation curves for air-cooled hot dip galvanised coatings with Mn and Al additions in 0.1 M NaCl with pH 6 with a scan rate of 1 mV/s. Tests were carried out by using the droplet cell.

Table 6.5 Comparison of cathodic current density of air-cooled hot dip galvanised coatings after the cathodic polarisation tests in 0.1 M NaCl solution with pH 6 (average of three measurements)

Hot dip galvanised coating	Cathodic current density ($\mu A/cm^2$) at -1.1 V (vs SCE)
G-CP-Al-air	50.0
G-Pb-Al-air	70.0
G-0.3Sb-Al-air	52.0
G-0.4Mn-Al-air	16.0
G-0.8Mn-Al-air	20.0
G-0.2Cu-Al-air	57.0
G-0.8Cu-Al-air	57.0
G-0.8Mn-0.2Cu-Al-air	20.0
G-0.8Mn-0.8Cu-Al-air	30.0

The additions of Cu and Sb were found to have no significant effect on the cathodic reactivity of the hot dip galvanised coating. Again, G-Pb-Al-air shows the highest cathodic current density. Table 6.5 summaries the cathodic current density of each hot dip galvanised coating at a potential of -1.1 V (*vs* SCE). The data were collected from repeated measurements which showed good reproducibility. The result shows that the cathodic current densities of all Mn-containing coatings are significantly lower than that of G-CP-Al-air as shown in Fig 6.8. The cathodic current densities of the Mn-containing coatings (with addition of 0.4 wt % and 0.8 wt % Mn) are almost same. The Mn-containing coating G-0.8Mn-0.8Cu-Al-air shows a slightly higher cathodic current density than other Mn coatings. It should be noted that the cathodic current densities of all hot dip galvanised coatings measured in the droplet cell were higher than that measured in the beaker cell. This is probably because that the oxygen can easily transfer into solution due to the direct contact with air when a droplet cell is used.

6.2 Linear polarisation resistance

Linear polarisation measurements were also carried out to investigate the corrosion resistance of hot dip galvanised coatings. The details of linear polarisation resistance (LPR) measurement can be found in Section 3.3.4. The corrosion current density i_{corr} is proportional to the value of LPR^{-1} [140]. The proportionality constant k can be calculated from the Tafel slopes of anodic and cathodic polarization curves (see Equation 3.1). In corrosion systems, however, distinct Tafel regions do not always appear on the polarization curves. Thus, it is preferable that the k value should be determined in advance from the correlation between the measured LPR and i_{corr} determined from mass loss measurement. Accordingly, in this study, the LPR obtained was used as an index of the corrosion resistance, assuming that the k value does not change during the immersion test. The solution was the accelerated solution (described in Section 3.3.2) which is to simulate the marine atmospheric corrosion environment. All hot dip galvanised coatings were immersed in this naturally aerated accelerated solution. The instantaneous linear polarisation resistances (LPR) were monitored by using a continuous LPR technique which can be achieved by using Corrware electrochemical measurement software during the corrosion tests. All LPR measurements were carried out at open circuit potential (OCP).

6.2.1 Water-quenched coatings

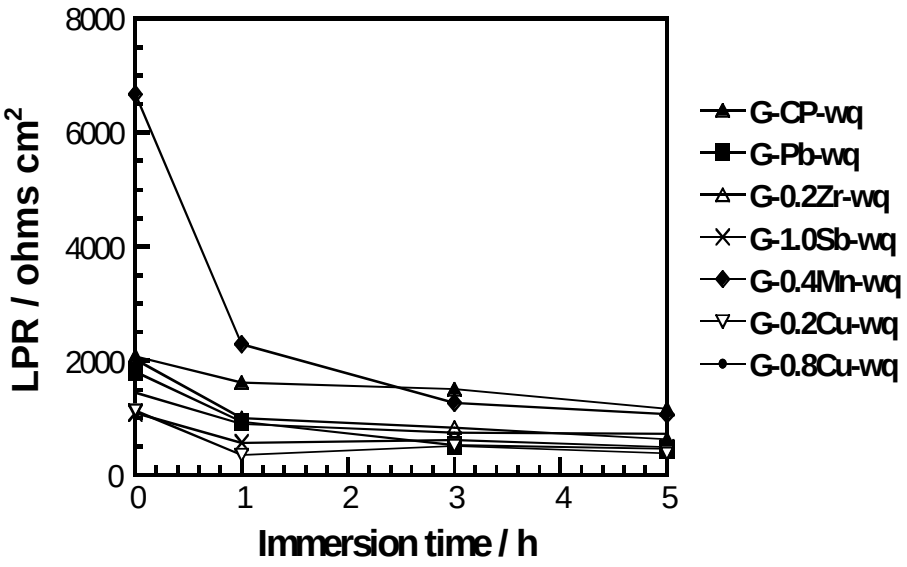

Fig 6.9 LPR (linear polarization resistance) as a function of immersion time for water-quenched hot dip galvanised coatings in the accelerated solution (0.1 M NaCl + 0.1 M Na_2SO_4 + 0.01 M $NaHCO_3$)

Fig 6.9 shows LPR of water-quenched hot dip galvanised coatings with and without additions (Cu, Sb, Zr and Mn) as a function of immersion time in the accelerated solution. Initially, the Mn-containing coating (G-0.4Mn-wq and G-CZM-wq) show a higher LPR than the commercially-pure Zn coating (G-CP-wq). All other coatings have slightly lower LPR than G-CP-wq. With increasing immersion time, the LPR of Mn-containing coatings decrease rapidly. After 3 h immersions in the accelerated solution, it is close to the LPR of G-CP-wq. After LPR tests, the corrosion morphology was examined by digital imaging at low magnification. Fig 6.10 and Fig 6.11 show the surface morphologies of the hot dip galvanised coatings after 5 h LPR tests in the accelerated solution. It is evident that localised corrosion has occurred on the surface for the coatings without Mn addition. Many pits and corrosion products were found on the surface of hot dip galvanised coatings without Mn addition. Fewer pits and corrosion products were found on the surface of the

Mn-containing coating (G-0.4Mn-wq). The low LPR of the hot dip galvanised coatings is due to localized corrosion on the surface. The higher LPR of the Mn-containing coating than other coatings reveals that Mn-rich oxide on the Mn-containing coatings can inhibit corrosion of hot dip galvanised coating in the accelerated solution especially during the first hour of immersion test.

The corrosion behaviour of the as received hot dip galvanised coatings immersed in the accelerated solution is different from that of polished Zn alloys. As shown in previous results (Fig 4.26), the LPR of most polished Zn alloys (except for Z-0.8Cu-wq and Z-Pb-wq) increased with the increasing of immersion time. This result suggests that the corrosion behaviour of hot dip galvanised coating and Zn alloys is sensitive to the preparation conditions. This result indicated that the hot dip galvanised coatings are more susceptible to corrosion in the accelerated solution than the polished Zn alloys.

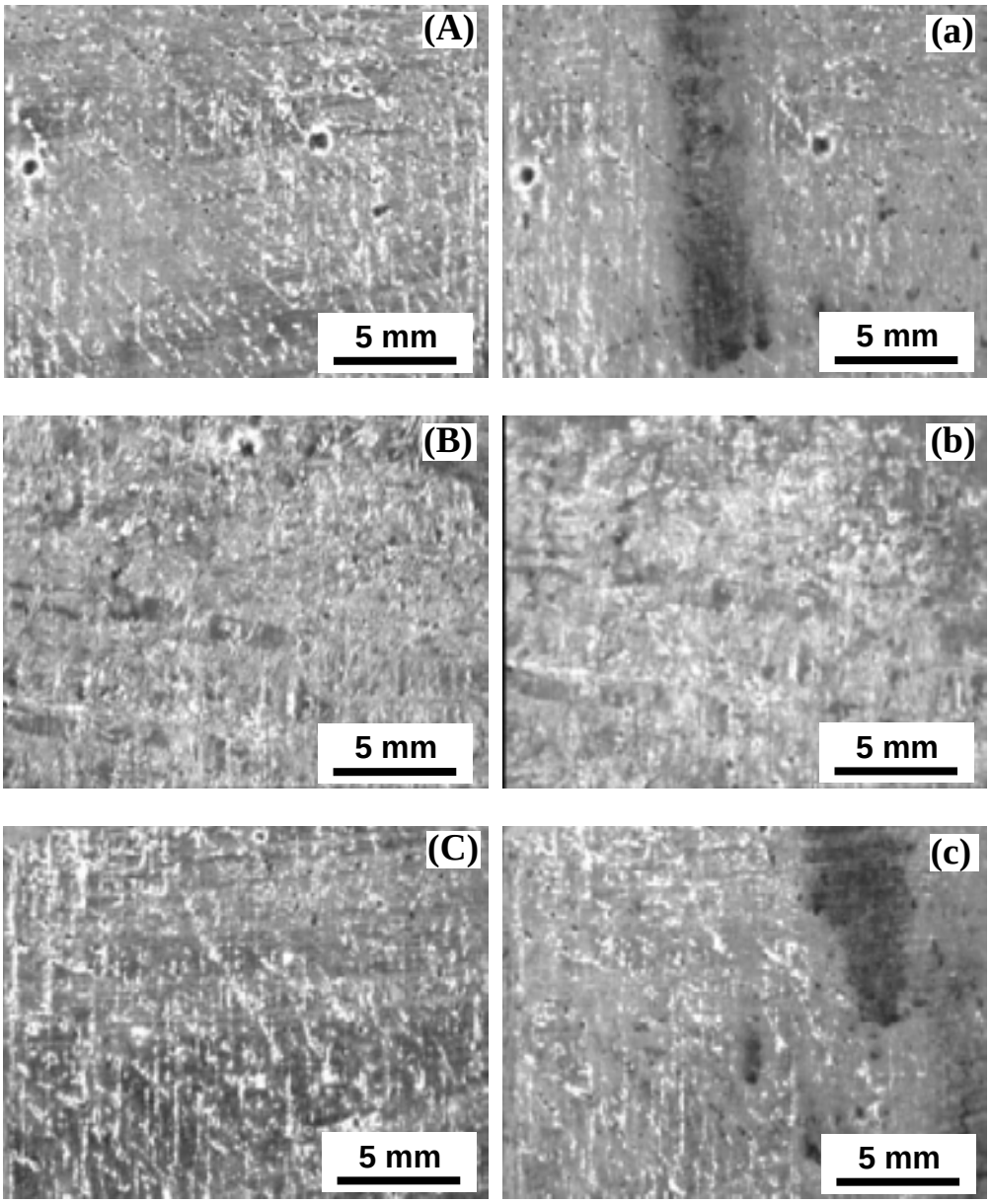

Fig 6.10 Digital images of (A) and (a) G-CP-wq, (B) and (b) G-0.4Mn-wq, (C) and (c) G-0.2Zr-wq before (A-C) and after (a-c) 5 h LPR tests in the accelerated solution (0.01 M NaCl + 0.01M Na_2SO_4 + 0.001 M $NaHCO_3$).

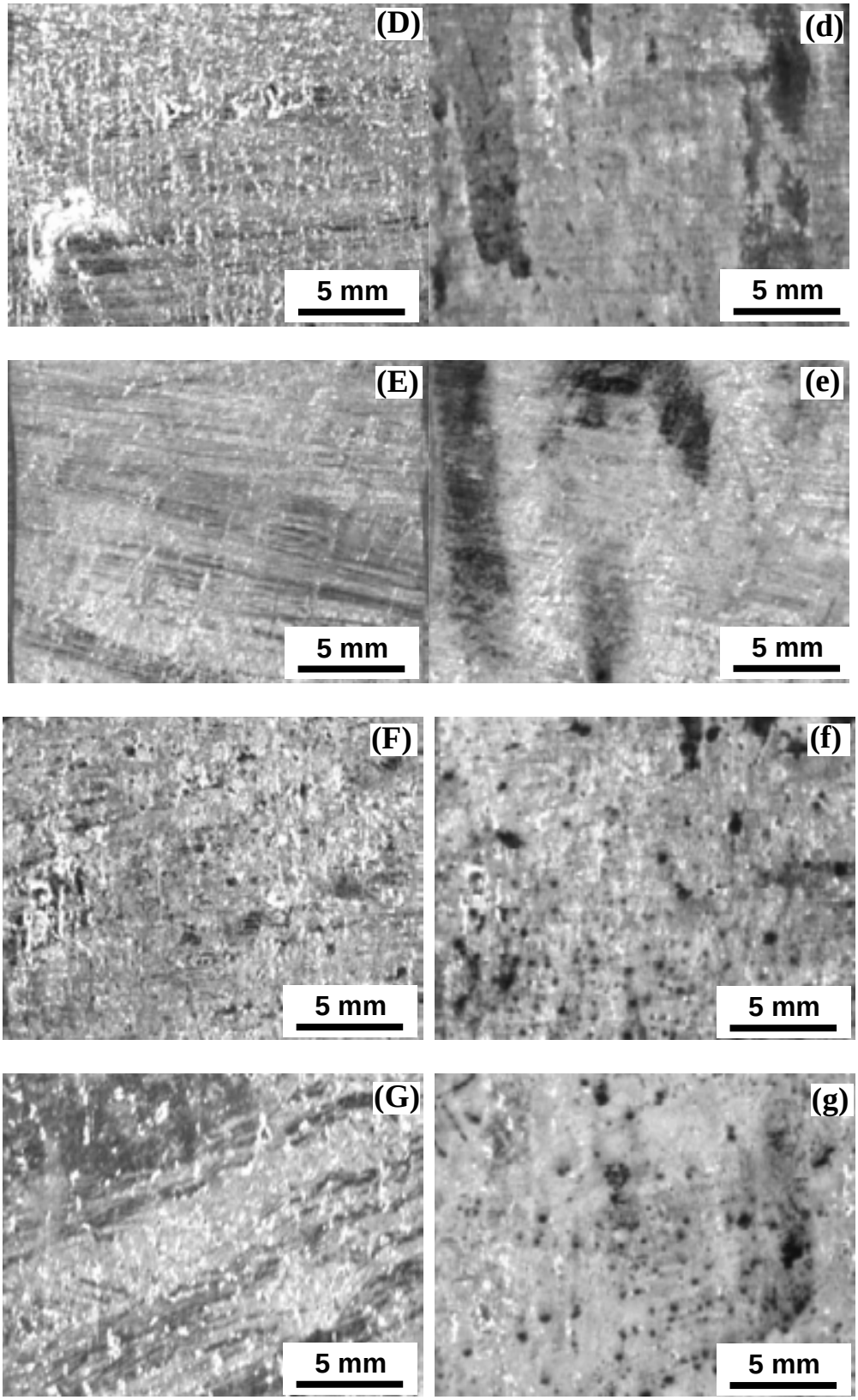

Fig 6.11 Digital images of (D) and (d) G-0.2Cu-wq, (E) and (e) G-0.8Cu-wq, (F) and (f) G-1.0Sb-wq, (G) and (g) G-Pb-wq before (D-G) and after (d-g) 5 h LPR tests in the accelerated solution (0.01 M NaCl + 0.01M Na_2SO_4 + 0.001 M $NaHCO_3$).

6.2.2 Air-cooled Mn-coatings

To further confirm the superior corrosion behaviour of Mn-containing hot dip galvanised coatings. LPR tests were also carried out on air-cooled hot dip galvanised coatings with Mn addition of two levels (0.4 wt % and 0.8 wt %). For comparison, the LPR of the air-cooled commercially-pure Zn coating was also measured. The results are shown in Fig 6.12. Similar to those found for water-quenched coatings; the Mn-containing coatings (G-0.4Mn-Al-air and G-0.8Mn-Al-air) show higher LPR than the commercially-pure Zn coating (G-CP-Al-air). The LPR of both G-0.8Mn-Al-air and G-0.4Mn-Al-air were found to decrease with increasing immersion time. The LPR of G-0.8Mn-Al-air is higher than that of G-0.4 Mn-Al-air.

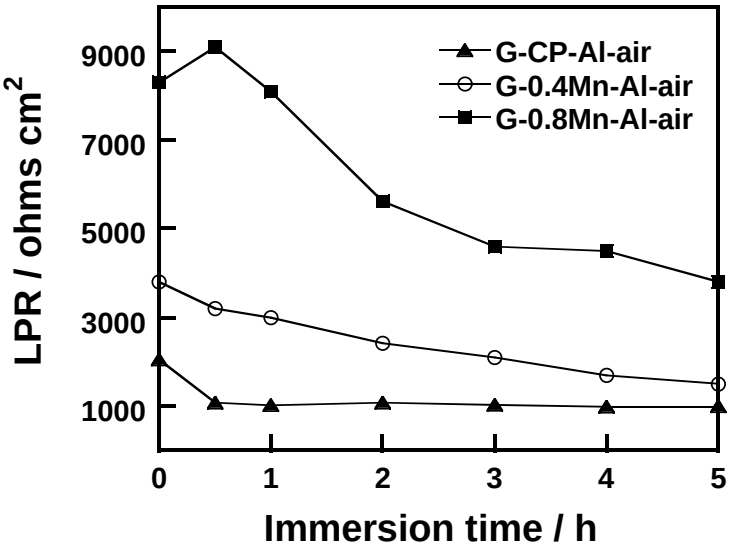

Fig 6.12 LPR (linear polarization resistance) as a function of immersion time for air-cooled hot dip galvanised coatings with Mn addition in the accelerated solution (0.01 M NaCl + 0.01M Na_2SO_4 + 0.001 M $NaHCO_3$).

Fig 6.13 shows the surface morphologies of the hot dip galvanised coatings after 5 h LPR tests in the accelerated solution. It is clear that localised corrosion occurred on the surface for all hot dip galvanised coatings. However, more pits and corrosion products were found on the surface of the commercially-pure Zn coatings, while fewer pits and corrosion products were found on the surface of the Mn-containing coatings. This result is consistent

with those found on water-quenched coatings, which indicates that Mn-rich oxides on the Mn-containing coatings can inhibit corrosion of hot dip galvanised coating in the accelerated solution, especially during the first stage of corrosion.

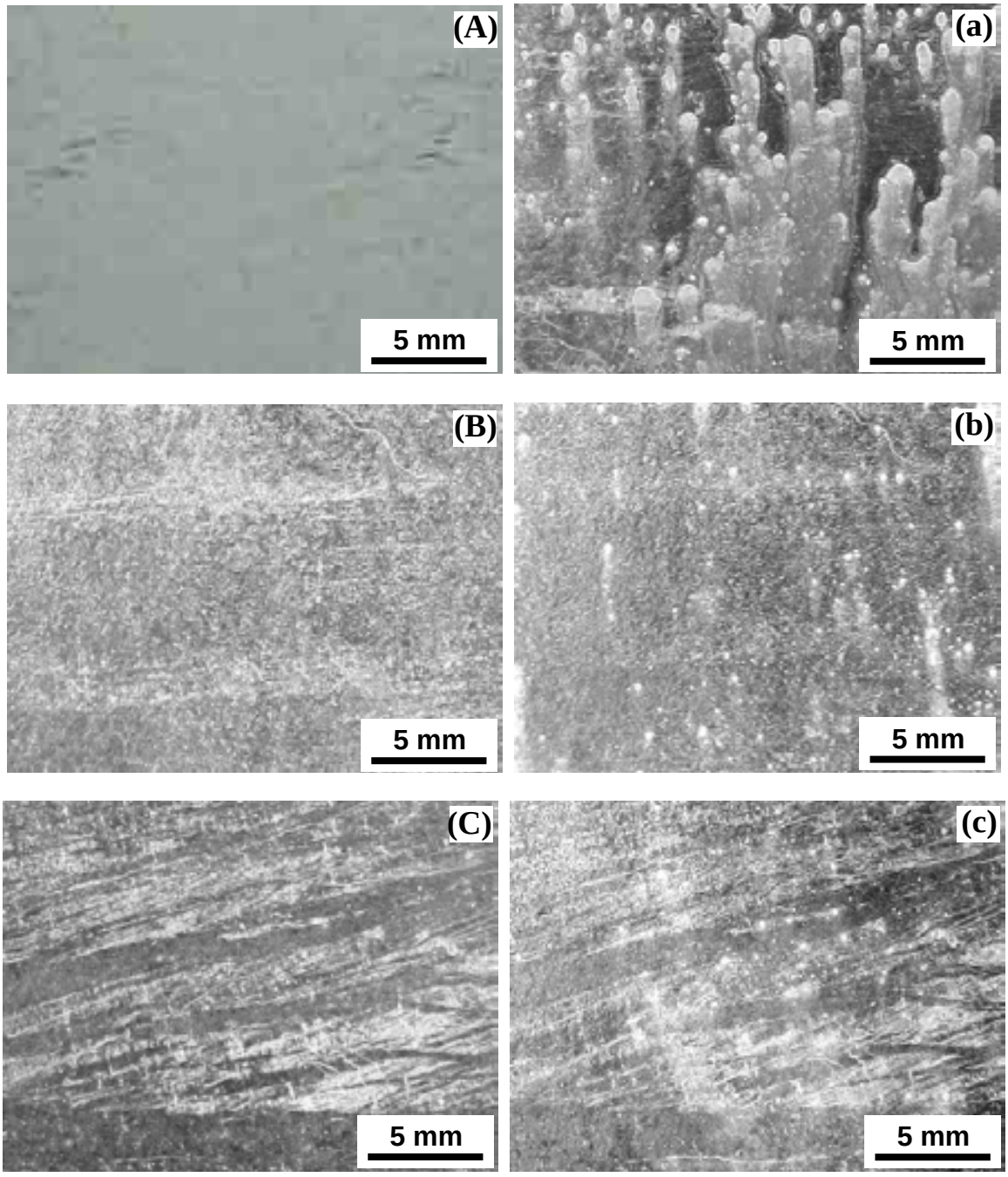

Fig 6.13 Digital images of (A) and (a) G-CP-Al-air, (B) and (b) G-0.4Mn-Al-air, and (C) and (c) G-0.8Mn-Al-air before (A-C) and after (a-c) LPR measurements in the accelerated solution (0.01 M NaCl + 0.01M Na_2SO_4 + 0.001 M $NaHCO_3$) for 5 h.

6.3 Immersion tests in 0.01 M NaCl solution

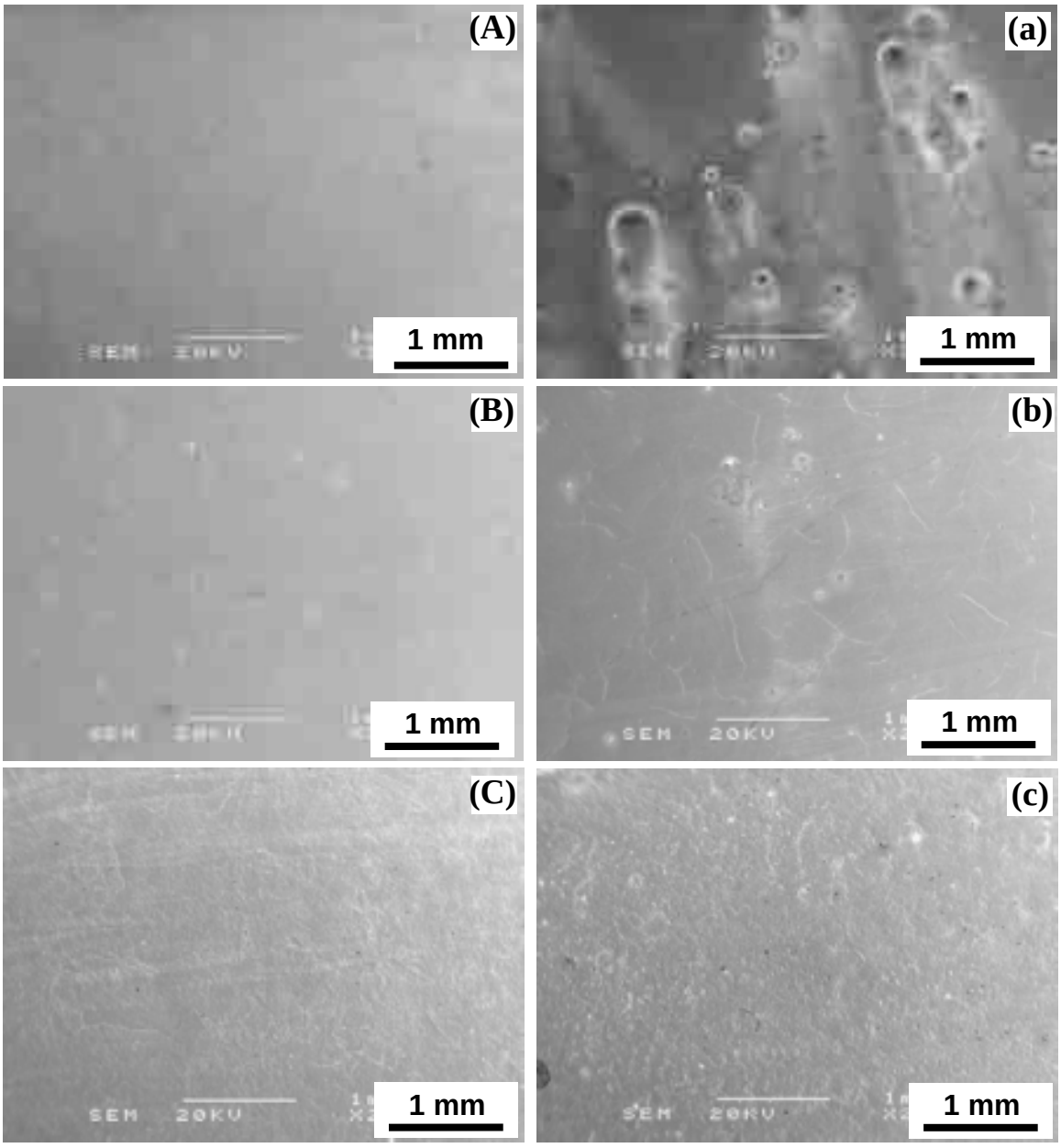

Fig 6.14 SEM images of (A) and (a) G-CP-Al-air, (B) and (b) G-0.4Mn-Al-air, (C) and (c) G-0.8Mn-Al-air before (A-C) and after (a-c) immersion test in naturally aerated 0.01 M NaCl with pH 6 for 2 h.

In-situ immersion tests of the commercially pure Zn coating and Mn-containing coatings in naturally aerated 0.01 M NaCl with pH 6 were also investigated. Fig 6.14 shows the surface morphologies of the hot dip galvanised coatings after a 2 h immersion test. It is

evident that localised corrosion occurred on the surface of the commercially pure Zn coating (G-CP-Al-air). Many pits and corrosion products were found on the surface of this coating after the immersion test. In contrast, few pits and less corrosion products were found on the surface of the Mn-containing coatings. This result further confirms that the Mn-containing coatings have higher corrosion resistance than the commercially-pure Zn coating.

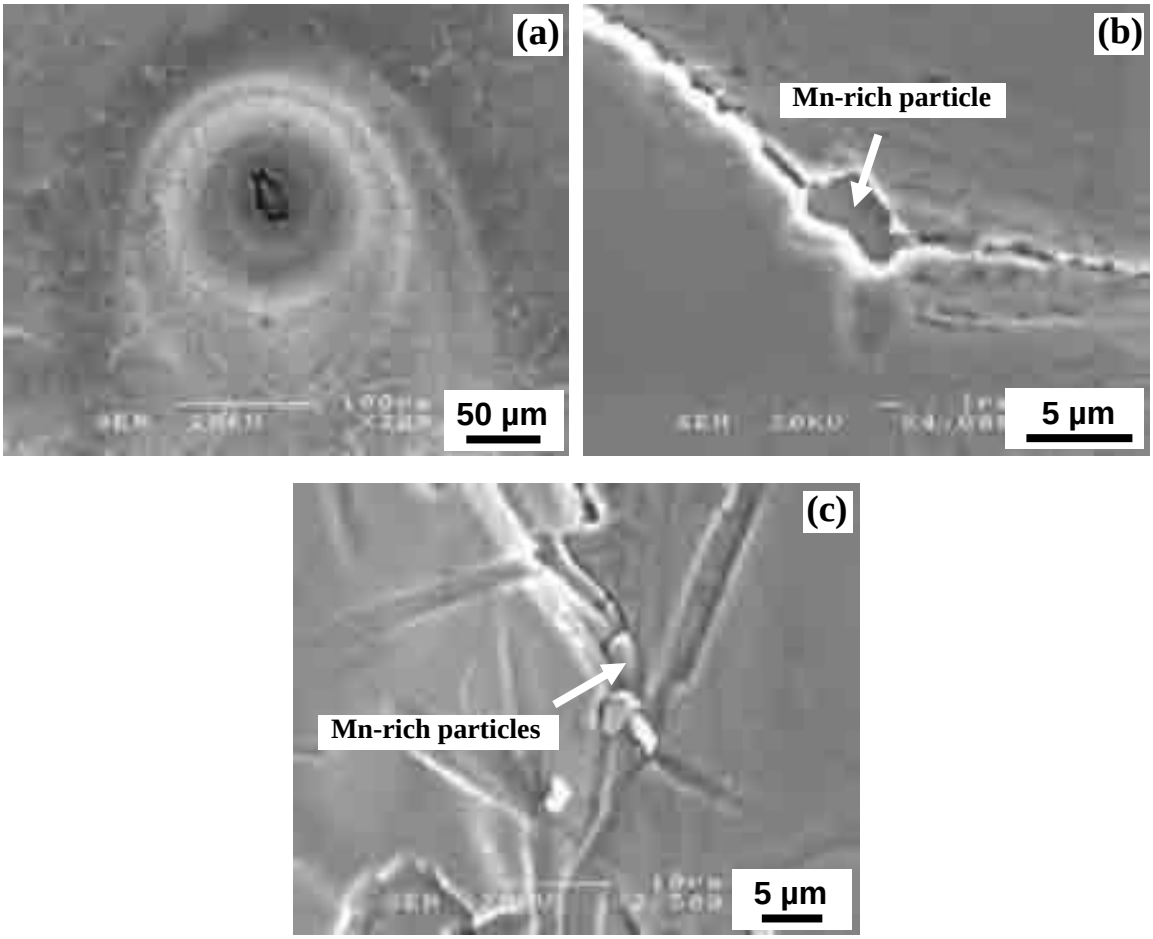

Fig 6.15 SEM images of (a) G-CP-Al-air, (b) G-0.4Mn-Al-air, and (c) G-0.8Mn-Al-air after immersion test in naturally aerated 0.01 M NaCl with pH 6 for 2 h.

As shown in the previous results (Section 5.1.6.2), there are Mn-rich particles on the surface of Mn-containing hot dip galvanised coatings. However, no pits and corrosion products were found around the Mn-rich particles for the Mn-containing coatings after the

immersion test in 0.01M NaCl solution as shown in Fig 6.15 (b) and (c). This result indicates that the Mn-rich particles are not pit initiation sites. For the commercially pure Zn coatings, significant pits were found on the surface after the immersion test. A typical pit morphology is shown in Fig 6.15 (a). There is an obvious pit on the corroded surface which is surrounded by the corrosion products. Although there are no detectable particles responsible for the pit initiation, impurities and fine intermetallic particles could be pit initiation sites for G-CP-Al-air.

6.4 Cyclic tests

The cyclic test is an accelerated corrosion testing method which has been developed recently to simulate atmospheric corrosion of Zn and hot dip galvanised coatings. In this study the cyclic wet-dry was conducted by exposing the samples to an alternate condition of 1 h-immersion in the accelerated solution and 23 h-drying in air. During 1 h immersion in solution, the LPR was recorded every 30 minutes. All the experiments were repeated to examine the reproducibility.

6.4.1 Water-quenched Mn-coating

Fig 6.16 shows the LPR of the water-quenched Mn-containing coatings and the commercially pure Zn coating as a function of immersion time in the accelerated solution. Initially, the Mn-containing coating (G-0.4Mn-wq) showed a higher LPR than the commercially-pure Zn coating (G-CP-wq). With increasing testing cycles, the LPR of G-0.4Mn-wq decreases, whereas the LPR of G-CP-wq remains the same. This is consistent with previous findings in which the Mn-containing coating showed higher LPR than the commercially-pure Zn coating at the initial period (Fig 6.9). The cyclic corrosion test further confirmed the beneficial effect of Mn addition on improving corrosion resistance of hot dip galvanised coating.

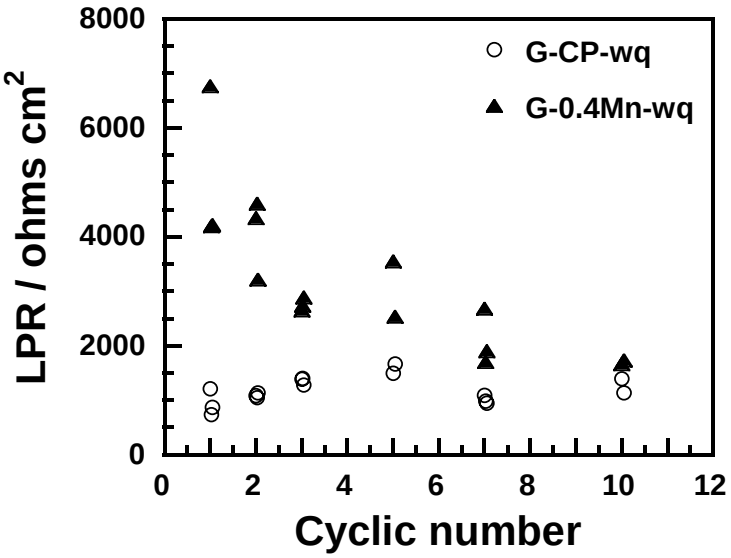

Fig 6.16 Cyclic tests of hot dip galvanised coatings with and without 0.4 wt % Mn in the accelerated solution 0.1 M NaCl + 0.1 M Na_2SO_4 + 0.01 M $NaHCO_3$ (1 cycle = 1 h in solution + 23 h in air).

6.4.2 Air-cooled coatings

The effects of alloying elements on the corrosion behaviour of air-cooled hot dip galvanised coating with addition of 0.005 wt % Al were also investigated by cyclic tests. Fig 6.17 shows the LPR of the air-cooled hot dip galvanised coatings with Cu, Mn and Mn-Cu additions as functions of immersion time in the accelerated solution (0.01 M NaCl + 0.01 M Na_2SO_4 + 0.001 M $NaHCO_3$). It is evident that the Mn-containing coating (G-0.4Mn-Al-air and G-0.8Mn-Al-air) show significantly higher LPR values than the commercially-pure Zn coating (G-CP-Al-air) during 3 days of cyclic tests. Coatings with Cu additions show similar low LPR to G-CP-Al-air. A slightly higher LPR than the commercial coating was also found for the coating with a combination of Mn and Cu (G-0.8Mn-0.2Cu-Al-air). This is in agreement with those found in previous sections in which Mn-containing coatings showed higher LPR than commercially-pure Zn coatings. Once again, this cyclic corrosion test further confirmed the beneficial effect of Mn addition on improving corrosion resistance of hot dip galvanised coatings. In the following sections, the atmospheric corrosion tests were carried out to give a final evaluation of the hot dip galvanised coatings, especially the Mn-containing coatings developed in this study.

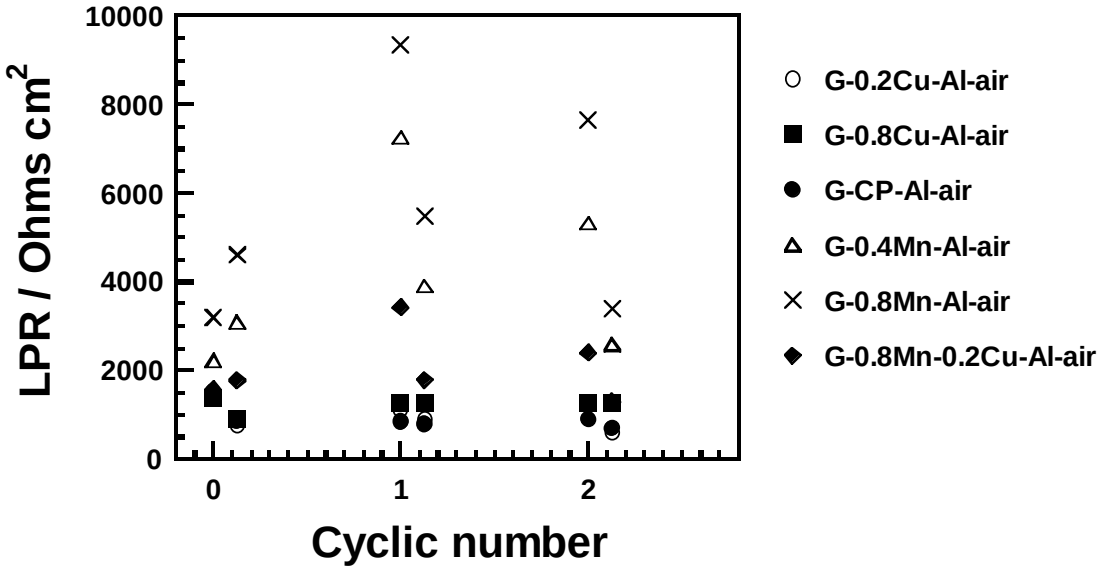

Fig 6.17 Cyclic tests of air-cooled hot dip galvanised coatings (with 0.005%Al) in 0.01NaCl + $0.01Na_2SO_4$ + $0.001NaHCO_3$ simulated solution (1 cycle = 3h in solution and 21h in air).

6.5 Atmospheric corrosion tests

To evaluate the corrosion resistance of hot dip galvanised coatings with alloying additions, atmospheric corrosion tests were also carried out. The advantage of an atmospheric corrosion test is that it can provide a real evaluation of the corrosion behaviour of hot dip galvanised coatings which are used in atmospheric environments. However, this corrosion testing method takes much longer time than the electrochemical methods and any accelerated tests.

In this study, four-month atmospheric corrosion tests were carried out. Two atmospheric corrosion sites were selected: Lyme Regis (mild marine atmosphere) and Birmingham (industrial atmosphere). The coatings with additions of Mn, Cu, Sb and Mn-Cu combination were examined for the atmospheric corrosion test. Both air-cooled and water-quenched coatings were investigated. For comparison, the results of two commercial hot dip galvanised coatings were also included.

6.5.1 Corrosion morphology

6.5.1.1 Air-cooled coatings exposed in a marine environment

The surface morphologies of the air-cooled hot dip galvanised coatings after 4 months atmospheric corrosion tests in a light marine environment are shown in Fig 6.18-25. It is evident that significant corrosion products are present on the surfaces of the two commercial hot dip galvanised coatings G-CP-Al-air (Fig 6.18) and G-Pb-Al-air (Fig 6.19).

For the Mn-containing coatings with additions of 0.4 and 0.8 wt % Mn, less corrosion had occurred on the surfaces and corrosion morphologies are uniform as shown in Fig 6.20 and Fig 6.21. This result indicates that the Mn-containing coatings G-0.4Mn-Al-air and G-0.8Mn-Al-air have better corrosion resistance than the commercial coatings G-CP-Al-air and G-Pb-Al-air in the marine environment at least for 4 months. This is probably due to the beneficial effect of Mn-rich layer which can suppress the cathodic reduction as found in the previous sections (Section 6.1.2). The Mn-rich layers were found on the top surfaces of both Mn-containing hot dip galvanised coatings with and without small Al additions (Section 5.1.6.3).

Addition of Cu was found to have no significant effect on the corrosion resistance of hot dip galvanised coating as shown Fig 6.22 and Fig 6.23. The Cu-containing coatings (G-0.2Cu-Al-air and G-0.8Cu-Al-air) show similar corrosion morphologies to G-CP-Al-air.

The coating with additions of both Mn and Cu (G-0.8Mn-0.2Cu-Al-air) shows similar corrosion morphology to the coating with only Mn addition as shown in Fig 6.24. No obvious corrosion products can be seen on the surface and the corrosion morphology is uniform compared with the commercial coating G-CP-Al-air. It can be concluded that this coating has a significant higher corrosion resistance than G-CP-Al-air in marine environments. The higher corrosion resistance of the coating with Mn and Cu combination is probably due to the beneficial effect of Mn-rich oxide layer on the surface.

For the coatings with additions of Sb, significant corrosion attack was found as

shown in Fig 6.25. This indicates that addition of Sb has no beneficial effect on the improvement of corrosion resistance of hot dip galvanised coating.

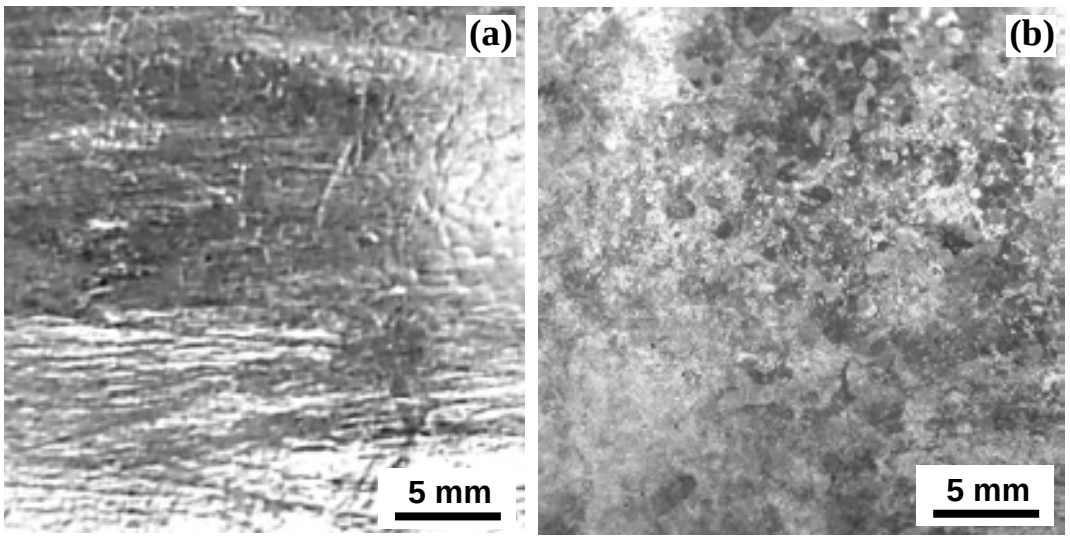

Fig 6.18 Digital camera images of the air-cooled coating G-CP-Al-air (a) before, and (b) after an atmospheric corrosion test in a marine environment at Lyme Regis for 4 months.

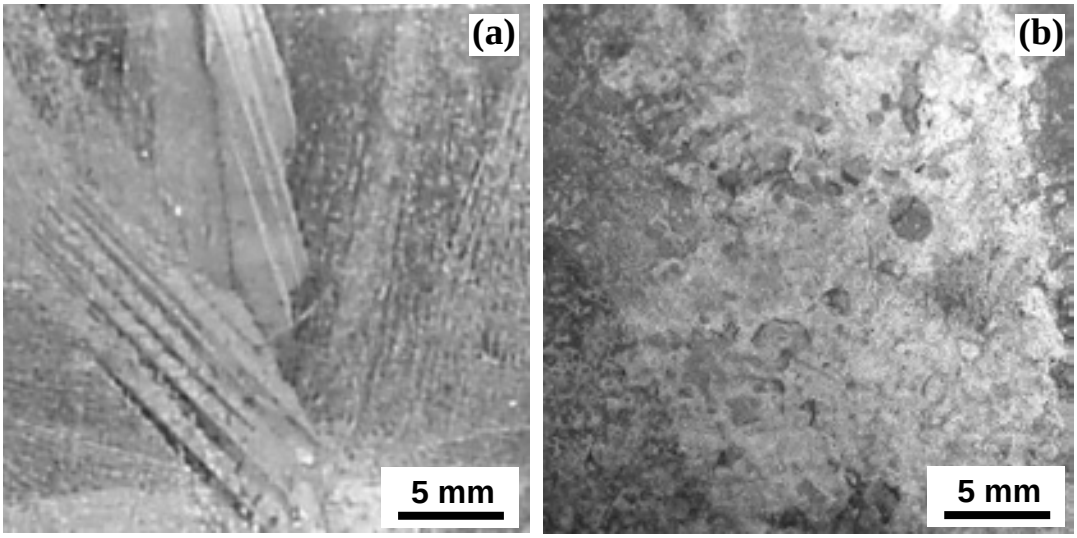

Fig 6.19 Digital camera images of the air-cooled coating G-Pb-Al-air (a) before, and (b) after an atmospheric corrosion test in a marine environment at Lyme Regis for 4 months.

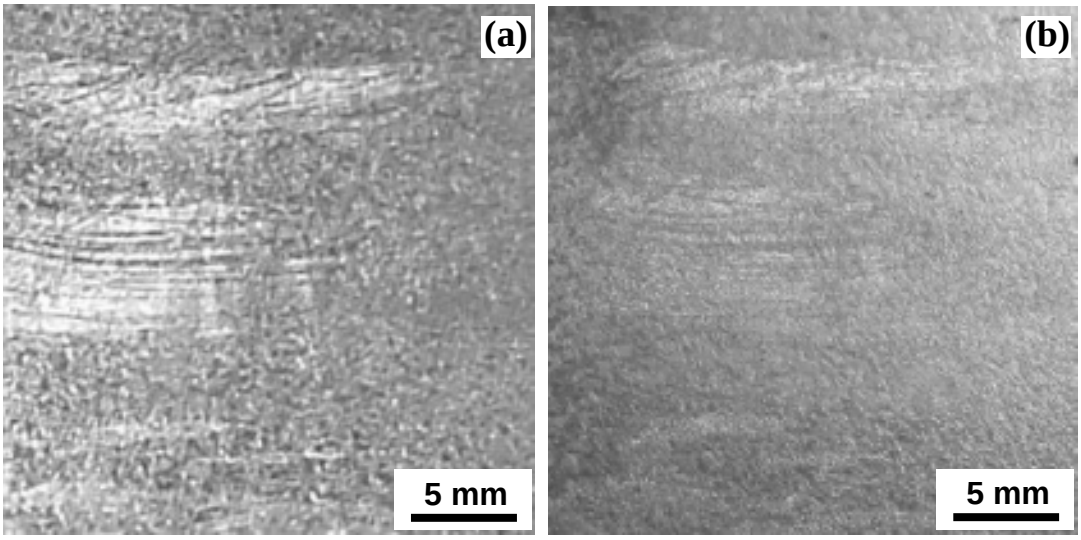

Fig 6.20 Digital camera images of the air-cooled coating G-0.4Mn-Al-air (a) before, and (b) after an atmospheric corrosion test in a marine environment at Lyme Regis for 4 months.

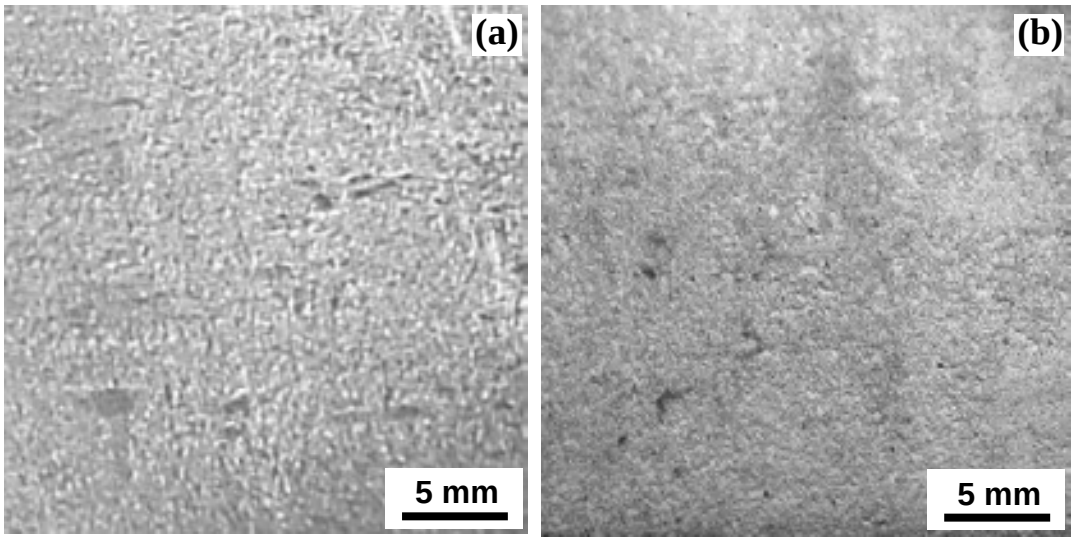

Fig 6.21 Digital camera images of the air-cooled coating G-0.8Mn-Al-air (a) before, and (b) after an atmospheric corrosion test in a marine environment at Lyme Regis for 4 months.

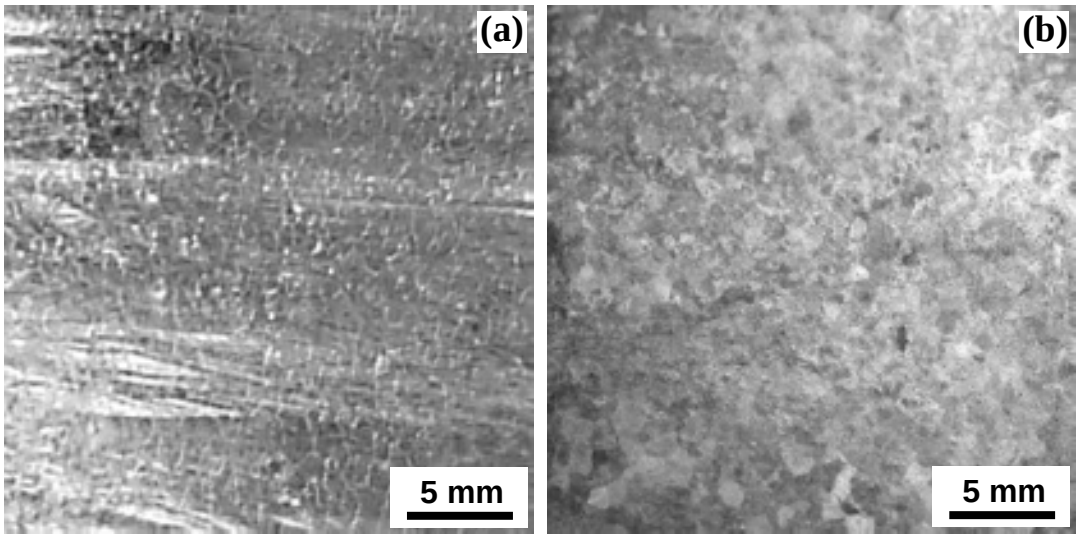

Fig 6.22 Digital camera images of the air-cooled coating G-0.2Cu-Al-air (a) before, and (b) after an atmospheric corrosion test in a marine environment at Lyme Regis for 4 months.

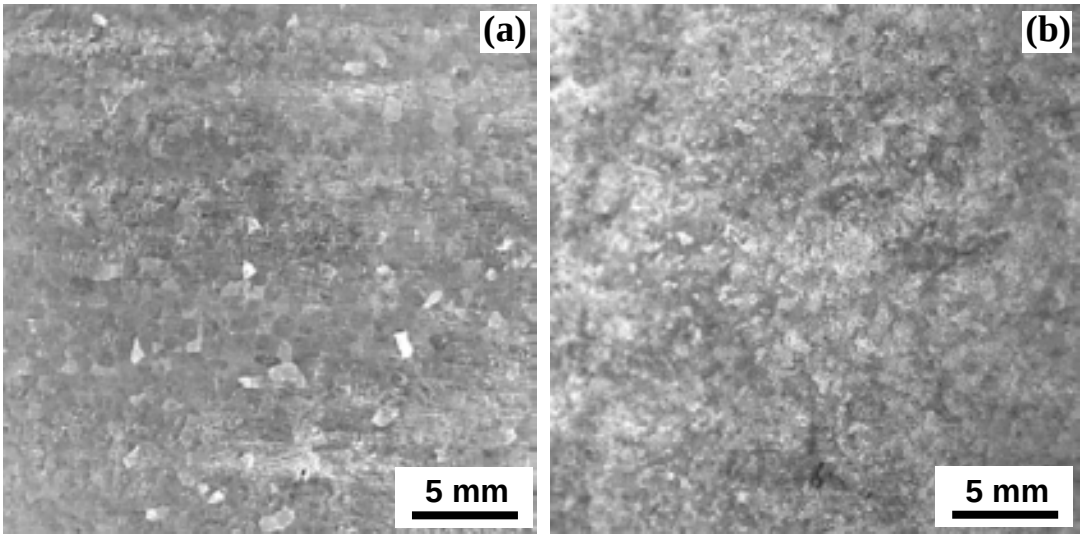

Fig 6.23 Digital camera images of the air-cooled coating G-0.8Cu-Al-air (a) before, and (b) after an atmospheric corrosion test in a marine environment at Lyme Regis for 4 months.

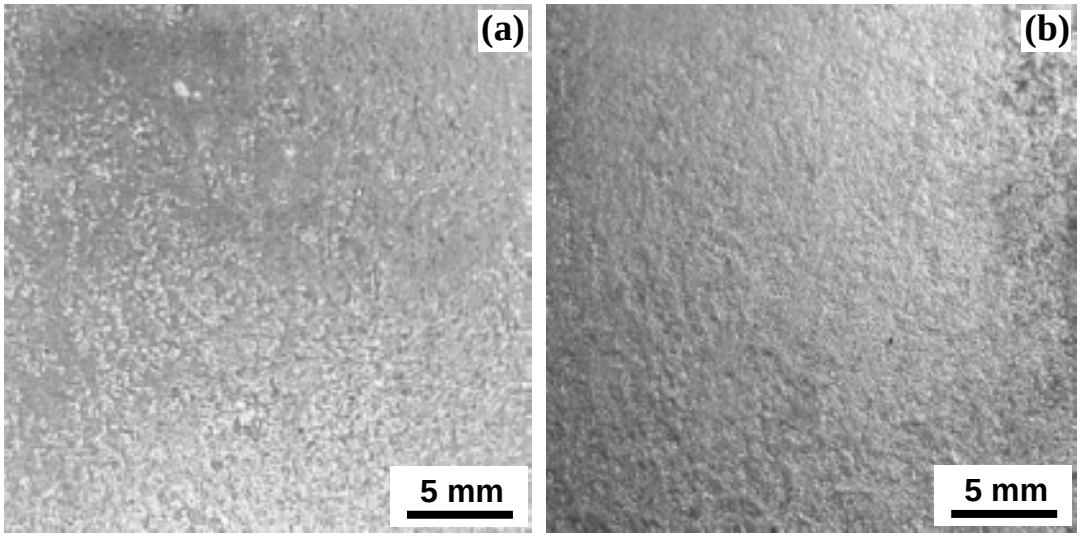

Fig 6.24 Digital camera images of the air-cooled coating G-0.8Mn-0.2Cu-Al-air (a) before, and (b) after an atmospheric corrosion test in a marine environment at Lyme Regis for 4 months.

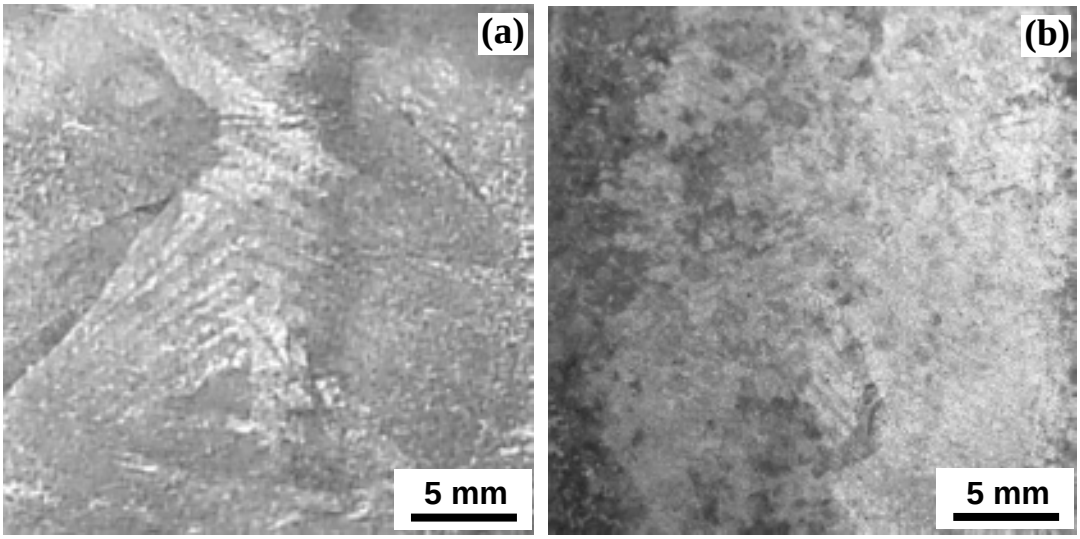

Fig 6.25 Digital camera images of the air-cooled coating G-0.3Sb-Al-air (a) before, and (b) after an atmospheric corrosion test in a marine environment at Lyme Regis for 4 months.

6.5.1.2 Water-quenched coatings exposed in a marine environment

The typical surface morphologies of the water-quenched hot dip galvanised coatings after 4 month atmospheric corrosion tests at light marine environment (Lyme Regis, UK) are shown in Fig 6.26 - Fig 6.32. Each water-quenched coating shows similar corrosion morphologies to the air-cooled coatings. This is not surprising as cooling method has no significant effect on the anodic and cathodic reaction activity of the coating surface (see Section 6.1.2.2).

Significant corrosion products were present on the surfaces of the two commercial hot dip galvanised coatings (Fig 6.26 and Fig 6.27) and the coatings with Cu (Fig 6.30 and Fig 6.31) and Sb (Fig 6.33) additions. These results indicate Cu, Sb and Pb additions have no beneficial effect on the improvement of corrosion resistance of hot dip galvanised coating.

For the water-quenched Mn-containing coatings with additions of 0.4 and 0.8 wt % Mn, more corrosion products were found on the surface than an air-cooled Mn coatings as shown in Fig 6.28 and Fig 6.29. Dark corrosion products were found near the edge of exposed area for the coating G-0.8Mn-Al-wq (Fig 6.29), while the surface in the centre is still shiny. Nevertheless, the surfaces are still better than that of G-CP-Al-wq. This result indicates that the Mn-containing coatings G-0.4Mn-Al-wq and G-0.8Mn-Al-wq may have better corrosion resistance than the commercial coatings G-CP-Al-wq and G-Pb-Al-wq in the marine environment.

The water-quenched coating with additions of both Mn and Cu (G-0.8Mn-0.2Cu-Al-wq) shows similar corrosion morphology to the air-cooled coating as shown in Fig 6.32. No obvious corrosion products can be seen on the surface and the corrosion morphology is quite uniform. It is expected that this coating has significantly higher corrosion resistance than G-CP-Al-wq in marine environments.

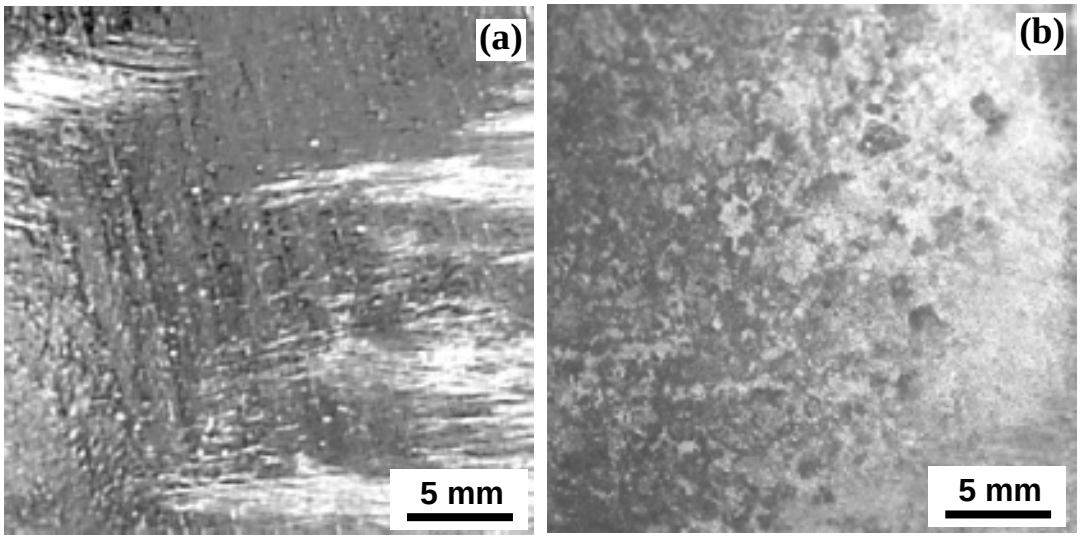

Fig 6.26 Digital camera images of water-quenched coating G-CP-Al-wq (a) before, and (b) after an atmospheric corrosion test in a marine environment at Lyme Regis for 4 months.

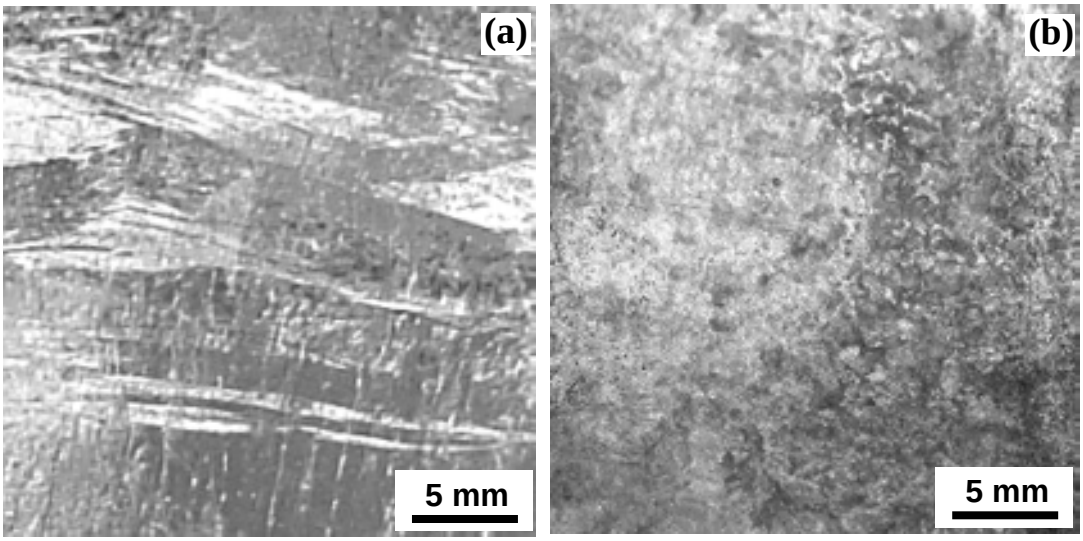

Fig 6.27 Digital camera images of water-quenched coating G-Pb-Al-wq (a) before, and (b) after an atmospheric corrosion test in a marine environment at Lyme Regis for 4 months.

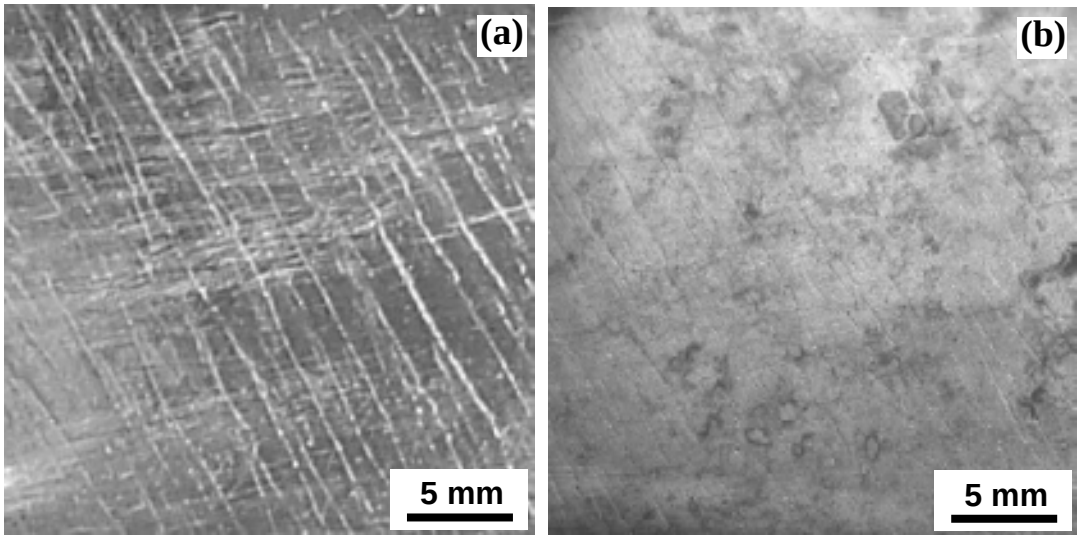

Fig 6.28 Digital camera images of water-quenched coating G-0.4Mn-Al-wq (a) before, and (b) after an atmospheric corrosion test in a marine environment at Lyme Regis for 4 months.

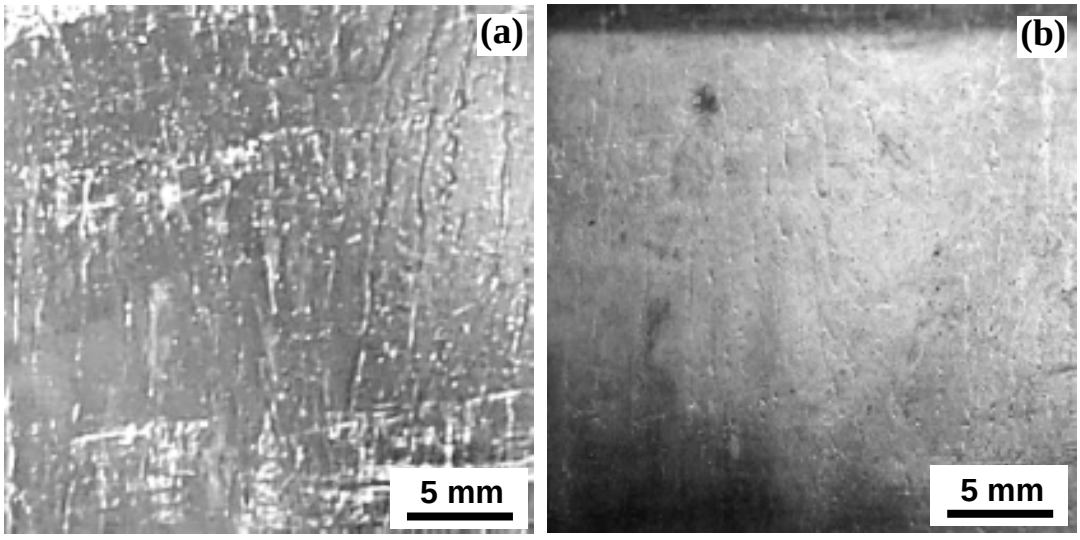

Fig 6.29 Digital camera images of water-quenched coating G-0.8Mn-Al-wq (a) before, and (b) after an atmospheric corrosion test in a marine environment at Lyme Regis for 4 months.

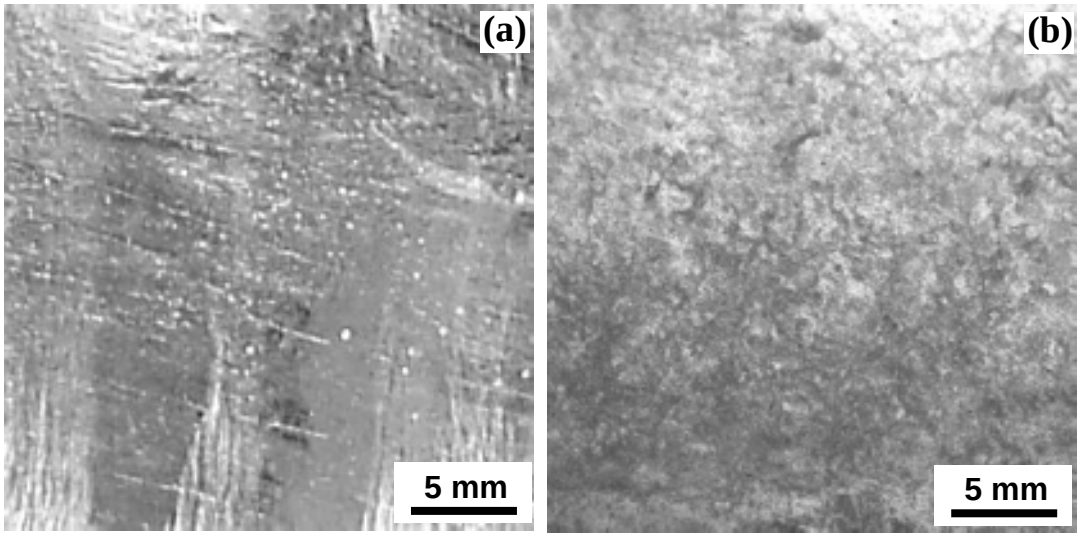

Fig 6.30 Digital camera images of water-quenched coating G-0.2Cu-Al-wq (a) before, and (b) after an atmospheric corrosion test in a marine environment at Lyme Regis for 4 months.

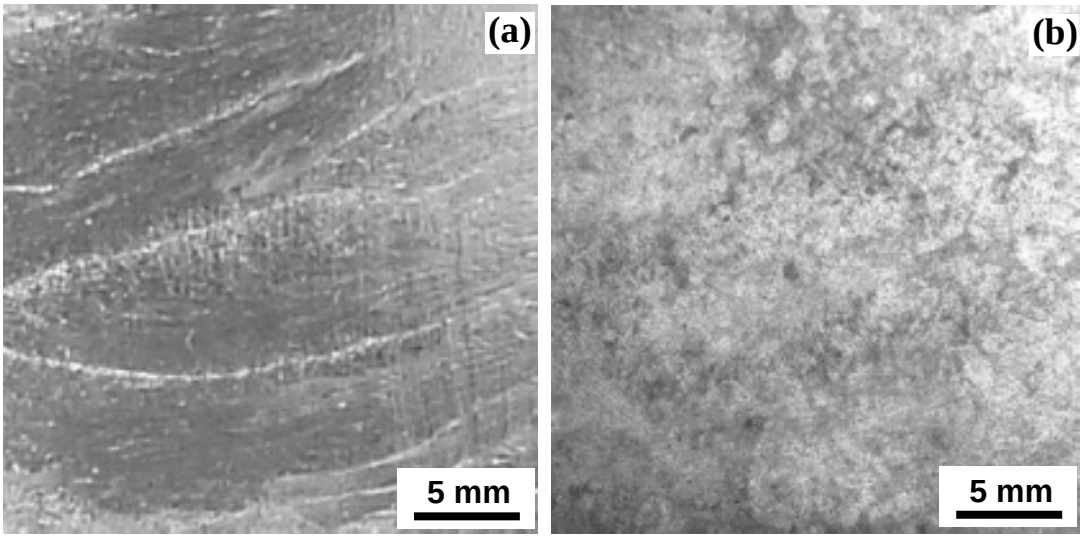

Fig 6.31 Digital camera images of water-quenched coating G-0.8Cu-Al-wq (a) before, and (b) after an atmospheric corrosion test in a marine environment at Lyme Regis for 4 months.

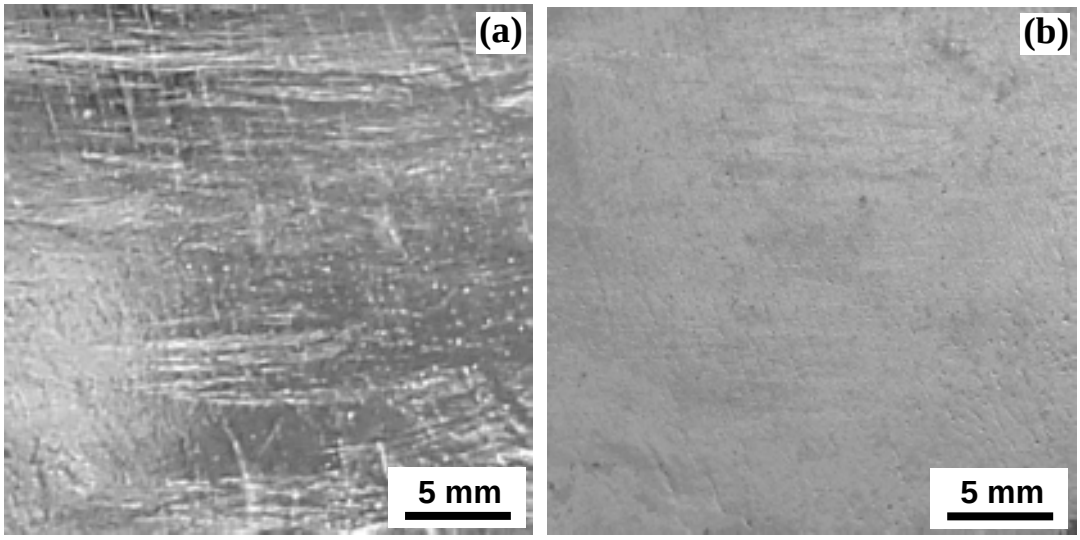

Fig 6.32 Digital camera images of water-quenched coating G-0.8Mn-0.2Cu-Al-wq (a) before, and (b) after an atmospheric corrosion test in a marine environment at Lyme Regis for 4 months.

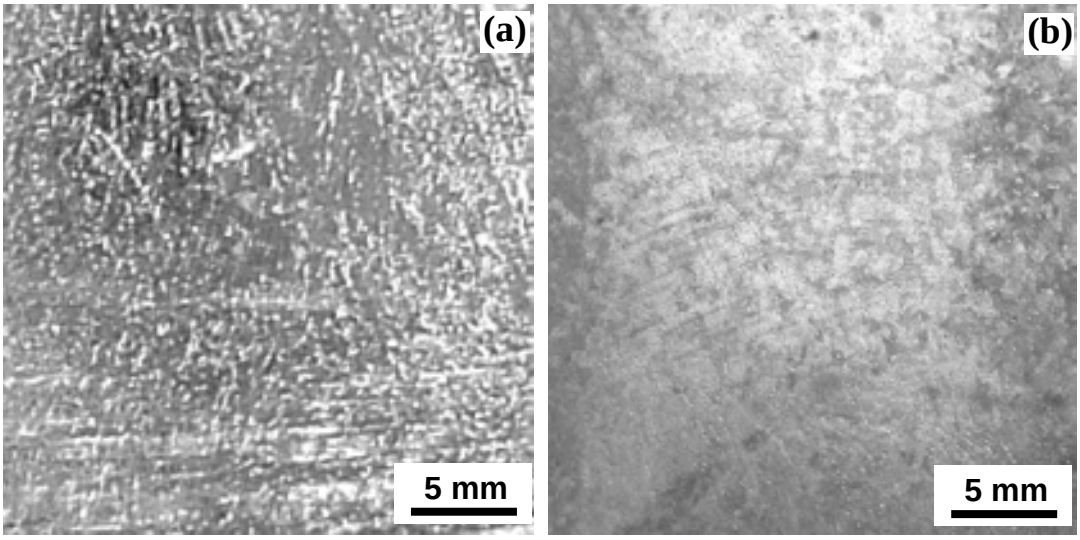

Fig 6.33 Digital camera images of water-quenched coating G-0.3Sb-Al-wq (a) before, and (b) after an atmospheric corrosion test in a marine environment at Lyme Regis for 4 months.

6.5.1.3 Air-cooled coatings exposed in an industrial atmosphere

The surface morphologies of the air-cooled hot dip galvanised coatings after 4 month atmospheric corrosion tests at industrial atmosphere are shown in Fig 6.34-42. When compared with results from the marine atmosphere, alloying additions have similar effects on the corrosion resistance of hot dip galvanised coatings. Again, Cu and Sb additions were found to have no beneficial effect on the improvement of corrosion resistance of hot dip galvanised coating. Significant corrosion products were present on the surfaces of the two commercial hot dip galvanised coatings (G-CP-Al-air (Fig 6.34) and G-Pb-Al-air (Fig 6.35)) and the coatings with Cu (Fig 6.38 and Fig 6.39) and Sb (Fig 6.42) additions.

The beneficial effect of Mn addition to improve corrosion resistance of hot dip galvanised coating was also found in the industrial atmosphere test. For these Mn-containing coatings (G-0.4Mn-Al-air, G-0.8Mn-Al-air and G-0.8Mn-0.2Cu-Al-air), significantly less corrosion products were present on the surfaces, and the surfaces were more uniform than those of other coatings without Mn additions as shown in Fig 6.36, Fig 6.37 and Fig 6.40. However, for the Mn-containing coating with additions of 0.8 wt % Mn and 0.8 wt % Cu, there were many “cracks” on the corroded surface. As shown in Section 5.3.1.2, Cu additions can significantly increase the growth of the galvanised layers, thus the top surface of G-0.8Mn-0.2Cu-Al-air mainly consists of Zn-Fe-Cu alloy phases. Eta phases may also remain on the top surface, which is between the Zn-Fe-Cu alloy phases. As eta phase is more active than the alloy phase, the formation of “cracks” is probably due to the selection dissolution of eta phase. However, more evidences are needed in order to provide a reasonable explanation for this result.

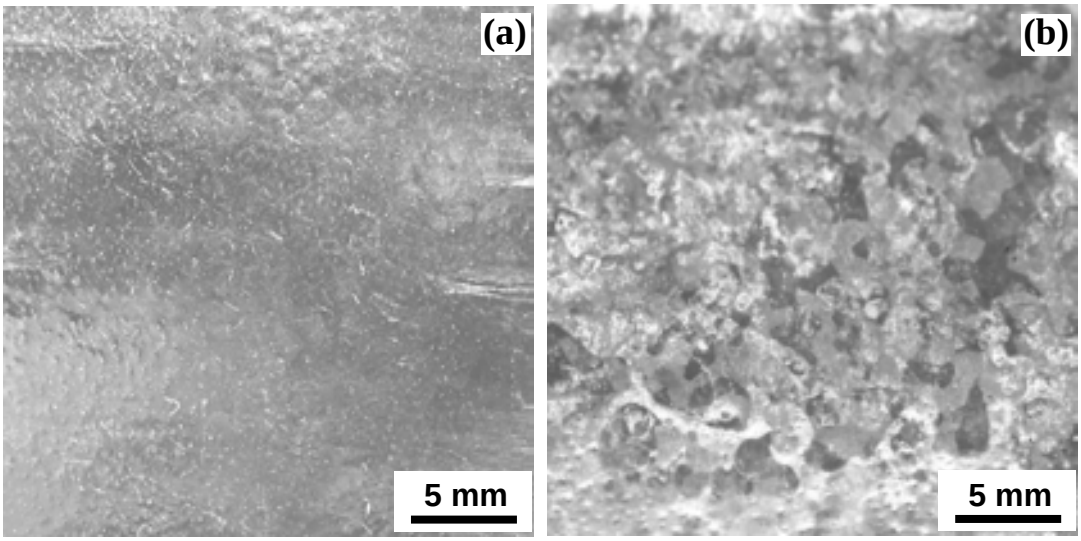

Fig 6.34 Digital camera images of the air-cooled coating G-CP-Al-air (a) before, and (b) after an atmospheric corrosion test in an industrial atmosphere at Birmingham for 4 months.

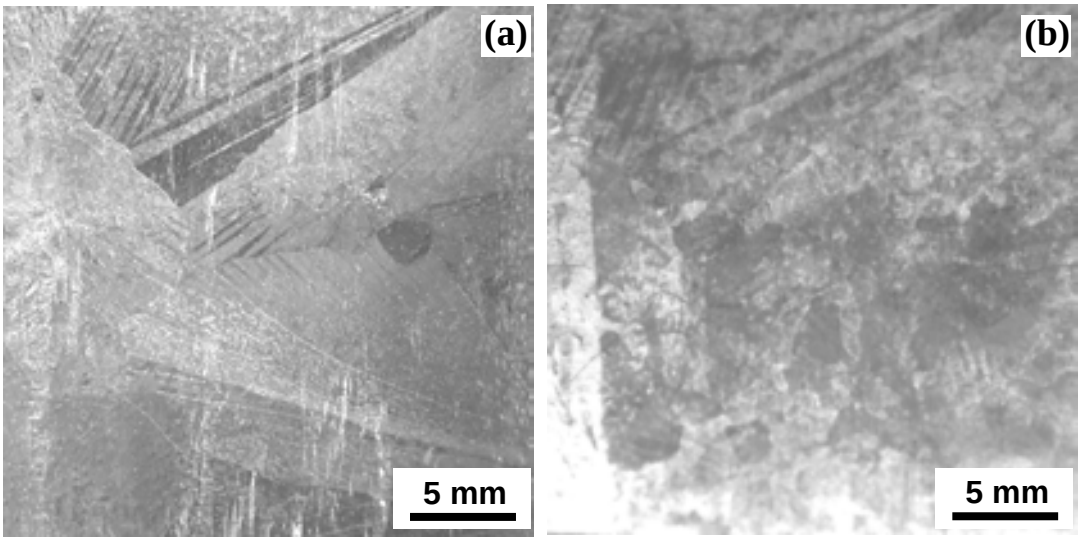

Fig 6.35 Digital camera images of the air-cooled coating G-Pb-Al-air (a) before, and (b) after an atmospheric corrosion test in an industrial atmosphere at Birmingham for 4 months.

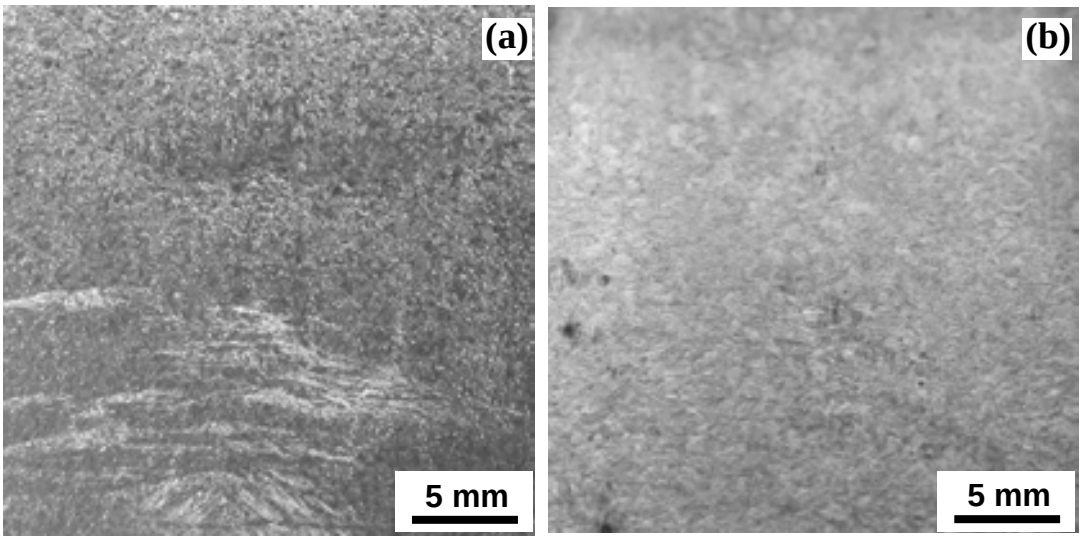

Fig 6.36 Digital camera images of the air-cooled coating G-0.4Mn-Al-air (a) before, and (b) after an atmospheric corrosion test in an industrial atmosphere at Birmingham for 4 months.

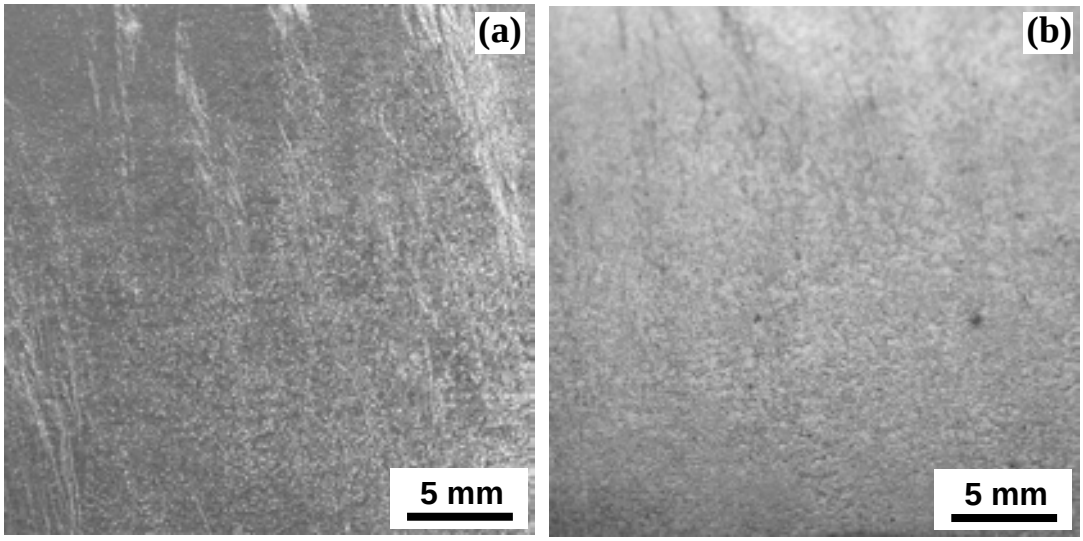

Fig 6.37 Digital camera images of the air-cooled coating G-0.8Mn-Al-air (a) before, and (b) after an atmospheric corrosion test in an industrial atmosphere at Birmingham for 4 months.

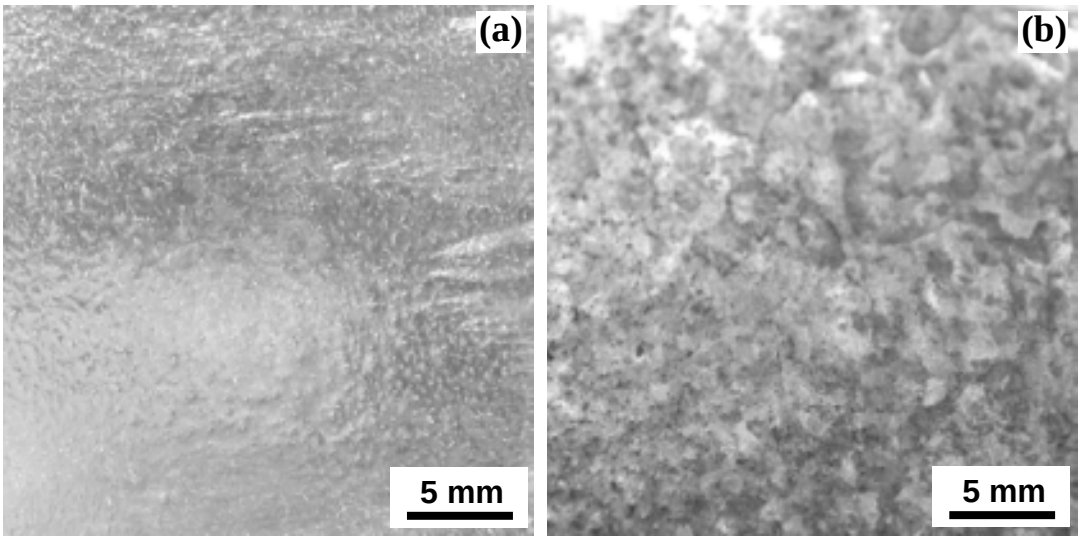

Fig 6.38 Digital camera images of the air-cooled coating G-0.2Cu-Al-air (a) before, and (b) after an atmospheric corrosion test in an industrial atmosphere at Birmingham for 4 months.

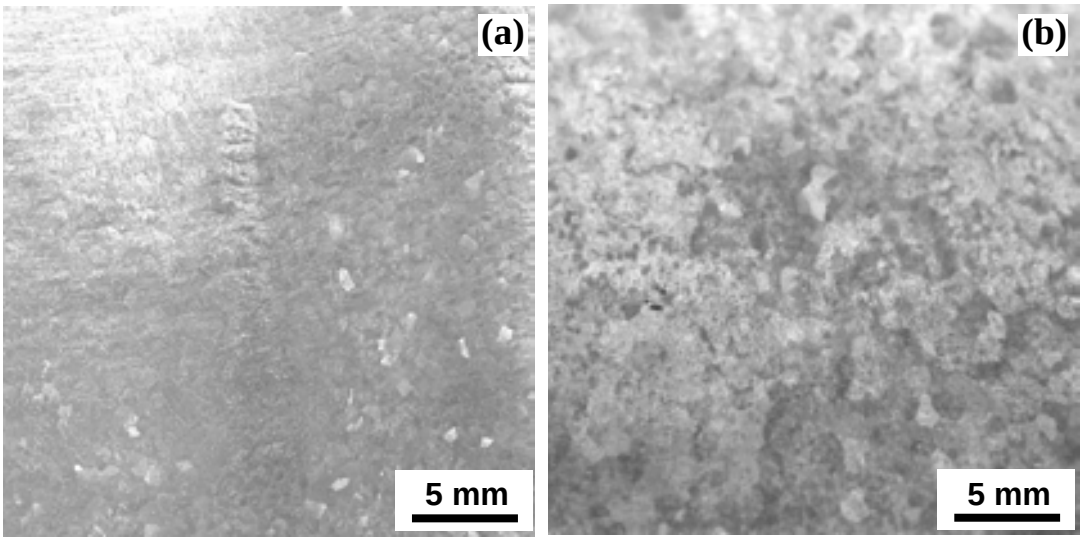

Fig 6.39 Digital camera images of the air-cooled coating G-0.8Cu-Al-air (a) before, and (b) after an atmospheric corrosion test in an industrial atmosphere at Birmingham for 4 months.

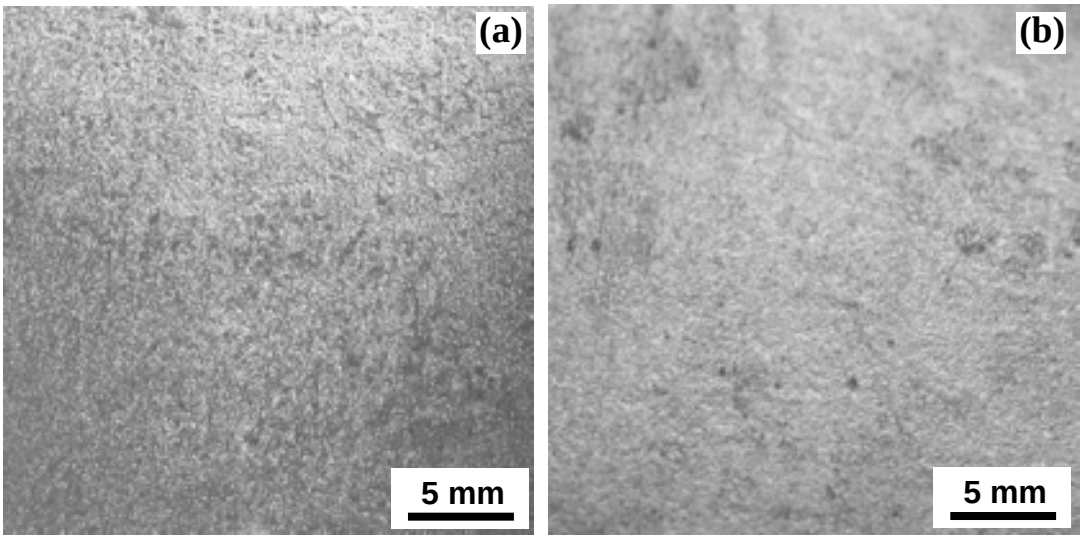

Fig 6.40 Digital camera images of the air-cooled coating G-0.8Mn-0.2Cu-Al-air (a) before, and (b) after an atmospheric corrosion test in an industrial atmosphere at Birmingham for 4 months.

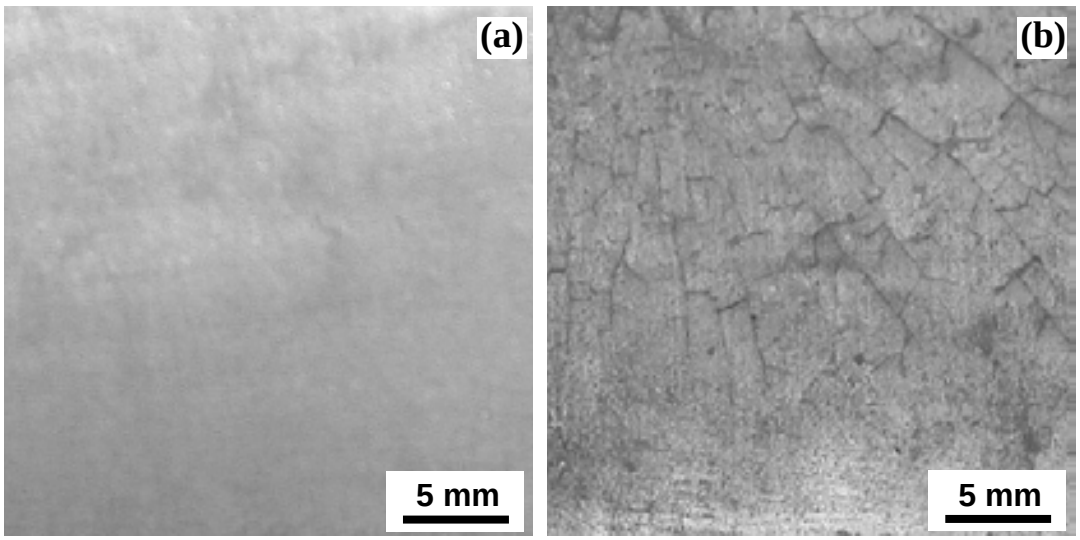

Fig 6.41 Digital camera images of the air-cooled coating G-0.7Mn-0.8Cu-Al-air (a) before, and (b) after an atmospheric corrosion test in an industrial atmosphere at Birmingham for 4 months.

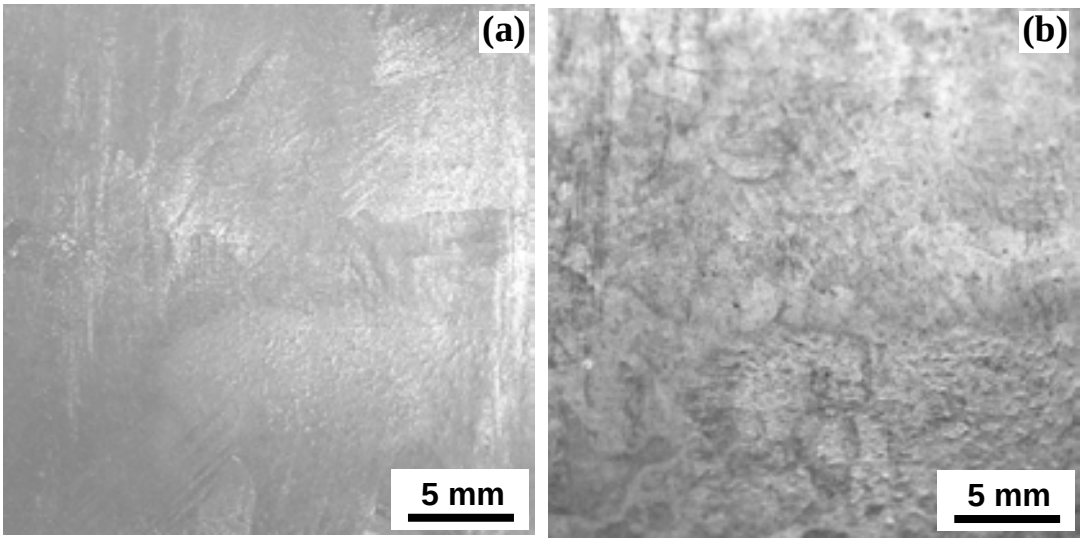

Fig 6.42 Digital camera images of the air-cooled coating G-0.3Sb-Al-air (a) before, and (b) after atmospheric corrosion test in industrial atmosphere at Birmingham for 4 months.

6.5.1.4 Water-quenched coatings exposed in an industrial atmosphere

The surface morphologies of the water-quenched hot dip galvanised coatings after four month atmospheric corrosion tests in an industrial atmosphere are shown in Fig 6.43 - Fig 6.51. Compared with those in the marine atmosphere, the alloying additions show similar effect on the corrosion morphologies of the hot dip galvanised coatings.

It is shown in Fig 6.43 and Fig 6.44 that significant corrosion products are present on the surfaces of the two commercial hot dip galvanised coatings (G-CP-Al-wq and G-Pb-Al-wq). The corrosion morphologies are similar to those found in the marine environment. Furthermore, there is no difference in the corrosion morphology between the air-cooled and water-quenched coatings after the atmospheric exposure.

The corrosion morphologies of the water-quenched Mn-containing coatings with additions of 0.4 and 0.8 wt % Mn are shown in Fig 6.45 and Fig 6.46. Some localised corrosion products were found on the surface of water-quenched coatings. Similar corrosion morphologies were also found for the water-quenched Mn-containing coatings after atmospheric tests in the marine environment. However, compared with the commercial pure Zn coating G-CP-Al-wq (Fig 6.43), much less corrosion products were

found on the water-quenched Mn-containing coatings. This result suggests that the Mn-containing coatings G-0.4Mn-Al-wq and G-0.8Mn-Al-wq still have better corrosion resistance than the commercial coatings G-CP-Al-wq and G-Pb-Al-wq in the industrial environment.

Addition of 0.2 wt % Cu was found to have no significant effect on the corrosion resistance of the water-quenched hot dip galvanised coating in the industrial environment as shown Fig 6.47. Slightly less corrosion product was found on the surface of water-quenched hot dip galvanised coating with addition of 0.8 wt % Cu compared with G-CP-Al-wq as shown Fig 6.48.

For the water-quenched coating with additions of both 0.8 wt % Mn and 0.2 wt % Cu (G-0.8Mn-0.2Cu-Al-wq), quite uniform corrosion morphology was found as shown in Fig 6.49. No obvious corrosion product was found on the surface. It is expected that this coating could have higher corrosion resistance than G-CP-Al-wq in the marine environment. The water-quenched coating with additions of both 0.8 wt % Mn and 0.8 wt % Cu (G-0.8Mn-0.8Cu-Al-wq) was found to have less corrosion products than G-CP-Al-wq as shown in Fig 6.50.

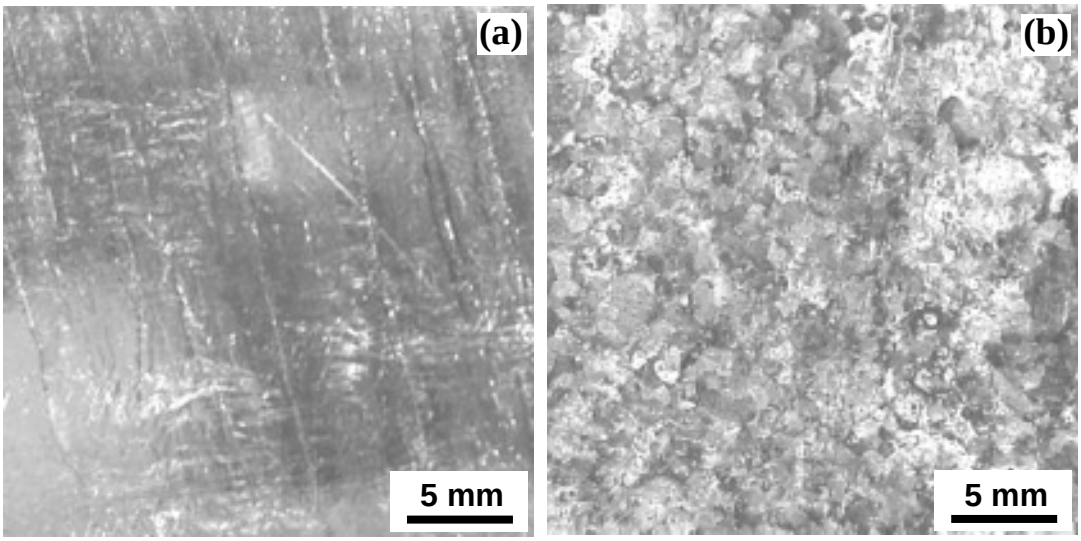

Fig 6.43 Digital camera images of the water-quenched coating G-CP-Al-wq (a) before, and (b) after an atmospheric corrosion test in an industrial atmosphere at Birmingham for 4 months.

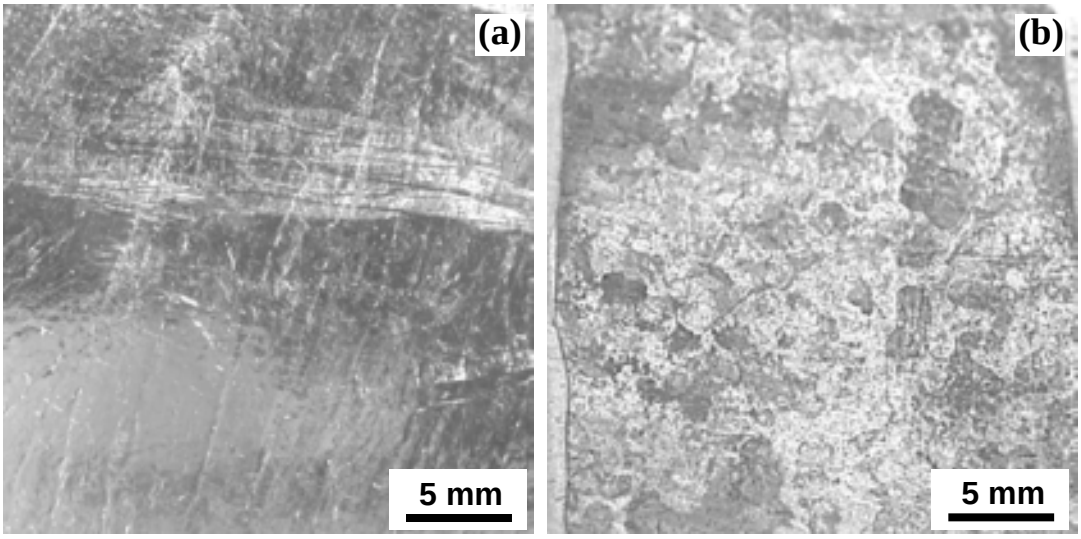

Fig 6.44 Digital camera images of the water-quenched coating G-Pb-Al-wq (a) before, and (b) after an atmospheric corrosion test in an industrial atmosphere at Birmingham for 4 months.

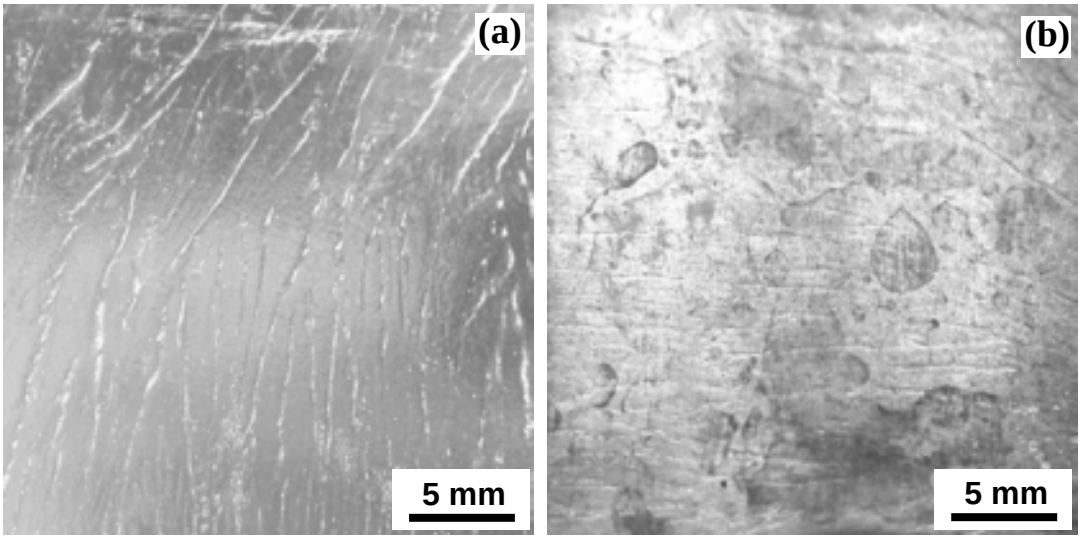

Fig 6.45 Digital camera images of the water-quenched coating G-0.4Mn-Al-wq (a) before, and (b) after an atmospheric corrosion test in an industrial atmosphere at Birmingham for 4 months.

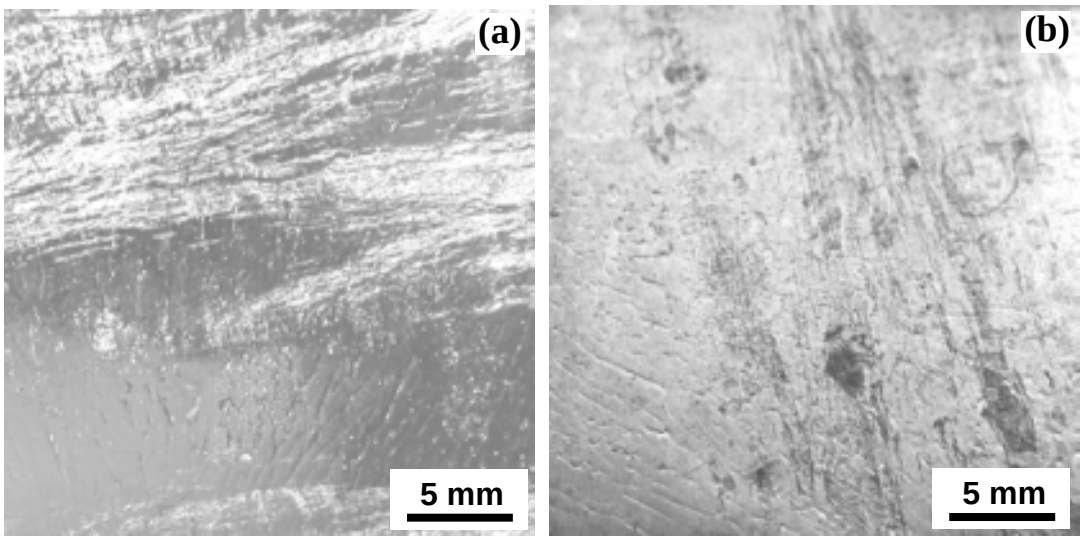

Fig 6.46 Digital camera images of the water-quenched coating G-0.8Mn-Al-wq (a) before, and (b) after an atmospheric corrosion test in an industrial atmosphere at Birmingham for 4 months.

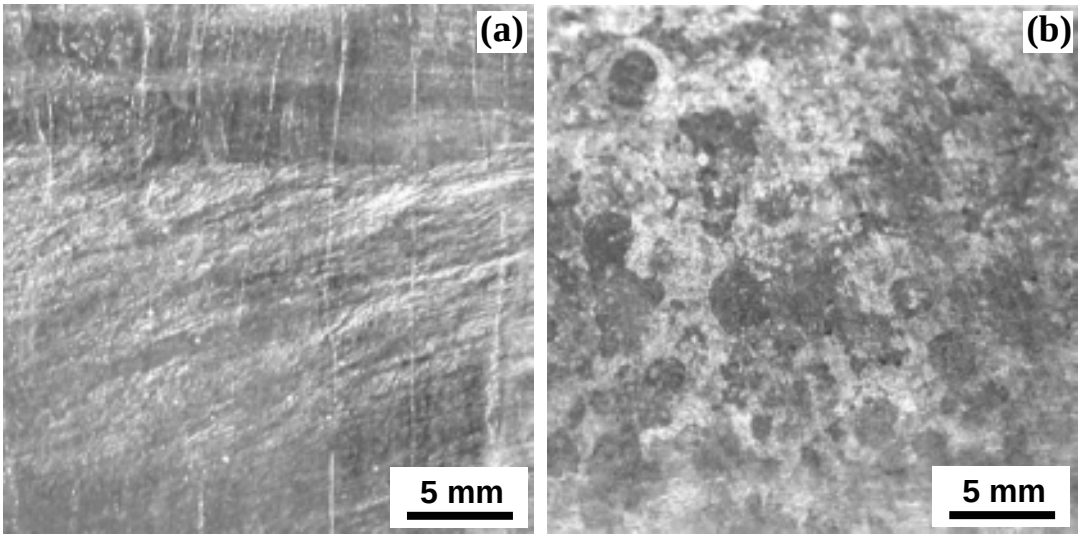

Fig 6.47 Digital camera images of the water-quenched coating G-0.2Cu-Al-wq (a) before, and (b) after an atmospheric corrosion test in an industrial atmosphere at Birmingham for 4 months.

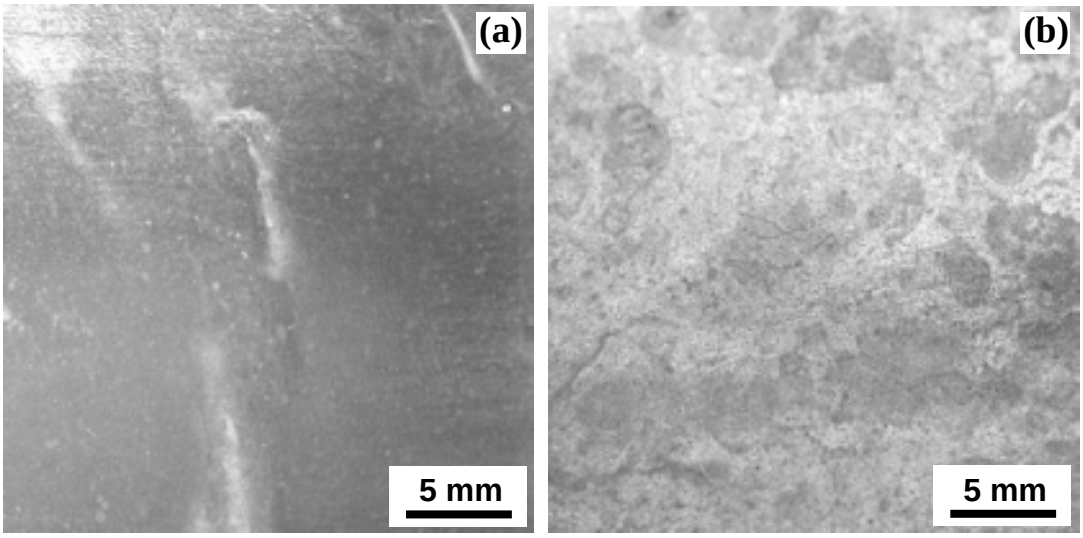

Fig 6.48 Digital camera images of the water-quenched coating G-0.8Cu-Al-wq (a) before, and (b) after an atmospheric corrosion test in an industrial atmosphere at Birmingham for 4 months.

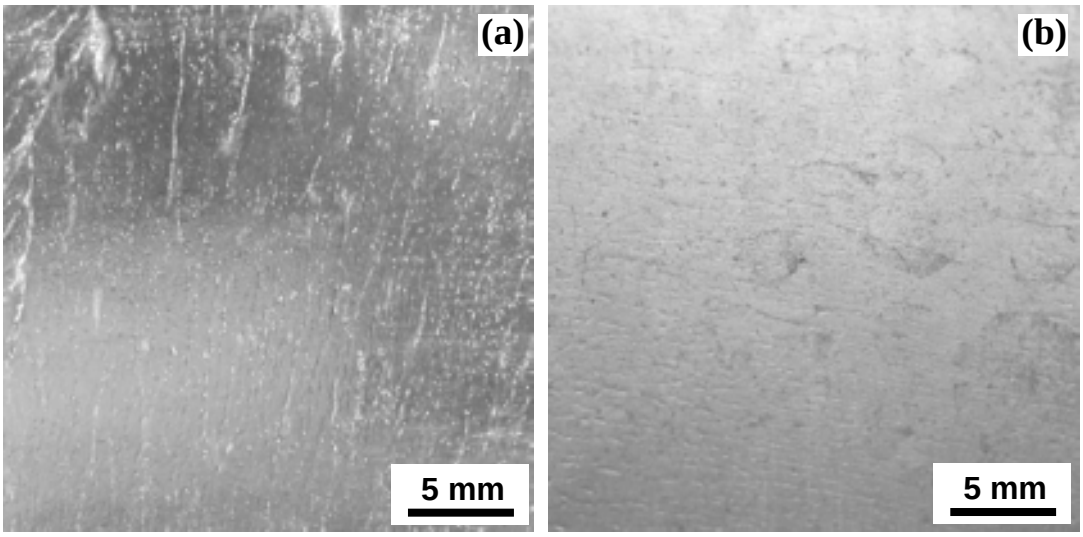

Fig 6.49 Digital camera images of the water-quenched coating G-0.8Mn-0.2Cu-Al-wq (a) before, and (b) after an atmospheric corrosion test in an industrial atmosphere at Birmingham for 4 months.

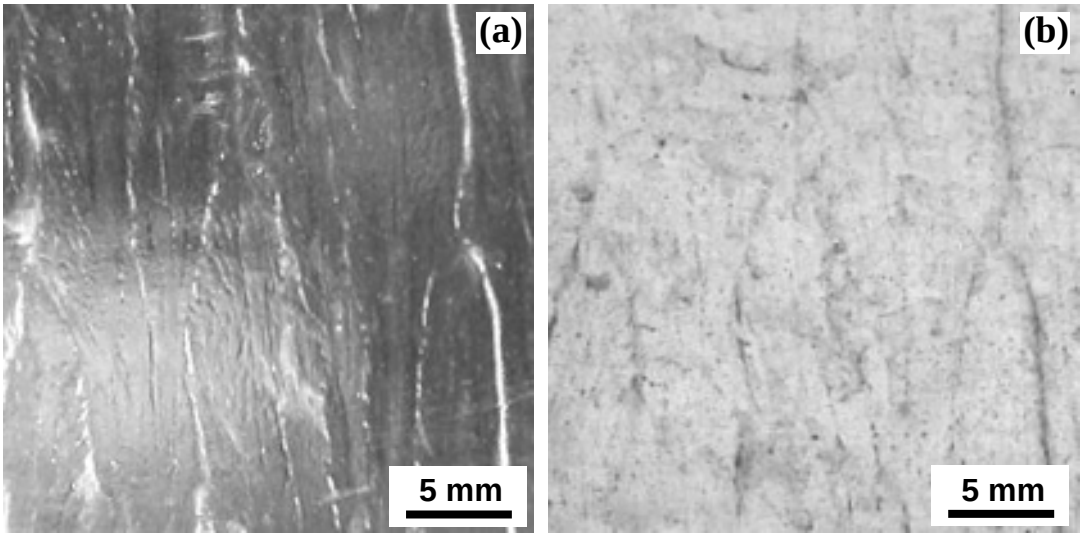

Fig 6.50 Digital camera images of the water-quenched coating G-0.7Mn-0.8Cu-Al-wq (a) before, and (b) after an atmospheric corrosion test in an industrial atmosphere at Birmingham for 4 months.

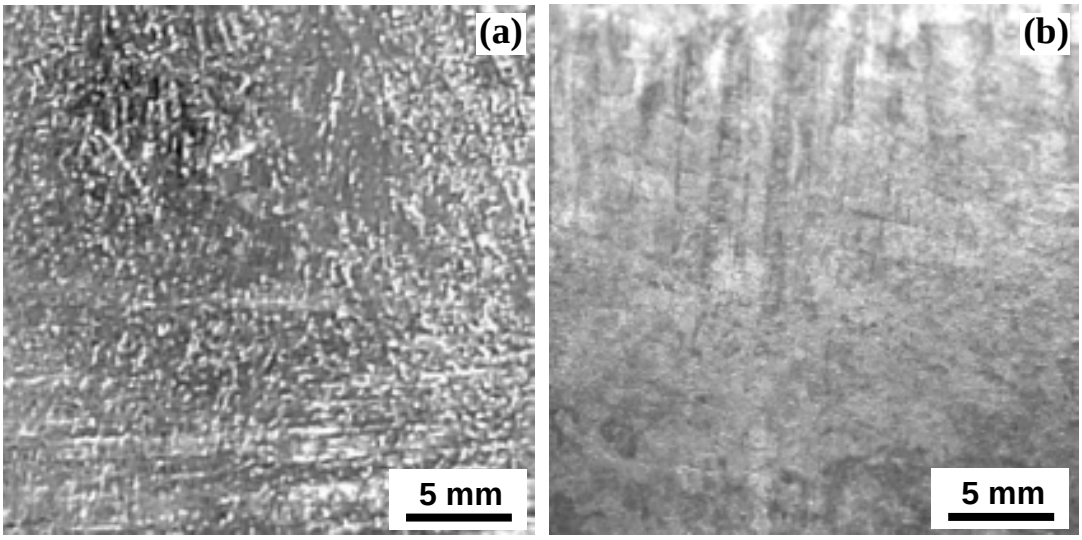

Fig 6.51 Digital camera images of the water-quenched coating G-0.3Sb-Al-wq (a) before, and (b) after an atmospheric corrosion test in an industrial atmosphere at Birmingham for 4 months.

6.5.2 Weight loss

Table 6.6 shows the weight loss of air-cooled hot dip galvanised coatings after 4 month exposure tests in the industrial atmosphere and the marine atmosphere. This result is also plotted in Fig 6.52. The results show that there is not much different in weight loss between industrial and marine atmosphere. In both environments, the weight loss of the Mn-containing coatings (G-0.4Mn-Al-air, G-0.8Mn-Al-air and G-0.8Mn-0.2Cu-Al-air) is about 50 % of the commercially-pure Zn coating (G-CP-Al-air). This further confirms the beneficial effect of Mn addition on the improvement of corrosion resistance of hot dip galvanised coatings. The weight loss results are in good agreement with the results of LPR and cyclic tests (Section 6.2.2 and 6.4.2). The weight loss of G-Pb-Al-air is about 20 - 35 % higher than that of G-CP-Al-air. This is not surprising as Pb globules were found to promote the cathodic reaction activity of the galvanised surface found in the previous results (Section 6.1.1). The weight loss of the coating with addition of Cu (0.2 wt % and 0.8 wt %) is similar to that of G-CP-Al-air. This indicates that Cu addition up to 0.8 wt % has no significant effect on the atmospheric corrosion resistance for about 4 month exposure. For the coating with addition of 0.3 wt % Sb, weight loss is higher than that of G-CP-Al-air.

It is not clear why G-0.3Sb-Al-air shows such a higher weight loss than others.

Table 6.6 Weight loss of air-cooled hot dip galvanised coatings after 4 month exposure tests at Birmingham (industrial atmosphere) and Lyme Regis (marine atmosphere), average of two measurements

Hot dip galvanised coating	Weight loss (mg/cm^2) at industrial atmosphere, ± 0.02	Wieght loss (mg/cm^2) at marine atmosphere, ± 0.02
G-CP-Al-air	0.41	0.36
G-Pb-Al-air	0.50	0.56
G-0.3Sb-Al-air	0.51	0.61
G-0.4Mn-Al-air	0.26	0.17
G-0.8Mn-Al-air	0.23	0.14
G-0.2Cu-Al-air	0.41	0.39
G-0.8Cu-Al-air	0.42	0.32
G-0.8Mn-0.2Cu-Al-air	0.23	0.12

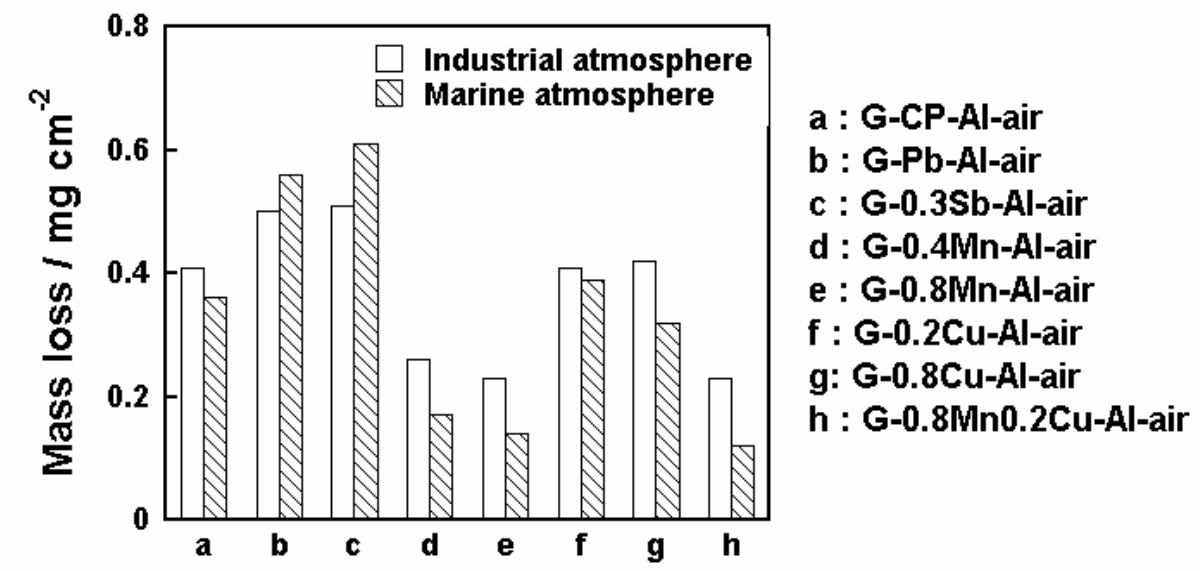

Fig 6.52 Weight loss of air-cooled hot dip galvanised coatings after 4 month exposure tests at Birmingham (industrial atmosphere) and Lyme Regis (marine atmosphere), average of two measurements

6.6 Discussion

Most of the hot dip galvanised coatings (except Mn-containing coatings) show higher cathodic reactivity than the freshly polished Zn alloys. The reason is not clear. The higher cathodic reactivity makes the OCP shift towards a more positive potential which is close to the pitting potential. In this case, no transient passive range was found on the anodic polarisation curves.

6.6.1 Small Al additions

The results of dynamic polarization showed that small Al additions (0.005 wt % Al), which are used to suppress the rapid oxidation of molten Zn, can slightly decrease both anodic and cathodic reactivity of the polished commercially-pure Zn. This is probably due to the presence of Al oxide formed during the galvanising process whereas it slightly decreases the corrosion resistance of the Mn-containing coating.

Small Al additions were found to have no effect on the LPR of Mn-containing coating, but to slightly increase the LPR of the commercially-pure Zn.

6.6.2 Effect of Cu

In the previous results (Section 4.2.3), Cu-rich intermetallic particles found in the Cu-containing alloys are the catalytic sites for the oxygen reduction reaction. Thus, a high level of Cu (0.8 wt % Cu) has a deleterious effect on the corrosion resistance of Zn. For a low level of Cu (0.2 wt % Cu), contradictory results have been found (see Section 4.3.1). However, in the present work no significant deleterious (0.8 wt %) and beneficial (0.2 wt %) effects of Cu addition on atmospheric corrosion resistance was observed. The reason for this is not clear. It is supposed that the effect of Cu-rich particles on the cathodic reactivity of galvanised surface is suppressed due to the higher cathodic activity of the hot dip galvanised coating compared with the Zn alloy.

In the literature, observations of the effect of Cu additions on atmospheric

corrosion of hot dip galvanised coating are contradictory. Some authors reported that Cu additions can increase the atmospheric corrosion resistance of hot dip galvanised coatings [4, 5], while others claimed that it decreases the corrosion resistance [101]. It was reported that addition of up to 0.82 wt % Cu increased the corrosion resistance by as much as 20 wt % in a two-year industrial exposure test [5]. In contrast, Dunbar and Showak [101] reported that adding 1.0 wt % Cu to rolled Zn sheet decreased the corrosion resistance in a severe marine environment. This enhancement of the corrosion rate was attributed to a galvanic effect between Zn matrix and the Cu-rich intermetallic phase which is always found to be an effective cathode site [101]. This is consistent with the present work. The high corrosion resistance of the Cu-containing hot dip galvanised coating was not observed in this study. It was shown in the previous results that addition of 0.8 wt % Cu significant changes the coating structure and up to 3 wt % Cu was found in the alloy layers. For air-cooled coatings, the eta layer almost disappears. Thus the atmospheric corrosion results reported in previous work [5] is probably the results of the Zn-Fe-Cu alloy layer and not the eta layer. This implies that the ternary Zn-Fe-Cu phase may have higher resistance to atmospheric corrosion than the pure Zn coating. Further work is required to confirm this.

6.6.3 Effect of Mn

The electrochemical polarisation reveals that the Mn-containing coating (G-0.4Mn-wq) shows significantly lower cathodic and anodic current density than the commercially-pure Zn coating as shown in Fig 6.1 and Fig 6.2. This result is consistent with the literature [14], where 0.5 wt % Mn was reported to slightly increase the corrosion resistance of galvanised coating by the dynamical polarisation tests. The results indicate that the Mn-rich oxide (Fig 5.9 and Fig 5.13) can decrease both cathodic and anodic reactivity of the hot dip galvanised coating. Therefore it is not surprising that this coating has higher corrosion resistance than the commercially-pure Zn coating by LPR measurements (Fig 6.9) and cyclic tests (Fig 6.12) in the accelerated solution. It is evident that this oxide layer forms during the withdrawal of the coating from the molten Zn-Mn

bath. The Mn-rich oxide is relatively thick (about 0.75 μm). When small Al additions are made, which are always required in general galvanising to reduce the rapid oxidation of molten Zn, the thickness of the oxide layer on the top surface of the hot dip galvanised coating is significantly reduced. XPS surface analysis revealed that the oxide layer mainly consists of a mixture of Mn and Al oxide. The mixed oxides decrease the cathodic reactivity but increase the anodic activity of the hot dip galvanised coating compared with the commercially-pure Zn coating (G-CP-Al-wq) as shown in Fig 6.3, Fig 6.4, Fig 6.5 and Fig 6.6. Under free corrosion conditions in neutral solution, the corrosion rate of Zn is mainly controlled by the reduction of oxygen [2]. G-0.4Mn-Al-air was found to have a significantly lower cathodic current density than that of G-CP-Al-air (Fig 6.5). This explains why G-0.4Mn-Al-air has a higher LPR than the commercially-pure Zn coating as shown in the LPR measurements (Fig 6.12) and cyclic tests (Fig 6.17).

As shown in the previous section, addition of 0.8 wt % Mn can slightly increase the cathodic reactivity of Zn. This effect was not observed for the hot dip galvanised coating. As shown in Fig 6.5 and Fig 6.12, the coating with addition of 0.8 wt % Mn shows a significantly lower cathodic current density and higher LPR than the commercially-pure Zn coating. It is supposed that the effect of Mn-rich particles on promoting the cathodic reactivity of Zn could be suppressed by the Mn and Al oxide formed during the galvanising process.

The atmospheric corrosion tests show that the weight loss of the Mn-containing coatings (G-0.4Mn-Al-air and G-0.8Mn-Al-air) is about 50 % of that of the commercially-pure Zn coating (G-CP-Al-air) after 4 month exposure tests as shown in Fig 6.52. Meanwhile, less corrosion products were found on the surface of these Mn-containing coatings. This is in good agreement with the electrochemical results.

The protective ability of this layer was found to decrease with the increase of immersion time in aqueous solution as demonstrated by the LPR (Fig 6.9 and Fig 6.12) and cyclic tests (Fig 6.16 and Fig 6.17). Nevertheless, as Mn favours the formation of ZHC (see Section 4.3.2), it is expected that the Mn-containing coating would still have better

corrosion resistance than the commercially-pure Zn coating in the long period of atmospheric corrosion tests.

6.6.4 The combined effect of Mn-Cu additions

For hot dip galvanised coatings, it has been shown that the combined additions of Mn and Cu (0.8 % Mn + 0.2 % Cu) can significantly improve the corrosion resistance to both industrial and marine atmosphere after 4 month exposure tests. This result indicates that Mn addition dominates the corrosion behaviour of hot dip galvanised coating when the combined additions of Mn and Cu are used. This is due to the formation of Mn-rich oxide layers on the galvanised top surface, which can significantly decrease the cathodic reactivity.

Based on the discussion on the effect of Cu and Mn, it can therefore be concluded that the effect of additions of Mn and Cu on the corrosion resistance is a result of the following mechanisms. Mn decreases the cathodic reactivity by the formation of corrosion resistant passive film/corrosion products. Cu inhibits anodic dissolution of Zn within pits and possibly by the formation of intermetallic layers (Zn-Fe-Cu) which are difficult to dissolve; but adding Cu to a Mn-containing coating doesn't affect corrosion resistance.

6.6.5 Effect of Pb

It has been shown that Pb has a deleterious effect on the corrosion resistance of Zn. This is because Pb promotes both anodic and cathodic reactivity of Zn. In this Chapter, Pb was also found to promote anodic activity (Fig 6.1) and increase the cathodic reactivity (Fig 6.2) of the hot dip galvanised coating although its effect on the cathodic reaction of hot dip galvanised coating is less when compared with that of Zn alloys. Atmospheric corrosion tests also revealed that Pb decreases the corrosion resistance (Fig 6.52). The result is consistent with the literature [38, 129, 136, 137], where Pb was reported to promote anodic activity of Zn. It was suggested that the interstitial localisation of Pb can cause tension in the crystalline lattice, creating greater heterogeneity in the surface, and

therefore increasing the surface activity [137].

6.6.6 Effect of Sb

In the literature, the beneficial effect of Sb additions was reported [17, 18]. It has been reported by Rädeker [17] that Sb reduced weight loss over 3 years in an industrial atmosphere by 20 %. Such a beneficial effect of Sb was not observed in the study. The current work shows that addition of Sb has no significant effect on both anodic and cathodic reaction activity of coatings. The results of atmospheric corrosion tests indicate that weight loss of the Sb-containing coating is higher than the commercially-pure Zn coating (G-CP-Al-air) after 4 month exposure tests in both marine and industrial atmospheres. The higher corrosion rate is not expected. Thus further work is needed to confirm this.

6.6.7 Effect of Zr

It has been shown that addition of 0.2 wt % Zr has no effect on either anodic or cathodic reactivity of Zn and hot dip galvanised coatings. Zr-rich particles were found to be pit initiation sites as shown in Fig 4.16. As Zr has no beneficial effect on the improvement of corrosion resistance of Zn, atmospheric corrosion tests of the Zr-containing coatings were not investigated in this study.

6.7 Summary

Based on the electrochemical corrosion tests and atmospheric corrosion tests, Mn addition was found to be the most beneficial alloying element to the Zn bath and can significantly increase the resistance to atmospheric corrosion. The additions of Cu and Sb have no significant effect on the improvement of atmospheric corrosion resistance. Pb impurities in the commercial Zn coating promote both anodic and cathodic reactivity of the coating; therefore it has harmful effect on the corrosion resistance to atmosphere. The results are summarised as follows:

1. Additions of Mn up to 0.8 wt % significantly increase the resistance of the coating to atmospheric corrosion in both marine and industrial atmospheres. The beneficial effect is due to the Mn-rich oxide layer formed during the withdrawal of the coating from the molten Zn bath as it can decrease the cathodic reactivity of the Zn surface;
2. Additions of Cu (0.2 wt % and 0.8 wt % Cu) have no significant effect on both anodic and cathodic reaction activity of coating, and it has no effect on the resistance of the coating to atmospheric corrosion in both marine and industrial atmospheres;
3. The combined additions of Mn and Cu (0.8 % Mn + 0.2 % Cu) also can significantly improve the corrosion resistance in both industrial and marine atmospheres, which is mainly due to the beneficial effect of Mn additions;
4. Addition of Sb up 1.0 wt % has no significant effect on either the anodic and cathodic activity of coating, however a slightly higher weight loss was found for this coating after atmospheric exposure in both marine and industrial atmospheres compared with the commercially-pure Zn coating;
5. Addition of 0.2 wt % Zr has no significant effect on both anodic and cathodic reaction activity of coating;
6. Addition of 0.005 wt % Al to the bath can slightly improve the corrosion resistance of the commercial-pure Zn coatings, but slightly decreases the corrosion resistance of the Mn-containing coating;
7. Cooling method has no significant effect on the corrosion resistance of the commercial-pure Zn coatings;
8. LPR and cyclic tests in the accelerated solution can provide a rapid corrosion evaluation of the hot dip galvanised coatings. The results are comparable with those in atmospheric environments.

CHAPTER 7 CONCLUDING DISCUSSION

This thesis focuses on the development of corrosion resistant alloys for hot dip galvanising. The addition of alloying elements to Zn changes its electrochemical properties, such as electrode potential, dissolution kinetics, cathodic reactivity, and formation of solid surface films [2]. The corrosion resistance of Zn can be improved through the following mechanisms: 1) Formation of corrosion resistant passive films or corrosion products; 2) Inhibition of anodic dissolution of Zn within pits; 3) Formation of intermetallic layers difficult to dissolve; and 4) Inhibition of cathodic reduction reaction of Zn. It seems that there is a broad selection of the alloying elements (e.g. Cr, Al, Ni, Co etc) that can improve the corrosion resistance of hot dip galvanised coatings. However, due to the natural thermal process required for the hot dip galvanising, alloying additions to the Zn bath are limited. One of the fundamental problems is that it is difficult to produce hot dip galvanised coating with alloying elements that possess high melting points compared to pure Zn. Another problem is that most of alloying elements have very low solubility in Zn (e.g. Cr) at the normal galvanising temperature (450°C) which gives rise to problems in making the alloying bath.

In the literature additions of Al [3], Cu [4, 5], Mg [6, 7], Ni [8], Co [9, 10], Mn [11-14] , V [15], Cd [16] and Sb [17, 18] etc have been reported to increase the corrosion resistance of Zn coatings. However, most of the Zn coatings were made either by electrodeposition (e.g. Ni, Co and Mn). For hot dip galvanised coating, little work has been done towards the improvement of corrosion resistance. Furthermore, the mechanisms of the effect of these additions are still not clear, since the information on their effect on the corrosion resistance and structure of the coating is rather controversial [2].

In this work, an investigation into the effect of alloying additions (Mn, Cu, Sb and Zr) on microstructure and corrosion of Zn alloys and hot dip galvanised coatings was undertaken. The modification of the coating properties by the addition of alloying elements, apart from its practical importance, presents a theoretical interest. In the following sections,

the effect of alloying elements (Mn and Cu) on corrosion of coating will be discussed with the aim to understand the mechanisms.

7.1 Corrosion mechanisms – the effect of Mn and Cu

Among the galvanising alloys examined in this study, Mn is the most beneficial addition to the Zn bath, which can significantly improve the resistance of the hot dip galvanised coating to atmospheric corrosion (Fig 6.52). In the absence of low levels of Al addition, Mn-rich oxide layers (Fig 5.9) were always found on the top surface during the galvanising process, which can greatly inhibit both the anodic (Fig 6.1) and cathodic (Fig 6.2) reactivity of the hot dip galvanised coating. It is noted that the ash formation due to the oxidation of the molten Zn bath containing Mn is higher than that of pure Zn bath. This will cause a great waste of Mn and Zn. Small Al additions (0.005 wt %) to the Zn bath can overcome this problem, which has been shown to successfully inhibit the rapid ash formation of the Mn-containing Zn bath. In this case, a shiny instead of a blue or yellow surface is present as shown in Fig 5.13 and Fig 5.14. XPS analysis shows that the oxides on the top surface of the coating after the additions of Mn and low levels of Al are a mixture of Mn, Al and possible Zn oxides. These oxides also inhibit the cathodic reactivity of the galvanised coating. Therefore the corrosion resistance to the atmosphere can be improved as shown in Fig 6.52.

As Mn has low solubility in solid Zn at room temperature, Mn-rich particles can be found in the Zn alloys (Fig 4.8, Fig 4.9 and Fig 4.10) and in the eta layer (Fig 5.15 and Fig 5.17) of the galvanised coating, especially for the coating with a high level of Mn (0.8 wt %). These Mn-rich intermetallic particles are found to slightly promote the cathodic reduction reaction on Zn (Fig 4.31). However, Mn-rich particles are not pit initiation sites (Section 4.2.1.1). LPR tests indicate that addition of 0.4 wt % Mn shows a higher LPR than the commercially-pure Zn (Fig 4.26 and Fig 4.32). The higher LPR indicates that the corrosion products formed on the Mn-containing alloys are more protective against corrosion. In the literature, Boshkov *et al.* [12] reported that an Zn-11 wt % Mn alloy has

higher corrosion resistance than pure Zn. He suggested that the high corrosion resistance is due to the rapid formation of corrosion product $Zn_5(OH)_8Cl_2{\cdot}H_2O$ (ZHC) on the Zn-Mn alloy. Mn is electrically a more negative element than Zn, it dissolves first as Mn^{2+} ions (**Equation** 7.1), causing evolution of hydrogen and consequently a slight increase in pH (**Equation** 7.2), which favours the formation of ZHC. It is general believed that ZHC is more compact than ZnO [118] and it can decrease the oxygen reduction rate [117]. From the long term corrosion point of view, the ability to form a more protective corrosion product is very important.

Equation 7.1 $Mn \rightarrow Mn^{2+} + 2e^-$

Equation 7.2 $2H_2O + 2e^- \rightarrow H_2 + 2OH^-$

This mechanism may explain whey Mn-rich particles are not pit initiation sites. Based on the theory of local acidification widely accepted for the pitting corrosion of Zn [94, 98, 104], to initiate and maintain an active pit, local acidification is considered to be necessary. This local acidification is a result of metal dissolution:

Equation 7.3 $Zn \rightarrow Zn^{2+} + 2e^-$

Equation 7.4 $Zn^{2+} + H_2O \rightleftharpoons ZnOH^+ + H^+$

Equation 7.5 $ZnOH^+ + H_2O \rightleftharpoons Zn(OH)_2 + H^+$

According to this model, if the dissolution in a pit is not fast enough to maintain sufficient acidity to prevent repassivation, a new passive film will form and pitting corrosion can stop. As the dissolution of Mn can cause a slight increase of the pH, pitting corrosion around the Mn-rich particles is not likely to occur.

The higher corrosion resistance of Mn-containing alloy may also due to the passivation of Mn. The passive film could be γ-Mn_2O_3 [13]. It is reported that this passive film can suppress oxygen reduction thus decrease the corrosion rate of Mn-containing alloy.

Apart from its beneficial effect on the atmospheric corrosion resistance, Mn has

also been demonstrated to inhibit the alloy layer growth on active steels with a high Si content (Fig 5.36). Thus, Mn might be an alternative addition to Ni, which can control the excessive reaction of some steels to reduce the cost of galvanising. Coupled with the relatively low cost and ease of alloying of this element, these various factors suggest that Mn might have broader applications in general galvanising.

The other alloying elements investigated in this study, however, have minor effects on the corrosion resistance of the galvanised coating. The present work has shown that the effect of Cu on corrosion of Zn depends on its content. For the Zn alloys with addition of 0.8 wt % Cu, the Cu-rich particles present in these alloys were found to be the catalytic sites for the oxygen reduction reaction as shown Section 4.2.1. This result indicates that a high Cu content has a deleterious effect on the corrosion resistance of Zn as confirmed by the LPR measurements in the accelerated solution. The enhanced cathodic reaction at the Cu-rich particles will significantly increase dissolution of Zn around the particles. Thus pits are likely to initiate at the Cu-rich particles as shown Fig 4.16 and Fig 4.25. This result is consistent with the literature [101]. It should be noted that the present work also shows that addition of 0.8 wt % Cu slightly increase the pitting potential when measurements start immediately upon immersion of the fresh polished samples in solution. As discussed in Section 4.3.1, the slightly higher pitting potential is probably due to the beneficial effect of the dissolved Cu in solid solution. It seems that there is a competition between Cu in the intermetallic particles and the dissolved Cu in the matrix. Under the conditions of open circuit in aerated solutions, cathodic reduction of oxygen dominates the corrosion process. Localised corrosion is likely to develop at Cu-rich particles and the corrosion resistance is then significantly reduced. It is therefore expected that more Cu in solid solution and less in intermetallic particles would make a Zn-Cu alloy with higher corrosion resistance. As shown in Section 4.1.3, there are no detectable Cu-rich particles in the Zn alloy with the addition of 0.2 wt % Cu. However, both higher (Fig 4.26) and lower LPR (Fig 4.32) were found in the accelerated solution. This is probably because the Zn alloy used for the LPR tests (Fig 4.32) has a slightly higher Cu content (0.21 wt % Cu) than

that (0.16 wt % Cu) used for the LPR tests (Fig 4.26). Thus more Cu-particles are likely to be developed in the alloy with more Cu content. This result suggests that the control of Cu content is very important in order to obtain high corrosion resistance of Zn by alloying with Cu. But for galvanised coatings, corrosion resistance is not sensitive to the Cu content. This is probably due to the well known fact that corrosion of Zn is markedly affected by the electrode preparation and by the experimental procedure [89].

It should be noted that the combined additions of Mn and Cu (0.8 % Mn + 0.2 % Cu) can also significantly improve the corrosion resistance in both industrial and marine atmospheres after 4 month exposure tests (Fig 6.24, Fig 6.32, Fig 6.40, Fig 6.49 and Fig 6.52). However, the LPR of Zn alloy (Z-0.8Mn-0.2Cu-Al-wq) in accelerated was found to be lower than that of Z-CP-Al-wq. The higher corrosion resistance of this coating is probably due to the formation of Mn-rich oxide layers on the galvanised top surface, which can significantly decrease the cathodic reactivity. The effect of additions of Mn and Cu on the corrosion resistance is a result of the following mechanisms. Mn decreases the cathodic reactivity by the formation of corrosion resistant passive film/corrosion products. Cu inhibits anodic dissolution of Zn within pits and possibly by the formation of intermetallic layers (Zn-Fe-Cu) which are difficult to dissolve; but adding Cu to a Mn-containing coating doesn’t affect corrosion resistance.

CHAPTER 8 CONCLUSIONS

This project has concentrated on the investigation of galvanising alloys with improved corrosion resistance. The effect of additions of Cu, Mn, Sb, Zr, Pb and Al on the corrosion behaviour and microstructure of Zn alloy and hot dip galvanised coating are summarised as follows.

1. Small Al additions (0.005 wt % Al) can slightly decrease both anodic and cathodic reactivity of the polished commercially-pure Zn, whereas it slightly increases the cathodic reactivity of both Mn-containing alloys and coatings. Al addition has no observed effect on the LPR of both Zn alloys and galvanised coatings in the accelerated solution. Al addition (0.005 wt %) has no effect on the thickness and microstructure of the galvanised coating.
2. The Cu-rich intermetallic particles were found to be pit initiation sites and promote the cathodic reactivity of Zn. Thus, addition of a high level of Cu has a deleterious effect on the corrosion resistance of Zn. Cu in solid solution was found to increase the corrosion resistance of Zn. For hot dip galvanised coating, additions of Cu (0.2 wt % and 0.8 wt % Cu) have no significant effect on corrosion resistance. The effect of Cu on thickness of hot dip galvanised coating depends on its concentration in Zn bath and the type of the steel substrate. Addition of 0.2 wt % Cu has no significant effect on the coating structure and thickness of both the galvanised steels (0.2 wt % Si and 0.02 wt % Si). However, addition of 0.8 wt % Cu to the bath was found to significantly increase the coating thickness of the galvanised hypo-Sandelin steels (0.02 wt % Si) especially at longer immersion time. In this case, the growth kinetics of the alloy layers follows a linear law indicating that the growth is interface controlled. Cu is incorporated into the Fe-Zn alloy layer of hot dip galvanised coating in some depth.
3. Mn-rich particles are found in the Zn alloys with Mn additions (0.4 and 0.8 wt %). For hot dip galvanised coatings, Mn-rich particles were found on the top surface

and in the eta phase of the Mn-containing coatings. The addition of 0.4 wt % Mn can decrease the cathodic reactivity of Zn but has no significant effect on the anodic activity. Addition of 0.8 wt % Mn slightly increases the cathodic reduction reactivity of Zn.

4. Additions of Mn (0.4 and 0.8 wt %) significantly increase the resistance of the coating to atmospheric corrosion in both marine and industrial atmosphere. Mn has no significant effect on the thickness and growth kinetics of alloy layer for the galvanised steel containing 0.02 wt % Si. However, Mn decreases the coating thickness of galvanised steels containing 0.2 wt % Si to about 30 % compared with the commercially-pure Zn coating. Therefore, Mn might be an alternative addition to Ni which can control the excessive reaction of some steels to reduce the cost of galvanising. Mn was incorporated into the Zn/Fe alloy layers in some depth, with a high concentration throughout the zeta layer.
5. Significant amounts of Pb globules are present in the commercial Zn alloy containing 1.0 wt % Pb. No detectable Pb is found in the matrix of this Zn alloy. Significant amount of Pb globules were also found in the eta layer of the hot dip galvanised coating. Pb impurities in the commercial Zn alloys promoted both anodic and cathodic reactivity of Zn. Pb produces larger spangles on the top surface and it has no effect on the thickness of the alloy layer.
6. Significant amount of Sb-rich intermetallic particles present in Zn with addition of 1.0 wt % Sb. No detectable Sb is found in the matrix of this Zn alloy. Significant amounts of Sb-rich particles were also found in the eta layer. Sb-rich particles are not catalytic sites for oxygen reduction reaction or pit initiation sites. Addition of Sb has no observable effect on the corrosion resistance of commercially-pure Zn. For hot dip galvanised coatings, addition of Sb was found to have no significant effect on either anodic or cathodic reaction activity of coating. Similar to Pb, Sb has no effect on the thickness of the alloy layer. Sb also produces spangles on the top surface.

7. Zr-rich intermetallic particles are found in the Zn alloy with 0.2 wt % Zr and in the eta phase layer. No Zr was detected in the alloy phase layers. Zr-rich particles were found to be pit initiation sites. For the hot dip galvanised coating containing 0.2 wt % Zr, no observed effect on both cathodic reactivity and anodic activity was found. The addition of 0.2 wt % Zr has some beneficial effect on inhibiting the growth of the alloy layers of the galvanised hyper-Sandelin steel (0.2 wt % Si).
8. The combined additions of Mn and Cu shows no significant effect on cathodic reactivity when a low level of Cu is added but significantly increases cathodic reactivity when high level of Cu is used. The combined additions of Mn (0.8 wt %) and Cu (0.2 wt % and 0.8 wt %) decrease the LPR compared with the commercially-pure Zn. However, the results of atmospheric exposure tests show that the combined addition of 0.8 % Mn and 0.2 % Cu can significantly improve the corrosion resistance to both industrial and marine atmosphere, which is mainly due to the beneficial effect of Mn additions.

CHAPTER 9 FUTURE WORK

1. Investigation of the corrosion behaviour of the Mn-containing coating in a long period of atmospheric exposure;
2. Electrochemical and atmosphere corrosion investigation of the corrosion behaviour of Zn-Fe-Mn and Zn-Fe-Cu alloy layers;
3. Explore other alloying additions (e.g. Bi) for improving the fluidity of the Zn bath without impairing corrosion resistance;
4. More detailed kinetic study of the effect of Cu additions on the coating thickness of Sandelin steel.

References:

1 X. G. Zhang, *Corrosion*, **55**, 787-794 (1999).
2 X. G. Zhang, *Corrosion and electrochemistry of zinc*, Plenum Press, New York, (1996).
3 Y. Uchima, M. Hasaka, and H. Koga, in *GALVATECH '89*, Tokyo, p. 545, The Iron and Steel Institute of Japan, (1989).
4 P. T. Gilbert, *J. Appl. Chem*, **3**, 174-181 (1953).
5 W. Radeker, F. K. Peters, and W. Friehe, in *Proceedings of 6th International Conference on Hot Dip Galvanizing*, Interlaken, p. 238-264, London: Zinc Development Association, (1961).
6 T. Johnsson and V. Kucera, in *INTERGALVA '82, 13th Conference on Hot Dip Galvanizing*, (1982).
7 J. A. Heath, *New Scientist*, **15**, 455 (1962).
8 R. Ramanauskas, L. Muleshkova, L. Maldonado, and P. Dobrovolskis, *Corros. Sci.*, **40**, 401-410 (1998).
9 A. Y. Hosny, M. E. El-Rafei, T. A. Ramadan, B. A. El-Gafari, and S. M. Morsy, *Met. Finish.*, **93**, 55-59 (1995).
10 R. Fratesi, G. Roventi, C. Branca, and S. Simoncini, *Surf. Coat. Technol.*, **63**, 97-103 (1994).
11 L. Diaz-Ballote and R. Ramanauskas, *Corro. Rev*, **17**, 411-422 (1999).
12 N. Boshkov, *Surf. Coat. Technol.*, **172**, 217-226 (2003).
13 R. Munz, G. K. Wolf, L. Guzman, and M. Adami, *Thin Solid Films*, **459**, 297-302 (2004).
14 L. Diaz-Ballote, R. Ramanauskas, and P. Bartolo-Perez, *Corro. Rev.*, **18**, 41-51 (2000).
15 M. S. Ho, *Atmospheric Corrosion Results of ZM-113 Galvanised Samples after Fifteen Years of Exposure*, 1, Cominco PTC Project No. 84-5-511, (1985).
16 W. Radeker, F. K. Peters, and W. Friehe, *The effect of alloy additions on the properties of hot galvanised coatings*, p. 238-264, Proceedings of the 6th International Conference on Hot Dip Galvanizing, Zinc Development Association, Interlaken, (1961).
17 W. Radeker and W. Friehe, in *Proceedings of 7th International Conference on Hot Dip Galvanizing*, Paris, p. 167-178, Pergamon Press, (1964).
18 F. Hanna and N. Nassif, *Surface Technology*, **21**, 27-37 (1984).
19 H. Leidheiser and I. Suzuki, *Corrosion*, **36**, 701 (1980).
20 F. C. Porter, *Zinc handbook: properties, processing, and use in design*, Marcel Dekker, New York, (1991).
21 A. R. Marder, *Progress in Materials Science*, **45**, 191-271 (2000).
22 L. Felloni, R. Fratesi, E. Quadrini, and G. Roventi, *Journal of applied electrochemistry*, **17**, 574 (1987).

23 M. Gavrila, J. P. Millet, H. Mazille, D. Marchandise, and J. M. Cuntz, *Surf. Coat. Technol.*, **123**, 164-172 (2000).
24 M. Hansen, R. P. Elliott, and F. A. Shunk, *Constitution of binary alloys*, McGraw-Hill, New York, (1958).
25 J. Mackowiak and N. R. Short, *Int. Met. Rev.*, **No. 1, Review 237**, (1979).
26 J. Ainsworth, *Met. Finish.*, **75**, 83 (1975).
27 O. Kubaschewski, *Binary alloy phase diagrams*, p. 1128, T. B. Massalski Editor. ASM, Metals Park, OH, (1986).
28 J. L. Murray, *Binary alloy phase diagrams*, p. 185, T. B. Massalski Editor. ASM, Materials Park, OH, (1986).
29 S. F. Radtke and D. C. Herrschaft, *J. Less Common Met.*, **93**, 253 (1983).
30 A. F. Skenazi, D. Davin, D. Coutsouradis, and F. G. Goodwin, in *Proceedings of 1st International Conference on Zinc Coated Steel*, Munich, London, Zinc Development Association, (1985).
31 A. Marder, *Microstructural characterization of zinc coatings*, p. 55, Zinc-based steel coating systems: metallurgy and performance, G. Krauss and D. Matlock Editors., TMS, Warrendale, PA, (1990).
32 A. F. Skenazi, D. Davin, D. Coutsouradis, and F. G. Goodwin, in *Proceedings of 1st International Conference on Zinc Coated Steel*, Munich, London, Zinc Development Association, (1985).
33 F. C. Porter, *Corrosion resistance of zinc and zinc alloys*, M. Dekker, New York, (1994).
34 J. H. Selverian, A. R. Marder, and M. R. Notis, *Met. Trans.*, **19A**, 1193 (1988).
35 J. H. Selverian, A. R. Marder, and M. R. Notis, *Met. Trans.*, **20A**, 543 (1989).
36 J. J. Sebisty and R. H. Palmer, in *Proceedings of 6th International Conference on Hot Dip Galvanizing*, Interlaken, p. 215-237, London: Zinc Development Association, (1961).
37 F. A. Fasoyino and F. Weinberg, *Met. Trans.*, **21B**, 549 (1990).
38 S. Chang and J. C. Shin, *Corros. Sci.*, **36**, 1425-1436 (1994).
39 R. Fratesi, N. Ruffini, M. Malavolta, and T. Bellezze, *Surf. Coat. Technol.*, **157**, 34-39 (2002).
40 P. Beguin, M. Bosschaerts, D. Dhaussy, R. Pankert, and M. Gilles, in *Proceedings of 19th International Galvanizing Conference*, Berlin, p. 1-5, EGGA, (2000).
41 M. Gagne, in *Proceedings of 18th International Galvanizing Conference*, Birmingham, p. 1-4, EGGA, (1997).
42 C. E. Jordan and A. R. Marder, *J. Mat. Sci.*, **32**, 5593-5602 (1997).
43 C. Allen, *Ph.D. Thesis*, University of London, (1963).
44 D. Horstmann, *Reaction between iron and zinc*, Zinc Development Association, London, (1978).
45 M. Onishi, Y. Wakamatsu, and H. Miura, *Trans JIM*, **15**, 331 (1974).
46 C. Allen and J. Mackowiak, *J. Inst. Met.*, **91**, 369-372 (1963).
47 *http://www.ckit.co.za/Secure/Conveyor/Troughed*.
48 H. Bablik, F. Gotzl, and R. Kukaczka, *Sheet Metal Industries*, **29**, 173-174 (1952).

49 G. D. S. Price and J. A. Charles, *J. Iron Steel Inst.*, **211**, 871-874 (1973).
50 R. W. Sandelin, *Wire and Wire products*, **15**, 655-676 (1940).
51 R. W. Sandelin, *Wire and Wire products*, **15**, 721-749 (1940).
52 R. W. Sandelin, *Wire and Wire products*, **16**, 28-35 (1941).
53 R. W. Sandelin, *Modern trends in steel as affecting hot-dip galvanizing*, American Hot Dip Galvanizers Association, Pittsburgh, (1963).
54 L. Habraken, in *Proceedings of 12th International Galvanizing Conference*, Paris, p. 121, Zinc Development Association, (1979).
55 M. Guttmann and P. Niessen, *Can. Metall. Quart.*, **11**, 609 (1972).
56 J. Foct, P. Perrot, and G. Reumont, *Scr. Met. Mat.*, **28**, 1195-1200 (1993).
57 Y. Lepretre and J. M. Mataigne, *A new interpretation of the Sandelin effect*, p. 303, Zinc-based steel coating systems: production and performance, F. E. Goodwin Editor. TMS, Warrendale, PA, (1998).
58 M. S. Kozdras and P. Niessen, *Metallography*, **22**, 253 (1989).
59 G. Reumont, P. Perrot, and J. Foct, in *Edited Proceedings: Seventeenth International Galvanizing Conference, Paris 1994*, p. 83-88, (1994).
60 S. Belfrage and P. Ostrom, in *Proceedings of 15th International Galvanizing Conference*, Rome, ZDA, GE3, (1988).
61 R. Sokolowski, in *Proceedings of 15th International Galvanizing Conference*, Rome, ZDA, GE1, (1988).
62 R. P. Krepski, in *Proceedings of 15th International Galvanizing Conference*, Rome, ZDA, GE4, (1988).
63 G. Reumont, P. Perrot, and J. Foct, *J. Mat. Sci.*, **33**, 4759-4768 (1998).
64 Z. W. Chen, N. F. Kennon, J. B. See, and M. A. Barter, *JOM-J. Miner. Met. Mater. Soc.*, **44**, 22-26 (1992).
65 T. Gladman, B. Holmes, and F. B. Pickering, *J. Iron Steel Inst.*, **211**, 765-777 (1973).
66 J. J. Sebisty and G. E. Ruddle, *Hydrogen atmosphere galvanizing of iron-base alloys*, Research Report No. R 255, Department of Energy, Mines and Resources, Mines Branch, (1972).
67 M. Dubois, *Mn in the galvanised coating*, p. 39, Zinc-based steel coating systems: production and performance, F. E. Goodwin Editor. TMS, Warrendale, PA, (1998).
68 M. A. Haughton, in *Proceedings of 2nd International Conference on Hot Dip Galvanizing*, London, p. 59-83, ZDA, (1952).
69 J. Strutzenberger and J. Faderl, *Met. Mater. Trans.*, **29A**, (1998).
70 R. P. Krepski, in *Proceedings of 14th International Galvanizing Conference*, London, p. 6/6-6/12, Zinc Development Association, (1985).
71 J. Strutzenberger and J. Faderl, *Metall. Mater. Trans. A-Phys. Metall. Mater. Sci.*, **29**, 631-646 (1998).
72 F. A. Fasoyinu and F. Weinberg, *Metallurgical Transactions B-Process Metallurgy*, **21**, 549-558 (1990).
73 J. J. Sebisty and J. O. Edwards, in *Proceedings of 5th International Conference on Hot Dip Galvanizing*, London, ZDA, (1958).
74 G. Reumont and P. Perrot, in *Proceedings of 18th International Galvanizing*

Conference, Birmingham, **Paper 4**, p. 1, EGGA, (1997).
75 T. Langill, in *Proceedings of 18th International Galvanizing Conference*, Birmingham, EGGA, (1997).
76 E. Nell, in *Proceedings of 9th International Conference on Hot Dip Galvanizing*, Redhill, UK, p. 140-151, Industrial Newspapers, (1970).
77 N. Katiforis and G. Papadimitriou, *Surf. Coat. Technol.*, **78**, 185-195 (1996).
78 E. Nell, in *Proceedings of 9th International Hot Dip Galvanization Conference*, Redhill, UK, p. 140-151, Industrial Newspapers, (1970).
79 J. J. Sebisty and R. H. Palmer, in *Proceedings of 7th International Conference on Hot Dip Galvanizing*, Paris, p. 235-265, Pergamon Press, (1964).
80 G. Reumont, J. Foct, and P. Perrot, in *Proceedings of 19th International Galvanizing Conference*, Berlin, **paper 4**, p. 1-9, EGGA, (2000).
81 G. R. Adams and J. Zervoudis, in *Proceedings of 18th International Galvanizing Conference*, Birmingham, **Paper 8**, p. 1-8, EGGA, (1997).
82 M. Gilles and R. Sokolowski, in *Proceedings of 18th International Galvanizing Conference*, Birmingham, **Paper 10**, p. 1, EGGA, (1997).
83 R. H. Palmer, H. R. Thresh, and J. J. Sebisty, in *Proceedings of 9th International Conference on Hot Dip Galvanizing*, Redhill, UK, p. 140-151, Industrial Newspapers, (1970).
84 M. Pourbaix, *Atlas of electrochemical equilibrium diagrams in aqueous solutions*, p. 406-413, NACE, Houston, TX, (1974).
85 L. M. Baugh, *Electrochim. Acta*, **24**, 657-667 (1979).
86 R. D. Armstrong and M. F. Bell, *Electroanal. Chem. Interfacial Electrochem.*, **55**, 201-211 (1974).
87 J. O. M. Bockris, Z. Nagy, and A. Danjanovic, *J. Electrochem. Soc.*, **119**, 285-295 (1972).
88 V. S. Muralidharan and K. S. Rajagopalan, *J. Electroanal. Chem.*, **94**, 21-36 (1978).
89 C. Cachet, F. Ganne, G. Maurin, J. Petitjean, V. Vivier, and R. Wiart, *Electrochim. Acta*, **47**, 509-518 (2001).
90 T. S. Lee, *J. Electrochem. Soc.*, **122**, 171-173 (1975).
91 H. Krug and H. Borchers, *Electrochim. Acta*, **13**, 2203-2205 (1968).
92 H. E. Townsend, in *ASM Metals Handbook*, American Society for Metals, Materials Park, Ohio, (1994).
93 G. D. Bengough and O. F. Hudson, in *Presented at the Annual General Meeting*, London, (1919).
94 U. R. Evans and D. E. Davies, *Corrosion*, **8**, 165-170 (1952).
95 K. F. Lorking and J. E. O. Mayne, in *The 1st International Congress on Metallic Corrosion*, London, p. 144-146, (1961).
96 E. A. Anderson and C. E. Reinhard, *zinc*, p. 331-346, The Corrosion handbook, H. H. Uhlig Editor. John Wiley & Sons, New York, (1948).
97 M. G. Alvarez and J. R. Galvele, *Corrosion*, **32**, 285-294 (1976).
98 D. E. Ddvies and M. M. Lotlikar, *Br. Corros. J.*, **1**, 149-155 (1966).
99 F. H. Assaf, S. S. A. E. Rehim, and A. M. Zaky, *Mat. Chem. Phy.*, **58**, 58-63 (1999).

100 E. E. Foad EI Sherbini and S. S. Abd EI Rehim, *Corros. Sci.,* **42**, 785-798 (2000).
101 S. R. Dunbar and W. Showak, *Effect of 1 percent copper addition on atmospheric corrosion of rolled zinc after 20 years' exposure,* p. 135-162, Atmospheric corrosion of Metals, **STP 767**, American Society for Testing and Materials, Philadelphia, (1982).
102 R. Lindstrom, J. E. Svensson, and L. G. Johansson, *J. Electrochem. Soc.,* **147**, 1751-1757 (2000).
103 T. Falk, J. E. Svensson, and L. G. Johansson, *J. Electrochem. Soc.,* **145**, 2993-2999 (1998).
104 A. D. Keitelman, S. M. Gravano, and J. R. Galvele, *Corrosion Science,* **24**, 535-545 (1984).
105 B. E. Roetheli, G. L. Cox, and W. B. Littreal, *Met. Alloys,* **3**, 73-76 (1932).
106 M. Selvam and S. Guruviah, *Bull. Electrochem.,* **6**, 485-486 (1990).
107 M. K. Budinski and B. E. Wilde, *Corrosion,* **43**, 60-62 (1987).
108 N. R. Short, A. Abibsi, and J. K. Dennis, *Trans. Inst. Met. Finish,* **67**, 73-77 (1989).
109 M. Sagiyama, A. Hiraya, and T. Watanabe, *J. Iron Steel Inst. Jpn.,* **77**, 251-257 (1991).
110 W. Feitknecht, *Chem. Ind.,* 1102-1109 (1959).
111 T. E. Graedel, *J. Electrochem. Soc.,* **136**, 193-203 (1989).
112 T. Falk, J. E. Svensson, and L. G. Johansson, *J. Electrochem. Soc.,* **145**, 39-44 (1998).
113 I. Odnevall and C. Leygraf, *J. Electrochem. Soc,* **138**, 1923-1928 (1991).
114 I. Odnevall and C. Leygraf, *Corros. Sci.,* **34**, 1213-1229 (1993).
115 I. Odnevall and C. Leygraf, *Corros. Sci.,* **36**, 1551-1567 (1994).
116 M. Mabuchi, K. Takao, H. Ogishi, H. Kimura, and T. Ichida, in *Zinc-based steel coating systems: metallurgy and performance,* G. Krauss and D. K. Matlock, Editors, p. 207-218, TMS, Warrendale, PA, (1990).
117 H. Satoh, K. Shimogori, H. Nishimoto, K. Miki, k. Ikeda, M. Iwai, H. Sakai, and S. Nomura, in *Automotive Corrosion and Prevention Conference,* Dearbon, Michigan, p. 8-10, SAE Technical Paper No. 862018, Society of Automotive Engineers, (1986).
118 J. Kawafuku, J. Katoh, M. Toyama, H. Nishimoto, k. Ikeda, and H. Satoh, *J. Iron Steel Inst. Jpn.,* **77**, 995-1002 (1991).
119 M. Keddam, A. Hugot-Le-Goff, H. Takenouti, D. Thierry, and M. C. Arevalo, *Corros. Sci.,* **33**, 1243-1252 (1992).
120 V. Ligier, M. Wery, J. Y. Hihn, J. Faucheu, and M. Tachez, *Corros. Sci.,* **41**, 1139-1164 (1999).
121 N. R. Short, S. Zhou, and J. K. Dennis, *Surf. Coat. Technol.,* **79**, 218-224 (1996).
122 F. J. F. Miranda, I. C. P. Margarit, O. R. Mattos, O. E. Barcia, and R. Wiart, *Corrosion,* **55**, 732-742 (1999).
123 D. Sylla, J. Creus, C. Savall, O. Roggy, M. Gadouleau, and P. Refait, *Thin Solid Films,* **424**, 171-178 (2003).
124 J. C. Zoccola, H. E. Townsend, A. R. Borzillo, and J. B. Horton, in *Atmospheric factors affecting the corrosion of engineering metals,* **STP 646,** p. 165-184, American Society for Testing and Materials, Philadelphia, (1978).
125 F. E. Goodwin, in *Zinc-based steel coating systems: metallurgy and performance,* D.

K. Matlock, Editor, p. 183, TMS, Warrendale, PA, (1990).
126 I. Suzuki, *Corrosion-resistant coatings technology*, p. 11, Marcel Dekker, New York, (1989).
127 H. E. Townsend, *Corrosion*, **44**, 229-230 (1988).
128 E. A. Anderson, *The atmospheric corrosion of rolled zinc*, p. 126-134, ASTM 58th Annual Meeting, Symposium on Atmospheric Corrosion of Non-Ferrous Metals, **STP 175**, American Society for Testing and Materials, Philadelphia, (1953).
129 P. R. Sere, J. D. Culcasi, C. I. Elsner, and A. R. D. Sarli, *Surf. Coat. Tech.*, **122**, 143-149 (1999).
130 A. M. Alfantazi and U. Erb, *Corrosion*, **52**, 880-888 (1996).
131 J. E. Svensson and L. G. Johansson, *Corros. Sci.*, **34**, 721-740 (1993).
132 A. Askey, S. B. Lyon, G. E. Thompson, J. B. Johnson, G. C. Wood, M. Cooke, and P. Sage, *Corros. Sci.*, **34**, 233-247 (1993).
133 I. L. Muller and J. R. Galvele, *Corros. Sci.*, **17**, 179-193 (1977).
134 I. L. Muller and J. R. Galvele, *Corros. Sci.*, **17**, 995-1007 (1977).
135 A. D. Keitelman, S. M. Gravano, and J. R. Galvele, *Corros. Sci.*, **24**, 535-545 (1984).
136 S. I. Pyun, J. S. Bae, S. Y. Park, J. S. Kim, and Z. H. Lee, *Corros. Sci.*, **36**, 827-835 (1994).
137 M. A. Arenas, M. Bethencourt, F. J. Botana, J. d. Damborenea, and M. Marcos, *Corros. Sci.*, **143**, 157-170 (2001).
138 N. Boshkov, S. Nemska, and S. Vitkova, *Met. Finish.*, **100**, 14 (2002).
139 http://www.webelements.com/.
140 M. Stern and A. L. Geary, *J. Electrochem. Soc.*, **104**, 56 (1957).